Tau spreading and accumulation with a focus on tyrosine kinases Pyk2 and Fyn in the context of Alzheimer‘s Disease

Dissertation

zur Erlangung des Grades eines

Doktors der Naturwissenschaften

der Mathematisch-Naturwissenschaftlichen Fakultät

und

der Medizinischen Fakultät

der Eberhard-Karls-Universität Tübingen

vorgelegt

von

Sarah Helena Nies

aus Köln, Deutschland

2022

Tag der mündlichen Prüfung:	07.12.2022
Dekan der Math.-Nat. Fakultät:	Prof. Dr. Thilo Stehle
Dekan der Medizinischen Fakultät:	Prof. Dr. Bernd Pichler
1. Berichterstatter:	Prof. Dr. Philipp Kahle
2. Berichterstatter:	Prof. Dr. Stephen Strittmatter
Prüfungskommission:	Prof. Dr. Philipp Kahle
	Prof. Dr. Stephen Strittmatter
	Prof. Dr. Peter Heutink
	Jun. Prof. Dr. Michela Deleidi

Erklärung / Declaration:

Ich erkläre, dass ich die zur Promotion eingereichte Arbeit mit dem Titel: “Tau spreading and accumulation with a focus on tyrosine kinases Pyk2 and Fyn in the context of Alzheimer‘s Disease” selbständig verfasst, nur die angegebenen Quellen und Hilfsmittel benutzt und wörtlich oder inhaltlich übernommene Stellen als solche gekennzeichnet habe. Ich versichere an Eides statt, dass diese Angaben wahr sind und dass ich nichts verschwiegen habe. Mir ist bekannt, dass die falsche Abgabe einer Versicherung an Eides statt mit Freiheitsstrafe bis zu drei Jahren oder mit Geldstrafe bestraft wird.

I hereby declare that I have produced the work entitled “Tau spreading and accumulation with a focus on tyrosine kinases Pyk2 and Fyn in the context of Alzheimer‘s Disease”, submitted for the award of a doctorate, on my own (without external help), have used only the sources and aids indicated and have marked passages included from other works, whether verbatim or in content, as such. I swear upon oath that these statements are true and that I have not concealed anything. I am aware that making a false declaration under oath is punishable by a term of imprisonment of up to three years or by a fine.

Tübingen, den ....

Datum / Date Unterschrift /Signature

Table of Contents

Table of Figures

Table of Tables

Abbreviations

Abbreviation	Long Name
AD	Alzheimer's Disease
ADAM10	A Disintegrin and metalloproteinase domain-containing protein 10
AICD	APP intracellular domain
APLP	Amyloid precursor like proteins
APP	Amyloid precursor protein
ARIA	Amyloid-related imaging abnormalities
Aß	Amyloid-ß
Aßo	Amyloid-ß oligomers
BACE1	Beta-site APP cleaving enzyme 1
BBB	Blood-brain barrier
BCA	Bicinchoninic acid
CAA	Cerebral amyloid angiopathy
CADTK	Calcium-dependent protein tyrosine kinase
CAKß	Cell adhesion kinase ß
CaMKII	Calcium/calmodulin-dependent kinase II
CDK5	Cyclin-dependent kinase 5
CK1	Casein kinase 1
CMA	Chaperone-mediated autophagy
CSF	Cerebrospinal fluid
CTF83	C-terminal fragment 83
CTF99	C-terminal fragment 99
DYRK-1A	Dual-specificity tyrosine-phosphorylation regulated kinase 1A
EDTA	Ethylenediaminetetraacetic acid
eEF2	Eukaryotic elongation factor 2
eEF2K	Eukaryotic elongation factor 2 kinase
EGFR	Epidermal growth factor receptor
EM	Electron microscopy
EOAD	Early-onset AD
EphA4	Ephrin type-A receptor
EphB2	Ephrin type-B receptor
ER	Endoplasmic reticulum
fAD	Familiar AD
FAK	Focal adhesion kinase
FAT	Focal adhesion targeting
FcγRIIb	Fcγ receptor IIb

Graf1	GTPase regulator associated with FAK-1
GSK3ß	Glycogen synthase kinase 3 ß
GWAS	Genome wide association studies
HDL	High density lipoprotein
hsc 70	Heat shock cognate protein of 70kd
IR	Insulin receptor
LilrB2	Leukocyte immunoglobulin-like receptor subfamily B2
LOAD	Late-onset AD
LTP	Long term potentiation
MAPK	Mitogen activated protein kinase
MARK	Microtubule affinity-regulating kinase
MCI	Mild cognitive impairment
mGluR5	Metabotropic glutamate receptor 5
MHC	Major histocompatibility complex
MRI	Magnetic resonance imaging
mTORC1	Mammalian target of rapamycin complex 1
MWM	Morris Water Maze
nAchRα7	Nicotinic acetylcholine receptor α7
Nct	Nicastrin
NF-κ-B	Nuclear factor kappa-light-chain-enhancer of activated B cells
NFT	Neurofibrillary tangles
NGF	Nerve growth factor
NgR1	Nogo-66 receptor 1
NMDA	N-methyl D-aspartate
NMDAR	NMDA receptor
NMR	Nuclear magnetic resonance
NOR	Novel Object Recognition
NR2A	NMDA receptor subunit 2A
NR2B	NMDA receptor subunit 2B
p-Fyn	Phosphorylated Fyn
p-GSK3ß	Phosphorylated GSK3ß
p-Pyk2	Phosphorylated Pyk2
p-Tau	Phosphorylated Tau
$p75^{NTR}$	Low-affinity nerve growth factor receptor
PBS	Phosphate-buffered saline
PBST	Phosphate-buffered saline with Tween-20
Pen-2	Presenilin enhancer 2
PET	Positron electron tomography
PF-719	N-cyclopropyl-4-(4-((1R,2R)-2-(dimethylamino)cyclopentylamino)-5-(trifluoromethyl)-pyrimidin-2-ylamino)benzamide dihydrochloride

PKA	Cyclic AMP-dependent protein kinase A
PKC	Protein kinase C
PP2A	Protein phosphatase 2A
PrP^C	Cellular prion protein
PSD	Post synaptic density
PSEN1	Presenilin 1
PSEN2	Presenilin 2
Pyk2	Proline-rich tyrosine kinase 2
RAFTK	Related adhesion focal tyrosine kinase
RAGE	Receptor for advanced glycation end products
RIPA buffer	Radioimmunoprecipitation assay buffer
sAD	Sporadic AD
sAßo	Synthetic Amyloid-ß oligomers
SDS	Sodium dodecyl sulfate
SPR	Surface plasmon resonance
STEP	Striatal-enriched protein tyrosine phosphatase
TBI	Traumatic brain injury
TBST	Tris-buffered saline with Tween-20
TCR	T-cell antigen receptor
TREM2	Triggering receptor expressed on myeloid cells 2
WT	Wild type

Abstract

In Alzheimer's disease (AD), deposition of pathological tau and amyloid-β (Aβ) is thought to drive synaptic loss and cognitive decline. Major questions in the field center around possible connections between the two pathologies and what molecular mechanisms can impact tau pathology progression. We aimed to determine, if different proteins reported to modify tau pathology could modify tau phosphorylation *in vitro* and tau spreading *in vivo*.

Two kinases, Pyk2 (*Ptk2b*) and Fyn, are part of a signaling cascade activated by Aß oligomers binding to the cellular prion protein receptor (PrP^C) and have also been reported to interact with GSK3ß, one of the best characterized tau kinases. We hypothesized that Aß might induce tau phosphorylation through Prp^C-mGluR5-Fyn-Pyk2-GSK3ß signaling. We first studied the interactions of the three kinases and tau in different *in vitro* model systems, including HEK-293T over-expression system and iPSC-derived neurons. In HEK-293T cells, Pyk2 and Fyn worked in synergy to increase GSK3ß phosphorylation and subsequent tau phosphorylation. Furthermore, GSK3ß co-immunoprecipitated with Pyk2, and Fyn kinase inhibition reduced Fyn's proximity to tau as well as reduced tau spreading in mouse cortical neuron cultures seeded with human tau. Thus, initial data supported a role for the three kinases in contributing to tau hyperphosphorylation and spreading. Contrary to these results, GSK3ß phosphorylation remained unchanged in human iPSC-derived neurons upon inhibition of Pyk2 and Fyn kinases. Surprisingly, tau phosphorylation on some epitopes was even increased upon Pyk2 inhibition. In addition, iPSC-derived neurons were incubated either short- or long-term with synthetic Aßo. Upon long-term treatment, neurons showed decreases in synaptic density as expected. In contrast to expectations, short-term treatment with sAßo did not activate Pyk2 and Fyn kinases and showed no effect on GSK3ß, tau or other downstream targets.

To study modulation of tau spreading by different factors, misfolded tau aggregates extracted from human AD brains were injected into WT and transgenic mice to drive templated spreading of tau pathology. We assessed the impact of Aβ co-pathology, of deleting loci known to modify AD risk (*Ptk2b, Grn, and Tmem106b*) and of pharmacological intervention with a Fyn kinase inhibitor on tau spreading after injection of AD tau extracts. The density and spreading of tau inclusions triggered by human tau seed were unaltered in the hippocampus and cortex of *APPswe/PSEN1ΔE9* transgenic and $App^{NL\text{-}F/NL\text{-}F}$ knock-in mice. In mice with human tau sequence replacing mouse tau, template matching enhanced neuritic tau burden. Human AD brain tau-enriched preparations contained aggregated Aβ, and the Aβ co-injection caused a redistribution of Aβ aggregates in mutant AD model mice. The injection-induced Aβ phenotype was spatially distinct from tau accumulation and could be ameliorated by depleting Aβ from tau extracts. These data suggest that Aβ and tau pathologies propagate by largely independent mechanisms after their initial formation. Altering the activity of the Fyn and Pyk2 kinases involved in Aβ-oligomer–induced signaling, or deleting expression of the progranulin and TMEM106B lysosomal proteins, did not alter the somatic tau inclusion burden or spreading. However, mouse aging had a prominent effect to increase the accumulation of neuritic tau after injection of human AD tau seeds into WT mice.

Overall, these results suggest that observations from over-expression non-neuronal model studies of Pyk2 and Fyn acting on GSK3ß and tau do not translate faithfully into neuronal model systems. Further, these studies refined our knowledge of factors (in-)capable of modulating tau spreading and lend evidence to the hypothesis of a more complex role of tau phosphorylation regulation by Fyn and Pyk2 in different model systems.

Introduction

Alzheimer's Disease

A Brief History of AD

What is today classified as Alzheimer's Disease (AD) was first reported on in 1906 at a neuroanatomist meeting in Tübingen by Alois Alzheimer, but his report only garnered little attention from attending scientists[1,2]. Nevertheless, Alzheimer published his findings on the pathology and symptoms of patient Auguste D. the following year[3]. Auguste D. exhibited clinical symptoms we now associate with AD including aphasia, erratic behavior, memory disruptions, paranoia and progressive confusion[3,4]. After her death, she was autopsied and Alzheimer examined her brain, describing what are now considered the hallmarks of AD: extracellular amyloid plaques and intracellular neurofibrillary tangles (NFT), accompanied by brain atrophy, neuronal loss and gliosis (see Figure 1)[3]. Alzheimer himself did not believe that he was describing a new disease, but rather an unusual case or sub-type of senile dementia occurring in younger patients. The presence of amyloids in the brain had been described previously by other scientists[5,6], but he was the first to identify them as markers for this sub-type of dementia.

In the same year as Alzheimer's first publication, another scientist located in Prague, Oskar Fischer, published a description of neuritic plaques[7]. These findings were confirmed later on by Alzheimer in his 1911 paper that also described the case of Johann F.[8]. Fischer published several additional papers[9–11] investigating neuritic plaques and even attempted to define stages of the disease process by comparing plaque development to clinical progression of 'presbyophrenic' dementia[9]. Even though both scientists were important in describing and characterizing what would later be called Alzheimer's Disease, only one of them was honored by having the disease named after him. This can be traced back to Emil Kraepelin, who published a textbook for medical students in which he named this sub-type of dementia after his former colleague, Alois Alzheimer[5,12,13].

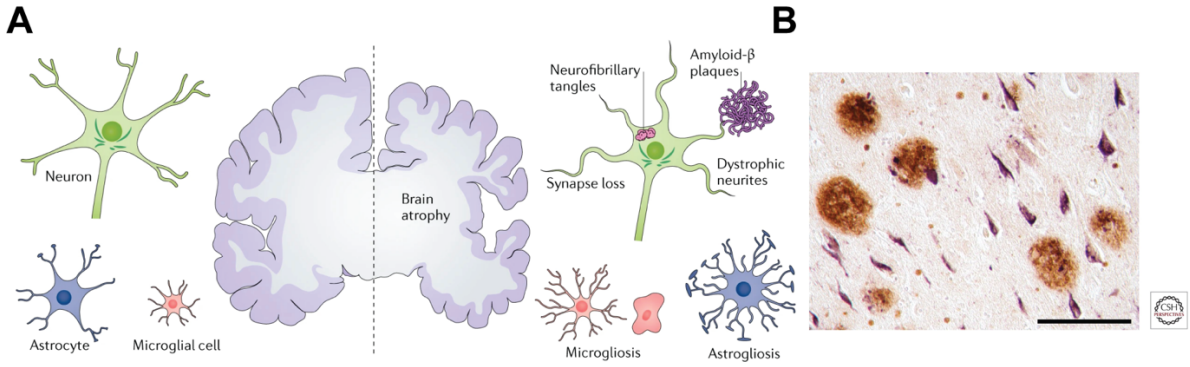

Figure 1: Hallmarks of AD.
A) Overview of AD hallmark pathologies. At the macroscopic level Alzheimer's disease is characterized by brain atrophy, driven by loss of synapses and neurons. At the microscopic level, the hallmark pathologies of AD, extracellular amyloid-β plaques and intraneuronal neurofibrillary tangles are observed. In addition, there are dystrophic neurites and loss of synapses, as well as microgliosis and astrogliosis**.** Image reprinted from Nature Reviews Neurology, Issue 14, Pages 399–415, Congdon, E.E., Sigurdsson, E.M., 2018, E.M. *Tau-targeting therapies for Alzheimer disease,* doi: https://doi.org/10.1038/s41582-018-0013-z , ©2018 by Springer Nature, with permission from Springer Nature[14]. **B)** Histopathological example of AD hallmarks. Amyloid-β (Aβ) plaques (brown; detected by immunostaining with a polyclonal antibody to Aβ), and intracellular neurofibrillary tangles (NFTs) (purple; detected by immunostaining with a monoclonal antibody to tau). Scale bar, 100 µm. Image reprinted from Cold Spring Harbor Perspectives in Medicine, Volume 6, Issue 7, Pages a024398, Walker et al., 2016, *The Prion-Like Properties of Amyloid-b Assemblies: Implications for Alzheimer's Disease,*

In the six decades following its first description and discovery, research into Alzheimer's Disease remained a niche topic in psychiatry and neurology[6,16]. From the 1970s onwards, the number of research articles published about AD steadily increased every decade[16] and progress was made to further characterize and link the underlying molecular causes of AD to the clinical presentation and progression of the disease[17–19].

Looking at the clinical aspects of AD, there were several shifts in definitions, diagnosis, and treatment of patients throughout the decades. Until the late 1970s, AD (presenile dementia) and senile dementia were regarded as separate diseases and not as part of the same disease spectrum that shares underlying causes[6,16]. This view shifted due to further investigations into dementia sub-forms and neuropathological examinations[20,21]. In the 1980s, several papers identified deficits in episodic memory as an early symptom of AD[22–25]. In the 1990 and early 2000s, the concept of mild cognitive impairment (MCI) was developed, following the realization that AD and other dementias are preceded by a phase of progressive cognitive decline that can span several years[26–33]. The term MCI has helped to identify and categorize people in early dementia stages, but also led to some confusion, as there is no clear delineation between MCI and early stages of clinical AD and some people never progress from MCI into full blown dementia[16,34,35]. During MCI, amyloid-ß (Aß) plaques and NFT are already deposited throughout the brain, and neuronal destruction takes place. Current efforts on the clinical side are focused on developing biomarkers that can accurately predict the onset of MCI and AD[19]. This would be helpful to allow for early, disease-modifying interventions once they become available[19,36].

On the research side, scientists investigated the role of the cholinergic system in cognitive decline in the 1970s[37,38], which lead to the cholinergic hypothesis, stipulating that the dysregulation of acetylcholine metabolism in the brain contributes significantly to cognitive dysfunction and progression of AD[16,39]. This hypothesis carries less weight nowadays, due to the emergence of the amyloid cascade hypothesis, which suggested Aß accumulation as the primary and causative factor in AD[40]. It was driven by work from Hyman[41], as well as Braak and Braak[42,43] in the 80s and 90s, focusing on the pathological examination of AD cases. This shifted the focus towards tau and Aß pathologies. Furthermore, advances in imaging techniques, helped to visualize changes in brain metabolism[44,45] and plaque deposition[46], leading to a better understanding of the temporal progression (staging) of AD. The past 30 years have also seen rapid advances in genetics, strengthening our understanding of familial forms of AD (fAD)[47–52] and risk genes for sporadic AD (sAD)[53–57]. Another AD research area that has seen great advances in recent decades are the molecular mechanisms underlying AD. Receptors that might mediate Aß-induced damage and their downstream signaling cascades have been identified (reviewed in Smith and Strittmatter 2017[58]) and the role of microglia, astrocytes and oligodendrocytes in AD has begun to be investigated. Nevertheless, our understanding of the molecular underpinnings of AD remains patchy and no holistic model has been reached on how all the different molecular players interact with one another[13,59,60].

Clinical Symptoms and Course of AD

Currently, Alzheimer's disease progression is categorized into three main periods: preclinical, prodromal (MCI) and AD dementia[19,61]. Research into the molecular causes underlying AD has shown that protein accumulation of amyloid-ß and tau can precede the onset of clinical symptoms by several decades, promoting the idea of AD progression as a continuum (see

Figure 2)[36]. The early phase of the disease has been named preclinical (or pre-symptomatic), since pathological processes have begun, but patients do not yet experience any cognitive decline[19,61]. This disease stage has received increased attention in recent years, as the damage to the brain is still developing and disrupting the pathological events at this timepoint could halt disease progression[19]. It remains difficult though to identify preclinical AD patients, since the only available tools currently are CSF biomarkers for Aß, tau and phospho-tau, or evaluation through neuroimaging (PET and MRI)[19,35,62]. Unfortunately, these procedures are either invasive or costly, having spurred research into blood and plasma biomarkers that would enable easy detection of preclinical pathology[19,36,59].

The clinical onset of Alzheimer's Disease is often gradual and early symptoms are easily overlooked[19,35,63]. Furthermore, differentiating AD from other forms of dementia remains difficult in early stages, since symptoms can overlap[19]. During the prodromal disease stages (MCI due to AD), symptoms are very mild and do not interfere with a person's everyday life[19,26–33]. Over time, most MCI patients progress from MCI to dementia and AD is often diagnosed when patients already have full-blown dementia, since symptoms become more pronounced[35]. Dementia is defined as having impairments in multiple domains, leading to a loss of function that impairs daily life[19]. Common symptoms include becoming more forgetful of recent events, names or conversations, losing track of time or failing to recognize formerly familiar places[19,64]. This can also be accompanied by changes in mental state, specifically apathy or depression, as well as additional symptoms such as disorientation, confusion and behavioral changes[64]. In the late stages of AD, patients frequently experience complications such as difficulty to communicate (impaired speech), immobility, swallowing disorders and subsequent malnutrition. These symptoms can increase the risk for acquiring serious acute conditions, often from respiratory illnesses or circulatory diseases, leading to death[65].

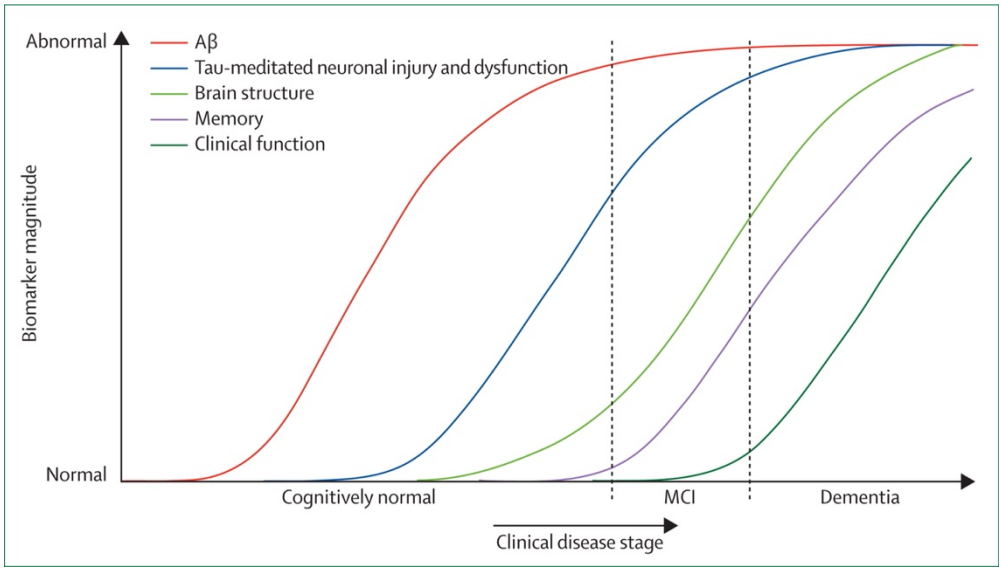

Figure 2: Alzheimer's Disease progression and biomarkers.
Biomarkers indicate that amyloid-ß accumulates first, followed by hyperphosphorylated tau, leading to neuronal dysfunction. This is followed by changes in brain structure, memory decline and subsequent clinical dysfunction. Image reprinted from The Lancet Neurology, Volume 12, pages 207-216, Jack CR Jr et al., *Tracking pathophysiological processes in Alzheimer's disease: an updated hypothetical model of dynamic biomarkers*, https://doi.org/10.1016/S1474-4422(12)70291-0 , ©2013 by Elsevier, with permission from Elsevier[36].

Genetic Risk Factors of AD

There are several genetic mutations known to cause familial AD and many more genetic loci that increase risk for sporadic AD have been identified in large genome wide association studies (GWAS) (see Figure 3). Disease symptoms in fAD usually occur around 40-60 years of age, leading to fAD often being categorized as early-onset AD (EOAD). In contrast, most sporadic AD cases have a later onset (late-onset AD, LOAD) at 65+ years of age. Only 5-10% of AD cases are caused by rare, monogenetic mutations that are inherited with an autosomal dominant pattern (fAD), while the remaining 90-95% of AD cases are considered sporadic, with unknown, complex, and likely multifactorial causes. Moreover, it has been suggested through twin studies, that 58-79% of the risk for developing LOAD can be attributed to genetics[66].

Rare mutations in the amyloid precursor protein (*APP*) or the presenilin 1 and 2 genes (*PSEN1* and *PSEN2*) are the cause of autosomal dominant AD[52,67–74]. Notably, all three genes are implicated in Aß production and to date, there are 73 *APP*[75], 348 *PSEN1*[76] and 87 *PSEN2*[77] known mutations in these genes. Not all mutations are disease causative, but at least 32 *APP*, 179 *PSEN1* and 14 *PSEN2* mutations result in EOAD, while only one *APP* mutation (Icelandic mutation, A673T) and none of the *PSEN1* or *PSEN2* mutations are classified as neuro-protective[78]. In APP, some mutations have been used to generate AD mouse models and thus become more well known, including the Swedish (KM670/671NL)[79], Florida (I716V)[80], London (V717I)[51], Iberian (I716F)[73], and Arctic (E693G)[81,82] mutations. The Swedish mutation is adjacent to the ß-site APP cleaving enzyme 1 (BACE1) cleavage site, even though most disease-causing mutations cluster around the γ-secretase cleavage site in APP. In the *PSEN* loci, disease causing mutations are clustered in the nine amino acid transmembrane domain of the proteins, leading to an increase of $Aß_{42}$ over $Aß_{40}$ production (see 'Generating Amyloid-ß from APP' for more information on APP processing)[78].

In contrast, mutations in *MAPT*, the gene giving rise to protein tau, are not disease-causing for AD, but can be causative for other tauopathies including frontotemporal dementia (FTD), progressive supranuclear palsy (PSP) and Pick's disease. The lack of disease causing *MAPT* mutations in AD is often cited as a reason for the validity of the amyloid cascade hypothesis, suggesting that Aß pathology rather than tau pathology is causative for the disease.

Apart from mutations causing EOAD, the best characterized risk gene for LOAD is the gene encoding apolipoprotein E (*APOE)*[53,54]. *APOE* exists in three variants (*ε2, ε3* and *ε4*) and encodes three different proteins (ApoE2, ApoE3 and ApoE4). Physiologically, ApoEs are the predominant apolipoprotein in high density lipoprotein complexes (HDL), where they are thought to facilitate Aß clearance from the brain. They play a role in binding Aß, with sequence differences at only two amino acids resulting in altered binding affinities for Aß. ApoE2 binds Aß best, followed by ApoE3 still displaying tight binding of Aß, while ApoE4 shows markedly lower binding[83]. This results in the *APOE ε2* allele being neuroprotective for AD and *APOE ε4* allele increasing AD risk. Conversely, a recent study associated ApoE3 with increased hyperphosphorylated tau deposition upon seeding of K18 tau in a PS19 mouse model[84]. People who are heterozygous for the *APOE ε4* allele have a threefold higher risk of developing AD, and homozygous carriers even have a 15-fold increased AD risk[85]. An estimated 10-20% in different populations across the globe carry at least one *APOE ε4* allele[86], making it one of the most important risk factors for AD.

There are too many genetic risk factors of LOAD to go into detail on all of them, but some additional risk factors that are considered to have more impact than others include sortilin-related receptor 1 (*SORL1*), A Disintegrin and metalloproteinase domain-containing protein 10 (*ADAM10)* and Triggering receptor expressed on myeloid cells 2 (*TREM2). SORL1* encodes the

protein SorL1 which has been implicated in regulating APP localization inside cells, with reduced SorL1 expression leading to increased APP proteolysis and thus increased Aß generation[55]. ADAM10 is the most important α-secretase that cleaves APP at the cell surface in the non-amyloidogenic pathway. Thus, its disruption can shift APP processing towards the amyloidogenic processing pathway, resulting in increased Aß levels[56,57]. Furthermore, ADAM10 also sheds TREM2 from microglia[87]. In microglia, TREM2 regulates phagocytosis and removal of apoptotic cells. Reduced TREM2 surface expression can impair these functions, likely leading to impaired clearance of debris (e.g. Aß aggerates) and prolonged neuroinflammation[87,88].

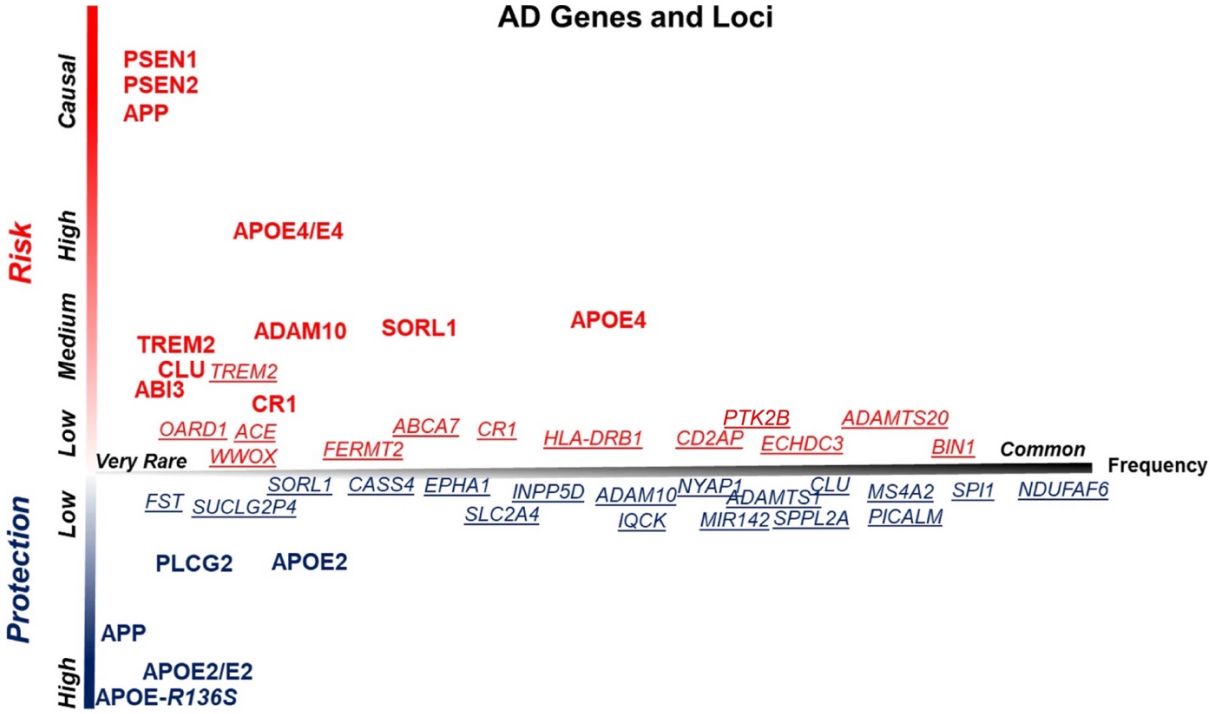

Figure 3: Genetic Risk Factors associated with Alzheimer's Disease.
Loci implicated by genome wide association studies (GWAS) are underlined, while AD causing genes are written in bold text. The X-axis indicates mutation or variant frequency, and the Y-axis indicates bidirectional risk. Some AD genes have both harmful and protective mutations or variants. For most loci implicated by GWAS, the genes and functional variants that are driving the association remain unknown. GWAS loci depicted in this figure are derived from Kunkle et al. 2019[57]. Image modified from Molecular Neurodegeneration, Vol. 17, Issue 1, Todd E. Golde, *Alzheimer's disease – the journey of a healthy brain into organ failure,* pages1-19, doi: https://doi.org/10.1186/s13024-022-00523-1 , ©2022 Springer Nature, with permission from Springer Nature[13].

Non-Genetic Risk Factors of AD

In addition to genetic risk factors, there are many other non-genetic risk factors thought to influence AD risk (reviewed in Reitz et al. 2011, Rochoy et al. 2019 and Golde 2022)[13,55,89]. They include advanced age, sex[65,90–92], cerebrovascular disease[93,94], obesity and type 2 diabetes[95], high blood pressure[93], sleep apnea[96], smoking, traumatic brain injury[97,98], other mental disorders such as depression and stress, diet, physical and intellectual activity[55,89,99].

The most common forms of cerebrovascular disease are ischemic and hemorrhagic strokes. Risk factors for cerebrovascular disease include hypertension, smoking and diabetes, which are also known risk factors for AD. Strokes are thought to increase AD risk through several mechanisms: they can directly damage brain regions and thus memory function, they can lead to increased Aß deposition[93], and inflammatory responses and the resulting

hypoperfusion of tissue can lead to aberrant cyclin-dependent kinase 5 (CDK5) signaling, increasing tau hyperphosphorylation and dysregulating synaptic plasticity[55,94].

Furthermore, hypertension in middle age has also been reported to increases the risk of AD by negatively impacting the integrity of the neuro-vascular unit and thus the integrity of the blood-brain barrier (BBB)[55,89,93]. The connection between traumatic brain injury (TBI) and AD remains controversial, but recent meta-analyses pooling results from 17 studies reported a higher incidence of AD in TBI patients[98]. The suspected cause for the increase in AD upon TBI is once more disruption of neurovascular unit integrity.

Obesity and diabetes[95,100] in middle life have also been reported to increase dementia risk, most likely through downstream effects of dysregulated insulin-signaling[95]. Interestingly, being underweight in middle age also seems to increase risk of dementia, and inversely, in the prodromal phase of AD, cognitive impairments can cause patients to lose weight too[55].

Up to 50% of AD patients experience depressive symptoms after AD onset, but longitudinal studies have also found an increased risk of dementia in patients that had depressive symptoms before AD onset[55,89]. Furthermore, stress might also increase AD risk by accelerating Aß and tau pathologies through dysfunction of the hypothalamic pituitary axis[13,101].

In contrast, lifestyle factors that potentially decrease AD risk include physical activity[89] and a Mediterranean diet[102]. The underlying reasons for the protective effects are not well established and likely complex. Another protective factor might be higher levels of educational attainment or engaging in cognitively stimulating activities[13,99]. This is hypothesized to build up a "brain structure and cognitive reserve" allowing people to retain cognitive function longer even though the brain is damaged by AD pathologies[103]. The impact of smoking on AD risk remains controversial, with more studies associating smoking with increased AD risk[89], and fewer finding none or even a protective impact[55,89]. The protective effects of smoking might stem from an increase in nicotinic acetylcholine receptors in the brain of smoker's that counter cholinergic deficits in AD. Conversely, the negative effects of smoking are likely mediated through increased oxidative stress, neuroinflammation and cerebrovascular damage[55].

Disease Prevalence and Costs

For a long time, there was little interest in researching the molecular causes of AD, but as public health improved and led to longer lifespans, the number of elderly people worldwide also increased. For example, the number of people above age 65 in the US was around 13 million in 1950, but is currently 58 million and will rise to 88 million by 2050[65,104]. In people age 60 and older, 60-80% of dementia cases are classified as AD, and currently, more than 1 in 9 people above the age of 65 in the US have AD [55,65]. The World Health Organization now classifies AD as the 7th leading cause of death worldwide[105].

As people get older, the percentage of dementia patients rises steadily with 5.3% of people age 65-74, 13.8% of people age 75-84, and 34.6% of people age 85 and older suffering from AD in the US[55,65]. This amounts to an estimated 6.2 million people suffering from AD in the US in 2022 and this number is projected to increase to 13.8 million people by 2050[65]. Worldwide, the number of AD cases is projected to increase from around 50 million in 2015 to 152 million cases by 2050[106]. It is also important to note, that the prevalence of AD is higher in women (2/3 of patients are female)[65,107]. The reasons for the sex difference remain controversial, with theories ranging from women's lifespan being longer on average[90], to hormonal differences[91], or differences in education levels in the current above age 65 population[65,99].

From the time of diagnosis, the average patient lives for another 4-8 years, which results in significant medical costs associated with AD, since unassisted living becomes impossible in later stages of the disease[65]. Current AD cases in the US, lead to an estimated yearly cost of $355 billion in traditional (institutional) care and treatment, as well as an additional $257 billion in unpaid care delivered by family members and volunteers[65]. Estimates vary, but due to the aging population, the cost of care is expected to balloon in coming years. In 2050, an estimated $1.1 trillion will be spent in traditional care in the US[65] (or $2 trillion worldwide[106]). This will put significant strain on healthcare systems, especially in developed countries like Germany, Japan or the US where the ratio of elderly to young people is rapidly shifting in favor of the elderly[104].

Treatment of AD

Until the early 2000s, little funding was directed towards investigating causes or treatment of AD and other dementias. This rapidly shifted when government and public interest rose due to increasing case numbers. For example, funding of dementia research has increased more than 7-fold in the last 10 years from $448 million to $3.4 billion annually in the US[108,109].

Still, scientific progress in understanding the causes of AD proves difficult to translate into disease-modifying therapies. In the late 1990s and early 2000s, cholinesterase inhibitors (donepezil, galantamine and rivastigmine) and N-methyl D-aspartate (NMDA) receptor antagonists (memantine) became widely available to treat AD, but they are unable to stop disease progression and only provide symptomatic benefit. Cholinesterase inhibitors block the degradation of acetylcholine, leading to higher amounts being available in the brain. This does not stop cholinergic neurons from dying as AD progresses and eventually the medication becomes ineffective as the number of cholinergic cells diminishes[110]. In contrast, memantine prevents NMDA glutamate receptor over-activation to alleviate AD memory symptoms[110]. Once more, this does not prevent neurons from dying and thus does not halt disease progression.

There have been (and still are) a plethora of clinical trials going on for drugs aiming to modify AD progression (reviewed in Vaz et al. 2020)[111]. Most of them target Aß or tau production, aggregation or removal, but except for one, these trials have remained unsuccessful[111]. In 2021, the first potentially disease-modifying drug (aducanumab) was approved in the US for early-stage AD patients (including MCI) by the FDA. Aducanumab is a monoclonal antibody targeting specific forms of Aß to be removed from the brain[112]. As accumulation of amyloid-ß is one of the pathological events thought to initiate or contribute to neuron destruction and memory decline, it is hypothesized that removal of Aß could slow down further cognitive decline, but is likely unable to reverse existing damage[111]. Currently, the approval of the drug remains controversial in the scientific community, due to its clinical trials[113,114] demonstrating low or no efficacy and patients suffering from potentially severe side effects, including amyloid-related imaging abnormalities (ARIA, indicative of brain swelling and/or bleeding) and allergic reactions[115,116]. Furthermore, the per patient costs associated with aducanumab are quite high, because of the price of the drug itself[112] and the cost and risks associated with the necessary diagnostic tests (e.g. positron electron tomography (PET) imaging or cerebrospinal fluid (CSF) collection). As of today, there are no therapies available that can reverse disease progression, making further research into the molecular mechanisms underlying AD of vital importance.

Molecular Pathologies in AD

Amyloid-ß

Generating Amyloid-ß from APP

One of the hallmark pathologies in AD is the accumulation of amyloid-ß (Aß) in extracellular plaques. Aß is generated through cleavage of the amyloid precursor protein (APP), which belongs to the family of amyloid precursor like proteins (APLP). It is the only family member that can produce an amyloidogenic fragment, since it is the only protein containing an Aß region. In humans, eight APP isoforms exist through alternative splicing, and the 695 amino acid isoform is the most common in the CNS[78]. Furthermore, APP is both produced and metabolized rapidly in neurons[117]. APP has large extracellular domains as well as a single-pass transmembrane domain. The function of APP is not entirely known yet, but it has been implicated in neuronal migration during brain development[118], as well as synaptic pruning and neuritic outgrowth[119,120]. Furthermore, when wild type (wt) APP is overexpressed in adult mice, cell growth and survival are enhanced, leading to enlarged neurons[121]. Conversely, when several members of the APLP family are knocked out in mice, brain development is disrupted, and mice die shortly after birth. This phenomenon is not observed when only one APLP family member is knocked out, suggesting that the family members have overlapping functions[120,122].

APP is first processed in the endoplasmic reticulum (ER) and Golgi apparatus, and then transported to synaptic terminals via fast axonal transport (see Figure 4)[123]. Depending on the pathway, further processing then occurs either at the cell surface (non-amyloidogenic pathway) or in endosomal compartments (amyloidogenic pathway)[124]. During non-amyloidogenic processing, α-secretase (a membrane-bound endoprotease) cleaves APP into secreted APPα (sAPPα) and the carboxyterminal fragment 83 (CTF83 or CTFα). Since α-secretase cleaves APP within the Aß sequence, there is no opportunity for Aß fragments to be generated[78]. Afterwards, γ-secretase cleaves CTF83 at the cell surface to generate two more fragments: the APP intracellular domain (AICD) and P3. All these fragments can be degraded by the cell and are not prone to aggregate.

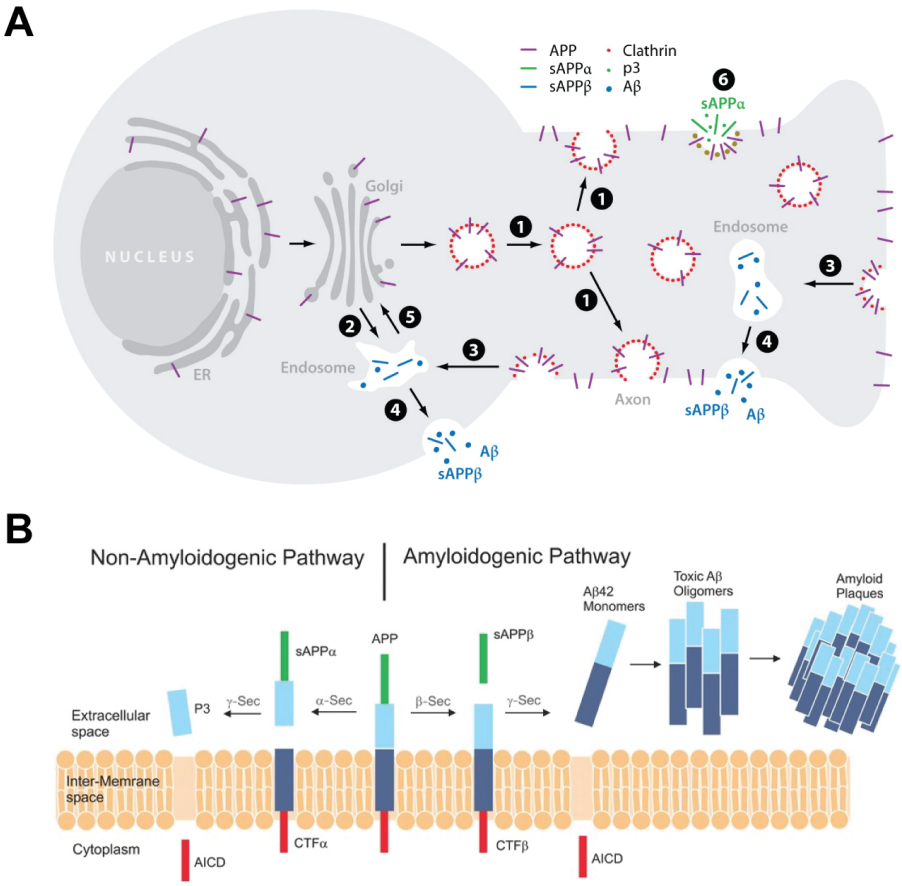

Figure 4: APP trafficking and processing to generate Aß.
A) Schematic of APP and Aß trafficking inside the cell. APP (purple) is transported from the ER and Golgi down the axon (1) or into a cell body endosomal compartment (2). If inserted at the cell membrane, some APP is cleaved through the non-amyloidogenic pathway by α-secretase (6) generating the sAPPα fragment, which diffuses away (green). Some APP that reached the cell surface is re-internalized into endosomes (3), where Aβ can be generated through amyloidogenic processing (blue). Following proteolysis, the endosome recycles to the cell surface (4), releasing Aβ (blue) and sAPPβ. Transport from the endosomes to the Golgi prior to APP cleavage can also occur, mediated by retromers (5). Image reprinted from Annual Review of Neuroscience, Volume 34, Pages 185-204, Richard J. O'Brien and Philip C. Wong, *Amyloid Precursor Protein Processing and Alzheimer's Disease,* doi: 10.1146/annurev-neuro-061010-113613 , ©2011 Annual Reviews, with permission from Annual Reviews[78].
B) Schematic of the non-amyloidogenic and amyloidogenic pathways as described in the text. Image reprinted from Medicinal Research Reviews, Volume 37, Issue 5, Pages 1186-1225, Bachurin et al. 2017, *Drugs in Clinical Trials for Alzheimer's Disease: The Major Trends*, doi: 10.1002/med.21434 , ©2017 Wiley Periodicals Inc., with permission from Wiley[125].

Instead of being processed on the cell surface, APP can also get trafficked directly, or get re-internalized from the cell membrane, via clathrin-coated vesicles to be transported to endosomes[78]. At the endosome, amyloidogenic processing of APP can take place. First, APP is cleaved by Beta-site APP cleaving enzyme 1 (BACE1), a transmembrane aspartic protease, which generates secreted APPß (sAPPß) and the carboxyterminal fragment 99 (CTF99 or CTFß). Second, γ-secretase cleaves CTF99 into Aß and AICD. Afterwards, Aß is secreted into the extracellular space where the brain tries to clear it[78,126]. Aß fragments are between 39-43 amino acids long, with $Aß_{40}$ and $Aß_{42}$ being generated most often. In familiar AD patients, an increased ratio of $Aβ_{42}$ over $Aß_{40}$ has been reported, suggesting that $Aß_{42}$ is more prone to aggregate and is thus more toxic[127,128]. It is important to note, that γ-secretase is a multiprotein complex consisting of presenilin 1 and 2 (PSEN1 and PSEN2), a type I transmembrane glycoprotein nicastrin (Nct), and two multipass transmembrane proteins, Anterior pharynx

defective 1 (Aph-1) and Presenilin enhancer 2 (Pen-2)[129]. Mutations causing autosomal dominant forms of AD are all located in either *APP, PSEN1* or *PSEN2* genes, leading to an increased production of Aß$_{42}$, and subsequently shifting the ratio of Aß$_{40}$ to Aß$_{42}$. Pharmacologically interfering with processing of APP through BACE1 or γ-secretase has so far proven unsuccessful, because other transmembrane proteins, like neuregulin and notch, are also cleaved by these proteins and impairing their processing leads to unwanted side effects[130].

Amyloid-ß: Types of Deposits and Spreading

Aß monomers do not have a defined secondary structure (random structure), but once they aggregate into Aß oligomers (Aßo) their structure becomes more stable and can be investigated through x-ray diffraction[131,132], solid-state[133,134] and solution NMR[135], electron microscopy (EM)[134] and cryo-EM[136]. In recent years, it has been reported, that different Aßo conformations[137], and subsequent fibril species with varying toxicity and propensity to aggregate, exist in patients[17,138,139]. Nevertheless, not all Aßo species aggregate further to form protofibrils, with the ones that continue to form fibrils being denoted as "on-pathway" and the ones that do not continue denoted as "off-pathway". Furthermore, the term oligomer is ill defined and encompasses a multitude of 3-15 nm diameter large aggregates, including Aß globulomers, amylospheroids and Aß-derived diffusible ligands[17,135]. If Aßo remain on-pathway to form protofibrils, they are likely to aggregate further into fibrils and later on plaques. Of note, it has been suggested that Aß$_{42}$ filaments (fibrils) from LOAD (sAD) patients have a different structure than filaments from fAD cases[136]. There are common characteristics though that all amyloid fibrils share, mainly parallel, anti-parallel or mixed ß-sheets and that several protofilaments interact to form a mature amyloid fibril[17].

Fibrils can aggregate further to ultimately form focal plaques, diffuse plaques, or vascular deposits (cerebral amyloid angiopathy, CAA). Three stages have been suggested by Braak and Braak in 1997[140], to describe Aß plaque deposition throughout the course of AD. Plaques appear first in the basal and temporal lobes (stage A), then extend into the association neocortices and hippocampus (stage B) and lastly reach the primary cortex, cerebellum and subcortical nuclei (stage C)[42,140]. Often, Aß deposits are concentrated in certain cell layers (e.g. outer and inner pyramidal cell layer in the hippocampus CA1), while other layers (usually heavily myelinated ones) display less plaques[140]. Diffuse Aß deposits appear first during AD disease progression and start out in the neuropil[140]. Focal Aß deposits arise later, replacing many diffuse plaques and are characterized by a spherical, dense core of tightly packed Aß fibrils and a periphery of more loosely packed Aß filaments[141]. They can be stained with the amyloid-detecting dyes thioflavin S and Congo Red, and are often surrounded by dystrophic neurites and/or tau deposits[141]. Diffuse Aß plaques, as well as the looser filaments surrounding dense-core plaques consist mostly of Aß$_{42}$, while focal plaque cores and vascular Aß deposits consist of both Aß$_{40}$ and Aß$_{42}$[142].

In recent years, several groups have injected Aß that is part of human brain extracts into APP transgenic mice brains to induce Aß deposition and plaque formation[143–149]. A few months after the injection of this material, Aß deposits emerged directly proportional to the amount of injected Aß. Neither WT mice injected with Aß-containing brain extracts nor APP transgenic mice injected with Control brain extracts or AD brain extracts immunodepleted of Aß showed Aß deposition upon injection. This suggests that both a template and "freely available" APP/Aß are necessary for plaque formation[15,149].

Furthermore, vascular Aß deposits are found in more than 80% of AD patients, but also 30-40% of elderly people without AD display CAAs[93]. The original of vascular Aß is likely neuronal and thought to enter the vasculature through impaired perivascular clearance[150]. Two types of CAA are distinguished depending on the localization of CAA deposits: type I deposits are often localized in cortical capillaries, while type II CAA aggregates are deposited in arteries, arterioles, veins and venules[93].

The amount of soluble Aβ oligomers (Aßo) correlates best with the severity of AD symptoms and disease progression[151,152], while plaque load does not[153]. Although controversial, this lead to the hypothesis that soluble, oligomeric Aß, not deposited plaques, are the Aß species causing most neuronal damage and synaptic loss[154,155]. Thus, Aβ plaques might serve a neuroprotective function by sequestering Aβo[156,157], even though they also induce neuroinflammation[158].

Amyloid-ß Oligomer Binding Partners and Suggested Mechanisms of Toxicity

Functionally. the physiological role of Aß has been suggested to include synaptic vesicle release[159], as well as synapse physiology and scaling[160]. In contrast, the mechanisms of Aß to cause toxicity resulting in neuronal loss in AD remain under debate. It has been proposed that Aß can interact with different cell surface receptors[58] leading to caspase signaling resulting in apoptosis[78] or activate signaling cascades leading to (hyper-) phosphorylation, mislocalization and cleavage of tau[161]. Furthermore, Aß is also thought to promote the generation of reactive oxygen species (ROS) and free radicals, resulting in peroxidized lipids, oxidized proteins and DNA damage due to oxidative stress[162]. Increased ROS likely also promote chronic inflammation and prolonged microglial activation observed in AD patient brains that can result in synaptic loss[162] . Other proposed mechanisms of toxicity include mitochondrial dysfunction triggered by Aß accumulation[163–165], as well as modulating NMDA receptor trafficking leading to dysregulated intracellular calcium homeostasis[161].

More specifically, the receptors that have been reported to bind Aßo include low-affinity nerve growth factor receptor ($p75^{NTR}$), receptor for advanced glycation endproducts (RAGE), nicotinic acetylcholine receptor α7 (nAchRα7), sortilin, Nogo-66 receptor 1 (NgR1), ephrin type-B receptor (EphB2), ephrin type-A receptor (EphA4), Fcγ receptor IIb (FcγRIIb), leukocyte immunoglobulin-like receptor subfamily B2 (LilrB2), insulin receptor (IR), EGFR and cellular prion protein receptor PrP^C (reviewed in Smith and Strittmatter, 2017[58], see Figure 5, A). It is of note, that out of these receptors only PrP^C, NgR1 and LilrB2 were shown to bind synaptotoxic Aßo, with PrP^C showing the strongest binding affinity[166]. This would make involvement of these receptors in the pathogenesis of AD more likely.

One of the first receptors where Aß binding triggered cellular apoptosis was the cell-surface transmembrane protein $p75^{NTR}$. It contains an intracellular death domain which can induce apoptosis through nuclear factor kappa-light-chain-enhancer of activated B cells (NF-κ-B) signaling, as well as an extracellular nerve growth factor (NGF) binding domain[58,167]. In 1989 scientists found that cholinergic neurons in the nucleus basalis, a region susceptible to degeneration in AD, express threefold higher levels of $p75^{NTR}$ [168,169]. A decade later, Aß and $p75^{NTR}$ were shown to interact through co-immoprecipitation experiments in cell lines and rat neurons[167,170]. The binding affinity of $p75^{NTR}$ to monomeric Aß was determined to be in the low nanomolar range (13nM) and slightly higher for aggregated Aß (23 nM)[170].

Another receptor that was detected early on to bind Aß was RAGE in 1996[171]. It is a transmembrane receptor expressed in endothelial cells and neurons with extracellular Ig-like C-

and V-type domains that can bind glycosylated proteins[172,173] and (on neurons) can bind neurite growth-promoting protein p30/amphoterin and thus modulate neuronal plasticity[174]. RAGE had been speculated to mediate Aß binding, due to its expression in both endothelial cells and neurons and Aß binding experiments had shown similar binding affinities for both cell types[171]. Du Yan et al. showed that RAGE was responsible for Aß binding to endothelial cells and that Aß binding could be disrupted by blocking the binding site on RAGE[171]. Later on, it was discovered that RAGE also mediates the transport of Aß across the BBB and that Aß accumulation was slowed down in RAGE KO animals or when soluble RAGE (sRAGE) was administered peripherally[175]. While slowed Aß deposition upon RAGE KO was confirmed in a separate study, memory deficits could not be rescued through RAGE KO in mice overexpressing human APP with Swedish and Arctic mutations[176]. Conversely, crossing human APP (hAPP) mice with mice overexpressing RAGE resulted in earlier onset and more severe AD pathology, including increased nuclear translocation of NF-κ-B, gliosis, synapse loss, memory deficits, increased activation of p38, ERK1/2, and cAMP response element-binding protein (CREB)[175]. Clinical trials for drugs targeting RAGE-Aß interaction have been undertaken but discontinued due to interim results showing limited efficacy[58].

nAchRα7 consists of five α7 subunits forming a ligand-gated ion channel with high Ca^{++} permeability that can be activated through acetylcholine binding[177]. The loss of cholinergic neurons was noted early on in AD and led researchers to investigate cholinergic signaling. At the turn of the millennia the ability of nAchRα7 to bind $Aß_{42}$ monomers in the range of femto- to picomolar concentrations was shown[178]. Furthermore, rat hippocampal slices incubated with $Aß_{42}$ showed a nAchRα7-specific response of increased phospho-ERK2 (MAPK signaling) and cells seemed desensitized to nicotine treatment after a two hour pre-treatment with $Aß_{42}$[179]. In the same study, increased nAchRα7 receptor density in Tg2576 transgenic AD-model mice was shown to negatively correlated with memory test performance.

NgR1 had been hypothesized to be involved in AD pathogenesis due to its role in regulating neurite sprouting, a process thought to contribute to the formation of dystrophic neurites surrounding Aß plaques[58]. In 2006, NgR1 was discovered to physically interact with Aß and to bind Aß monomers and oligomers with an affinity of around 60 nM[180]. The same paper showed that intracerebroventricular infusion of a soluble ectodomain of NgR1 (NgR(310)ecto-Fc) into APP/PS1 could decrease dystrophic neurites, concentrations of Aß in the brain as well as Aß plaque burden. A follow up study focused on administering the NgR1 ectodomain peripherally in APP/PS1 mice obtained similar results in lowering total Aß burden, plaque load and number of dystrophic neurites through increased Aß clearance, as well as attenuating animal's learning deficits in radial-arm water maze[181].

Obesity and type II diabetes are known risk factors of AD and insulin resistance and decreased glucose metabolism can be early symptoms in AD. In 2002, neuronal IR was shown to bind both $Aß_{40}$ and $Aß_{42}$ with an affinity of 20 μM and to inhibit autophosphorylation of IR[182]. The relevance of this binding remains controversial though, since the inhibitory constants for Aß were reported as 8 μM (for $Aß_{40}$) and 25 μM (for $Aß_{42}$)[182], and a separate group found Aß binding to IR dependent on NMDA receptor activity [183]. Furthermore, when staining IR expressing cells exposed to Aß with immunocytochemistry not all cells showed Aß binding, suggesting that the binding of Aß to IR might be dependent on the formation of an unknown receptor complex[58,183].

Chronologically, Aßo binding to PrP^C was identified next[184], but further information on this receptor and downstream signaling cascade will be provided in the next section as it is of importance for this thesis. The following four receptors discussed below were discovered more

recently and evidence of their interaction with Aßo is often based on evidence from a few publications or from a single lab. Further validation and evaluation of their relevance for disease processes in AD is needed, but they deserve to be mentioned as potentially important receptors mediating Aßo-induced damage.

The evidence for Aßo binding to EGFR is scant and based on a singular 2012 study[185]. In this study, co-overexpression of $Aß_{42}$ and EGFR lead to synergistic learning and memory impairments that could be rescued when mice were treated with an EGFR inhibitor. Furthermore, in an over-expression model $Aß_{42}$ could be co-immunoprecipitated with EGFR from COS-7 cells.

Ephrin receptors type-A and type-B were discovered to interact with Aß in 2014 and 2011 respectively[186,187]. Aß was shown to directly bind the fibronectin repeats of EphB2 in the presence of NMDA receptors. Furthermore, EphB2 expression was decreased in primary neurons exposed to Aßo and delivering EphB2 through a lentiviral vector to the hippocampus hAPP transgenic mice improved their memory and cognition[58,186]. There are two ephrin type-A receptors implicated in AD: EphA1 has been identified by several GWAS as a risk modifying locus for AD[58], and EphA4 was shown to bind Aß in a cell-free pull-down assay[187]. Furthermore, ligand-bound EphA4 leads to dendritic spine retraction through CDK5 signaling and blocking EphA4 activity in hippocampal slice cultures treated with Aß returned synaptic activity to normal levels[187].

FcγRIIb is a transmembrane receptor primarily found on the surface of B cells preventing autoimmune responses upon binding of antigen-bound IgG complexes, but is also expressed on non-immune cells in the nervous system with unknown function[58]. In 2013, Aßo was shown to interact with the ectodomain of FcγIIb with a dissociation constant of 56 nM (monomer equivalents) and FcγIIb and Aßo could be co-immunoprecipitated from human AD brain lysates, cell lysates and from recombinant proteins[188]. Knocking out FcγIIb rescued dendritic spine loss and cell death in primary hippocampal neurons, as well as ER stress marker upregulation. Furthermore, incubation with Aßo triggered FcγIIb-dependent c-Jun N-terminal kinase (JNK) signaling[188]. In transgenic mouse models of AD, loss of FcγIIb prevented LTP depression and rescued learning and memory deficits. Furthermore, a recent study suggested that PrP^C, LilrB2 and FcγIIb are able to recognize a common, end-specific structural motif on Aß fibrils[189].

LilrB2 and its murine ortholog PirB are also primarily implicated in autoimmune responses. The transmembrane receptor LilrB2 is expressed on antigen presenting cells and recognizes major histocompatibility complex (MHC) class 1 molecules. In addition, PirB had been shown to be expressed in neurons and to bind myelin inhibitor proteins to regulate synaptic plasticity[58]. In the same year as FcγIIb, LilrB2 and Aßo were shown to interact in co-immunoprecipitation and immunocytochemistry expeirments[190]. The dissociation constant of Aßo binding to LilrB2 expressed in HEK293 cells was determined to be 250 nM (monomer equivalents), while Aß monomer binding was minimal[190,191]. Furthermore, through domain deletion experiments and crystallography the Aßo binding site on LilrB2 was determined[192]. Functionally, PirB2 deletion in AD transgenic mice restored LTP in the striatum radiatum in Aßo treated slices and abolished cofilin activation normally observed in AD transgenic mice[190]. Mechanistically, cofilin activation is mediated by protein phosphatase 2A (PP2A) and calcineurin, which are two phosphatases also implicated in Aßo-dependent dendritic spine loss, as well as tau hyperphosphorylation. This makes LilrB2-Aßo interaction an interesting target for further studies.

Sortilin is a member of the vacuolar protein sorting 10 (VPS10) domain receptors and can bind pro-BDNF, pro-NGF and extracellular progranulin, the latter accumulates in FTLD[58]. Also in 2013, sortilin was shown to bind $Aß_{40}$ (unknown if monomeric or oligomerized) with a K_D of

800 nM (monomer equivalents) with and without the presence of ApoE. Mechanistically, the interaction was not further characterized, but seems to play a role in Aß clearance from the extracellular space through neuronal uptake[193].

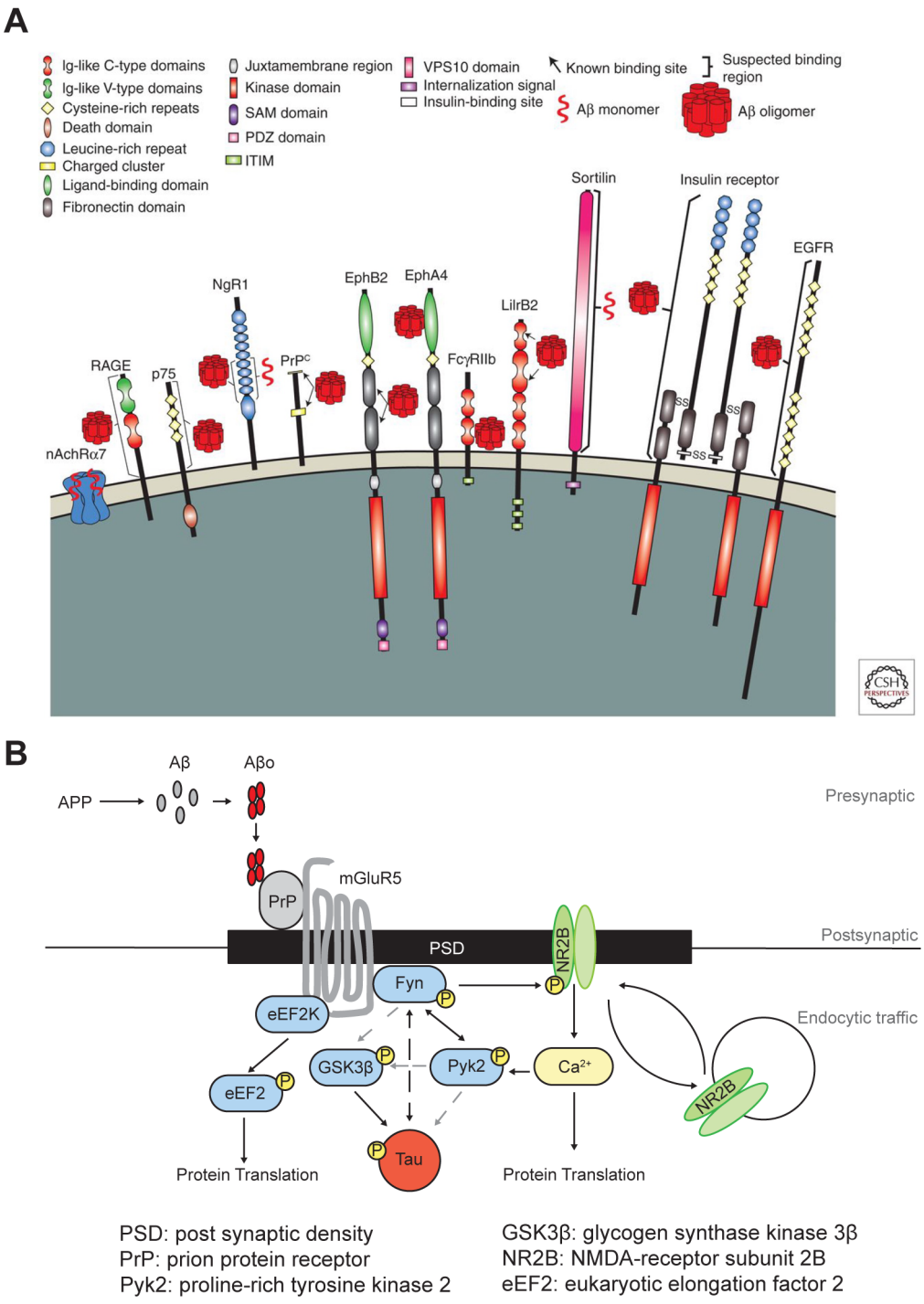

Figure 5: Receptors binding Aßo and signaling cascade downstream of Aßo-PrPC binding.
A) Suggested binding receptors of Aß monomers and oligomers. Known receptor domains (see legend above image for receptor domain symbols) and reported Aß binding sites are indicated with arrows (specific site) or brackets (unclear binding site). See text for further receptor information. Abbreviations in legend: Sterile a motif (SAM), vacuolar protein sorting 10 (VPS10), immunoreceptor (ITIM). Figure reprinted from Cold Spring Harbor Perspectives in Medicine, Volume 7, Issue 5, Article a024075, 2017, Levi M. Smith and Stephen M. Strittmatter, *Binding Sites for Amyloid-β Oligomers and Synaptic Toxicity,* doi: 10.1101/cshperspect.a024075 ©2017 by Cold Spring Harbor Laboratory Press. **B**) Schematic overview of proposed signaling cascade downstream of Aßo

binding to PrPC in mouse primary neurons. Briefly, Aβ oligomerizes and binds to PrpC (located at postsynaptic densities (PSD)) that associates with metabotropic glutamate receptor 5 (mGluR5). Intracellularly, mGluR5 recruits guanine nucleotide-binding protein subunit alpha-11 (Gαq/11), Homer1b/c (both not shown in picture), proline-rich tyrosine kinase 2 (Pyk2), Src kinase Fyn as well as eucaryotic elongation factor 2 kinase (eEF2K). Fyn is able influence NMDA receptor trafficking, and thus dendritic spine stability, through phosphorylation of N-methyl D- aspartate receptor (NMDA-R) subunits (NR2A and NR2B) and is reported to influence tau phosphorylation as well as protein translation. Tau in turn is responsible for recruiting Fyn to dendritic spines. In addition to calcium influx through NMDA-R, the activation of the heterotrimeric G protein Gαq/11 and following signaling cascade causes a rise in intracellular calcium concentration. This rise in intracellular calcium and/or phosphorylation via Fyn activate Pyk2, which in turn is hypothesized to phosphorylate GSK3β. Furthermore, GSK3β is also reported to be directly phosphorylated by Fyn. Dashed grey arrows between kinases Fyn, Pyk2 and GSK3ß indicate putative connections that have not been well validated. See "The Aßo-PrP^C-mGluR5 signaling cascade" for further details. Figure adapted from Nygaard et al. 2014[194].

The Aßo-PrP^C-mGluR5 signaling cascade

One of the most investigated signaling cascades initiated by Aßo lies downstream of the glycosyl phosphatidylinositol (GPI)-anchored cellular prion protein receptor (PrP^C) (see Figure 5B, reviewed in Brody and Strittmatter 2017[195] and Salazar and Strittmatter 2016[196]). This receptor is enriched in post synaptic densities (PSD) and was identified as a target of Aβo binding (K_d of 0.4 nM) in a genome wide expression screen in 2009 testing more than 225,000 cDNA clones[184,196,197]. In this study, two independent clones of mouse PrP^C (mPrP^C) were transfected into Cos-7 cells and shown to have Aßo binding affinities nearly identical to the ones observed in primary hippocampal mouse neurons. Furthermore, PrP^C was found to bind Aßo with >21 selectivity compared to monomeric Aß and the binding region for Aßo on PrP^C was determined to encompass amino acids 95-110[184]. Immunocytochemistry for Aßo bound to PrP^C KO mouse neurons compared to WT neurons revealed that Aßo binding was decreased by 50%, suggesting that PrP^C deletion has a large effect on Aßo binding, but that additional receptors must also be present on the cell surface to mediate binding. Furthermore, other publications confirmed Aßo-PrP^C binding through surface plasmon resonance (SPR) and co-immunoprecipitation[198,199].

At post-synaptic densities, PrP^C associates with the group I metabotropic glutamate receptor 5 (mGluR5) upon Aßo binding, initiating aberrant signaling[200–203]. mGluR5 activates the cytoplasmic Src family tyrosine kinase Fyn[199,204] and activated Fyn can phosphorylate N-methyl D-aspartate receptor (NMDA-R) subunits NR2A and NR2B, modulating their trafficking and thus dendritic spine stability[199]. Fyn is also able to phosphorylate the late onset AD (LOAD) associated risk factor proline-rich tyrosine kinase 2 (*PTK2B*, Pyk2)[205], that has been shown to activate glycogen synthase kinase 3β (GSK3β)[206]. In addition to influencing spine stability, Fyn can influence the hyperphosphorylation of tau[204,207] and in return tau is responsible for recruiting Fyn to dendritic spines[161]. Interestingly, PrP^C has also been shown to bind mGluR5 independently of Aßo with no disruption to mGluR5 regular signaling[201].

Through its interaction with mGluR5, PrP^C also associates with guanine nucleotide-binding protein subunit alpha-11 ($G\alpha_{q/11}$), Pyk2, calcium/calmodulin-dependent protein kinase II (CamKII) and Homer1b/c (CamKII and Homer1b/c not shown in Figure 5)[200]. mGluR5s association with the heterotrimeric G protein $G\alpha_{q/11}$ leads to the activation of phospholipase C (PLC), consecutive signaling through inositol 1,4,5-triphosphate (IP_3), followed by the release of calcium from endoplasmic reticulum (ER) stores and the activation of protein kinase C (PKC)[208]. Rising intracellular calcium concentrations, as well as other kinases can also cause the activation of Pyk2[209]. Knocking out, pharmacologically inhibiting, or interfering with the binding of any central member of this cascade to the next (PrP^C, mGluR5 or Fyn), results in a rescue of

synapse loss and long-term potentiation (LTP) suppression in acute brain slices, as well as in a rescue of behavior and memory deficits in transgenic APP$_{Swe}$/PS1ΔE9 mice[200,210–212]. More information on Fyn and Pyk2 and their potential connection to GSK3ß and tau will be provided in the respective sections of this thesis.

Another downstream component of the Aßo-PrP^C-mGluR5 signaling cascade are eukaryotic elongation factor 2 kinase (eEF2K) and its substrate eEF2[200,201,213,214]. eEF2K associates with mGluR5 and phosphorylates (activated) eEF2 at threonine 56 (T56) upon mGluR5 activation. This ultimately leads to suppression of protein translation and might mediate synaptic deficits[213]. In APP transgenic mice, eEF2 phosphorylation was observed to be increased[200,201,211,213], while deletion of PrP^C was shown to rescue aberrant eEF2 activation[214].

There is a growing body of evidence for the physiological relevance of Aßo-PrP^C interaction. Upon Aßo treatment, there is PrP^C-dependent inhibition of LTP in hippocampal slices and alive mice upon Aßo[184,215–217]. In addition, mice injected with antibodies or inhibitors blocking the Aßo binding site on PrP^C show decreased synapse loss and memory impairment[218–220] and when APP transgenic mice are crossed with PrP$^{C-/-}$ mice, their hippocampal synapse loss and behavioral deficits are rescued[210,214]. Lastly, Aßo-induced synapse loss in cultured cells is reduced upon PrP^C KO[221]. In contrast, some groups have reported none or limited effect of PrP^C on synaptotoxicity[198,222,223]. More specifically, in some mice strains early behavioral deficits occur independent of PrP^C [198,222–224], and certain forms of fibrillar Aß can inhibit LTP independent of PrP^C in hippocampal slice cultures[225]. The biological importance of fibrillar Aß (not) binding to receptors remains under debate, since Aβo are thought to predominantly mediate and correlate well with cognitive decline in patients[154,226].

Amyloid Cascade Hypothesis

One hypothesis that has shaped the field of AD research significantly in the past 30 years is the amyloid cascade hypothesis[227]. Several observations led to the emergence of this hypothesis in the early nineties, which proposed Aß accumulation to be the main causative event in AD[40] . The first observation supporting this hypothesis was that all familial AD cases carry mutations in the *APP* gene or genes encoding APP processing proteins. Furthermore, EOAD follows the same trajectory, with the same pathologies and symptoms, as LOAD, except for an earlier age of onset[52,67–74]. The second line of evidence were CSF biomarker measurements in AD patients, where the concentration of Aß$_{42}$ was reduced long before p-tau concentrations increased, indicating an earlier timepoint for Aß accumulation compared to tau deposition[36]. A third body of evidence are the results of many animal studies conducted with transgenic mice (e.g. overexpressing APP with familial AD mutations or containing presenilin mutations). These transgenic mice develop age-dependent AD-like phenotypes, including senile plaques, synapse loss and impaired memory and cognition[228–231].

In contrast to the above listed evidence, there are also critical voices challenging the amyloid cascade hypothesis and leading to its continued reevaluation. The main point of criticism is that plaque deposition and clinical disease progression seem to be decoupled from one another. More specifically, significant Aß plaque load has been observed in the brains of non-symptomatic individuals[155,232], and the measure that correlates best with patients' cognitive impairment and clinical symptom duration is p-tau, not Aß deposition[233]. Furthermore, clinical trials, that have focused on developing treatments (mainly antibodies) against Aß pathology, have mostly failed to improve patient outcome, even though some of them led to reduced Aß plaque burden[111].

One response to these critical arguments is that these facts do not intrinsically contradict the amyloid cascade hypothesis, but rather complement it. This would be the case, if the hypothesis about the long pre-clinical phase of AD is correct and that Aß accumulation triggers disease-relevant processes long before the Aß accumulation itself becomes noticeable in patients. That way, further downstream effects that are induced by Aß would correlate better with clinical symptom onset than Aß deposition itself (see Figure *2*) and any treatment of Aß plaques at clinical disease stages occurs too late, as the disease-causing effects of Aß accumulation have already been initiated decades earlier.

Nevertheless, the criticisms of the amyloid cascade hypothesis are valid in pointing out that AD research for a long time focused only on Aß and failed to address other aspects of the disease, including tau pathology, neuroinflammation and glial involvement. This is now changing, and more resources are spent on investigating these aspects of the disease and how Aß is connected to them[13]. Central questions that remain to be answered include, if and how Aß and tau deposition impact one another, why the pre-clinical phase of AD is so long and what factors impact it most, how different species of Aß elicit different degrees of toxicity and how important the role of the brain's immune system and vasculature is during the course of the disease (reviewed in Golde 2022[13]).

Kinases of interest: Pyk2, Fyn and GSK3ß

Pyk2

Pyk2 (PTK2B, FAK2), also referred to as related adhesion focal tyrosine kinase (RAFTK), cell adhesion kinase beta (CAKβ) or calcium-dependent protein tyrosine kinase (CADTK), is a non-receptor protein tyrosine kinase that is highly expressed in the mature brain. The only other known member of this family is focal adhesion kinase (FAK), which shares around 45% sequence homology with Pyk2 (up to 60% in the catalytic domain). FAK is higher expressed than Pyk2 in the developing brain, while Pyk2 is stronger expressed in the mature brain[234]. Pyk2 structure was first investigated in rats but quickly determined to be highly conserved between rats and humans[235]. The 115.7 kDa protein Pyk2 consists of 1009 amino acids, with a 418 amino acid N-terminal, a 330 amino acid C-terminal noncatalytic domain containing a focal adhesion targeting (FAT) domain, as well as a catalytic kinase domain spanning from amino acids 418-680[209,234–236]. Both FAK and Pyk2 have a conserved sequence (ESNIYAEI) allowing other proteins to bind to them through their SH2-domain. Conversely, Pyk2 and FAK themselves lack transmembrane domains, as well as SH2 and SH3 domains[235].

In addition, there are two more splice variants of Pyk2 called Pyk2 splice form (Pyk2s) and Pyk2-related non-kinase (PRNK). Pyk2s lacks 42 amino acid of full-length Pyk2 in the C-terminal domain and PRNK consists of only the C-terminal domain of Pyk2[236]. These splice variants are expressed at a lower level than full-length Pyk2 in the brain but might contribute to the functional diversity of Pyk2 interactions. In the brain, full-length Pyk2 is expressed strongest in the hippocampus, olfactory bulb, and cerebral cortex. PRNK and Pyk2s are only able to bind substrates that bind in a SH3-dependent manner, e.g. paxillin, but not Graf or p130FAK. Pyk2 as well as its splice variants are all able to localize at focal adhesions, since the FAT domain is located at the C-terminus and present in all three variants[236].

Pyk2 can be activated through increases in intracellular calcium concentration leading to autophosphorylation[237] or through interactions with other kinases (e.g. Fyn or protein kinase C (PKC))[238–240], leading to phosphorylation at tyrosine 402 (Y402). Conversely, Pyk2 is also able to synergistically co-activate Fyn[211,238,240]. Functionally, Pyk2 has been implicated in multiple cellular processes (reviewed by de Pins 2021[241] and Kumar 2022[242]), including modulating

synaptic stability[243], modulating mitochondrial calcium homeostasis[244], participating in several cell signaling cascades (e.g. mitogen activated protein kinase (Ras/MAPK), Wnt/β-catenin)[209], T- and B-cell signaling[238,245,246], apoptotic cell death[247], as well as cell migration and survival[248], cancer biology and most recently in AD[205,211,243,249].

In 2013, Pyk2 was identified as a late-onset AD risk allele in a GWAS study[205]. There is evidence, that Pyk2 is a downstream member of the PrP^C-mGluR5-Fyn signaling cascade, because inhibiting Fyn kinase activity pharmacologically causes a reduction in the levels of phosphorylated Pyk2 (p-Pyk2)[211], and Pyk2 interaction with Fyn had previously been reported in T-cell antigen receptor signaling[238]. Additionally, when comparing the p-Pyk2 levels in wild type and APP_{Swe}/PS1ΔE9 (APP/PS1) mouse brains, p-Pyk2 levels are significantly increased in transgenic AD mice[211]. In return, deleting Pyk2 in AD transgenic mice reduced spatial memory deficits in these mice[249]. In acute brain slices from WT or $Pyk2^{-/-}$ mice, LTP deficits induced by Aßo were rescued through Pyk2 deletion[249]. Furthermore, when WT brain slices were treated with both Aβo and the Pyk2-selective, ATP-competitive small molecule inhibitor PF-719 (N-cyclopropyl-4-(4-((1R,2R)-2-(dimethylamino)cyclopentylamino)-5-(trifluoromethyl)-pyrimidin-2-ylamino)benzamide dihydrochloride)[250], LTP impairments were also ameliorated[249]. In addition, synapse loss in APP/PS1 mice was shown to be dependent on the presence of Pyk2[249]. Furthermore, Pyk2 interaction with the RhoGAP protein GTPase regulator associated with focal adhesion kinase-1 (Graf1) is necessary to convey Aßo-induced synapse loss in primary mouse neurons by modulating dendritic spine loss and F-actin dependent spine motility via RhoA GTPase[243].

In contrast, Pyk2 has been reported to play a different role in studies with 5XFAD mice (carrying the mutations APPSwe, I716V (Florida), V717I (London) and PSEN1 M146L, L286V[251]). When 5XFAD mice were crossed with *Ptk2b-/-* mice, plaque burden decreased but behavioral deficits and other histological phenotypes remained unchanged[252]. Conversely, Pyk2 phosphorylation levels were lower in 5XFAD mice to begin with and overexpression of Pyk2 rescued this decrease, improved synapse density and mouse performance in behavioral tasks[252]. This line of inquiry is further supported by evidence that Pyk2 overexpression protected hippocampal neurons from $Aß_{1\text{-}42}$ toxicity in microfluidic cultures[253]. In addition, decreases in Pyk2 phosphorylation could be due to its role as a substrate for striatal-enriched protein tyrosine phosphatase (STEP), which is over-activated in AD and leads to dephosphorylation and decreased surface expression of NMDAR[254–257].

The reasons for these differential outcomes in various mouse models remain elusive, but one potential explanation might lie in the dysregulation of tyrosine phosphorylation having divergent effects in different model systems[241].

Another way Pyk2 might impact AD pathology is its function in microglia[241]. *PTK2B* variants associated with increased AD risk have been shown to lead to higher Pyk2 expression in monocytes and macrophages[258,259]. Treating microglia *in vitro* with Aß leads to downstream activation of PKC and Pyk2, resulting in the secretion of neurotoxic factors (e.g. TYROBP)[258,260]. Furthermore, Pyk2/ERK signaling can be activated by Transient receptor potential melastatin 2 (TRPM2), a ROS-sensitive calcium channel, expressed in various brain tissues and lead to microglial activation and tumor necrosis factor α (TNFα) production[261,262]. The relevance of Pyk2 function in microglia and macrophages for AD has not been thoroughly investigated yet but might be relevant to elucidate a potential role of Pyk2 in inflammation.

Pyk2 has also been connected to tau pathology in AD with studies reporting a *Drosophila Melanogaster* homolog of Pyk2 to modulate tau-dependent neurodegeneration[263]. Furthermore, Pyk2 has been suggested to bind tau directly[207,264] and in histological examinations of

AD patients and pR5 mouse brains Pyk2 co-localized with hyperphosphorylated tau[263,265]. Its capability to phosphorylate Fyn and potentially GSK3ß[206] in the context of AD have suggested Pyk2 as a potential link for connecting Aß and tau pathologies.

Fyn

FYN is located on chromosome 6q21 and encodes three splice variants of the Src family non-receptor tyrosine kinase (SFK) protein Fyn[266–268]. Fyn is 59 kDa large and the three isoforms are denoted as Fyn-B, Fyn-T and Fyn-D7[266,269]. Fyn-B is highly expressed in the brain, but also found throughout the body, while Fyn-T is mainly expressed in cells of hematopoietic origin and Fyn-D7 is found in peripheral blood mononuclear cells[266,269]. The other eight members of the SFK family are Src, Lck, Lyn, Yes, Fgr, Hck, Blk and Yrk, with Fyn and the first four proteins in the list being highly expressed in the CNS[266,267,270]. SFK family members share a common domain structure, with a Src homology 4 (SH4) domain, followed by an SH3 and SH2 domain, a kinase domain (SH1) containing the activation site (Y420 on human Fyn), and lastly a short C-terminal tail with an autoinhibition phosphorylation site (Y531 on human Fyn)[267,268,271]. Phosphorylation on Y531 promotes protein-internal interactions between the SH2 and SH3 domains, preventing kinase activity of Fyn. In contrast, phosphorylation of Y420 induces conformational changes exposing the catalytic site, increasing Fyn activity. Physiologically, Fyn is involved in a variety of cellular processes, including T-cell function and humoral immune response[272–275], cellular proliferation and metastasis[276,277], platelet function[278,279], bone physiology[280] and central nervous system myelination[281].

For a review of Fyn's role in AD, see reviews by Nygaard 2018[282] and Guglietti et al. 2021[271]. Before Fyn's importance in AD became apparent, Fyn was shown to be necessary for regulating LTP through NMDA receptor subunit (NR2A and NR2B) trafficking and to associate with postsynaptic density protein 95 (PSD-95)[283–286]. *In vitro*, Fyn's role in Aßo-mediated neurotoxicity was first noted in 1998[287] and *in vivo*, AD transgenic mice overexpressing Fyn showed accelerated synapse loss and memory impairments that were rescued by Fyn deletion[288,289]. In addition, histopathological staining of AD patient brains demonstrated an overlap of increased Fyn and hyperphosphorylated tau deposition[290]. This led to the hypothesis that in addition to regulating LTP through spine stability, Fyn might also contribute to tau hyperphosphorylation[207,291,292]. In turn, tau is responsible for recruiting Fyn to dendritic spines[161,204,293]. Thus, for a long time Fyn was known to be important for AD pathogenesis, but the signaling cascade components connecting Aßo with Fyn remained unknown.

As described in the chapter "The Aßo-PrPC-mGluR5 signaling cascade", Fyn was connected to Aßo-dependent signaling in 2012 through its interaction with mGluR5, which in turn associates with PrP^C upon sAßo binding[199–202,204]. Upon mGluR5 activation, Fyn is phosphorylated at Y420 and synergistically co-activates Pyk2[199]. In turn, removing PrP^C or mGluR5 from the signaling cascade will abolish the Aßo-dependent increases in Fyn phosphorylation[200,201]. Interestingly, chronic Aßo exposure *in vivo (*e.g. in J9 transgenic mice) and *in vitro* does not seem to lead to chronically elevated p-Fyn levels, while other kinases (e.g. Pyk2 and eEF2) remain activated for longer time spans upon Aßo exposure[200,211]. The de-activation of Fyn is thought to occur through STEP, since STEP activity is inversely correlated with Fyn phosphorylation in cultured mouse cortical neurons, but the mechanisms underlying the differential treatment of Pyk2 and Fyn by STEP remain unclear[199,294].

When Fyn activation is pharmacologically inhibited (e.g. through the small molecule inhibitor saracatinib (AZD0530))[211,295,296], Pyk2 activation and synapse loss through Aßo-dependent

signaling are diminished in AD transgenic mice and *in vitro*[199,289,297]. This makes Fyn an interesting target for pharmacological interventions for AD and there are several drugs currently undergoing clinical trials for their efficacy in AD either targeting Fyn directly (saracatinib) or more generally inhibiting tyrosine kinases (e.g. masitinib, bosutinib, ponatinib and dasatinib)[211,282]

Many of these tyrosine kinase inhibitors are already being used or tested as cancer treatment drugs, since tyrosine kinases are often implicated in cancer metabolism[282]. The high conservation of SFK family kinases and their expression in many different tissues leads to challenges in designing Fyn-specific inhibitors that do not show excessive off-target effects. Most currently available Fyn inhibitors bind to its catalytic site as competitive ATP inhibitors and thus, also act on other SFK family kinases[282].

Masitinib inhibits c-kit, lyn and Fyn, as well as PDGF and FGF receptors[298] and chronic treatment with masitinib in APP/PS1 mice was reported to restore spatial learning and synaptic density in the hippocampus in a preclinical study[299]. A Phase III clinical trial is ongoing (NCT01872598) and reported meeting its primary goal with their 4.5 mg/kg treatment cohort in 2020[300]. Another two cancer drugs are bosutinib and ponatinib which both bind Fyn with low nanomolar IC50 (0.36 nM-1.8 nM) but are fairly unspecific and thus likely unsuitable as Fyn-specific drugs[301–303]. In contrast, dasatinib is more specific, inhibiting only a subset of SFK kinases, Fyn, Lck and Src, with low nanomolar IC50 (0.2-0.5 nM)[295,304]. In pre-clinical studies dasatinib was shown to improve memory function in transgenic AD mice and to modulate microglial activation[305]. Unfortunately, a clinical study suggested dasatinib to have immunosuppressive effects[306]. Currently, there are ongoing Clinical Phase I and II studies for dasatinib combined with quercetin in the context of AD (NCT04685590, NCT04063124 and NCT04785300).

Saracatinib (AZD0530) is an orally bioavailable inhibitor originally developed for cancer treatment and inhibits Fyn (IC50 of 8-10 nM), Src (IC50 2.7 nM), Yes (IC50 4nM), Lyn (IC50 5nM) and Abl (IC50 30-156 nM)[282]. It has been investigated in pre-clinical as well as in two Clinical Phase I and II studies for its efficacy and potential off-target effects for cancer and AD treatment (NCT01864655,). In pre-clinical studies, 50% chronic inhibition of Fyn in mice brains was achieved through an oral dosing paradigm of 5 mg/kg/day (10 nM) and resulted in rescue of spatial memory impairments and synaptic loss in APP/PS1 and 3XTg-AD mice after 4-6 weeks of treatment that was sustained even after a washout period of 1-4 weeks[211,307,308]. The Kaufman et al. study also reported reduced microgliosis after the AZD0530 treatment[211]. Conversely, one known side-effect of saracatinib is reduced osteoclast activity in rodents and humans, but bone density changes were not measured[279,280,309]. In human Clinical Phase I trial (NCT01864655), 100-125 mg/day oral saracatinib were reported as sufficient to yield brain saracatinib concentrations >10 nM and showed only mild to moderate side effects over the course of a one month treatment paradigm[282,309]. Unfortunately, a Clinical Phase IIa study (NCT02167256) showed no effects in its primary or secondary outcome measures of reduction in relative CMRgl, measured by 18F-fluorodeoxyglucose (18F-FDG) PET in regions of interest and changes in cognition, function, and other biomarkers[310]. This calls into question Saracatinib's usefulness as a drug for already symptomatic patients, but it remains to be investigated if it could be used in pre-clinical stages of AD.

GSK3ß

Glycogen synthase kinases (GSKs) are a family of serine-threonine protein kinases with three members, GSK1, GSK2 and GSK3[311–313]. There are two paralogs of GSK3, the larger GSK3α with a molecular weight of 51 kDa and the smaller GSK3ß with 47 kDa[314]. The two paralogs share around 98% amino acid identity, but in addition to several shared targets they also still have independent binding partners and functions[315]. For example, GSK3α knockout mice are viable but have shortened lifespans and brain structure abnormalities[316], while GSK3ß knockout mice die *in utero*[317]. Structurally, GSK3ß consists of a polar, disordered N-terminus, followed by its protein kinase domain and a disordered C-terminus. Its activity can be regulated by phosphorylation at certain serine (S), threonine (T) and tyrosine (Y) residues. The two main regulatory points are phosphorylation at S9 (through Wnt/β-catenin signaling, PI3K-Akt, protein kinase A (PKA) and protein kinase C (PKC)) which will result in diminished GSK3β activity, while phosphorylation at tyrosine 216 (Y216) (including by Pyk2[206], Fyn kinase[318] or by autophosphorylation[319]) leads to increased activation. However, the exact mechanism of GSK3β phosphorylation at Y216 still remains to be investigated. It is important to mention that GSK3ß is one of few constitutively active kinases and Y216 phosphorylation is most often used to restore previously inhibited protein activity[320]. The regulation through S9 is better understood with phosphorylation at S9 leading to GSK3ß N-terminal domain to act as a pseudo-substrate, competing with pre-phosphorylated substrates and thus inhibiting its activity[321]. Many substrates of GSK3ß need to be pre-phosphorylated by another kinase before GSK3ß can act on them (most common sequence pattern is S/T-X-X-X-S/T(P) with GSK3ß acting on the latter S/T)[321–325]. This is facilitated by a primed substrate binding domain adjacent to the kinase domain on GSK3ß. In addition, GSK3ß is also able to phosphorylate non-primed substrates (e.g. tau), but it's activity is further enhanced when these substrates are primed.

GSK3ß is one of the best studied kinases phosphorylating tau at multiple residues[326], but it is also implicated in numerous other cellular processes, including glycogen metabolism[311–313], microtubule stabilization, neurite outgrowth and retraction[327], hippocampal neurogenesis[328,329], cancer formation[330], synaptic plasticity and memory[331,332], and neuroinflammation[333]. GSK3ß is often considered a hub for signal integration, due to the multitude of signaling cascades modulating its activity and its more than 100 likely substrates[334,335]. Conversely, how GSK3ß achieves substrate specificity is an important question and current research suggest it depends on post-translational modification status of GSK3ß, its subcellular localization, substrate priming, as well as association to multi-protein complexes[320]. See Beurel et al. 2015[320] for a detailed review on GSK3ß regulation.

In AD, elevated levels of oligomeric Aβ seem to cause heightened activation of GSK3β and tau hyperphosphorylation *in vivo* and *in vitro*[336,337]. In return, reduced GSK3ß activity through inhibition with lithium leads to decreased Aß production[338–340], likely through its interaction with PS1 and BACE1 during the APP cleavage process[341,342]. In support of this hypothesis, PS1 phosphorylation by GSK3ß increases PS1 activity leading to heightened Aß production[343]. Furthermore, BACE1 activity and expression is dependent on GSK3ß activity *in vitro*[344,345]. Other mechanisms impacting Aß and tau pathologies are clearance mechanisms including autophagy[346]. Autophagy can be inhibited through mTOR-GSK3ß signaling, and insulin degrading enzyme (IDE), an important protein for Aß degradation[347], is negatively correlated with GSK3ß levels suggesting more ways how GSK3ß can contribute to AD pathologies[348,349]. For a detailed review of GSK3ß in AD see Lauretti et al. 2020[350].

With regards to its interaction with tau, GSK3ß has long been known to phosphorylate tau at several residues (potential phosphorylation sites include T181, S199, S202, T205, T212,

S214, T217, T231, S396, S404, S409, S413, S422, S198/S199/S202, S396/S404) *in vivo* and *in vitro*[351–353]. In addition, activated GSK3β co-localizes with NTFs in the brain of AD patients[354] and GSK3ß expression levels in the CNS are known to increase with age[355]. Activation of GSK3ß by Aß exposure was shown to increase tau phosphorylation. This suggests that GSK3β could be a key link between Aβ and tau pathologies, but the exact molecular mechanisms underlying this connection remain under debate[356–358]. One suggested connecting pathway is Wnt signaling, which in its normal state inhibits GSK3ß but is disrupted by Aß[359].

Mechanistically, there is evidence, that Pyk2 and GSK3β can interact with one another, either indirectly through a protein complex or through directly interaction at several domains, since kinase-dead Pyk2 still co-immunoprecipitates with GSK3β[206,327]. Moreover, previous studies in AD mouse models have reported elevated levels of GSK3β and Pyk2 *in vivo*, as well as GSK3β-mediated phosphorylation of tau in AD mice[265,356,358].

Inhibiting GSK3ß as a therapeutic approach to AD remains difficult due to lack efficacy or low tolerability of the inhibitors[360]. Lithium, one of the best studied GSK inhibitors, is not well tolerated in the elderly[361], has a small therapeutic window and off-target effects on other kinases leading frequently to unwanted side effects or difficulties identifying which cellular process is responsible for observed changes[362]. Other specific GSK3ß inhibitors (e.g. AZD1080 and AZD2858) showed promise in animal models but did not pass toxicological or Phase II Clinical trials[360]. For an overview of other GSK3ß inhibitors being tested in the context of AD see D'mello 2021[360] and Lauretti et al. 2020[350].

Tau

Structure and Function

The second molecular hallmark of AD is the intracellular deposition of hyperphosphorylated protein tau. In recent years, research into tau pathology has increased due to its promise as a CSF biomarker for AD and the fact that tau deposition correlates better with neuronal loss and memory deficits in patients with AD than Aβ plaque load[363,364].

There are six tau isoforms present in the adult human brain that are generated through alternative splicing of exons 2, 3 and 10 of the *MAPT* gene that is located on chromosome 17 (see Figure 6 A). The six isoforms are between 45 - 65 kDa large and differ in the number of N-terminal inserts (0N, 1N or 2N) and microtubule- (MT-) binding domains (3R or 4R)[365,366]. Many of the 85 potential phosphorylation sites on tau are located in or close to the MT-binding domain[367], making 4R tau more prone to aggregate, but to also bind microtubules better in its native form[368]. Structurally, the MT-binding domains of monomeric tau form ß-sheets, while the N- and C-termini of the protein are disordered[369]. In healthy brains, the ratio of 3R:4R tau isoforms is 1:1, but in some tauopathies (e.g. FTD or progressive supranuclear palsy (PSP)) the ratio is altered, favoring the 4R isoforms[370].

Functionally, tau is mainly implicated in regulating axonal transport by promoting microtubule assembly and stability[371,372] and interacting with proteins at PSDs (e.g. recruiting Fyn), giving it a potential role in cell signaling events[161,207]. In addition, tau has also been suggested to regulate transcription in the nucleus both directly and indirectly[373]. Studies have identified dephosphorylated tau in the nucleus of neuroblastoma cells, where it localized with chromosome scaffolds and nuclear organization centers. Furthermore, the MT-binding domain of tau seems capable of binding DNA as well as RNA[370,374]. Moreover, tau was also reported to regulate the transcription of *PRNP* via JNK/c-jun-AP-1 signaling, resulting in increased levels of PrP^C upon increases in tau levels[373]. It is also of note, that tau knockout is not lethal in mice

models[375], but depending on the genetic background of the mice, it can lead to delayed neuronal maturation[376].

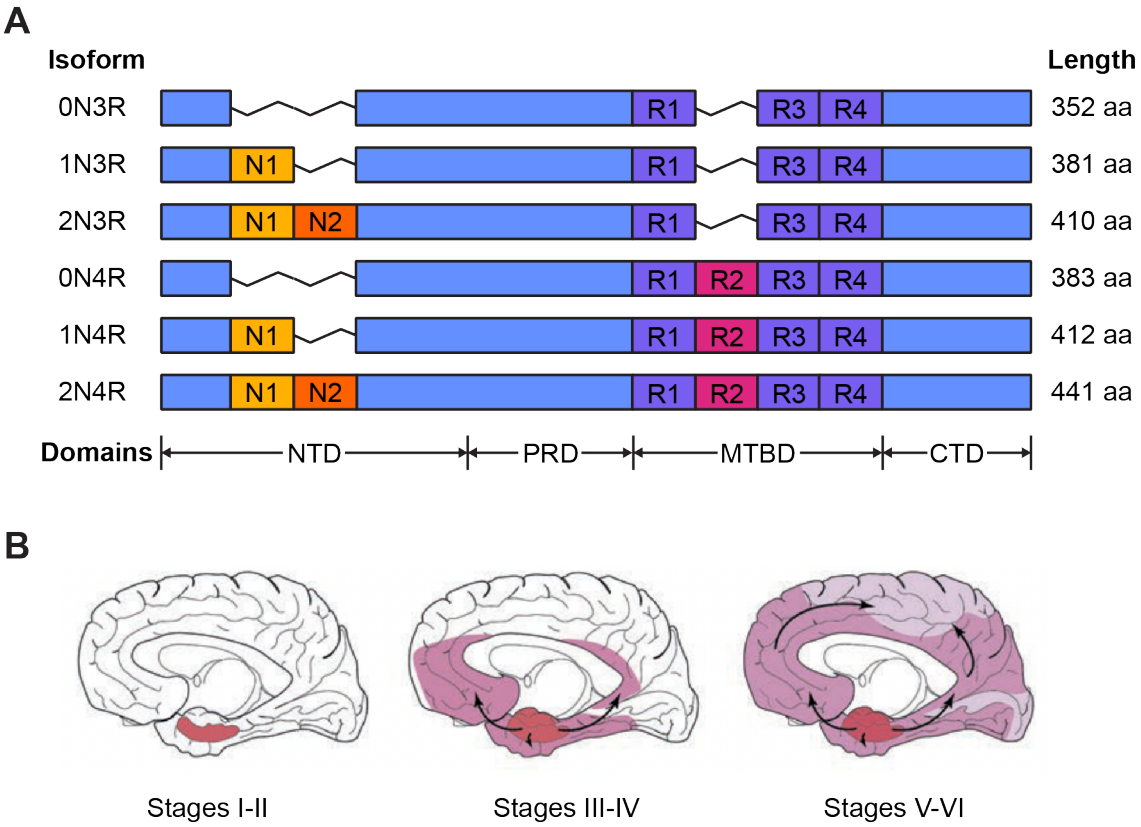

Figure 6: Tau isoforms and spreading in AD.
A) Isoforms of tau present in the human brain. Tau can contain 0N, 1N or 2N terminal domains (spliced from exons 2 and 3) and either 3R or 4R microtubule-binding domains (spliced from exon 10). NTD: N-terminal domain, PRD: proline-rich domain, MTBD: microtubule-binding domain, CTD: C-terminal domain. **B)** Tau spreading in AD displayed according to Braak stages. Tau pathology starts in the trans-entorhinal cortex, spreading via the entorhinal cortex and hippocampus (stage I and II) into the EC-adjacent neocortical regions (stages III-IV). In stage V-VI, tau inclusions spread further into all areas of the neocortex. For more detailed description of tau spreading see the section "Tau Seeding and Spreading in AD". Figure B reprinted from Advances in Experimental Medicine and Biology, Volume 1184, Pages 305-325, 2019, Simon Dujardin and Bradley T. Hyman, *Tau Prion-Like Propagation: State of the Art and Current Challenges,* doi: 10.1007/978-981-32-9358-8_23 , ©2019 by Springer Nature, reprinted with permission from Springer Nature.

Tau Hyperphosphorylation and Accumulation in Disease

Hyperphosphorylated tau forms deposits in a variety of neurodegenerative diseases, including the 'primary' tauopathies frontotemporal lobar dementia (FTLD), progressive supranuclear palsy (PSP), corticobasal degeneration (CBD), chronic traumatic encephalopathy (CTE), primary age-related tauopathy (PART) and Pick's disease. These diseases are classified as primary tauopathies because tau accumulation is considered the causative event in these diseases. On the other hand, AD is classified as a secondary tauopathy, since Aß likely is the disease initiating protein in AD. Furthermore, there are no known tau mutations that are disease causative for AD, while other tauopathies like FTLD can occur due to mutations in the *MAPT* gene (reviewed in Kovacs 2015[377] and Leveille et al. 2021[378]). It is important to note, that the various tauopathies exhibit different tau phosphorylation patterns, types of inclusions, and inclusion cell type specificity (neurons, astrocytes, or oligodendrocytes), allowing them to be distinguished histochemically[377]. In AD, both 3R and 4R tau get hyperphosphorylated and after

forming oligomers, aggregate further and are deposited intracellularly in neurons as neurofibrillary tangles (NFTs), neuritic plaques (NPs), and neuropil threads (NTs)[377,379–382].

Tau conformation and function can be regulated by post-translational modifications such as phosphorylation, N- and O- glycosylation, acetylation, SUMOylation, ubiquitination, oxidation[242], as well as through cleavage by caspase-3, and -6, and calpain-1[370,383,384]. Especially O-GlcNAcylation (modification of S/T residues by O-linked N-acetylglucosamine)[385,386], truncation[387], and phosphorylation have emerged as relevant mechanisms for tau aggregation. O-GlcNAcylation of tau is known to occur at six sites and can have two, sometimes overlapping, purposes: (de-)priming tau for phosphorylation by kinases and partaking in reciprocal regulation of tau phosphorylation[385,386,388]. In AD patients, it has been observed that O-GlcNAcylation is decreased, and this decrease inversely correlates with an increase of tau hyperphosphorylation[386]. Furthermore, O-GlcNAcylation might connect AD and diabetes since O-GlcNAcylation is a sensor of intracellular glucose metabolism. O-GlcNAcylation is also decreased in diabetes patients and thus might elevate the risk of tau hyperphosphorylation[367,389]. Tau truncation by caspases generates tau fragments, containing the MT-binding repeats that are then more prone to aggregate and form PHFs[387]. These fragments and their aggregates have been observed in AD brain extracts as well as in transgenic rats overexpressing truncated human tau[383].

Nevertheless, most research into tau aggregation has focused on (de-)phosphorylation mechanisms of tau, with the hypothesis that an imbalance of kinase and phosphatase activity on tau leads to its hyperphosphorylation. There is evidence that tau hyperphosphorylation precedes tau aggregation, which would support the notion of phosphorylation being involved in tau conformational changes and ultimately aggregation[354]. 85 putative phosphorylation sites, mostly flanking the MT-binding domain, have been identified on tau, with around 45 of them being implicated in AD[370]. Soluble, healthy tau is only phosphorylated at few residues, while aggregated, fibrillar tau in the brain of AD patients shows phosphorylation at four times the number of residues (for review see Noble et al. 2013[370] and Iqbal et al. 2016[367]). Importantly, phosphorylation of tau (e.g. at S214 and T231) decreases its binding affinity for tubulin and thus inhibits its normal function[390,391]. In return, tau that is not associated with microtubules is a better substrate for kinases, than tau that is bound to microtubules[392]. Furthermore, phosphorylation of tau at certain N-terminal residues seems to decrease its plasma membrane association, potentially disrupting signaling cascades (e.g. mislocalizing Fyn)[370,393–395]. Treating tau transgenic mice with kinase inhibitors results in reduced numbers of tau aggregates[396,397], while overexpressing tau kinases[398–400] or inhibiting tau phosphatase PP2A leads to increased tau phosphorylation[401].

In general, there are three different types of kinases that can phosphorylate tau: proline-directed serine/threonine kinases, non-proline directed serine/threonine kinases and tyrosine kinases. Proline-directed serine/threonine kinases require a proline residue to follow the serine/threonine that the kinase will act on, while the non-proline directed kinases do not. The first group includes GSK3ß[326,397,402], CDK5[398,399,403] and AMPK[404,405], while the second group contains kinases like casein kinase 1 (CK1)[406], PKA[407,408], dual-specificity tyrosine-phosphorylation regulated kinase 1A (DYRK-1A)[409,410] and microtubule affinity-regulating kinases (MARKs)[411,412]. The last group entails Fyn[204,207], Abl[413], Syk[414], and potentially Pyk2[263–265]. Some kinases (e.g. GSK3ß) require or prefer tau to be already phosphorylated (primed) at some residues before acting on it. Furthermore, all kinases listed above have been purified together with NFT from AD patient brains and it is thought that different combinations of these kinases

act in concert to lead to tau hyperphosphorylation and deposition in AD[367]. For a review of tau phosphorylation see Noble et al. 2013[370].

Other important players in regulating tau phosphorylation are phosphatases (protein phosphatases-1, -2A and -5), with PP2A being the most important one[370]. In the 1990s, PP2A was shown to be downregulated in the brains of AD patients[415] and to act on hyperphosphorylated tau in AD[416]. Furthermore, PP2A does not only act on tau, but also regulates the activities of multiple tau kinases (e.g. GSK3ß, CaMKII, PKA and CDK5)[367,417]. PP2A activity can be downregulated through phosphorylation at Y307 by Src kinase and through the I_1^{PP2A} and I_2^{PP2A} proteins, whose expression is upregulated in AD patient brains[367]. Furthermore, cleavage products of I_2^{PP2A} , that get generated if acidosis conditions are present in the brain due to ischemic stroke, CTE or hyperglycemia, can also inhibit PP2A activity, providing a potential connection of these conditions to tau hyperphosphorylation[367]. In support of this hypothesis, the activated state of the enzyme necessary for cleaving I_2^{PP2A} is increased in AD patients, and the I_2^{PP2A} cleavage products co-localize with hyperphosphorylated tau[418,419]. Another interesting facet of PP2A regulation is that PP2A can associate with mGluR5 but dissociates from it upon mGluR5 activation. Once dissociated, it is more prone to be phosphorylated at Y307 and thus to become inactivated, leading to increased tau phosphorylation levels[420].

There is ongoing debate if soluble tau or the insoluble neurofibrillary tangles (NTFs) are the key mediator of tau-induced neurodegeneration, but increasing evidence shows that soluble, hyperphosphorylated tau might correlate best with synapse loss and behavioral deficits in mice[356,421]. Furthermore, hyperphosphorylated tau oligomers have been identified in AD patient synapses post-mortem, suggesting that they mislocalize there[422]. One apparent consequence of tau hyperphosphorylation is that tau ceases its normal function as a microtubule assembly and stability protein, but in addition, hyperphosphorylated tau has also been shown to have synaptotoxic effects[370,423]. The exact mechanisms by which tau aggregates cause synaptic toxicity are still under investigation, but one theory is that the lack of normal tau function and the accumulation of oligomeric, hyperphosphorylated tau in dendrites and synapses leads to impaired trafficking and/or anchoring of NMDA and AMPA receptors[423–426]. This would disrupt synaptic function and as well as the cells calcium homeostasis.

Tau Seeding and Spreading in AD

In AD, tau oligomerizes before it aggregates further and gets deposited as NFT, NP and NTs. The structure of tau oligomers has so far remained elusive, but in addition to post-translational modifications favoring tau conformational changes, disulfide-bonds and/or electrostatic interactions have been theorized to play a role in the formation of tau oligomers[427]. It is also known that tau can undergo liquid-liquid-phase separation, but whether this process contributes to tau aggregation or not remains controversial[428]. Furthermore, it has been shown that tau forms distinct oligomers in different tauopathies, that can then act as templates (‘seeds’) corrupting healthy tau to misfold and to cause distinct spreading patterns[429–436]. The differences of these seeds/strains are likely due to differences in the folding and isoform composition of their oligomers/NFTs[437]. This mode of transmission has been dubbed ‘prion-like’ and tau seeds have also been called ‘prionoids’, even though this terminology remains controversial[433].

In contrast to oligomers, the structure of NFTs has been determined through NMR, EM and cryo-EM studies for several different tauopathies[437]. The dense core of NFTs is comprised of the MT-binding domains (repeat regions of 3R and 4R tau for AD[438]), which are aligned in ß-sheets. In contrast, the remainder of the protein remains unstructured and forms a fuzzy

coat around the dense core[427,428,439–441]. In AD, 3R and 4R domains fold to form a 'C'-shaped filament, that then aligns back-to-back with another C-shaped filament to form a tau fibril[437].

On a macroscopic level, the spreading pattern of tau deposits in AD post-mortem brains was first characterized extensively and classified into stages by Braak and Braak in the 1990s and early 2000s[42,43,442]. In AD, tau inclusions are predominantly neuronal and inclusions first appear in the trans-entorhinal cortex (stage I) from which they progress along anatomical connections throughout the brain (see Figure 6 B) [43,442,443]. They spread via the entorhinal cortex to the hippocampus (stage II). Next, EC-adjacent neocortical regions like, the occipito-temporal gyrus and the lingual gyrus are affected (stage III). In stage IV, pathology in the hippocampus worsens and large portions of the insular cortex as well as the medial temporal gyrus contain significant numbers of inclusions. At this stage, patients often have dementia symptoms, while in previous stages they are often in pre-clinical stages of AD. In stage V, tau inclusions appear in the superior temporal gyrus and start to be present in the premotor and first order sensory association areas of the neocortex. In the final stage VI, tau deposits are present in the first order sensory association areas and the occipital neocortex. In addition, pathology in previously affected areas like the superior temporal gyrus becomes more pronounced[442].

Due to the progression of tau pathologies in AD brains, spreading of tau aggregates is hypothesized to occur along neuronal connections. There are two main mechanisms necessary for this cell-to-cell transfer: tau secretion and uptake[433,444–448]. For the secretion process, several mechanisms are likely to occur, since the majority of tau is found free in the extracellular space (not associated with any vesicles), but it has also been identified in microvesicles (ectosomes, 100 nm – 1 μm diameter) and exosomes (30-100 nm diameter) purified from mice overexpressing tau and from patient CSF[433,436,449–452]. The mechanism of how free extracellular tau is generated remains unclear, but type I unconventional protein secretion mechanism as well as chaperone-mediated translocation through membranes have been suggested[453,454]. Moreover, secreted tau appears to be dephosphorylated and is often truncated at the carboxy-terminus[455–458]. In support of the hypothesis that secretion occurs at synapses, neuronal activity leads to increases of extracellular tau[448,457,459]. For vesicle-associated tau, ectosomes are large vesicles that are directly budding from the plasma membrane, while intraluminal vesicles, the exosome-precursors, are generated inside the cell lumen. At endosomes, membrane invaginations lead to the formation of multivesicular bodies (MVBs), with intraluminal vesicles trapping intracellular matter. Then, these intraluminal vesicles are released as exosomes when MVBs fuse with the plasma membrane[433]. Most mechanistic studies of tau secretion to date have been conducted *in vitro* and thus, the relevance of these different mechanisms *in vivo* is yet to be determined[433].

Tau uptake has been studied both *in vitro*[446,460–464], in primary neurons, as well as human iPSC-derived neurons and astrocytes, and *in vivo*[462,465]. Both clathrin-mediated and clathrin-independent mechanisms (e.g. micropinocytosis) have been reported as potential uptake mechanisms for tau. Furthermore, heparan sulfate proteoglycans (HSPGs) and other receptors (e.g. LRP1) have been suggested to facilitate receptor-mediated uptake of free tau[466–469]. Another way tau might enter the cell could be through the membrane rupture of endocytic vesicles[470–472]. Upon rupture, autophagy pathways get activated and try to remove the released debris. In support of this uptake mechanism, inhibiting autophagy results in increase tau aggregation in recipient cells[471]. Furthermore, loss of function of BIN1, a LOAD risk factor and a protein involved in endocytosis, also leads to increased tau uptake and aggregation[470]. Lastly, uptake of tau into astrocytes seems to be reduce tau propagation, but to also negatively affect synaptic activity of nearby neurons[463,464].

To better model tau spreading and to further understand its underlying mechanisms, recent work has aimed to develop better *in vivo* rodent models (for review see Robert et al. 2021[473]). Previous 'traditional' tau mice models often relied on overexpressing human tau with *MAPT* mutations found in familiar FTLD patients (P301S or P301L, A152T or K280del), which has caveats due to side effects of the overexpression and because these mutations are not found in AD. Furthermore, expression of human tau in these models was most often pan-neuronal and not brain region specific, making any spreading studies difficult. One approach to better model tau spreading, was to generate a transgenic mouse model with mutant human tau expression localized to the EC and locus coeruleus[474–476]. It recapitulated tau spreading along anatomically connected regions characterized by Braak and colleagues, but still had the caveat of expressing only misfolded tau that forms seeds specific to FTLD, not AD. Another model system to study tau spreading that was developed in recent years was to inject AAV-based tau expression systems into wt mice[450,477–479]. Advantages of this system include that tau expression can be targeted through the location of injection as well as choice of promoter and that a fluorescent marker can be included in the expression cassette, easily visualizing transduced neurons vs tau spreading. Furthermore, it eliminates the need for time-consuming crossbreeding to generate transgenic mice. Conversely, since these models still locally overexpress tau with FTLD-mutations, this main drawback remains[473].

In addition, there are recently developed tau spreading model systems that utilize injecting patient-derived tau seeds from various tauopathies into either wt mice or rats[431,444,480–484] or different strains of transgenic (e.g. humanized tau (hTau) or APP transgene) mice[430,432,485–490]. This technique was pioneered by Virginia Lee's lab, and the first paper injecting seeds derived from human AD brain post-mortem tissue found that tau spread from the site of injection to anatomically connected regions[444]. These findings have now been replicated and expanded on in several studies, looking at different tau seeds from various tauopathies[473–476]. Most significantly, the cell type specificity that certain tauopathies display in humans seems to be conserved when their tau seeds are injected into wt mice (e.g. PSP seeds will induce astroglial tau inclusions)[484]. Furthermore, studies comparing tau injections in wt and transgenic mice expressing non-aggregation prone humanized tau (e.g. hTau[491] or 6hTau[430] models) confirmed that templating of human brain-derived tau seeds onto human tau works better than templating onto tau from a different species (mouse tau)[430,486,487]. When combining both Aß and tau pathologies by injecting APP mouse models (e.g. 5xFAD, APP/PS1 or APP knock-in mice), Aß plaques in some of these mouse models seemed to create a micro-environment close to the plaques facilitating increased dystrophic neurite and NP tau formation, but NFT numbers seemed unaffected[485,487,491].

Of note, none of the tau seed injected or local expression tau mice models show cognitive deficits. Likely this is because tau pathology is not severe enough without the overexpression of tau or presence of additional Aß pathology[476]. In addition, a recent study found that the amount and rate of tau spreading from hippocampal and EC neurons overexpressing tau, to neurons with normal tau levels was dependent on the genetic background of the mice[492]. This raises interesting questions about the inherent variability of tau spreading in different mice models and in patients and what other, currently unidentified genetic factors could impact tau spreading.

Autophagy: A Clearance Mechanisms for Misfolded Proteins

One cellular mechanism proposed to modify Aß and tau pathologies is autophagy, which is dysregulated in several neurodegenerative diseases[346,493,494]. Autophagy is a cellular degradation pathway that engulfs cytoplasmic proteins, organelles, or other aggregates to deliver

them to lysosomes for degradation and nutrient recycling. Autophagy is especially important in neurons, since they are post-mitotic and are unable to dilute toxic substance build-up through cell division[495]. In AD, autophagy/lysosomal degradation is thought to remove hyperphosphorylated tau, APP, as well as Aß and its aggregates from neurons. Conversely, inhibiting lysosomal function increases intracellular tau and Aβ aggregation[493,496]. There are three types of autophagy: macroautophagy, chaperone-mediated autophagy (CMA) and microautophagy. The first two have been reported to potentially play a role in AD, with macroautophagy being the most relevant form. For a review of autophagy in AD see Li et al. 2017[346] and Menzies et al. 2015[494].

Macroautophagy consists of three main stages: autophagosome biogenesis (subdivided into phagophore membrane isolation, elongation and engulfment of cellular content), autophagosome maturation and fusion with lysosomes[346]. The main regulator of autophagy activity is the mammalian target of rapamycin complex 1 (mTORC1). mTORC1 serves as a sensor for nutrient levels in the cell and is activated in nutrient-rich conditions. Upon its activation it negatively regulates autophagy initiation. In contrast to inhibition by mTORC1, other stimuli like presence of reactive oxygen species (ROS), hypoxia, subcellular organelle damage and protein aggregation can induce macroautophagy[346].

In AD, it is unclear if macroautophagy malfunction is a symptom or cause of AD. There is evidence that genetic mutations of *PSEN1* in familiar AD and ApoE4 allele status in sporadic AD can negatively impact macroautophagy. One physiological function of PSEN1, independent of γ-secretase, is to regulate lysosomal acidification through v-ATPase distribution. When PSEN1 is mutated in fAD, lysosomal acidification is reduced, and this can lead to decreased levels of autophagy. In addition, increased activation of GSK3ß has also been shown to disrupt lysosome acidification[497]. In sporadic AD, ApoeE4 expression has been shown to cause autophagy malfunction through increased levels of $Aß_{42}$ in lysosomes. This is then thought to cause lysosomal leakage, ultimately resulting in neuronal apoptosis[346]. In addition, tau hyperphosphorylation decreases its physiological role of stabilizing microtubules, which in turn might impair retrograde trafficking of autophagosomes, thus impairing autophagy further.

The second autophagy type implicated in AD is CMA. In contrast to macroautophagy, it targets mostly soluble, cytoplasmic proteins that selectively get translocated into lysosomes one after another. Heat shock cognate protein of 70kd (hsc70) is the cytosolic chaperone that recognizes target proteins at a conserved sequence (most often KFERQ), prompts their unfolding and delivers them to the lysosome. At the lysosome, lysosomal-associated membrane protein 2A (LAMP-2A) will form a channel in the lysosomal membrane to allow target protein translocation into the lysosome with the help of lysosome-resident hsc70. Both APP and tau have the KFERQ motif and are thus substrates for CMA. When this motif is disrupted through mutations or deletions, their degradation by CMA is impaired. APP will not be delivered to the lysosome and instead is increasingly cleaved, generating more Aß fragments. Tau on the other hand, is normally cleaved upon degradation and the C-terminal fragment is degraded through macroautophagy or CMA. If the cleavage occurs at the wrong position, the C-terminal fragment is still recognized and moved to the lysosome, but translocation fails, resulting in truncated tau accumulating at lysosomal membranes[346]. This can once more disrupt the lysosomal membrane, leading to lysosomal leakage and ultimately apoptosis.

Two lysosomal proteins of interest for this thesis are progranulin (PGRN) and transmembrane protein 106B (TMEM106B). Both are implicated in several neurodegenerative disorders including FTLD-TDP (FTLD with transcription factor TAR DNA binding protein 43 (TDP-43) accumulation) and AD[498–501]. In humans, complete loss of progranulin causes the lysosomal

storage disorder neuronal ceroid lipofuscinosis (NCL)[502], while a heterozygous mutation in *GRN*, the gene encoding PGRN, leads to PGRN haploinsufficiency, causing FTLD-TDP[503]. Furthermore, a reduction of PGRN levels was recently associated with increased total tau levels in human CSF and increased tau phosphorylation in mice[504–506]. Importantly, lysosome enzyme dysregulation and accumulation of lipofuscin are present in PGRN-deficient mice, making them an interesting model system to investigate PGRN deficiency in the context of neurodegenerative diseases[507–509]. The role of PGRN deficiency in AD is not fully understood yet. Having the T-allele of the rs5848 single-nucleotide polymorphism (SNP) results in decreased serum PGRN levels and thus has been associated with increased AD risk[510–513]. In mouse model studies of PGRN in the context of AD, results were contradictory with some studies reporting attenuated AD phenotypes when PGRN levels are increased[514,515] and others reporting PGRN deficiency to improve Aß deposition[499,504,516].

Several physiological and pathological functions have been described for PGRN, including its role as a growth factor involved in wound healing, inflammation and tumorigenesis[499]. Its connection to lysosomal health remains under investigation, but it is known that PGRN is localized at lysosomes through its interaction with sortilin or with the soluble lysosomal protein prosaposin (PSAP). Reduction in PGRN was shown to lead to reduced lysosomal PSAP levels, offering one potential explanation of how PGRN deficiency disrupts lysosomal homeostasis[499]. Another hypothesis for PGRNs involvement in lysosomal homeostasis is its role as a lipid metabolism regulator, since lipidomic and transcriptomic data from *GRN* deletion mice showed altered lipid metabolism[499].

Reduction or loss of the second protein of interest, TMEM106B, has been reported to cause multiple lysosomal abnormalities, including impaired acidification and dysregulated of lysosomal trafficking in mouse neurons [507,517–520]. Furthermore, three recent papers identified three different folds of TMEM106B inclusions in aged human brains via cryo-EM[521–523]. They surveyed frontal cortex tissue from patients with sporadic and inherited tauopathy, Aβ-amyloidosis, synucleinopathies and TDP-43 proteinopathies, as well as from three neurologically healthy individuals with no or only few amyloid deposits. Interestingly, the type of TMEM106B deposit was not specific to specific diseases.

Functionally, TMEM106B is a transmembrane protein localized to lysosomal membranes in neurons, glia and endothelial cells. It is known to interact with subunits of the vacuolar ATPase and loss of TMEM106B likely increases lysosomal acidification[507,519,520]. In addition, TMEM106B is also implicated in the axonal transport of lysosomes, with TMEM106B reduction causing decreased lysosomal numbers and a the same time increasing axonal transport of lysosomes[517,519]. A third function of TMEM106B is its role as a regulator of myelination, with TMEM106B deficiency leading to downregulation of genes implicated in the myelination process, loss of OLIG2-positive cells in the corpus callosum of mice and reduced levels of myelin sheath membrane proteins[524–526].

TMEM10B was first identified as a risk factor of FTLD-TDP in a GWAS study in 2010, with the minor alleles of three SNPs decreasing disease risk[527]. Importantly, *TMEM106B* alleles seem to have most impact on modifying disease risk caused by *GRN* or *C9orf72* mutations, leading to TDP-43 accumulation. Nevertheless, TDP-43 inclusions also occur in other neurodegenerative diseases, including Lewy body dementia (LBD), hippocampal sclerosis (HpScl) and AD, suggesting that TMEM106B might modify their disease risk as well[498]. From 2012 onwards, multiple studies found a neuroprotective effect of the minor allele *TMEM106B* variants for AD and HpScl patients with TDP-43 inclusions[498,528]. This makes TMEM106B an interesting

target for further study in AD, since its impact on lysosomal dysfunction in AD and potential downstream effects remain poorly understood.

Aims of This Project

Tau aggregation and spreading are likely distinct but connected processes. Furthermore, several mechanisms connecting Aß and tau pathologies exist in AD. Gaining a better understanding how these mechanisms influence one another and how their disruption could be beneficial for the treatment of AD, was a driving force behind this thesis. More specifically, my project aimed to investigate a potential connection of Aß pathology to tau aggregation and spreading by a) characterizing the interactions of Pyk2, Fyn and GSK3ß between one another and their impact on tau aggregation *in vitro* and in different cellular models and b) investigating the impact of Aß, Pyk2 and Fyn, lysosomal proteins TMEM106B and PGRN, as well as age on tau spreading in mice.

For tau aggregation, existing research suggests that the imbalance of kinase and phosphatase activity is a major contributor to tau hyperphosphorylation, with Pyk2, Fyn and GSK3ß all reported to phosphorylate and/or co-localize with tau. In AD, Pyk2 and Fyn are both part of a signaling cascade induced by Aß oligomers binding to PrP^{C}, which then interacts with mGluR5, and subsequently activates Fyn and Pyk2. Separately, Pyk2 and Fyn have both been reported to phosphorylate GSK3ß *in vitro*, and GSK3ß is one of the best characterized tau kinases in AD. Given this existing evidence, I wanted to understand, if these three kinases can act in concert to facilitate tau hyperphosphorylation and aggregation in different model systems, specifically downstream of the above mentioned Aßo-induced signaling cascade.

To achieve this, I first studied Pyk2 and Fyn interaction with GSK3ß in in vitro kinase assays and HEK293T overexpression model. Then, I characterized the effects of Pyk2 and Fyn inhibition on tau phosphorylation in mouse neurons and iPSC derived neurons, as well as tried to determine if synthetic Aßo can induce activation of Pyk2 and Fyn in iPSC-derived neurons.

It remains unclear, to what extent cell-autonomous intracellular tau aggregation and trans-neuronal spreading are dependent on one another in AD. Furthermore, the balance of de novo versus templated misfolding of tau in AD is also ill defined and there is ongoing debate regarding which aspects of cell biology in AD might alter the pattern and magnitude of tau spreading. Especially tau aggregation associated mechanisms, had not been studied yet in this context. To expand on our understanding of what mechanisms might contribute to tau spreading, I investigated what impact mouse age, Aß pathology, disrupting Pyk2 and Fyn kinases or perturbed lysosomal function had on tau spreading.

I studied tau spreading by injecting mice with human tau. First, I validated my model system by analyzing my extracted seeding material and injecting WT (C57BL/6J) mice with tau extracts from four different brains (three AD and one Control brain). Then, I monitored if Aß aggregation would exacerbate tau spreading, as there is conflicting evidence if Aß aggregation can enhance tau accumulation and spreading at various disease stages[60,485,529–533]. To achieve this, I injected APPswe/PSEN1ΔE9 as well as hTau x $App^{NL\text{-}F/NL\text{-}F}$ knock-in mice with human tau extracts. Next, I explored the effects of reducing Fyn and Pyk2 activity on tau spreading, by injecting WT mice treated long-term with the Fyn inhibitor AZD0530 or by injecting $Ptk2b^{-/-}$ mice. Lastly, I wanted to investigate if perturbing lysosomal regulation or advanced age would have an impact on tau spreading. Thus, I injected $Grn^{-/-}$ and aged Tmem106b-/- mice tau extracts to observe potential effects on tau spreading.

Materials and Methods

The Materials and Methods sub-sections titled: Animals, Chronic Oral Dose Preparation of AZD0530, Tau Extraction, Atomic Force Microscopy, In Vitro Tau Seeding in Mouse Primary Neurons, Stereotactic Surgery on Mice, Mouse Brain Tissue Collection and Processing, Immunohistochemistry, Quantification of Tau Inclusions, Imaging and Quantification of Fluorescent Staining, SDS-Page and Western Blotting, Immunoprecipitation of Aß from Tau Samples and Statistical Analysis, were adopted with minor changes from my first author paper (Nies et al. 2021[487]).

Plasmid DNA Constructs

Tau and Pyk2 sequences were subcloned into an AAV-CAG-GFP vector (#28014, Addgene, Watertown MA; USA). GSK3β and Fyn sequences were subcloned into a pcDNA3.0 (previously sold by Invitrogen, Waltham, MA, USA) vector which also served as a negative transfection control.

Cell Culture

HEK-293T cell culture

Human embryonic kidney-293T cells (HEK-293T, #CRL-3216, ATCC, Manassas, VA, USA) cells were maintained in Dulbecco's Modified Eagle Medium (DMEM, #11965-092, Gibco/Invitrogen, Waltham, MA, USA) supplemented with 10% fetal bovine serum (#16000044, Gibco). Cells were maintained at 37°C and 5% CO_2 and passaged with 0.25% Trypsin/EDTA (#25200-056, Gibco)when reaching 80 - 95% confluency.

Human iPSC line information and maintenance

Two cell lines with distinct differentiation protocols were used in this work. The first cell line (from now on called "Gibco" line) was a commercially available episomal human iPSCs line (#A18945, Gibco) and differentiated using a previously described and validated dual SMAD inhibition protocol (Sousa et al. 2017[534]). The second cell line (from now on called "i3N" line) was a kind gift from Martin Kampmann at UCSF and was differentiated through dox-inducible NGN2 expression as described in Tian et al. 2019[535]. This cell line was generated from the WTC11 line through insertion of doxycycline-inducible mouse NGN2 at the AAVS1 locus and additional insertion of a pC13N-dCas9-BFP-KRAB cassette at the CLYBL intragenic safe harbor locus[535].

Human induced pluripotent stem cells (iPSCs) were cultured on vitronectin-coated (5 μg/mL working concentration, #A14700, Gibco) 6-well plates (#3516, Costar/Corning, Bedford, MA, USA) in Essential 8 Flex Medium (#A2858501, Gibco). When ~80% confluent, cells were passaged in clumps using Gentle Dissociation Medium (#07174, StemCell Technologies, Vancouver, BC, Canada) or dissociated into single cells and plated for neuronal induction.

Differentiation into cortical neurons

Gibco cell line

Gibco iPSCs were differentiated as described in Sousa et al. 2017[534]. Briefly, iPSC were washed once in PBS and dissociated using Accutase (#07920, StemCell Technologies). Once lifted, they were diluted 1:5 in phosphate buffered saline (PBS) and centrifuged at 250 x g for

5 minutes at RT. Single cells were plated at a density of 2 x 10^5 cells per well on a vitronectin-coated 12-well plate (#665180, Greiner Bio-one, Monroe, NC, USA) in Essential E8 Flex medium with 2 µM thiazovivin (#72252, StemCell Technologies) to improve cell-survival. One day after plating (at ~75-90% confluence), Essential 8 Flex Medium was replaced with neural induction medium [a 1:1 mixture of DMEM/F12 (#11330-033, Gibco) and Neurobasal-A Medium (#10888-022, Gibco) containing 1x N-2 supplement (#17502-048, Gibco), 1x B-27 supplement (#17504-044, Gibco), 20 µg/ml insulin (#I0516, Sigma-Aldrich, Darmstadt Germany), 1 mM L-glutamine (#25030-081, Gibco), 100 µM MEM Non-Essential Amino Acids (#11140-050, Gibco), 0.1 mM β-mercaptoethanol (#21985, Gibco), 100 nM LDN-193189 (#19396, Cayman Chemical, Ann Arbor, MI, USA), 10 µM SB-431542 (#13031, Cayman Chemical) and 2 µM XAV-939 (#3748, Tocris Bioscience, Minneapolis, MN, USA)] and replaced daily for 12 days. On day 12, cells were dissociated using Accutase and seeded in neural induction medium with 2 µM thiazovivin at a density of 4 x 10^4 cells/well onto 24-well pre-coated poly-D-lysine plates (#354414, Costar/Corning) that had been additionally coated with 5 µg/ml mouse laminin (#23017-015, Invitrogen) overnight. Neural induction medium was replaced 2 - 3 days after seeding with terminal neural differentiation medium (now called "TD-medium", Neurobasal-A Medium containing 1x N-2 supplement, 1x B-27 supplement, 1 mM L-glutamine and 30 ng/ml BDNF (#PHC7074, Gibco). Cells were maintained in TD-medium for at least 90 days (up to 120 days) and replated once more time at 45-60 DIV as described above to promote cell health. 3⁄4 of TD-medium was replenished twice weekly and to prevent detachment, the medium was supplemented with 2.5 µg/ml laminin once weekly.

i3N cell line

i3N iPSC were differentiated according to the protocol in Tian et al. 2019[535]. Briefly, iPSCs were washed once in PBS and dissociated using Accutase. Once lifted, they were diluted 1:5 in PBS and centrifuged at 250 x g for 5 minutes at RT. Supernatant was removed and pelleted cells were resuspended in Essential E8 medium containing 2 µM thiazovivin to improve cell survival. iPSCs were then plated at 7 x 10^5 cells per matrigel-coated (#356234, Corning) well of a 6-well plate.

The next day, all Essential E8 medium was removed and replaced with Pre-Differentiation Medium (Knockout DMEM/F12 (#12660-012, Gibco) containing 1x MEM Non-Essential Amino Acids (#11140-050, Gibco), 1x N2 supplement, 10 ng/mL NT-3 (#450-03, PeproTech, Rocky Hill, NJ, USA), 10 ng/mL BDNF (#450-02, PeproTech), 1 mg/mL mouse laminin, 10 nM Y-27632 dihydrochloride ROCK inhibitor (#125410, Tocris Bioscience) or 2 nM thiazovivin), and 2 mg/mL doxycycline hydrochloride (#D3447-500MG, Sigma-Aldrich) to induce expression of NGN2. Medium was fully exchanged daily for three days.

On the third day, now called Day 0, pre-differentiated cells were dissociated and centrifuged as above. Supernatant was aspirated and pelleted cells were resuspended in Pre-Differentiation Medium and plated at 0.5 or 1 x 10^5 cells/well onto a Poly-D-lysine pre-coated 24-well plate (#353047, Falcon/Corning), pre-coated Poly-D-lysine/laminin 12 mm round glass coverslips (#354087, Corning), or at 1.5 x 10^4 cells/well for Poly-D-lysine pre-coated 96-well plates (#165305, ThermoFisher, Waltham, MA, USA).

The next day, all Pre-Differentiation medium was removed and Classic Neuronal Medium with doxycycline (1:1 mixture of DMEM/F12 (#11320-033, Gibco) and Neurobasal-A (#10888-022, Gibco) containing 1x MEM Non-Essential Amino Acids, 0.5x GlutaMAX Supplement (#35050-061, Gibco), 0.5x N2 Supplement, 0.5x B27 Supplement (#17504-044, Gibco), 10 ng/mL NT-3, 10 ng/mL BDNF, 1 mg/mL mouse laminin, and optionally 2 mg/mL doxycycline

hydrochloride) was added. On Day 7, half of the medium was removed and an equal volume of fresh Classic Neuronal Medium without doxycycline was added. On Day 14, half of the medium was removed and twice that volume of fresh medium without doxycycline was added. On Day 21, one-third of the medium was removed and twice that volume of fresh medium without doxycycline was added. On Day 28 and each week after, two-thirds of the medium was removed and an equal volume of fresh medium without doxycycline was added.

Phosphorylation Assays in HEK293T cells overexpressing kinases and tau

HEK293T cells were seeded at 7 x 10^4 cells/well in a 12-well plate and cultured until they reached ~90% confluency. Cells were transfected with appropriate DNA constructs (0.5 µg DNA/well in a 12-well plate, see 'Plasmid DNA constructs' for plasmid information) using Lipofectamine 3000 reagent (#L3000001, Invitrogen). After 24 hours, cells were washed once with PBS and harvested in 200 µL lysis buffer [1% Triton X-100 containing 50 mM Tris, 150 mM NaCl, 1 mM EDTA, 1 x c0mplete™ Mini protease inhibitor cocktail (#11836170001, Roche, Basel, Switzerland) and 1 x PhosSTOP™ (#4906845001, Roche)]. Lysates were centrifuged at 14,000 x *g* for 10 min at 4°C and supernatants were boiled in Laemmli sample buffer (#1610747, Bio-Rad, Hercules, CA, USA) for 10 min at 95°C. SDS-PAGE and Western blotting were performed as described in the corresponding sections. Primary antibodies (anti-Pyk2 (#3480, Cell Signaling Technology (CST, Danvers, MA, USA)), anti-pPyk2 Y402 (#3291, CST), anti-GSK3β (#9315, CST), anti-pGSK3β Y216/pGSK3α Y279 (#ab68476, Abcam, Cambridge, UK), anti-Fyn (#4023, CST), anti-pSrc Family Y216 (#6943, CST), anti-Tau (HT7) (#MN1000, ThermoFisher Scientific), anti-pTau S202/T205 (AT8) (#MN1020, ThermoFisher Scientific), anti-pTau S396/S404 (PHF-1) (Peter Davies Personal Request, RRID:AB_2315150) and β-Actin (#8457, CST)) were used at 1:1000 dilution in blocking buffer (#MB- 070-010F, Blocking Buffer for Fluorescent WB, Rockland, Bedford, PA, USA).

Co-immunoprecipitation of Pyk2 and GSK3ß

HEK293T cells were seeded at 1.2 x 10^6 cells/dish in 60 mm dishes and grown until 50-70% confluent. Then, cells were transfected with 1 µg DNA GFP-Pyk2 plasmid, 0.5 µg DNA GSK3ß plasmid or equivalent amount of empty vector using Lipofectamine 3000. 24h after transfection, cells were washed once with PBS and then each dish was lysed in 600 µL lysis buffer [150 mM NaCl, 50 mM Tris, 1% Triton-X-100, 1 mM EDTA]. The lysates were centrifuged for 5 minutes at 16,260 x g and 550 µL/sample were incubated for 2 h at 4°C with 20 µL GFPtrap_A beads (#gta-20, chromotek, Planegg-Martinsried, Germany). Afterwards, beads were washed 5 times in 500 µL lysis buffer and then eluted in 25 µL of 4 x Laemmli buffer + 10% ß-mercaptoethanol. SDS-PAGE and Western blotting was performed as described in the corresponding sections, with 2.5% input loaded compared to eluate. Primary antibodies buffer (rabbit anti-GFP (#ab290, Abcam), and rabbit anti-GSK3ß (27C10) (#9315, CST)) were used at 1:1000 dilution in Rockland blocking buffer.

In vitro Kinase Assay

Recombinant Fyn (#ab84696, Abcam), GSK3b (#ab63193, Abcam) and Pyk2 (#ab42622, Abcam) were combined with either Pyk2 or Fyn kinase at their physiological concentration (25 nM Fyn or 40 nM Pyk2, determined and from mouse hippocampus and cortex) and various concentrations (0, 1, 5, 10, 50, 100, 500 and 1000 nM) of GSK3ß being added in 50 µL kinase

buffer (#9082S, CST) and 200 µM ATP (#PV3227, Invitrogen). The reactions were stopped after 30 minutes by adding 1x Laemmli buffer + 5% ß-mercaptoethanol to samples and boiling them at 95°C for 5 minutes. SDS-PAGE and Western blotting was performed as described in the corresponding sections, with 2.5% input loaded compared to eluate. Primary antibodies: mouse anti-Pyk2 (#3480, CST), rabbit anti-pPyk2 Y402 (#3291, CST), mouse anti-GSK3b (11B9) (#sc-81462, Santa Cruz Biotechnology), rabbit anti-pGSK3[alpha + beta] (#ab68476, Abcam), rabbit anti-Fyn (#4023, CST), rabbit anti-pSrc Family Y216 (#6943, CST)were used at 1:1000 dilution in Rockland blocking buffer.

HEK-293 Proximity Ligation Assay (PLA)

PLA assay was conducted as described previously[536]. HEK-293T cells were plated at 40,000 cells/well onto 8-well chamber slides (#154941, Nunc/Thermo Scientific). Transient transfection with plasmids expressing human tau (#RC213312, Origene, Rockville, MD, USA) and Fyn (#RC224691, Origene) was conducted using Lipofectamine 2000. Three hours later, 2 µM AZD0530 in DMSO or DMSO (vehicle) was added to the treatment or control wells. After 24 h of treatment, cells were fixed in 4% paraformaldehyde in PBS at room temperature for 30 min and then washed three times in PBS for 5 min and stored until PLA was performed. Duolink In Situ Detection Reagents Green (#DUO92014, Sigma) were used for the PLA as described[537] with modifications. Cells were fixed on 8-well chamber slides and permeabilized/blocked with 10% normal donkey serum, 0.2% Triton X-100 in PBS for 30 min at room temperature. Wells were then incubated with primary antibodies (anti-Tau (#A0024, DAKO, 1:4000 dilution) and Fyn15 (#sc-434, Santa Cruz, 1:500 dilution) in 1% normal donkey serum in PBS overnight at 4°C. The next day, after removing wells, the slides were washed 3x for 5 min in PBS and then incubated for 1 h at 37 °C in 8 µL Duolink In Situ PLA Prole Anti-Rabbit PLUS (#DUO92002, Sigma) and 8 µL Duolink In Situ PLA Probe Anti-Mouse MINUS (#DUO92004, Sigma) in 24 µL 1% normal donkey serum in PBS per sample. Slides were then washed two times for 5 min with 1x Wash Buffer A (#DUO82049, Sigma) at room temperature. For the ligation step, slides were incubated for 1 h at 37°C in 8 µL 5x Ligation buffer and 1 µL of Ligase in 32 µL high purity water. Then, slides were washed two times for 5 min in 1x Wash Buffer A at room temperature. For the amplification step, the slides were incubated for 100 min at 37°C in 8 µL 5x Amplification buffer and 0.5 µL polymerase in 31.5 µL high purity water per sample. The slides were then washed two times for 10 min in 1x Wash Buffer B (#DUO82049, Sigma) and for 1 min in 0.01x Wash Buffer B and then 5 min in PBS at room temperature. For tau and Fyn visualization, slides were incubated for 1 h at room temperature in the secondary antibodies (donkey anti-rabbit conjugated with Alexa Fluor-568 and donkey anti-mouse conjugated with Alexa Fluor-647 (1:500 dilution, Thermo-Fisher)) with 1% normal donkey serum in PBS. Then, slides were washed four times for 5 min in PBS. Coverslips were mounted on the slides with Vectashield (Vector Laboratories) antifade mounting medium with DAPI and stored at 4°C until imaging.

APOE allele genotyping

To determine the APOE allele composition of i3N and Gibco cell lines, cells were genotyped according to a previously published protocol by Zhong et al. 2016[538]. Briefly, DNA was extracted from iPSC according to manufacturer's instructions (# QE09050, Lucigen, QuickExtract™ DNA Extraction Solution). Genotyping was performed by quantitative Real Time PCR (BioRad CFX96 + C1000 Touch Thermocycler), combining 1 × TaqMan® Genotyping Master Mix (#4371353, ThermoFisher), 0.5 µM of each APOE primer and APOE probe, 0.1 µM of each ACTB

primer and ACTB probe and 40 ng of genomic DNA per reaction (see Table 1 for primer and probe sequences). Initial activation of the polymerase occurred for 10 min at 95 °C, followed by 40 cycles of [denaturation at 95 °C for 15 sec, annealing/extension at 64 °C for 1 min]. The fluorescence signals were collected during the annealing/extension step.

Table 1: Probes and primers for APOE genotyping

Name	Sequence 5' – 3'
APOE Probe	6FAM-CAGCTCCTCGGTGCTCTGGC-QSY
ACTB Probe	VIC-TGCTGTCTGGCGGCACCACCATGTACC-QSY
APOE2-f	GCGGACATGGAGGACGTGT
APOE2-r	CCTGGTACACTGCCAGGCA
APOE3-f	CGGACATGGAGGACGTGT
APOE3-r	CTGGTACACTGCCAGGCG
APOE4-f	CGGACATGGAGGACGTGC
APOE4-r	CTGGTACACTGCCAGGCG
ACTB-f	GACGTGGACATCCGCAAAGAC
ACTB-r	CAGGTCAGCTCAGGCAGGAA

Validation of iPSC-derived neurons

For SDS-PAGE and Western Blotting, neurons were grown at 1 x 10^5 cells/well in 24-well plates and harvested (at DIV 28 or 46 for i3N, and at DIV50 or DIV65 for Gibco neurons) on ice in 100 µl/well lysis buffer [RIPA with 1% SDS, 1 x c0mplete™ Mini protease inhibitor cocktail and 1 x PhosSTOP™]. Samples from adjacent wells were pooled (pooled sample volume, 200 - 300 µl from 2-3 wells), briefly vortexed and centrifuged at 100,000 x *g* for 30 min at 4°C. SDS-soluble supernatants were boiled in 1x Laemmli sample buffer with 5% β-mercaptoethanol and 1% SDS at 95°C for 5 minutes. SDS-PAGE and Western Blotting was performed as described in the section about Western Blotting with the following primary antibodies at 1:1000 dilution: mouse anti-ß-actin (8H10D10) (#3700S, CST), rabbit anti-ß-tubulin (#2146B, CST), mouse anti-PrP^C (#SAF32, #189720, Cayman Chemical), rabbit anti-mGluR5 (D6E7B) (#920, CST), rabbit anti-NR2B (#4207S, CST), rabbit anti-SV2A (#ab32942, Abcam), rabbit anti-Fyn (#4023, CST) , rabbit anti-pSRC Y416 (D49G4) (#6943, CST), rabbit anti-eEF2 (#2332S, CST), rabbit anti-peEF2 T56 (#2331S, CST), mouse anti-GSK3b (11B9) (#sc-81462, Santa Cruz Biotechnology), rabbit anti-pGSK3[alpha + beta] (#ab68476, Abcam), mouse anti-Pyk2 (5E2) (#3480S, CST), rabbit anti-pPyk2 Y402 (#3291S, CST), rabbit anti-SAPK/JNK (#9252S, CST), mouse anti-pSAPK/JNK T183/Y185 (#9255S, CST), rabbit anti-PSD95 (#ab18258, Abcam), rabbit anti-MAP2 (#4542S, CST) and rabbit anti-NR2B (#4207S, CST).

For immunohistochemistry, cells were fixed in 4% PFA for 20 minutes at 37°C, then washed three times with 300 µL/well PBS and blocked/permeabilized for 30 minutes at RT in PBS containing 1% BSA and 0.1% Triton-X-100. Afterwards, cells were incubated overnight at 4°C in blocking buffer with primary antibodies: mouse anti-synaptophysin (#ab8049, Abcam, 1:250 dilution), rabbit anti-PSD95 (#ab18258, Abcam, 1:500 dilution), chicken anti-MAP2 (#ab5392, Abcam, 1:500 dilution). The next day, cells were washed three times for 10 minutes in PBS and incubated overnight at 4°C with secondary antibodies (AlexaFluor 488 goat anti-rabbit, AlexaFluor 568 goat anti-chicken, AlexaFluor 647 goat anti-mouse, all diluted 1:500, and DAPI at 1:5000) in blocking buffer. Afterwards, coverslips were washed three times in 300 µL PBS for 10 minutes each and mounted using ProLong Glass Antifade Mountant (#P36984,

Invitrogen). Coverslips were imaged as described in 'Imaging and Quantification of Fluorescent Staining'.

Pharmacological Inhibition of Pyk2 and Fyn in iPSC-derived neurons

For the four day inhibitor incubation experiments, cells were grown at a density of 1 x 10^6 or 2 x 10^6 cells/well in 24-well plates and 1 h prior to treatment, 3⁄4 of medium was replaced with fresh TD medium. For treatment, cells were treated with DMSO vehicle, 1 μM AZD0530, 1 μM PF-719 or 1 μM of both inhibitors diluted in TD medium. For each treatment condition, volumes of DMSO vehicle and DMSO-solubilized drugs were kept constant. Neurons were treated for 4 days at 37°C and afterwards immediately harvested on ice in 100 μl/well lysis buffer [1 x RIPA (diluted in ddH_2O from 10x stock, #20-188, Millipore) with 1% SDS, 1 x c0mplete™ Mini protease inhibitor cocktail and 1 x PhosSTOP™]. Samples were briefly vortexed and centrifuged at 100,000 x *g* for 30 min at 4°C. SDS-soluble supernatants were boiled in 1x Laemmli sample buffer with 10% β-mercaptoethanol at 95°C for 5 minutes before performing SDS-PAGE and Western Blotting as described in the appropriate sections. Primary antibodies used at 1:1000 dilution in blocking buffer for Western Blotting were: mouse anti-Pyk2 (#3480, CST), rabbit anti-pPyk2 Y402 (#3291, CST), anti-GSK3β (#9315, CST), anti-pGSK3β Y216/pGSK3α Y279 (#ab68476, Abcam), anti-Fyn (#4023, CST) and anti-pSrc Family Y216 (#6943, CST), mouse anti-Tau (#MN1000, Invitrogen), mouse anti-pTau AT8 (#MN1020, Invitrogen), mouse anti-pTau PHF1 (Peter Davies personal request, RRID: AB_2315150), mouse anti-pTau AT180 (#MN1040, Invitrogen) and mouse anti-pTau Y18 (#MM-0194-P, Medimabs).

For the 2 hour inhibitor incubation, the experiment was performed as above, but cells were treated with either DMSO vehicle or varying concentrations (0.5 μM, 1 μM or 2 μM) of PF-719 and two wells were pooled to have a larger sample volume.

Synthetic Amyloid-ß oligomer preparation

Synthetic amyloid-$ß_{1-42}$ peptide was obtained as lyophilized powder from the Keck Large Scale Peptide Synthesis Facility (Yale University). Preparation of synthetic Aß oligomers was performed as described previously[184] with minor modifications. Briefly, dried Aß peptide was reconstituted in anhydrous DMSO and then diluted in Ham-F12 medium (specially formulated Ham-F-12 medium without glycine, glutamine, L-glutamic acid, L-glutamine, and phenol red, Invitrogen) to a final concentration of 100mM. After 16 h incubation at 22°C, the preparation was centrifuged at 21,000 x g for 15min, and the supernatant was concentrated, and buffer exchanged to PBS in an Amicon Ultra 0.5 mL Centrifugal Filter 3K (#UFC500396, Millipore). For the buffer exchange, samples were collected in the filter through centrifugation at 14,000 x g for 15 minutes, then buffer exchanged twice in 500 μL PBS (centrifugation at 14,000 x g for 15 minutes for each exchange). For elution, the filter was inverted and placed in a fresh collection tube and centrifuged at 1,000 x g for 2 minutes. Protein concentration was assessed by measuring absorption at 280 nm with a Nanodrop® Spectrophotometer (#N-1000, ThermoFisher Scientific) and dividing the absorption by the extinction coefficient of sAßo (E280 = 1490/(M*cm)). The concentration of Aßo in all experiments is expressed in monomer equivalents, with 1 μM total $Aß_{1-42}$ peptide corresponding to around 10 nM oligomeric species[184].

Treatment of iPSC-derived neurons with synthetic Aß-oligomers

For short-term (30 minute) treatment, i3N neurons were grown in 24-well plates at a density of 1 x 10^6 cells/well. One hour prior to treatment, 3⁄4 of medium was replaced with fresh TD medium. For treatment, medium was replaced with 600 µL of Classic Neuronal medium containing vehicle or synthetic Aß-oligomers (sAßo) at 0.5 µM, 1 µM or 2 µM concentration. Cells were incubated for 30 minutes at 37°C, then lysed in 100 µL lysis buffer/well [1 x RIPA (diluted in ddH_2O from 10x stock, #20-188, Millipore) with 1% SDS, 1 x c0mplete™ Mini protease inhibitor cocktail and 1 x PhosSTOP™] on ice and centrifuged at 100,000 x *g* for 30 min at 4°C. SDS-soluble supernatants were boiled in 1x Laemmli sample buffer with 5% β-mercaptoethanol at 95°C for 5 minutes before performing SDS-PAGE and Western Blotting as described in the appropriate sections. Primary antibodies used at 1:1000 dilution in blocking buffer for Western Blotting were: mouse anti-Pyk2 (#3480, CST), rabbit anti-pPyk2 Y402 (#3291, CST), anti-GSK3β (#9315, CST), anti-pGSK3β Y216/pGSK3α Y279 (#ab68476, Abcam), anti-Fyn (#4023, CST) and anti-pSrc Family Y216 (#6943, CST), rabbit anti-SAPK/JNK (#9252S, CST), mouse anti-pSAPK/JNK T183/Y185 (#9255S, CST), rabbit anti-eEF2 (#2332S, CST), rabbit anti-peEF2 T56 (#2331S, CST), mouse anti-ß-actin (8H10D10) (#3700S, CST) and rabbit anti-ß-tubulin (#2146B, CST).

For long-term (7 day) treatment, Gibco neurons were grown on Poly-D-Lysine- and laminin-coated glass coverslips (#354087, Corning) at a density of 0.5 x 10^6 cells/coverslip. Cells were treated with 800 µL/well of vehicle or sAßo at 0.1 µM, 0.3 µM or 1 µM concentration in TD medium containing penicillin/streptomycin (#15140122, Gibco) at 1:100 dilution and returned to the incubator. After 3 days, 600 µL of the medium was replaced with new vehicle or sAßo containing medium. After 7days of treatment, cells were washed once in 500 µL PBS/well , then fixed with 4% PFA for 20 minutes at 37°C, washed three times for 5 minutes in 300 µL PBS and blocked with 250 µL/well blocking buffer [PBS containing 10% normal donkey serum and 0.2% Triton X-100] for 30 minutes. Neurons were incubated overnight at 4°C with primary antibodies (chicken anti-MAP2 (#ab5392, abcam, 1:5000 dilution), rabbit anti-PSD-95 (#ab18258, abcam, 1:500 dilution)) in PBS containing 1% normal donkey serum and 0.2% Triton X-100. The next day, samples were washed three times with 300 µL PBS for 10 minutes each and then incubated overnight at 4°C in secondary antibodies (donkey anti-rabbit Alexa Fluor 488 and goat anti-chicken Alexa Fluor 568 (both from Invitrogen, 1:500 dilution) and DAPI (1:5000 dilution)) diluted in PBS containing 1% normal horse serum and 0.2% Triton X-100. Afterwards, coverslips were washed three times in 300 µL PBS for 10 minutes each and mounted using ProLong Glass Antifade Mountant (#P36984, Invitrogen).

Tau Extraction

Pre-existing de-identified human autopsy brains were accessed for these studies under conditions considered exempt from Human Subjects regulations after review of Yale's Institutional Review Board. Fresh frozen brain had been stored at -80°C, see Table 2 for post-mortem information on the brains. Tau was extracted based on a previously published protocol[444] with some modifications as described in Nies et al. 2021[487].

Table 2: Post-mortem information of patients whose tissue was used for Tau extraction.
Table re-printed from JBC, Volume 297, Issue 4, Article 101159, Nies et al. 2021, *Spreading of Alzheimer tau seeds is enhanced by aging and template matching with limited impact of amyloid-ß,* doi: https://doi.org/10.1016/j.jbc.2021.101159 , Figure S1-A, © 2021 Elsevier, with permission from Elsevier under the CC-BY license.

Internal Name	Patient Age	Post mortem Interval [h]	NIA Classification or Braak Stage	Sex
Control Brain	47	25	0	F
Brain A	87	36	A2, B3, C2	M
Brain B	87	23	A2, B3, C2	M
Brain J	64	6	6	M

Briefly, 11–12 grams of cortical grey matter were dounce homogenized in 30 mL lysis buffer [10 mM Tris-HCl, 1 mM EDTA, 0.1% sarkosyl, 10% sucrose, freshly added 2 mM DTT, phosSTOP (Roche) and protease inhibitors (Roche)]. During the extraction, lysates were kept on ice. Homogenates were centrifuged at 12,000 rpm at 4 °C for 12 min (Ti 45 rotor, Beckman Coulter, Brea, CA, USA). The supernatant was pooled, and the pellets were re-extracted and centrifuged twice more as above. The pooled supernatant was centrifuged twice more at 12,000 rpm at 4 °C for 12 min (Ti 45 rotor, Beckman Coulter) to remove debris. Then, the sarkosyl concentration was increased to 1% and samples were nutated for 1 h at room temperature (RT). The samples were centrifuged at 300,000 x g for 1 h at 4°C (57,000 rpm, Ti 70 rotor, Beckman Coulter). The resulting pellet was washed with PBS supplemented with phosSTOP and protease inhibitors twice and then resuspended in PBS supplemented with phosSTOP and protease inhibitors. After sonication at 15% amplitude for 20 s with 0.5 s ON/ 0.5 s OFF pattern, the lysate was centrifuged at 100,000 x g for 30 min at 4 °C. The supernatant was discarded, and the pellet washed twice in PBS supplemented with phosSTOP and protease inhibitors. The pellet was once more resuspended in PBS supplemented with phosSTOP and protease inhibitors and sonicated at 30% amplitude for 60 s with 0.5 s ON/0.5 s OFF pattern. This was followed by a 100,000 x g spin for 30 min at 4 °C. The resulting supernatant contained the soluble tau and was aliquoted and stored at − 80°C until further analysis or experimental use. Tau extract concentration was determined by comparing tau extracts diluted to 10%, 5% or 2.5% in 1x Laemmli sample buffer to the same dilution curve of recombinant 2N4R tau (#842501, Biolegend) via Western blotting. Primary antibodies (anti-Tau (HT7) (#MN1000, ThermoFisher Scientific) and anti-Tau pThr231 (AT180) (#MN1040, Invitrogen)) were used at 1:100 dilution in Rockland blocking buffer. Total protein concentration in tau extracts was assessed by measuring absorption at 280 nm on a Nanodrop® Spectrophotometer (#N-1000, ThermoFisher Scientific).

Atomic Force Microscopy

Samples were prepared by splitting Mica discs (#50, 9.9mm diameter, Ted Pella Inc, PELCO Mica Discs, Redding, CA, USA) with a fresh razor and sticking them to a glass coverslip with a double-sided sticky tab (#16084-6, 6mm OD, Ted Pella Inc, PELCO Tabs). Tau extracts were diluted to a tau concentration of 5 ng/µL and mica discs were covered with 10 µL of tau extract for 2 minutes. Afterwards, the discs were washed twice with 100 µL ddH2O and stored protected from light at RT until imaging. Samples were scanned at a Dimension FastScan with ScanAsyst™ AFM (Bruker, Billerica, MA, USA) with a Fastscan-B (Bruker) cantilever in ScanAsyst air mode. Scans were 5 µm x 5 µm in size, with a scan rate of 3.38Hz and 1024 samples/line. After acquisition, images were processed with Research NanoScope software (Bruker) by flattening images and adjusting the z-scale from -10 to 20 nm. Tau fibril length was manually analyzed by measuring the distance between two points in Gwyddion (GPL, free software). For each tau extract 2-3 images were analyzed with 50-200 fibrils measured per image.

In Vitro Tau Seeding in Mouse Primary Neurons

Primary mouse neuronal culture and tau seeding were conducted as described previously[487,507,536]. Pregnant mice were euthanized with CO_2 and hippocampal and cortical tissues (1:1 ratio) were harvested from E17 embryos on ice cold Hibernate E media (#HibernateE, BrainBits, Springfield, IL, USA), digested in 0.05% Trypsin and 1 mg/mL DNase (#DN25, Sigma-Aldrich) in HBSS for 10 min at 37°C. After incubation, neurons were triturated manually into neuronal medium [Neurobasal-A media (Gibco) supplemented with 1x B27, 1 mM sodium pyruvate, 1x GlutaMAX, 100 U/mL penicillin-streptomycin (#15140122, Gibco)] and incubated at 37°C. Dissociated neurons were spun at 250 x g at 4°C for 6 minutes, then resuspended and plated at 50,000 - 75,000 cells/well onto PDL-coated 96-well plates (#354461, Corning) in neuronal medium.

On DIV 7, tau extracts (0.25% (v/v), around 150 ng of tau/well) from human AD brains were seeded into wells. For studies investigating the effect of AZD0530 on tau spreading, 0.5 or 1 μM AZD0530 dissolved in high purity water was also added to the medium. At DIV21, neurons were fixed with ice cold methanol for 30 min on ice and blocked with 10% normal donkey serum and 0.2% Triton X-100 in PBS for 30 min. Afterwards, neurons were incubated with primary antibodies (anti-MAP2 (#4542, CST, 1:150 dilution) and mouse tau (T49) (#MABN827, Millipore Sigma, 1:500 dilution) diluted in 1% normal donkey serum and 0.2% Triton X-100 in PBS overnight at 4°C. The samples were washed three times with PBS and incubated in secondary antibodies (Alexa Fluor donkey anti-mouse or anti-rabbit, Invitrogen, 1:500 dilution) and 0.5 μg/mL DAPI diluted in 1% normal donkey serum and 0.2% Triton X-100 in PBS for 1 h.

Animals

As described in Nies et al. 2021[487], all experiments with mice bred at Yale's animal facility used littermate control mice (C57BL/6J background) with no preference for male or female mice. See Table 3 for details on mice used for each injected cohort. All animals were cared for by Yale's Animal Resource Center until the time of injection (at around 12 weeks of age unless indicated otherwise) and returned there until they were perfused, and tissue was collected. All protocols were approved by Yale's Institutional Animal Care and Use Committee (IACUC). The animals were housed in groups of 2 – 4 animals per cage with *ad libitum* access to food and water. The housing light has a scheduled light period from 7 am to 7 pm and a dark period for the remaining 12 h.

C57BL/6J mice (RRID: IMSR_JAX: 000664) for cohorts injected with Brain A, B, AB, D, Brain D_{conc} or treated with Vehicle or AZD0530 were purchased from Jackson Laboratories (JAX, Bar Harbor, ME, USA) and arrived at 8-9 weeks of age. APPswe/PSEN1ΔE9 mice on a C57BL/6J background had been purchased from JAX (RRID: MMRRC_034832-JAX, Jankowsky et al. 2004[127]) and maintained in our institution's animal facility. Ptk2b$^{-/-}$ mice (RRID: MGI:3584536, Okigaki et al., 2003[539]) on the C57BL6J background after 10 backcrosses were generously provided by Dr. David Schlaepfer (UCSD) and maintained in our institution's animal care facility. Tmem106b$^{-/-}$ mice on the C57BL/6N background were generated previously by a lacZ gene trap strategy[507]. The Tmem106b$^{-/-}$ gene trap line is a hypomorph and expresses 5-10% residual full-length TMEM106B protein[520,526]. Grn$^{-/-}$ mice on a C57BL/6J background (RBRC02370, Kayasuga et al., 2007[540]) were obtained from RIKEN BioResource Center and bred at Yale's animal facility. App$^{NL-F/WT}$ heterozygous KI mice were imported from the RIKEN Institute. In these mice, one allele of the APP gene contains three point mutations to humanize the Aβ

sequence and also the Swedish (KM670/671NL) and Iberian (I716F) mutations[541]. The mice were backcrossed for more than 10 generations to C57BL/6J strain and then expanded to generate homozygous $App^{NL-F/NL-F}$ mice (NLF) and $App^{WT/WT}$ wild type (WT) controls. Subsequently, these homozygous mice were crossed with B6.Cg-Mapt<tm1.1(MAPT)Tcs> (from now on called hTau) KI mice (RBRC09995, Saito et al. 2019[491]) obtained from RIKEN BioResource Center to generate hTau-$App^{NL-F/NL-F}$ mice (DKI).

Stereotactic Surgery on Mice

Mice were injected as previously described[444,487]. For detailed information on animal numbers in injected mouse cohorts, see Table 3.

Briefly, mice received 0.05 mg/kg buprenorphine (Buprenex® Injection, 0.03 mg/mL, Reckitt Benckiser Healthcare Ltd., Hull, UK, diluted 1:10 in sterile PBS before use) 30 minutes before undergoing surgery. They were anesthetized by placing them in an isoflurane (Covetrus, Portland, ME, USA) and oxygen filled chamber and kept in anesthesia with 2-3% isofluorane mixed with oxygen (Quantiflex Low Flow V.M.C., Matrix Medical Inc, Minneapolis, MN; USA). Animals were immobilized in a stereotaxic frame (David Kopf Instruments, Tujunga, CA, USA) and their skull was shaved, followed by disinfecting the incision site three times with 70% ethanol and iodine. An incision of approx. 1 cm length was made on the animals' skull. Human tau extracts were aseptically injected using a Hamilton syringe (#901, Hamilton, Reno, NV, USA) with a 33G needle, 45° tip (#7803-05, Hamilton), controlled by a Micro4TM Microsyringe Pump Controller (World Precision Instruments, Sarasota, FL, USA) at a rate of 0.25 µl/minute under stereotactic guidance at two locations. The first location was in the hippocampus, the other in the overlying cortex (from bregma: anterior-posterior −2.5 mm; medial-lateral 2 mm; dorso-ventral −2.4 mm (for hippocampus) and dorso-ventral −1.4 mm (for cortex)). Each location received 2.5 µl of human tau. The hippocampus was injected first and after each injection there was a waiting period of three minutes to allow the injected solution to permeate into the tissue. After injections were completed, animals were closed with 2-3 surgical sutures (#J310, Synthetic Absorbable Vicryl Suture, Ethicon, Raritan, NJ, USA) and monitored until they regained responsiveness.

For post-operative pain management, animals received 0.05 mg/kg buprenorphine for 3 days (twice daily, 12 h apart) as analgesic, accumulating to a total of six buprenorphine injections per animal. The incision was checked daily for infections and/or pulled stitches, and if necessary, sutures were replaced.

Mouse Brain Tissue Collection and Processing

As previously described[487], six (or nine) months after injection, mice were anesthetized with CO_2 for 45 seconds, followed by transcardial perfusion with 20 mL of ice-cold PBS. Brains were extracted and post-fixed for 48h in 4% PFA. Afterwards, brains were stored in PBS containing 0.05% NaN_3 and sectioned with a vibratome into 40 µm thick coronal sections (#VT1000S, Leica Biosystems, Deer Park, IL, USA). To be able to identify ipsi- and contralateral hemispheres relative to the tau injection after IHC, the contralateral hemisphere received a small incision in the auditory cortex before sectioning.

Table 3: Overview of tau extract injected mouse cohorts.
Numbers in brackets indicate the number of animals analyzed from each group. Table re-printed from JBC, Volume 297, Issue 4, Article 101159, Nies et al. 2021, *Spreading of Alzheimer tau seeds is enhanced by aging and template matching with limited impact of amyloid-ß*, doi: https://doi.org/10.1016/j.jbc.2021.101159 , Figure S1-C,

Cohort	Average Age at injection [months]	Injected Material	Genotype	Male (analyzed)	Female (analyzed)	Combined (analyzed)
WT vs WT cohort	3	Control	WT	6	4	10
		Brain A	WT	6	4	10
		Brain B	WT	5	5	10
		Brain D	WT	5	5	10
		Brain D conc.	WT	5	5	10
WT vs APP/PS1 cohort I	3	Control	WT	4	1	5
			APP/PS1	5 (4)	5 (0)	10 (4)
		Brain A/B	WT	5	5	10
			APP/PS1	5 (3)	5 (3)	10 (6)
WT vs TMEM KO (aged) cohort	19	Control	WT	5 (3)	5 (4)	10 (7)
			TMEM KO	3 (2)	4 (3)	7 (5)
		Brain A/B	WT	5	5 (2)	10 (7)
			TMEM KO	4 (3)	5 (4)	9 (7)
WT vs Pyk2 KO cohort	3	Control	WT	2	3	5
			Pyk2 KO	1	4	5
		Brain A/B	WT	4	2	6
			Pyk2 KO	1	4	5
WT treated with AZD	3	Brain A/B	WT - Vehicle	10	10	20
			WT - AZD	10	10	20
WT vs Progranulin KO cohort	3	Control	WT	1	3	4
			Prgrn KO	5	2	7
		Brain A/B	WT	3	5	8
			Prgrn KO	9	3	12
WT vs APP/PS1 cohort II	3	Control	WT	3	2	5
			APP/PS1	2	2	4
		Control - D54D2	WT	3	2	5
			APP/PS1	2 (0)	2 (1)	4 (1)
		Brain D	WT	3	5	8
			APP/PS1	5 (3)	6 (5)	11 (8)
		Brain D - D54D2	WT	4	3	7
			APP/PS1	3	11 (7)	14 (10)
WT vs hTau vs hTau/NLF cohort	3	Control	WT	2	3	5
			hTau	0	4	4
			hTau/NLF	3	2	5
		Brain A/B	WT	1	3	4
			hTau	1	1	2
			hTau/NLF	3	5	8

Chronic Oral Dose Preparation of AZD0530

N-(5-chloro-1,3-benzodioxol-4-yl)-7-[2-(4-methylpiperazin-1-yl)ethoxy]-5-(tetra-hydro-2H-pyran-4- yloxy)quinazolin-4-amine (AZD0530, saracatinib) was prepared as described previously[487,536]. Mice received a drug dosage of 5 mg/kg per day through purified diet pellets. The drug dosage in the food was calculated to take into account the average amount of food eaten by a mouse in a single day per kg of weight[542]. The compound was incorporated into purified diet pellets by Research Diets, Inc. by dissolving the compound in a solution of 0.5% w/v Hydroxypropylmethylcellulose/ 0.1% w/v polysorbate 80 at 1.429 mg/ml to dose animals chronically. For vehicle pellets, diet pellets were purified with control vehicle solution (without drug).

Immunohistochemistry for Mouse Brain Sections

Fluorescent Staining

Mouse brain sections, unless indicated otherwise, were stained as free-floating sections. They were washed once in blocking buffer [1% BSA + 1% Triton- X in PBS] for 5 minutes, followed by incubation in blocking buffer for 1 h at RT. Sections were then incubated with primary antibodies (anti-amyloid-ß (D54D2) (#8243S, CST, 1:500 dilution), anti-CD68 (FA-11) (#MA5-16674, Invitrogen, 1:250 dilution) and anti-GFAP (#Z0334, DAKO, 1:250 dilution)) in blocking buffer for 48 h – 72 h at 4°C. Afterwards, sections were washed three times for five minutes in blocking buffer or PBS and incubated overnight at 4°C with the appropriate secondary antibodies (donkey anti-mouse or anti-rabbit AlexaFluor 488, 568 or 647, diluted 1:500 in blocking buffer). The next morning, sections were incubated three times for five minutes with PBS, followed by copper sulfate treatment to reduce autofluorescence. For copper sulfate treatment, sections were briefly transferred to ddH_2O, incubated for 15 minutes in copper sulfate solution [10 mM $CuSO_4$, 50 mM ammonium acetate, pH 5], briefly returned to ddH_2O and the incubated in PBS for at least 10 minutes. Afterwards, sections were mounted on microscope slides (#22-178-277, Fisher Scientific, Hampton, NH, USA) and coverslipped with VECTASHIELD Antifade Mounting Medium containing DAPI (#H-1200, Vector Laboratories, Burlingame, CA, USA).

For co-staining of total Aβ and dense core Aβ plaques, Thioflavine S (from now on called ThioS, #T1892-25G, Sigma-Aldrich, used at 0.1% (w/v) in 70% ethanol) staining was performed after sections had been stained for Aβ. Sections were incubated for 15 minutes, followed by two 5 minute washes in 70% ethanol and two 5 minute washes in ddH_2O. Sections were then returned to PBS and mounted as described before.

DAB Immunohistochemistry and Nissl stain

To perform 3,3'-Diaminobenzidine (DAB) Immunohistochemistry for p-Tau Ser202/Thr205 (AT8) the rabbit- specific HRP/DAB (ABC) Detection Kit (#ab64261, Abcam) was used according to manufacturer's instructions with small adjustments. Unless otherwise indicated, all steps were performed at RT. Sections were incubated for 10 minutes in Hydrogen Peroxide Blocking solution, followed by two washes in blocking buffer [1% BSA + 1% Triton-X in PBS] for 5 minutes each. Then, Protein Block solution was applied for 10 minutes, and sections were washed once for 5 minutes in blocking buffer. Afterwards, sections were incubated overnight at 4°C with primary antibody (biotinylated anti-pTau Ser202/Thr205 (AT8) (#MN1020B, Invitrogen, diluted 1:250 in blocking buffer)). The next day, sections were washed four times for 5 minutes in blocking buffer and the biotinylation step of the kit was left out, since the primary

antibody was already biotinylated. Next, Streptavidin Peroxidase solution was applied for 10 minutes, and sections were rinsed four times in blocking buffer afterwards. In the meantime, the DAB staining solution was freshly prepared by mixing 30 µl of DAB Chromogen with 1.5 mL DAB substrate. Sections were incubated with the resulting solution for 3 minutes under constant shaking and rinsed four times in PBS afterwards. Last, sections were mounted on positively charged coverslips (#22-037-246, Superfrost Plus Microscope Slides, FisherBrand, Pittsburgh, PA, USA) and left at RT to dry overnight.

The next day, sections were counterstained with cresyl violet (Nissl stain). Cresyl violet was dissolved at 1 g/L in ultrapure water under stirring overnight. The next day, 2.5 mL glacial acetic acid were added to 1 L of cresyl violet solution and stirred for 15 minutes at RT. The Nissl stain solution was then sterile filtered (0.22 µm filter) and heated to 50°C. Mounted sections were stained for 10 minutes in pre-warmed Nissl solution and then rinsed for 3 minutes in ultrapure water. Next, sections were de-stained for 10 minutes in 95% ethanol, followed by two 5 minute incubations in 100% ethanol. In the end, sections were incubated twice for 5 minutes in xylene and coverslipped with CytoSeal60 (#8310-4, ThermoFisher).

Quantification of Tau Inclusions

The experimenter was blinded to mice genotype and injection paradigm during the staining and data analysis of tau inclusions and other fluorescent stains. DAB-Nissl stained sections were scanned at 20x with an Aperio Scanner (Aperio CS2, Leica Biosystems, Deer Park, IL, USA). Subsequently, sections were exported as TIFs, and all further analysis was conducted in ImageJ/Fiji (open source developed by Wayne Rasband[543]). Channels were separated into a Nissl and DAB stain image through the Color Deconvolution function (parameters: [r1]=0.55554247 [g1]=0.77908224 [b1]=0.29052263 [r2]=0.2969366 [g2]=0.5443869 [b2]=0.78452 [r3]=0.77666026 [g3]=0.31092405 [b3]=0.54783666). Somatic inclusions in different regions were counted manually with the help of the Cell Counter function. Brain regions (see Figure ***7***) were identified based on coronal reference sections from the Allen Brain Atlas (Allen Institute for Brain Science, https://mouse.brain-map.org/static/atlas) in two standardized sections per mouse. For heat maps and somatic inclusion counts, the number of inclusions from both sections were added together when regions were present in both sections (RSA; motor cortex, primary somatosensory cortex, auditory cortex, ecto- and perirhinal cortex, entorhinal cortex and piriform cortex). The temporal association area was included in the counts for the auditory cortex and the amygdalar nuclei were included in the piriform cortex counts. For brain heatmaps, only schematics of Section 2 are shown in the main figures of the paper, since most regions (except dorsal hippocampus) where somatic inclusions were scored are visible. The ipsilateral hemisphere is always displayed on the right.

To analyze the neuritic inclusion burden, ROIs were drawn along anatomical regions on section's Nissl stain, applied to the thresholded DAB stain image and the percent area within the ROI was measured. The pre- programmed "Renyi" threshold was used on all cohorts except the WT vs TMEM106B KO cohort, where the pre-programmed "Default" threshold was used. Sections were thresholding failed were excluded from further analysis. The thresholding to measure the percent area occupied by neuritic inclusion in the hippocampus also recognized the somatic inclusions, but the area of somatic inclusions only constitutes a very small percentage of the measured total area. The number of neuritic plaque tau inclusions was counted manually by searching DAB stains of APP or DKI animals for neuritic deposits surrounding circular, unstained spaces (Aβ plaques).

In addition, higher magnification images of neuritic inclusions were taken on a Zeiss AxioImager Z1 fluorescent microscope (Zeiss, Oberkochen, Germany) with a 63x 1.4 oil-objective.

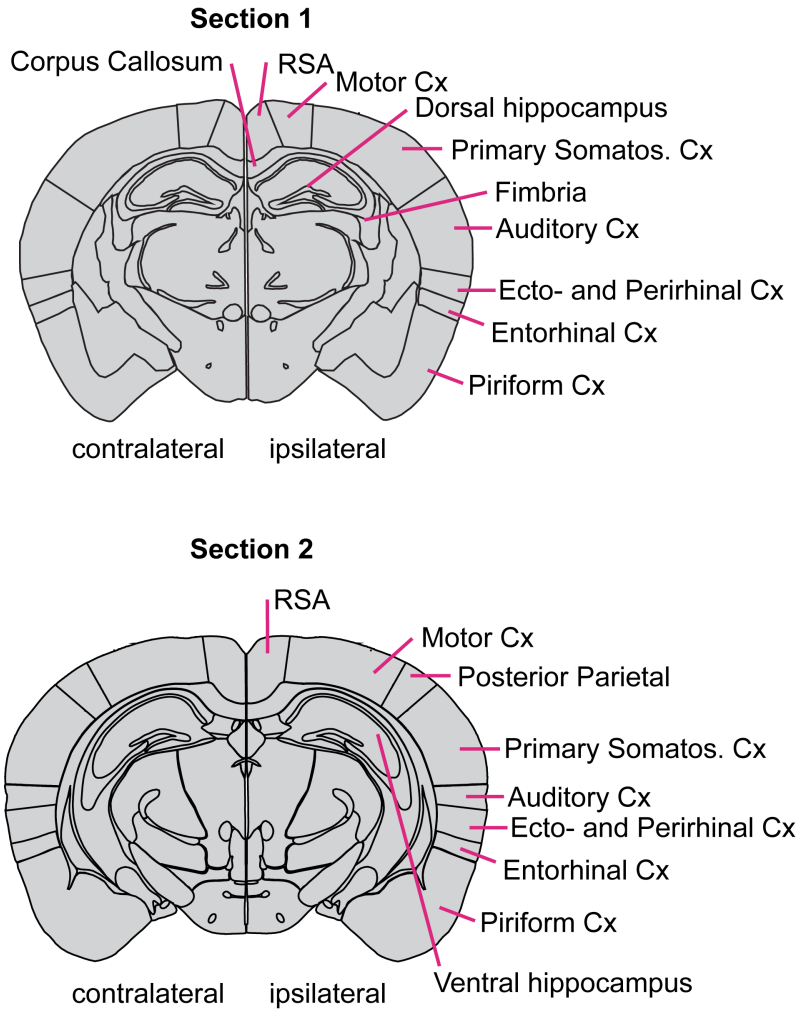

Figure 7: Schematics of analyzed mouse brain sections.
Hippocampal and cortical brain regions were identified based on coronal reference sections from the Allen Brain Atlas. Only schematics of Section 2 are shown in the main figures of the paper. Indicated regions are the ones used for counting somatic and neuritic inclusions. Figure re-printed from JBC, Volume 297, Issue 4, Article 101159, Nies et al. 2021, *Spreading of Alzheimer tau seeds is enhanced by aging and template matching with limited impact of amyloid-ß,* Figure S4, doi: https://doi.org/10.1016/j.jbc.2021.101159, © 2021 Elsevier, with permission from Elsevier under the CC-BY license.

Imaging and Quantification of Fluorescent Staining

For iPSC-derived neuron validation, images were taken with a 63x/1.4 oil-objective on the Leica DMi8 Inverted Fluorescent Microscope (Leica, Wetzlar, Germany). Images shown are maximum z-projections of a z-stack (5 steps, step size: 1 µm).

For in vitro tau seeding assays, images were taken using the automated ImageXpress Micro XLS (Molecular Devices, San Jose, CA, USA) with a 20x air-objective. Each experiment was performed in duplicate and four images were taken per well. With ImageJ/Fiji, MAP2-positive area was identified and masked over the corresponding T49 image. The percent of T49-positive area within the MAP2 mask was calculated.

Images for Aβ (D54D2) and ThioS staining were taken on a Leica DMi8 Inverted Fluorescent Microscope (Leica, Wetzlar, Germany) with a 10x 0.25 air-objective for tiled images of whole

brain sections or 20x 0.4 air- objective for higher magnification images of specific regions. In addition, tiled images of D54D2 and ThioS staining for hTau and DKI animals were taken on a Zeiss AxioImager Z1 fluorescent microscope (Zeiss, Oberkochen, Germany) with a 20x 0.8 air-objective. Images for GFAP and CD68 staining were taken on the same Leica microscope as mentioned above with 20X 0.4 air-objective. All image analysis was conducted using ImageJ/Fiji.

For tiled images of whole brain sections stained with D54D2 antibody and ThioS, ROIs were drawn according to the ThioS image along anatomical brain regions. D54D2 and ThioS stains were thresholded separately and the percent area occupied within each ROI was measured. For higher magnification images of D54D2 and ThioS stained section, images were converted to 8-bit, thresholded in each channel and the percent area was measured.

Images of cells stained for GFAP or CD68 were thresholded, followed by measuring the percent area occupied (for GFAP: objects above 15 and below 10.000 pixels were included, for CD68: objects above 5 and below 750 pixels in size were included).

SDS-Page and Western Blotting

All samples were heated for 5 min at 95°C prior to loading. Sodium dodecyl sulphate–polyacrylamide gel electrophoresis (SDS-Page) was performed by loading samples on 24-well 4-20% Criterion TGX Precast Gels (Bio-Rad) and running them in 1x Tris/Glycine/SDS Running Buffer (#1610772, Bio-Rad) for 45 minutes at 180 V.

For Western Blotting, proteins were transferred onto nitrocellulose membranes (iBlot2 Gel Transfer Device with #IB23001, iBlot2 NC Regular Stacks, Invitrogen) and blocked for 1 h at RT with blocking buffer (#MB-070-010F, Blocking Buffer for Fluorescent WB, Rockland). Afterwards, membranes were incubated overnight at 4°C with primary antibodies (1:1000 dilution in blocking buffer, see specific applications for primary antibodies). The next day, membranes were washed three times for 5 minutes in Tris-Buffered Saline + 0.1% Tween 20 Detergent (TBST), followed by incubation with secondary antibodies (donkey anti-mouse 680 or donkey anti-rabbit 800, diluted 1:10.000 in TBST, LI-COR Biosciences, Lincoln, NE, USA) for 1h at RT. Blots were washed again three times for 5 minutes in TBST and then imaged on an Odyssey Infrared Imaging System (LI-COR Biosciences, Lincoln, NE, USA). Densitometric quantification of protein bands was performed with Image Studio Lite (LI-COR Biosciences, Lincoln, NE USA).

Immunoprecipitation of Aβ from Tau Samples

Control Brain and Brain D tau extracts were thawed on ice and a sample to estimate the initial tau and Aβ concentration via Western blot was taken. Pure Proteome Protein G Magnetic Beads (#LSKMAGG10, Millipore, Burlington, MA, USA) were conjugated to either Rabbit IgG antibody (#2729, CST, Danvers, MA, USA) or β-Amyloid (D54D2) XP® Rabbit mAb (#8243, CST) according to manufacturer's instructions in PBS + 0.02% Tween 20 (PBST). For each 100 µL of tau extract, 25 µL of beads were conjugated to 1 µg of antibody. Extracts were incubated with beads overnight at 4°C under nutation. The next day, extracts were removed from beads, transferred to a new Eppendorf tube and a sample was taken to assess tau and Aβ concentration after clearing. Beads were washed three times in 200 µL PBS and bound protein was eluted by incubating beads for 10 minutes at 95°C with 1x Laemmli sample buffer (1/3 of initial sample volume, samples E1). After this first round of immuno-depletion, there was still Aβ present in the tau extracts, as well as residual antibody. To further reduce the amount of Aβ

in the samples, the process described above was repeated, but with a reduced amount of antibody (1/4 of the previous amount). After the extracts had incubated overnight with antibody-conjugated beads, the tau extracts were transferred to new Eppendorf tubes and to remove residual antibody, incubated with unconjugated Pure Proteome Protein G Magnetic Beads for 2 h at 4°C under nutation. In the meantime, the antibody-conjugated beads were eluted once more as described above (samples E2). After 2 h, the tau extracts were removed from the beads and a sample was taken for analysis. The beads of the third incubation were eluted again as described above (sample E3). The remaining tau extract was stored at 4°C until injection into mice the next day. The decrease in monomeric and oligomeric Aβ as well as total tau was measured by densitometric analysis using ImageStudio Lite (LI-COR Biosciences) by averaging the ratios of cleared/untreated extract band intensity per dilution.

Statistical Analysis

Figures were prepared using Adobe Illustrator CC (Adobe Inc., San Jose, California). All statistical analysis and graphing of data was conducted using GraphPad Prism 9 (GraphPad Software Inc, San Diego, CA, USA). One-way ANOVA with Tukey's multiple comparisons test, Kruskal-Wallis with Dunn's multiple comparisons test, Brown-Forsythe ANOVA test with Dunnett's multiple comparisons test or Two-way ANOVA with Sidak's multiple comparisons test were performed as indicated in figure legends. A $p<0.05$ was considered statistically significant and all values are displayed as mean ± S.E.M unless otherwise indicated in the figure legends. All n-values refer to individual mice unless indicated otherwise.

Results

Parts of the results of this thesis have been previously published in Nies et al. 2021[487] (all mouse data), Tang et al. 2020[536] and Brody et al. 2022[544] (parts of the *in vitro* data in HEK-293T cells). Figures that have been reproduced fully or in part from these publications are marked as such in the figure legends. The text describing Figures 13- 23 has been adapted from Nies et al. 2021[487].

Pyk2 activates GSK3ß in HEK293T cells and in in vitro kinase assays as well as increases GSK3ß-dependent Tau phosphorylation

Binding kinetics of GSK3ß with either Pyk2 (Figure 8, A) or Fyn (Figure 8, B) were assessed by conducting in vitro kinase assays. To determine Pyk2, Fyn and GSK3ß concentrations in mouse brains (Figure 8, C), hippocampus and cortex of two mice brains were lysed, immunoblotted, and compared to a dilution curve of BSA standards. For the in vitro kinase assays, physiologically relevant concentrations of Pyk2 or Fyn, (40 nM and 25 nM respectively, determined from mouse hippocampus and cortex, Figure 8, C) were incubated with varying GSK3ß concentrations for 30 minutes and phosphorylation levels of GSK3ß at Y216 were assessed through densitometric analysis of western blotted reactions. Fitting Michaelis-Menten kinetics was tested, and curves showed good fit with experimental results (R^2 = 0.9489 and R^2 = 0.8760 respectively). K_M = 416.5 nM for GSK3ß-Pyk2 and K_M = 25.64 nM for GSK3ß-Fyn interaction were calculated, indicating that the K_M measured for Pyk2-GSK3ß interaction was close to physiological concentrations of GSK3ß measured in mouse brains (378 nM).

To further investigate the interaction of Pyk2 and GSK3ß, GFP-tagged Pyk2 and GSK3ß were transfected into HEK-293T cells and GSK3ß was co-immunoprecipitated by trapping the GFP-tag of GFP-Pyk2 (Figure 8, D). GSK3ß successfully co-immunoprecipitated with GFP-Pyk2, while a minimal background band was seen if GFP alone was co-transfected with GSK3ß. Unfortunately, further characterization of the binding domains on Pyk2 and GSK3ß was not possible, because constructs of Pyk2 domain deletions expressed at highly variable levels and made differentiating GSK3ß binding from background levels of GSK3ß present in GFP only transfected cells impossible (data not shown).

To assess phosphorylation of our proteins of interest in cells, different combinations of Pyk2, Fyn, GSK3ß and tau were transfected and over-expressed in HEK-293T cells (Figure 8, E-G). Analysis of western blotted cell lysates revealed that Pyk2 alone was able to increase activation of GSK3ß (phosphorylation on Y216) three-fold. Cells expressing GSK3ß and Fyn without the presence of Pyk2 only saw a non-significant increase in GSK3ß Y216 phosphorylation, but co-expression of all three kinases led to a synergistic effect on GSK3ß activation (Figure 8, F). When monitoring phosphorylation of tau at pS202/T205 (AT8), GSK3ß proved necessary to achieve a significant increase in pTau AT8 phosphorylation. In accordance with GSK3ß phosphorylation levels, expressing Pyk2, GSK3ß and tau led to a three-fold increase in pTau AT8 phosphorylation, while expressing Fyn, GSK3ß and tau failed to increase pTau AT8 phosphorylation levels and co-expressing all proteins led to the greatest increase in pTau AT8 phosphorylation (Figure 8, G). Overall, this data suggested that Pyk2 and GSK3ß can interact both *in vitro* and when overexpressed in HEK-293T cells, while Fyn-GSK3ß interaction was theoretically possible *in vitro* but had no relevance in the over-expression model.

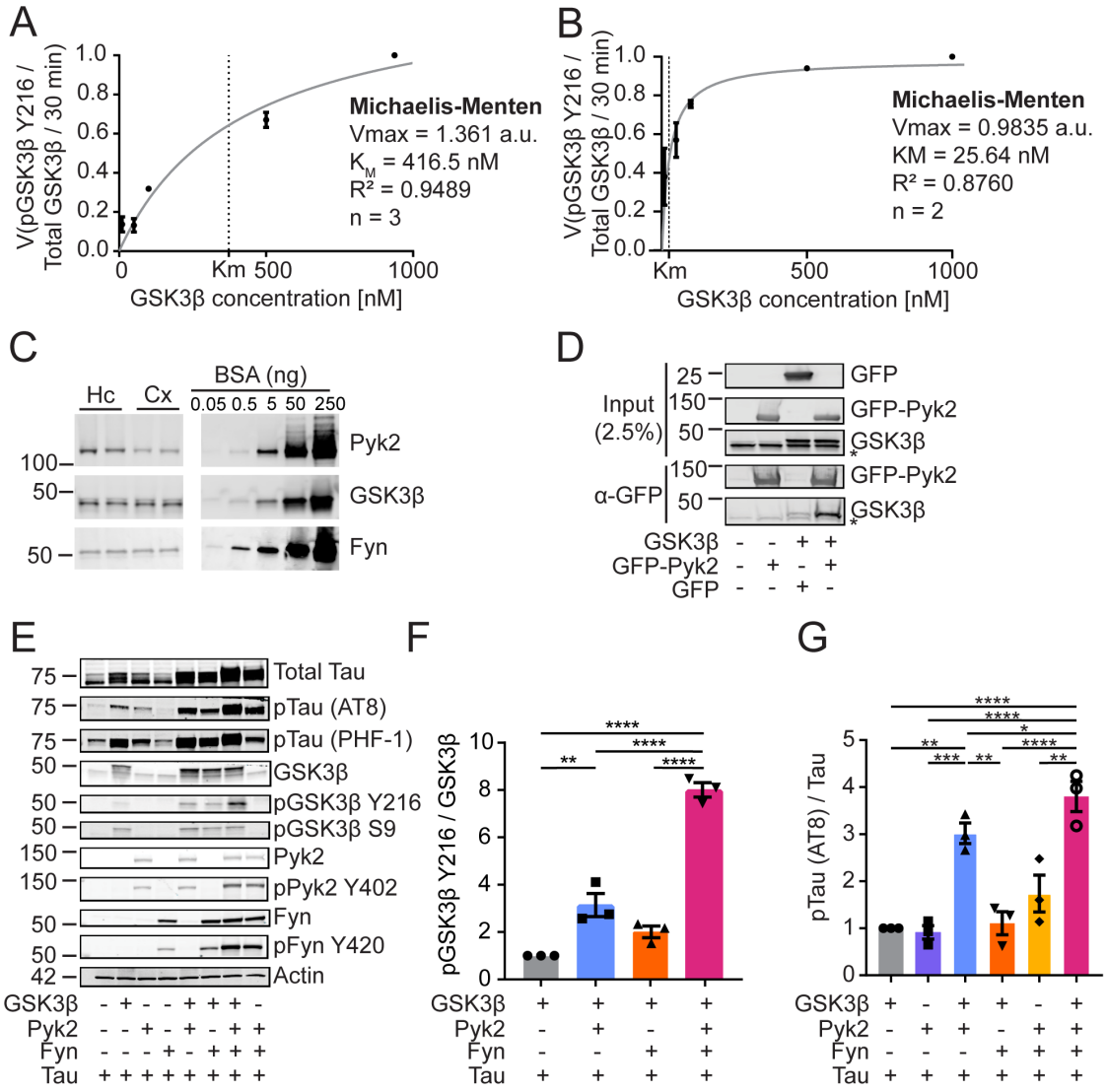

Figure 8: Pyk2 phosphorylates tau via GSK3β in a HEK293T over-expression system and in in vitro kinase assays. A-B) In vitro kinase assays of GSK3ß with Pyk2 **(A)** or Fyn **(B)**. Samples were obtained after 30 minutes of reaction time by adding Laemmli buffer to each reaction. Samples were separated by SDS-PAGE, Western Blotted and densitometric measurements of pGSK3ß Y216 / GSK3ß were graphed. Michaelis-Menten kinetics provided best fit for the data. **C)** Determining physiological levels of Pyk2, GSK3ß and Fyn in mouse hippocampus (Hc) and cortex (Cx). Mouse brain lysates and a BSA dilution curve (5 µL/lane) were immunoblotted and densitometric measurements were taken. Pyk2 concentration was measured to be 58 nM in the Hc and 24 nM in the Cx. GSK3ß concentration was measured to be 410 nM in the Hc and 346 nM in the Cx. Fyn concentration was measured to be 26.44 nM in the Hc and 23.9 nM in the Cx. **D)** Co-Immunoprecipitation of GFP-Pyk2 and GSK3β from transfected HEK-293T cells. GFP-trap beads were used to capture GFP-Pyk2 and lysates were probed for the presence of GSK3β. GSK3β was observed in the presence of GFP-Pyk2, but not GFP alone (* marks an unspecific band). **E)** HEK-293T cells were transfected with combinations of the proteins indicated, lysates were separated via SDS-PAGE and Western Blotted. Representative immunoblot images of transfected HEK-293T cells. **F-G)** Quantification of A. **(F)** Co-expression of Pyk2 and GSK3ß led to a significant increase in phosphorylation/activation of GSK3ß on Y216. This increase was further augmented by the co-transfection of Fyn with GSK3β and Pyk2. **(G)** The phosphorylation of tau at S202/T205 (AT8) normalized to total tau (HT7) was significantly increased when co-transfected with GSK3β and Pyk2, but not when co-transfected with either kinase alone. No further increase in normalized AT8 signal was observed when tau, Pyk2 and GSK3β were co-transfected with Fyn. Statistics: One-way ANOVA followed by Tukey's multiple comparisons test, *p<0.05, **p<0.01, ***p<0.001, ****p<0.0001, n = 3. Data for E-G has been previously published in Brody et al. 2022[544] and was generated by Fulin Guan (see contributions statement). Modified panels were re-printed from Molecular Neurodegeneration, Volume 17, Issue 32, Pages 1-33, *Alzheimer Risk Gene Product Pyk2 Suppresses Tau Phosphorylation and Phenotypic Effects of Tauopathy,* doi: https://doi.org/10.1186/s13024-022-00526-y , Figure 1, ©2022 BMC, with permission from BMC under the CC-BY license..

Fyn inhibition decreases Fyn-Tau interaction in a HEK-293T cell overexpression model and Tau seeding in mouse neurons

In addition to studying the combined interactions of Pyk2, Fyn and GSK3ß with one another and on tau, we wanted to ascertain the role of Fyn on tau independent of GSK3ß. This was important as Fyn had been reported to be tethered to post-synaptic densities (PSDs) through its interaction with tau[161,204,293] and to phosphorylate tau on certain residues independent of GSK3ß in AD[207,291,292].

To study Fyn-Tau interaction, both proteins were co-transfected into HEK-293T cells and three hours later treated with either nothing, vehicle (DMSO) or 2 μM AZD0530 (AZD). Cells were fixed 24 h after transfection and immunohistochemistry for both proteins as well as a proximity ligation assay (PLA) were performed (Figure 9, A-E). Upon treatment with AZD, Fyn-tau PLA signal decreased by approximately 45% compared to untreated or vehicle treated cells (Figure 9, A-B), while tau and Fyn expression were not significantly altered regardless of treatment (Figure 9, B-C). Furthermore, cells transfected with tau alone showed no background signal for Fyn-tau PLA, confirming the assay's specificity (Figure 9, E). These results indicated that inhibiting Fyn activity reduced the physical proximity of Fyn and tau in this overexpression model. It suggested that both roles Fyn takes on with tau, as a binding partner and kinase, might be disrupted when Fyn activity is diminished.

To investigate the effects of Fyn inhibition on tau seeding, mouse primary neurons were seeded for 14 days with tau extracted from non-diseased (Control) or AD human brains (Figure 9, F-I, further characterization of tau extracts is presented in Figure 13). In addition, for the duration of tau exposure, neurons were either left untreated, treated with water (vehicle), 0.5 μM or 1 μM AZD0530. Cells were fixed and immunohistochemistry with a mouse tau specific antibody was performed to only assess seeded, endogenous mouse tau and not added, human tau (Figure 9, G). Mouse tau seeding within total neuron area (measured by MAP2 staining) was quantified and upon AZD treatment, tau seeding was 40-50% reduced (Figure 9, H-I). This level of inhibition was in accordance with the decrease in Fyn-tau proximity observed earlier in the PLA assay and provided further evidence that decreased Fyn activation might also decrease tau pathology. However, most of our *in vitro* data so far had originated from an over-expression system in HEK-293T cells, so we wanted to expand on this data in a more relevant model system, human iPSC-derived neurons.

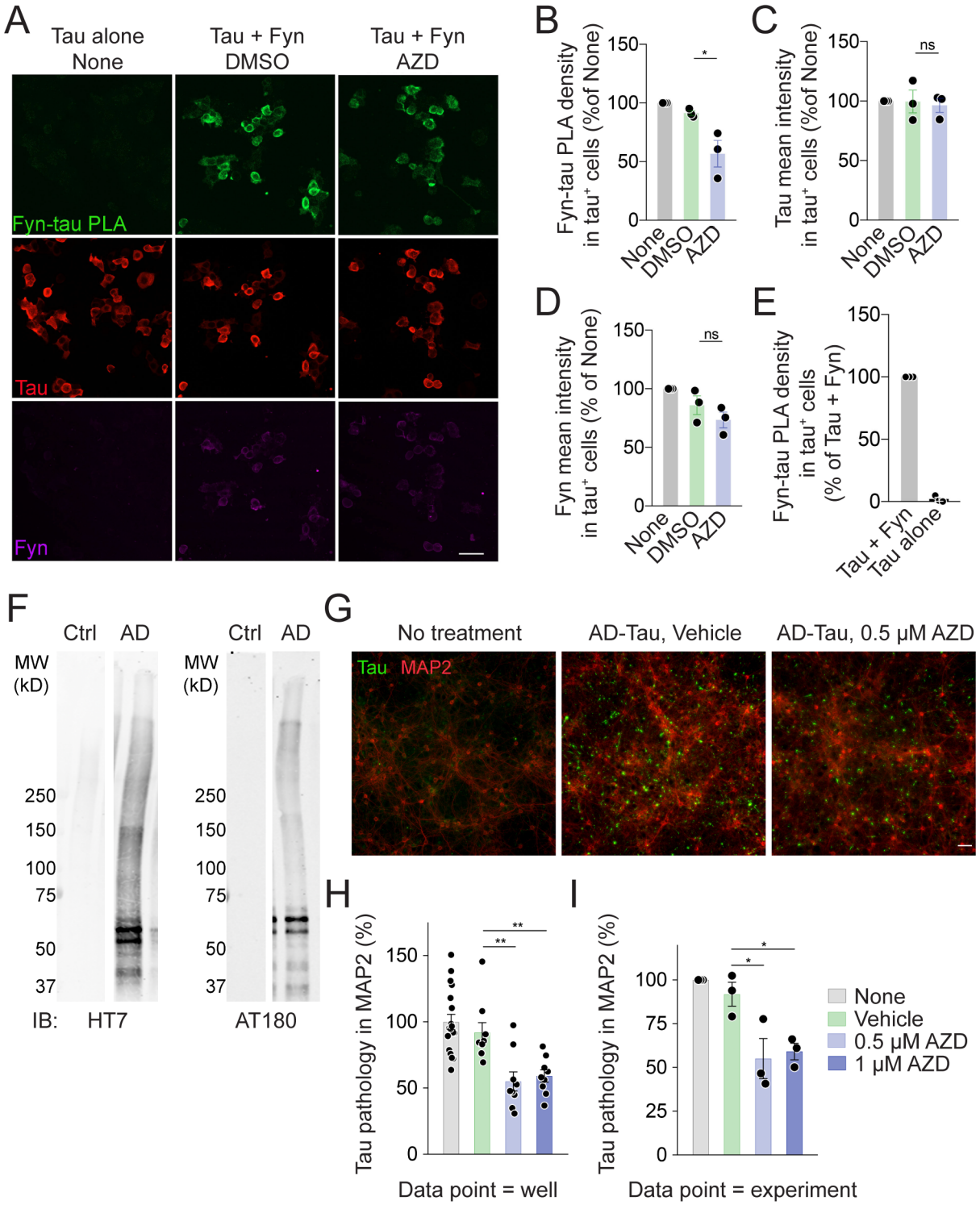

Figure 9: Inhibiting Fyn decreases Tau-Fyn interaction in HEK-293T cells and tau seeding in primary mouse neurons.

A-E) Proximity Ligation Assay (PLA) in HEK-293T cells overexpressing human Fyn and tau. Cells were treated for 24h with either 2 µM AZD0530 (AZD) dissolved in DMSO or Vehicle (DMSO). For B-E): each point represents the average of four images taken per experimental condition, N=3 and statistics performed were unpaired t-test. **A)** Representative immunofluorescent images, with Fyn-Tau PLA signal in green, tau-positive areas in red and Fyn-positive areas in magenta. Scale bar: 20 µm. **B)** Quantification of the area of Fyn- Tau PLA density within tau-positive area of HEK-293T cells expressing human Fyn and tau, normalized to the condition with no treatment. *$p < 0.05$. **C)** Quantification of mean intensity of tau within tau-positive area of HEK-293 T cells, normalized to the condition with no treatment. **D)** Quantification of mean intensity of Fyn within tau-positive area of HEK-293 T cells, normalized to the condition with no treatment. **E)** Quantification of the percent Fyn-Tau PLA density in HEK-293T cells expressing only human tau in tau-positive cells, normalized to the percent PLA density in tau- and Fyn-

transfected HEK-293T cells. **F)** Representative blots of tau extracts from human AD patient and a healthy control using HT7 (total tau) and AT180 (Tau pThr231) antibodies to show tau bands between 50 and 75kD. **G-I)** Mouse primary neurons were treated with human tau at DIV7, cultured until DIV21 and fixed with ice-cold methanol. **G)** Representative images of MAP2 and tau (endogenous mouse tau) immunostaining. Left panel shows neurons with no AD-tau seeding nor treatment. Middle panel shows neurons with AD-tau seeding and treatment with vehicle (water). Right panel shows neurons with AD-tau seeding and treatment with 0.5 µM AZD0530. **H-I**) Quantification of percentage of mouse tau-positive area within MAP2-positive area. Neurons were either not seeded with tau; only seeded with AD-tau; seeded with AD-tau and treated with water as vehicle; seeded with AD-tau and 0.5 µM AZD, or seeded with AD-tau and 1 µM AZD. The background signal from images of neurons without AD-tau treatment was subtracted. Experiments were performed in triplicate. Each data point represents the average of values obtained from four images taken from one well **(H)** or the average of three wells of each condition from one experiment **(I)**. **H)** N = 9–18 per experimental condition. **p < 0.01; One-way ANOVA with Dunnett's multiple comparisons test. **I)** N = 3. *p < 0.05; Repeated measures one-way ANOVA with Dunnett's multiple comparisons test. Modified figures were re-printed from Acta Neuropathologica Communications, Volume 8, Issue 1, Article 96, Tang et al. 2020[536], *Fyn kinase inhibition reduces protein aggregation, increases synapse density and improves memory in transgenic and traumatic Tauopathy,* doi: https://doi.org/10.1186/s40478-020-00976-9 , Figures 4E-I and 6, ©2020 Springer Nature, with permission from Springer Nature under the CC-BY license.

Validation of human iPSC-induced neuron culture

To further investigate the interactions of Pyk2, Fyn, GSK3ß and Tau *in vitro*, but without the caveat of using an over-expression model, differentiation of two different iPSC lines into neurons was established. The first cell line was commercially available from Gibco (called "Gibco" throughout the thesis) and underwent no additional modifications after reprogramming. These cells were differentiated into cortical neurons according to a previously published protocol[534] using dual SMAD inhibition and kept in culture for at least 65 days before experiments were conducted. The second cell line was kindly provided by Martin Kampmann at UCSF (i3N cell line[535]). This cell line was generated from the WTC11 line through insertion of doxycycline-inducible mouse NGN2 at the AAVS1 locus and additional insertion of a pC13N-dCas9-BFP-KRAB cassette at the CLYBL intragenic safe harbor locus[535]. Accordingly, these cells were differentiated into cortical neurons with a protocol using doxycycline[535] and experiments were conducted after at least 28 days of neuronal culture.

Before mechanistic experiments were started, confirmation of APOE genotype and validation of the neurons was conducted. For APOE genotyping, DNA was extracted from iPSC and Real Time quantitative PCR was performed according to a previously published protocol[538]. Both cell lines showed amplification and markedly earlier Cq for the APOE3 probe (Figure 10, A, C), while the internal control (ACTB) showed similar Cq and amplification for all three APOE probes and the negative control (water) did not show any amplification (Figure 10, A-C).

Next, it was determined if all proteins relevant to our signaling cascade of interest were expressed at DIV28-45 for i3N and at DIV50-65 for Gibco neurons (Figure 10, D-E). Neurons from both cell lines expressed the proteins of interest, only total Pyk2 and pPyk2 Y402 levels were sometimes difficult to reliably detect. To assess the synaptic connections in both cell lines, neurons were fixed and stained for MAP2, PSD-95 and synaptophysin (Figure 10, F-G). Neuronal cultures showed a dense network of neuronal processes and PSD-95 and synaptophysin puncta were shown to overlap, suggesting the formation of synapses.

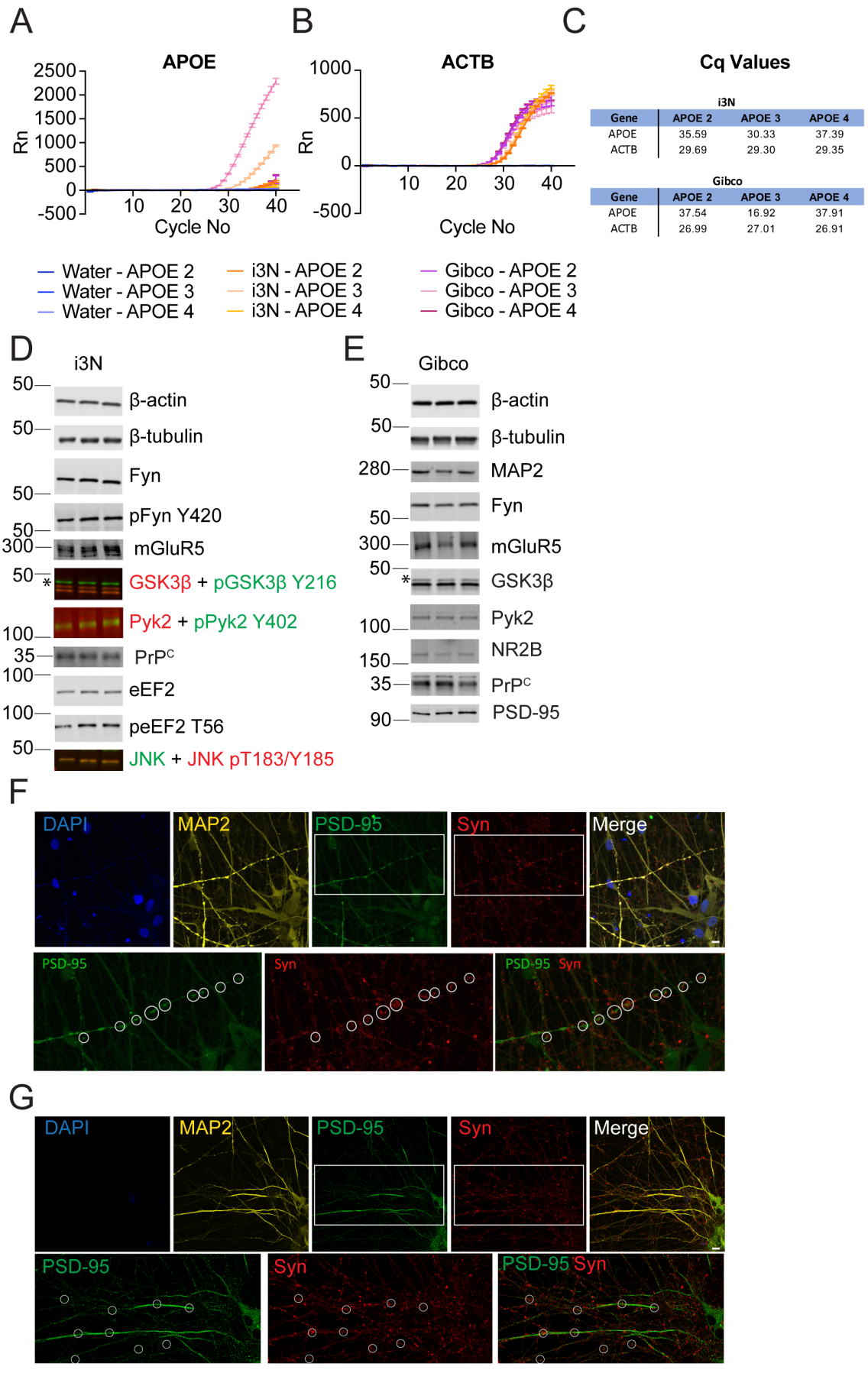

Figure 10: Validation of iPSC-derived neurons reveals that they have APOE 3 genotype and express all relevant proteins of interest after DIV46 (i3N) and DIV60 (Gibco).

A-C) APOE allele genotyping via RT-qPCR in i3N and Gibco cell lines with n = 4 samples/condition. Fluorescent signal for APOE **(A)** and internal control ACTB **(B)** were measured, and Cq values calculated **(C).** Fluorescent curves and Cq values suggest APOE 3 genotype for both cell lines. **D-E)** Immunoblots to evaluate expression of proteins of interest in iPSC-derived neurons from i3N **(D)** and Gibco **(E)** cell lines. Cells were lysed in RIPA + 1% SDS and lysates from two wells pooled to increase sample volume. i3N neurons were DIV 28 (for mGluR5 and PrP^C) or DIV 46 upon harvest, Gibco neurons were DIV 50 or DIV 65 (for mGluR5, NR2B and MAP2), N = 3 replicates. **F-G)** Gibco iPSC-derived neurons at DIV 95 **(F)** and i3N iPSC-derived neurons at DIV 60 **(G)** show colocalization of post- and pre-synaptic markers. Top row: DAPI (blue), MAP2 (yellow), PSD-95 (green), synaptophysin (red) and merged image, scale bar : 10 μm. Bottom row: zoom of white boxes shown in top panel images. White circles indicate synaptic colocalization of PSD-95 (green) and synaptophysin (red). Scale bar: 10 μm.

Pharmacologically inhibiting Pyk2 and Fyn in iPSC-derived neurons shows no effect on GSK3ß phosphorylation and potentially even increases Tau phosphorylation

Gibco neurons were treated either for four days (Figure 11, A-H) with 1 μM of Pyk2 inhibitor PF-719, 1 μM of Fyn inhibitor AZD-0530 (AZD), 1 μM of both inhibitors or an equivalent amount of vehicle (DMSO), to determine if the phosphorylation patterns observed in the HEK-293T overexpression model between Fyn, Pyk2, GSK3ß and tau were consistent in this more physiologically relevant model system.

Fyn activation (measured as phosphorylation on Fyn pY420 normalized to total Fyn levels) was around 20% decreased upon treatment with PF-719 and about 50% decreased when treated with AZD or both inhibitors combined (Figure 11, B), suggesting effective inhibition of Fyn. In contrast, Pyk2 inhibition upon inhibitor treatment was less clear cut and showed considerable amounts of variability, likely due to low signal intensity. Other commercially available antibodies were tested but did not improve signal intensity. There was a trend for decreases of Pyk2 activation upon inhibitor treatment, but they remained non-significant (Figure 11, A, C). When monitoring GSK3ß activation and phosphorylation of tau at different epitopes (AT180, pY18, AT8 and PHF-1), neither GSK3ß nor tau epitopes AT180 and pY18 showed changes in phosphorylation levels (Figure 11, A, D-F). This was surprising, especially because tau pY18 has been previously reported to be a direct phosphorylation target of Fyn. In addition, tau epitopes AT8 and PHF-1 even showed an unexpected, non-significant increase in phosphorylation upon Fyn and Pyk2 inhibition (Figure 11, A, G-H).

To further investigate if a higher dosage or shorter time frame would inhibit Pyk2 more effectively and improve variability, Gibco neurons were treated for 2 hours with 0.5 μM, 1 μM or 2 μM of PF-719 or vehicle (DMSO) equivalent in volume to the highest inhibitor concentration (Figure 11, I-M). With the highest dose of PF-719, a significant decrease in Pyk2 activation of about 40% could be detected (Figure 11, I-J). At the same time, GSK3ß activation still showed no changes upon inhibitor treatment, confirming the data obtained from the four day inhibitor treatment experiment. Interestingly, the trends observed for pTau AT8 and PHF-1 were also confirmed, with all concentrations of Pyk2 inhibitor treatment showing significant increases in phosphorylation at these two tau epitopes (Figure 11, I, L-M).

Overall, this experiment contradicted the results obtained from previous experiments in over-expression systems. It suggests that the interaction of Pyk2, Fyn, GSK3ß and tau in human cortical neurons is different and potentially involves additional interaction partners that lead to a differential effect of Pyk2 and Fyn on tau and GSK3ß phosphorylation. So far, the existence and identity of these potential interaction partners remains unclear, but the physiological relevance of the increase of tau phosphorylation upon Pyk2 inactivation was further supported by animal studies conducted by my colleague Harrison Brody[544], where Pyk2 KO animals crossed with PS19 transgenic mice also showed increases in tau hyperphosphorylation.

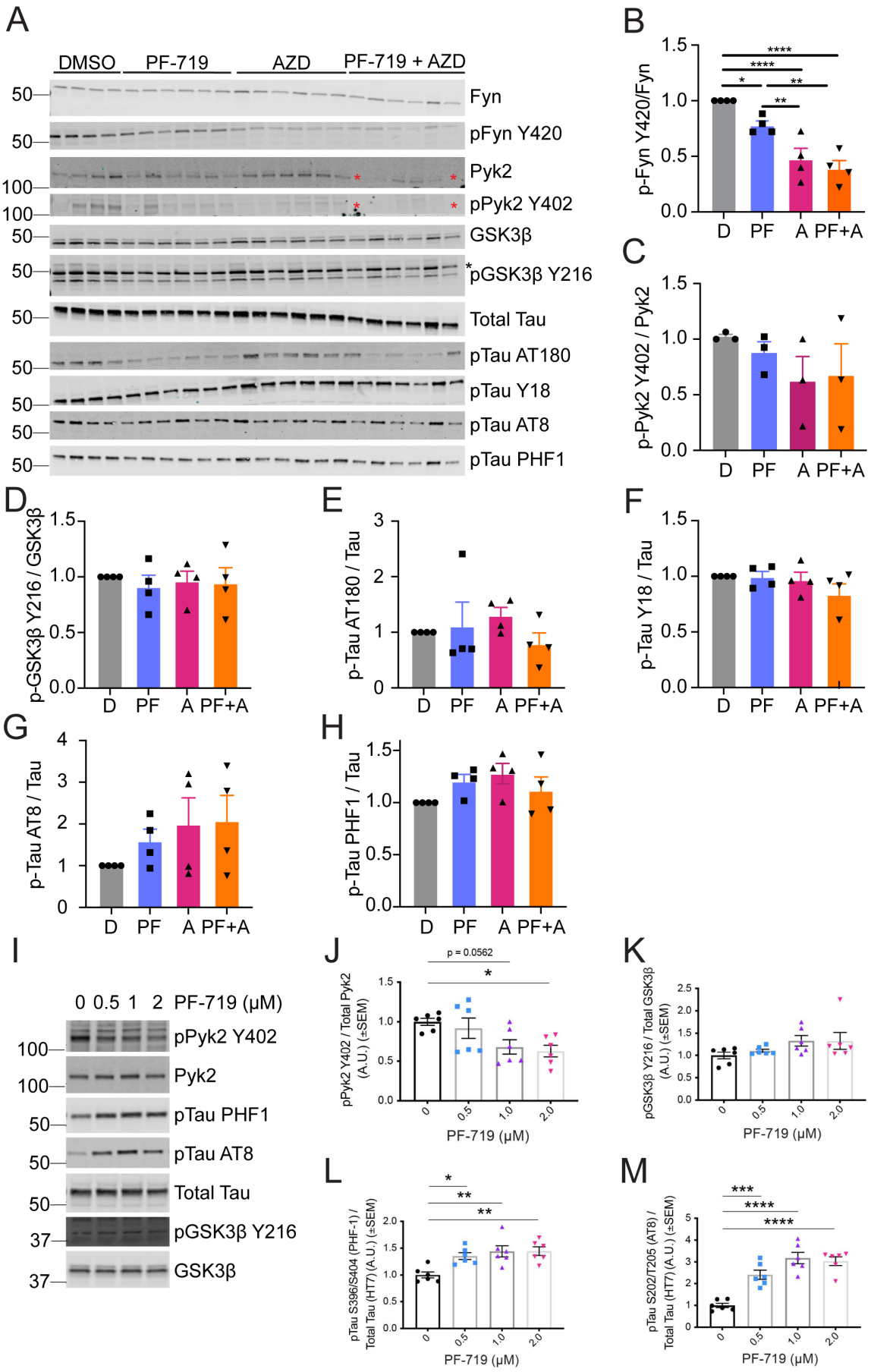

Figure 11: Inhibiting Pyk2 or Fyn in iPSC-derived neurons has no effect on GSK3ß and does not decrease tau phosphorylation.

Gibco iPSC-derived neurons at DIV 65-75 were treated for 4 days at 37°C with either Control (D), 1 μM PF-719 (PF), 1 μM AZD-0530 (A) or 1 μM of both inhibitors. Cells were harvested in RIPA + 1% SDS and changes in phosphorylation were evaluated through densitometric analysis of Western Blots. **A)** Representative images of immunoblots for relevant epitopes. Red asterisks indicate not quantified bands. **B-H)** Quantification of phosphoepitopes over total protein for Fyn **(B)**, Pyk2 **(C)**, GSK3ß **(D)**, pTau AT180 **(E)**, pTau Y18 **(F)**, pTau AT8 **(G)** and pTau PHF1 **(H)**. N = 3-4 experiments, with 4-6 replicates per treatment condition. Statistics: One-way ANOVA with Tukey's multiple comparisons test, *p<0.05, **p<0.01, ***p<0.005, ****p<0.0001. **I-M)** Gibco iPSC-derived neurons were treated for 2 hours at 37°C with Control (DMSO) or different concentrations (0.5 μM, 1 μM or 2 μM) of PF-719. After treatment, samples were processed as described for A-F). **I)** Representative immunoblot images. **J-M)** Quantification of I). PF-719 treatment significantly inhibited Pyk2 activity (pPyk2 Y402 normalized to total Pyk2) **(J)**, while no changes in GSK3β activity (pGSK3β Y216 normalized to total GSK3β) were observed at any concentration of PF-719 **(K)**. Pyk2 inhibition resulted in increased levels of tau phosphorylation at S396/S404 (PHF-1) normalized to total tau **(L)** and S202/T205 (AT8) normalized to total tau **(M)** at every concentration of PF-719 administered. Statistics: One-way ANOVA with Dunnett's multiple comparisons test, *p<0.05, **p<0.01, ***p<0.001, ****p<0.0001, n = 6. For **I-M)** Modified figures were re-printed from Molecular Neurodegeneration, Volume 17, Issue 32, Page 1-33, Brody et al. 2022[544], *Alzheimer Risk Gene Product Pyk2 Suppresses Tau Phosphorylation and Phenotypic Effects of Tauopathy,* doi: https://doi.org/10.1186/s13024-022-00526-y, Figures 2E-I, ©2022 BMC, with permission from BMC under the CC-BY license.

Long-term exposure of iPSC-derived neurons to synthetic Aßo reduces synaptic density, but short-term exposure does not activate kinases downstream of PrP^C-mGluR5 signaling

In addition to studying kinase interactions in iPSC-derived neurons when they were inhibited, I was interested to model kinase responses in the context of AD. For this purpose, neurons were incubated with synthetic Aßo (sAßo) for either seven days (long-term) to study responses on synaptic density (Figure 12, A-B) or for 30 minutes (short-term) to observe, if the signaling cascade downstream of Aßo binding to PrP^C, that caused mGluR5 activation and subsequent Fyn and Pyk2 phosphorylation in mouse neurons, was also activated in iPSC-derived neurons (Figure 12, C-H).

For the long-term exposure, neurons were treated with 0.1 μM, 0.3 μM or 1 μM of sAßo or equivalent volume of vehicle for seven days, then fixed and stained for MAP2 as well as PSD-95 to measure synaptic density normalized to MAP2 area (Figure 12, A-B). The highest treatment group showed a 30% decrease in synaptic density, while the other treatments showed no significant effect (Figure 12, B). Thus, long-term exposure of iPSC-derived neurons to sAßo recapitulated synaptic damage seen previously in cortical mouse neuronal cultures.

In contrast, when exposing iPSC-derived neurons for short periods of time to sAßo and lysing cells afterwards to study kinase activation downstream of sAßo-PrP^C-mGluR5 signaling, consistent activation of either Fyn, Pyk2 or GSK3ß could not be observed (Figure 12, D-F). Furthermore, other kinases reported to be activated downstream of this signaling cascade like eEF2 or JNK also failed to show activation (Figure 12, C, G-H). There are several potential reasons for our failure to observe the activation of these kinases in iPSC-derived neurons in response to sAßo treatment, ranging from too rapid dephosphorylation of our kinases of interest, to the wrong timepoint to analyze cells after treatment or the specificity of our sAßo preparation. Further experiments (see Discussion) will be required to determine the cause for these results that differ from previously published results from mice *in vivo* and mouse primary neuronal cultures *in vitro*.

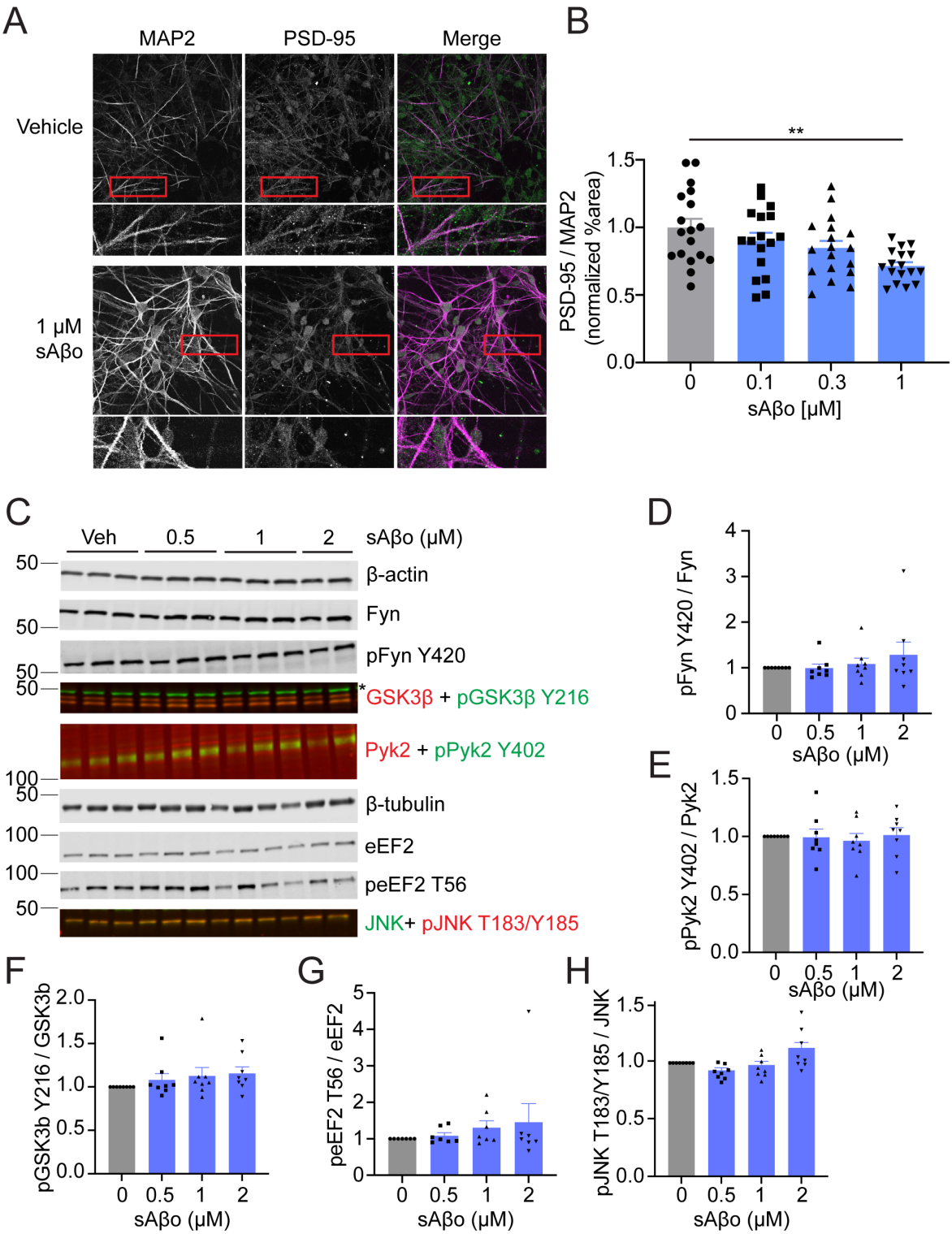

Figure 12: Exposing iPSC-derived neurons for seven days to synthetic Aßo reduces PSD-95 levels, but short-term exposure for 30 minutes has no impact on kinase activation downstream of PrP^C-mGluR5-Fyn signaling. **A-B)** Treating Gibco neurons at DIV 64-76 for 7 days with vehicle or sAßo at 0.1 µM, 0.3 µM or 1 µM. Treatment with 1 µM caused reduction in the %area of PSD-95 puncta. Cells were fixed with 4% PFA and immunostained for PSD-95 (green) and MAP2 (purple). **A)** Representative images of vehicle and 1 µM sAßo treated cells. Red boxes indicate enlarged area shown underneath each picture. **B)** Quantification of A), showing % area of PSD-95 normalized to %area of MAP2 and Vehicle treated group average. N = 3 experiments with 3 coverslips treated per condition and 4 images taken per coverslip, data points shown are averages per coverslip. Statistics: One-way ANOVA with Tukey's multiple comparisons test, **p<0.01. **C-H)** i3N neurons at DIV 28-104 were treated for 30 minutes at 37°C with synthetic Aß-oligomers (sAßo) or with vehicle. Afterwards, cells were lysed in RIPA + 1% SDS on ice, centrifuged for 30 minutes at 100,000 x g and supernatants were run on SDS-PAGE and

immunoblotted. **C)** Representative immunoblot images of proteins of interest. **D-H)** Quantification of C). Phosphorylation of relevant kinases was measured through densitometric analysis of Western Blots and normalized to the corresponding total protein signal and to respective vehicle treatment group. N = 8 experiments with 3 replicates per treatment group, data points are group averages per experiment. Statistics: One-way ANOVA with Tukey's multiple comparisons test.

Generating Tau Extracts from Neurologically Intact and AD Subject Brains

In addition to investigating intracellular interactions of Pyk2, Fyn, GSK3ß and tau *in vitro*, I also wanted to assess the impact of Aß, Pyk2, Fyn and other factors like mouse age, template matching and lysosomal health, that could potentially impact tau hyperphosphorylation, on inter-neuronal tau spreading. For this purpose, a model system in which mice were injected with tau extracted from human brains was established, following a previously published protocol[444]. Before injections could take place, tau had to be extracted from human autopsy brain tissue and tested for its stability, phosphorylation status as well as ability to seed *in vitro*.

To obtain tau extracts able to seed tau aggregation in mice or neuronal cell cultures, we followed a published tau purification protocol[444] with autopsy brain tissue from one neurologically intact (from now on called control) subject and three different AD subjects (brains A, B and D, see Materials and Methods - Tau Extraction for post-mortem information). To obtain concentrated brain D tau extracts, the final resuspension volume during the purification protocol was reduced to one quarter of the original amount. To assess the total tau and phospho-Tau (pTau) concentrations in extracts, we performed immunoblots with anti-total tau (HT7) and pTau (AT180) antibodies (Figure 13, A) and measured tau concentration by comparing tau extracts to a standard curve of recombinant 2N4R tau (Figure 13, B). Control subject–derived brain extract contained very low amounts of human tau while showing total protein concentration comparable to the extracts derived from AD subjects. The non-concentrated AD subject-derived extracts showed minor variation in their tau concentrations. To provide a larger stock for mouse injections with the same tau preparation, tau extracted from brain A and B was combined in a 1:1 ratio for most mouse injections (from here on termed AB extract). Next, we sought to test if the phosphorylation and aggregation of this tau material would remain stable over a 60 hour period when stored on ice. This was important to ensure that a cohort of mice injected over the course of up to 3 days would receive the same material. There were no significant changes in tau high–molecular-weight aggregates or phosphorylation when comparing samples from extracts stored at 4°C every 12 h (Figure 13, C). We also characterized the length of our extracted tau fibrils using atomic force microscopy (Figure 13, D). We observed similar average fibril lengths of 90 to 100 nm in all tau extracts from AD brains. To test the potency of our tau extracts *in vitro*, we treated days in vitro (DIV) 7 primary WT mouse neurons with 0.25% (v/v) tau extracts for 14 days and measured tau pathology within the area occupied by neurons (Figure 13, E). Treatment with control extract did not induce tau pathology, whereas all AD tau extracts caused significant increases in tau pathology. Of note, treating with about 10-fold higher concentration of tau (brain D_{conc}) resulted in a nonlinear increase in tau pathology.

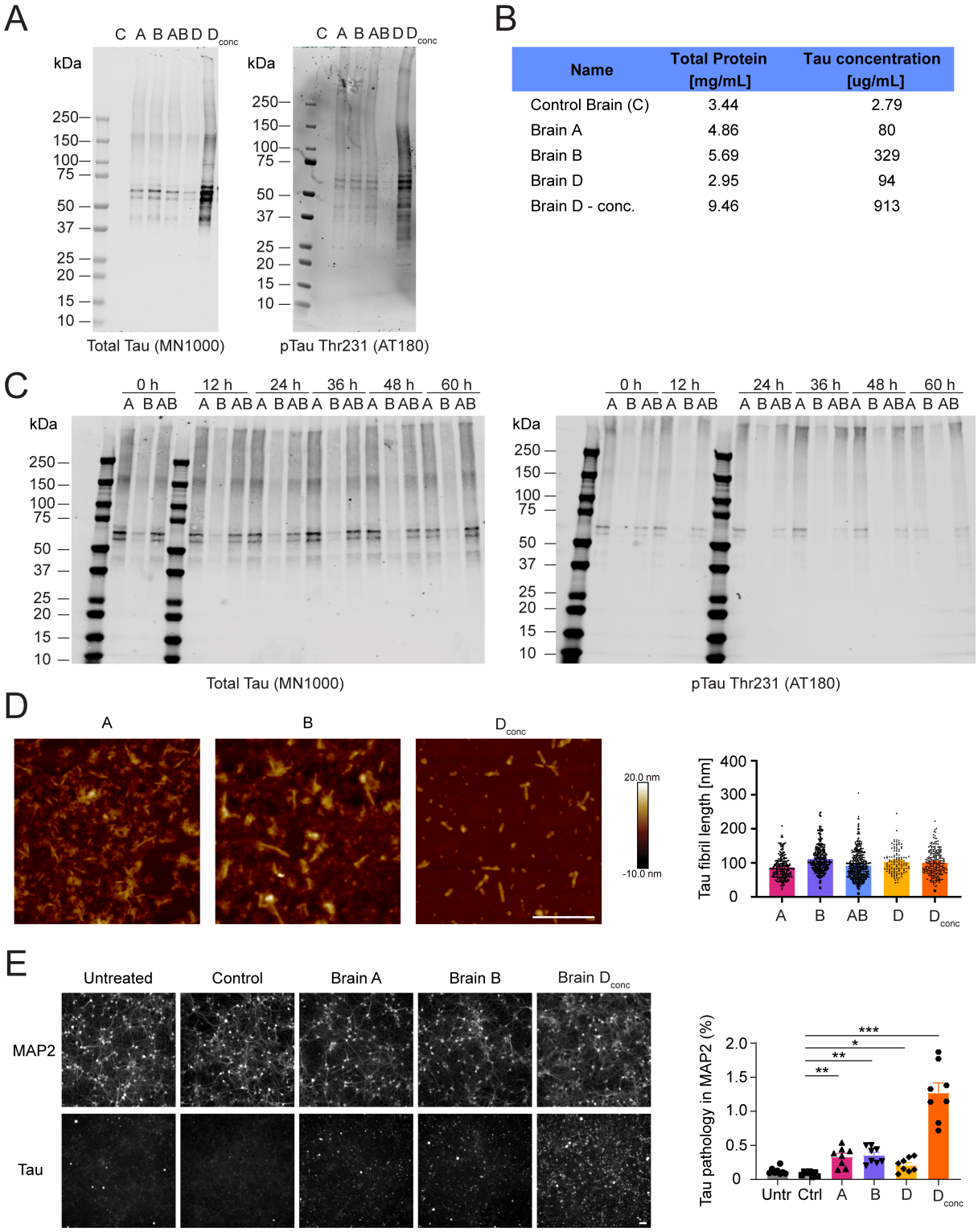

Name	Total Protein [mg/mL]	Tau concentration [ug/mL]
Control Brain (C)	3.44	2.79
Brain A	4.86	80
Brain B	5.69	329
Brain D	2.95	94
Brain D - conc.	9.46	913

Figure 13: Characterization of tau fibrils extracted from human AD subjects.
A) Immunoblots for total tau (HT7) and pTau-Thr231 (AT180) of the tau extracts used in this study (samples were C: Control, A: Brain A, B: Brain B, AB: 1:1 mixture of Brain A and B extracts, D: Brain D, and D_{conc}: 10x concentrated Brain D). **B)** Overview of total protein and total tau concentration in each extract. Total protein concentration was evaluated by measuring absorption at 280nm on a spectrophotometer. Total tau concentration was calculated by comparing densitometric quantifications of total tau (HT7) immunoblots to a dilution curve of recombinant tau (2N4R isoform). **C)** Immunoblots for total tau (HT7) and pTau-Thr231 (AT180) for samples from Brain A, B and a 1:1 mixture of Brain A and B (AB) to assess the tau isoform distribution and phosphorylation over a 60 h time course with measurements taken every 12h. **D)** Tau extracts were diluted in PBS to a concentration of 5 ug/mL and 5 µm x 5 µm images were taken by atomic force microscopy. Scale bar: 0.5 µm. Fibril length was quantified using Gwyddion. N(A)=219 fibrils from 2 images, N(B)=260 fibrils from 3 images, N(AB)=494 fibrils from

3 images, N(D)=116 fibrils from 2 images and N(D_{conc})=225 fibrils from 2 images. **E)** Primary mouse neurons were seeded at 50-75k density, treated with 0.25% (v/v) human tau extracts at DIV 7 and incubated until DIV21. Cells were fixed in ice-cold methanol and stained for MAP2 and mouse tau (T49). Tau seeding was measured by quantifying the percent area occupied by aggregated mouse tau within MAP2 positive area using ImageJ. Scale bar: 50 µm. Statistics: Brown-Forsythe ANOVA test (F = 43.85, p < 0.0001) with Dunnett's multiple comparisons test to compare all groups to Control treated cells. N=8 images per condition. *p<0.05, **p<0.01, ***p<0.005, ****p<0.0001. Figure re-printed from JBC, Volume 297, Issue 4, Article 101159, Nies et al. 2021[487], *Spreading of Alzheimer tau seeds is enhanced by aging and template matching with limited impact of amyloid-ß*, doi: https://doi.org/10.1016/j.jbc.2021.101159 , Figure 1, © 2021 Elsevier, with permission from Elsevier under the CC-BY license.

Tau from Different AD Subjects Generated Somatic and Neuritic Inclusions in WT Mice

To ascertain if our tau extracts showed seeding activity *in vivo*, we injected WT animals as described previously[444]. Tau extracts were injected into the hippocampus and overlying cortex of one hemisphere at 3 months of age (Figure 15, A and B). After a 6-month waiting period, we analyzed the number of somatic inclusions in the hippocampus and cortex in two standardized sections (see Material and Methods - Quantification of Tau Inclusions), as well as the percent area occupied by neuritic inclusions in hippocampus, fimbria, and corpus callosum (Figure 15, B and C). To be counted as a somatic inclusion, AT8-positive tau deposition was required to be present in a neuronal cell soma and outline the cell body. The somatic inclusions are likely to include deposition in pre-NFT and NFT stages. We did not assess mature NFTs separately by silver stain or electron microscopy. Neuritic tau inclusions counted by our thresholding include both very fine NTs within the hippocampus and slightly larger threads with the occasional round inclusion in white matter tracts (Figure 15 C). Since we injected tau from patients with AD, it is likely that NTs detected in white matter tracts are within neurites, not oligodendrocytes. In the dorsal and ventral hippocampus, the threshold to identify the percent area occupied by neuritic inclusions also recognizes and includes somatic inclusions, but the somatic fraction constitutes less than 5% of the total neuritic inclusion area measured. We monitored mouse health by monthly weighing (Figure 14) and detected no adverse effects of AD extract injection on mouse body mass.

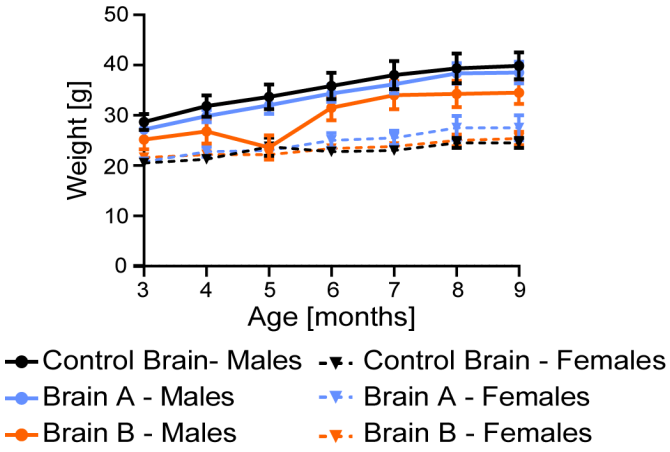

Figure 14: Injecting human tau extracts does not affect mouse weight.
Mice from the WT vs WT cohort injected with extracts from control brain, brain A or brain B were weighed every month to monitor effects of tau injection on mouse weight as a proxy for overall health. Mouse weight was not significantly altered by tau injection. Figure re-printed from JBC, Volume 297, Issue 4, Article 101159, Nies et al. 2021, *Spreading of Alzheimer tau seeds is enhanced by aging and template matching with limited impact of amyloid-ß,* doi: https://doi.org/10.1016/j.jbc.2021.101159 , Supplementary Figure 1B, © 2021 Elsevier, with permission from Elsevier under the CC-BY license.

When comparing the number of somatic inclusions on the ipsilateral hemisphere of control or AD extract–injected animals in each brain region (Figure 15, D), tau inclusions were only found to be seeded at significant levels by AD extracts in select brain regions (ventral hippocampus, retrosplenial area (RSA), and EC). A similar pattern was observed in the contralateral hemisphere (Figure 16, A), where only RSA and auditory cortex showed significantly higher levels of somatic tau inclusions. For AD-injected animals, the number of somatic inclusions in each contralateral region was lower than the one in their ipsilateral counterpart. Since tau fibrils were extracted from several different AD brains, we sought to evaluate whether injecting material from different subjects would alter the number of somatic inclusions per animal. Extracts A (80 μg tau protein/ml), B (329 μg tau protein/ml), AB (204 μg tau protein/ml), and D (94 μg tau protein/ml) were injected into mice directly, whereas the concentrated brain D extract was diluted in sterile PBS to a concentration of 500 μg/ml before injection. Increasing (brain D concentrated) or decreasing (brain A and D) the amount of injected tau did not translate into a proportional change in tau seeding in WT mice. Instead, the main difference in seeding was observed between tau extracts derived from different brains, with brain D resulting in more numerous tau inclusions (Figure 15, E and Figure 16, B). The regional distribution of tau inclusions between the different tau extracts though remained largely unchanged (Figure 15 , F), with ventral hippocampus, RSA, and EC on the ipsilateral hemisphere showing the most inclusions. The extract used to inject most cohorts was AB, and the tau spreading pattern for this extract remained the same throughout the WT animals of different cohorts (Figure 16, C). Furthermore, the neuritic tau burden in WT animals was elevated in all measured regions for brain D or D_{conc} injected animals compared with brain A, B, or AB injected ones (Figure 15, G). Altogether, these data are consistent with previous observations from other groups[444].

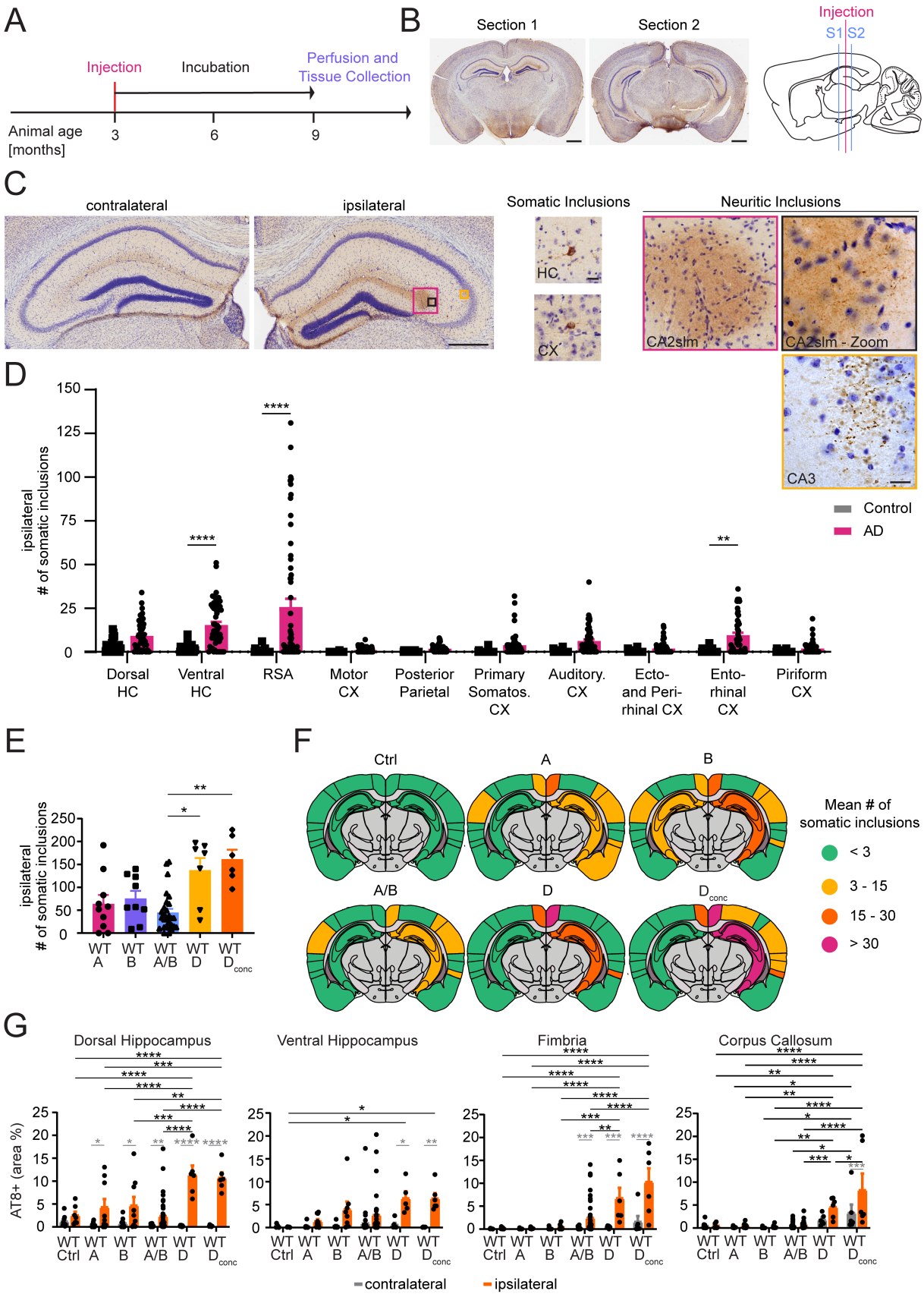

Figure 15: Injecting tau extracts into WT mice results in tau deposition and spreading in hippocampus and cortex.

A) Experimental timeline of mouse injections. Mice were injected unilaterally (right hemisphere) at 3 months of age with either Control or AD brain tau extract. Per animal, 5 µL of tau extract were injected distributed over two injection sites (2.5 µL/site). After injection, mice were housed under regular conditions for 6 months and then killed by perfusion. **B)** Example pictures of AT8b-DAB + Nissl stain sections that were analyzed and sagittal

schematic indicating injection site in pink and analyzed section location in blue. Section 1 is located anterior (from Bregma: ML +2.0 mm, AP -2.0) to the injection sites (from bregma: anterior-posterior −2.5 mm; medial-lateral 2 mm; dorso-ventral −2.4 mm (for hippocampus) and dorso-ventral −1.4 mm (for cortex)), section 2 is located posterior (ML +2.0 mm, AP -2.9) to the injection sites (scale bar: 1 mm). **C)** From left to right: magnified images of Section 1 contralateral and ipsilateral hippocampus (scale bar: 0.5 mm (ipsilateral HC) and 25 µm (CA3)). Example images of somatic inclusions quantified in this study. Example images of neuritic inclusions quantified in this study (scale bar: 20 µm). **D)** Mean number of somatic inclusions per brain region on the ipsilateral hemisphere of WT animals injected with Control or AD tau extracts. Inclusions were counted manually in ImageJ with the Cell Counter Tool. Statistics: Ordinary Two-way ANOVA test (Interaction: F (9, 841) = 8.431, p<0.0001; Row Factor: F (9, 841) = 9.852), p<0.0001; Column Factor: F (1, 841) = 72.28, p<0.0001) with Sidak's multiple comparisons test. N represent individual animals. N(Control)=27-28, N(AD)=60. **p<0.01, ****p<0.0001. **E)** Mean number of somatic inclusions on the ipsilateral hemisphere in animals injected with tau extracts extracted from different AD brains. Statistics: Kruskal-Wallis test (Approximate p-value: 0.0008, Kruskal-Wallis statistic: 18.91) with Dunn's multiple comparisons. N represents individual animals. N(A)=10, N(B)=9, N(AB)=28, N(D)=7, N(D_{conc})=6. *p<0.05, **p<0.01. **F)** Coronal section schematics of mean somatic inclusion burden in ipsi- and contralateral brain regions dependent on injected tau extract. Brain regions not analyzed are depicted in grey. Ipsilateral hemisphere is on the right. **G)** Area occupied by neuritic inclusions in four regions of animals injected with tau extracts from different AD brains. Statistics: Ordinary Two-way ANOVA (for dorsal hippocampus - Interaction: F(5,144) = 9.266, p<0.0001; Row Factor: F(5,144) = 9.041, p=0.0001; Column Factor: F(1,144) = 95.96, p<0.0001; for ventral hippocampus - Interaction: F(5,121) = 2.191, p=0.0596; Row Factor: F(5,121) = 2.120, p=0.0675; Column Factor: F(1,121) = 21.06, p<0.0001; for fimbria - Interaction: F(5,144) = 6.743, p<0.0001; Row Factor: F(5,144) = 11.41, p=0.0001; Column Factor: F(1,144) = 33.45, p<0.0001; for Corpus Callosum - Interaction: F(5,137) = 3.679, p=0.0037; Row Factor: F(5,137) = 18.48, p<0.0001; Column Factor: F(1,137) = 12.78, p=0.0005) with Sidak's multiple comparisons test. In grey: comparing ipsi- and contralateral hemisphere for the same injected extract. In black: comparing ipsilateral values of different tau extract injected groups. N represent individual animals. N(Ctrl)=8-9, N(A)=9-10, N(B)=8-9, N(AB)=30-39, N(D)=6-7, N(D_{conc})=6. *p<0.05, **p<0.01, ***p<0.005, ****p<0.0001. Figure re-printed from JBC, Volume 297, Issue 4, Article 101159, Nies et al. 2021, *Spreading of Alzheimer tau seeds is enhanced by aging and template matching with limited impact of amyloid-ß,* doi: *https://doi.org/10.1016/j.jbc.2021.101159* , Figure 2, © 2021 Elsevier, with permission from Elsevier under the CC-BY license.

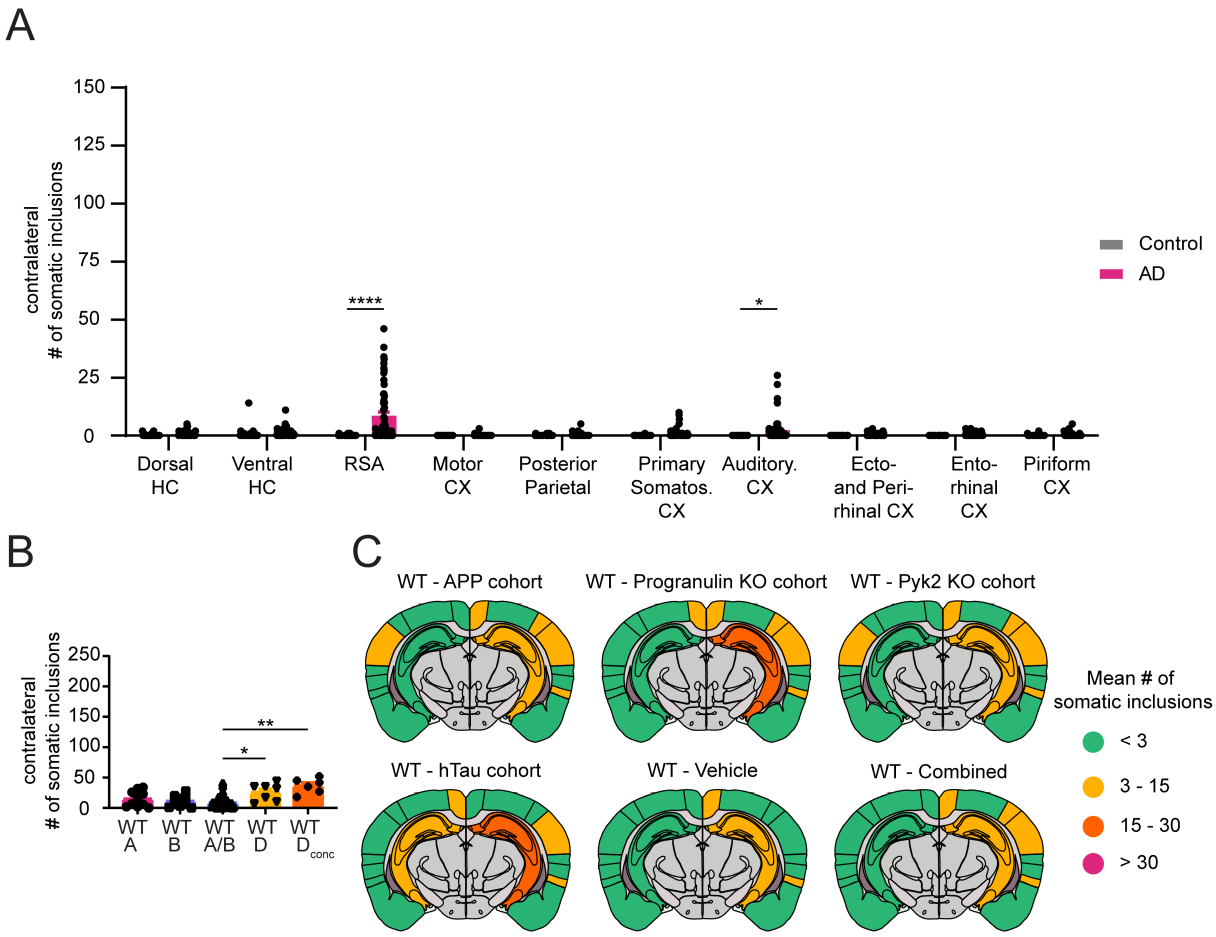

Figure 16: Contralateral hemisphere of AD extract injected animals shows lower numbers of somatic inclusions and tau spreading pattern remains the same in different mouse cohorts injected with brain AB tau.
A) Mean number of somatic inclusions per brain region on the contralateral hemisphere in WT animals injected with tau extracts extracted from Control or AD brains. Inclusions were counted manually in ImageJ with the Cell Counter Tool. Statistics: Ordinary Two-way ANOVA test (Interaction: F (9, 838) = 10.01, p<0.0001; Row Factor: F (9, 838) = 10.08), p<0.0001; Column Factor: F (1, 838) = 28.13, p<0.0001) with Sidak's multiple comparisons test. N represent individual animals. N(Control)=27-28, N(AD)=60. **p<0.01, ****p<0.0001. **B)** Mean number of somatic inclusions on the contralateral hemisphere in animals injected with tau extracts extracted from different AD brains. Statistics: Kruskal-Wallis test (Approximate p-value: 0.0008, Kruskal-Wallis statistic: 19.07) with Dunn's multiple comparisons. N represent individual animals. N(A)=10, N(B)=9, N(AB)=28, N(D)=7, N(Dconc)=6. *p<0.05, **p<0.01. **C)** Coronal section schematics of mean somatic inclusion burden in ipsi- and contralateral brain regions of WT animals injected with Brain AB tau extract in different animal cohorts. Brain regions not analyzed are depicted in grey. Ipsilateral hemisphere is on the right. Figure re-printed from JBC, Volume 297, Issue 4, Article 101159, Nies et al. 2021, *Spreading of Alzheimer tau seeds is enhanced by aging and template matching with limited impact of amyloid-ß,* doi: https://doi.org/10.1016/j.jbc.2021.101159 , Figure S2 A-B, © 2021 Elsevier, with permission from Elsevier under the CC-BY license.

Aβ Accumulation Did Not Alter Tau Inclusion Burden, but Human Tau Template Increased Neuritic Inclusions

Having established that AD tau injection leads to tau accumulation and spreading in WT animals, we investigated whether the presence of Aβ deposition would impact tau spreading using the APPswe/PSEN1ΔE9 transgenic (APP mice) and App$^{NL-F/NL-F}$ knock-in (KI) mouse models. APP mice develop Aβ plaques between 4 and 6 months of age. This mouse model is well established but has the caveat of Aβ overexpression via the transgene array. App$^{NL-F/NL-F}$ KI mice develop Aß plaques slightly later around 6 months of age[541]. For more extensive

description of the mouse models see Material and Methods - Animals. We intercrossed the KI mice with a mouse line containing humanized tau (hTau) to generate double homozygous hTau-App$^{NL-F/NL-F}$ mice (double KI [DKI])[491]. In addition, to discern if changes in tau spreading were caused by humanized Aβ or hTau, we also injected hTau animals not carrying the App$^{NL-F/NL-F}$ gene with tau extracts. After AD tau extract injection into these different Aβ plaque containing mice, we observed only a limited and nonsignificant trend towards an increase in the number of somatic tau inclusions in the cortex of AD mice compared to WT mice. Only in the dorsal hippocampus, AD tau extract-injected DKI animals showed a significant difference compared to WT animals (Figure 17, A and B). Moreover, we observed no change in the number of tau-positive NPs near amyloid plaques for either the APP or the DKI model (Figure 17, E). In contrast, the amount of neuritic inclusions was significantly increased in mice carrying hTau for all measured regions (Figure 17, C and D). Adding App$^{NL-F/NL-F}$ to the hTau genotype (DKI mice) did not cause further increase in the neuritic tau inclusion burden. Under these conditions, the presence of Aβ accumulation does not alter tau spreading. The findings support the hypothesis that misfolded human tau seeds can template hTau more efficiently than murine tau. We next sought to explore if there might be altered glial reaction, which in turn might alter tau aggregation in neurons. We stained brain sections for glial fibrillary acidic protein (GFAP) (Figure 18, A-B) and CD68 (Figure 18, C-D), which are astrocytic and microglial markers, respectively, and analyzed the percent area occupied by each staining in the hippocampus and cortex. The only injection-dependent difference detected was for CD68 signal in the hippocampus of AD tau extract–injected animals. In all other groups, the AD tau injection did not alter immunoreactivity of these glial markers. Thus, AD tau aggregate induced spreading of tau inclusions in these mice is enhanced by matching the template but is largely independent of Aβ pathology or gliosis.

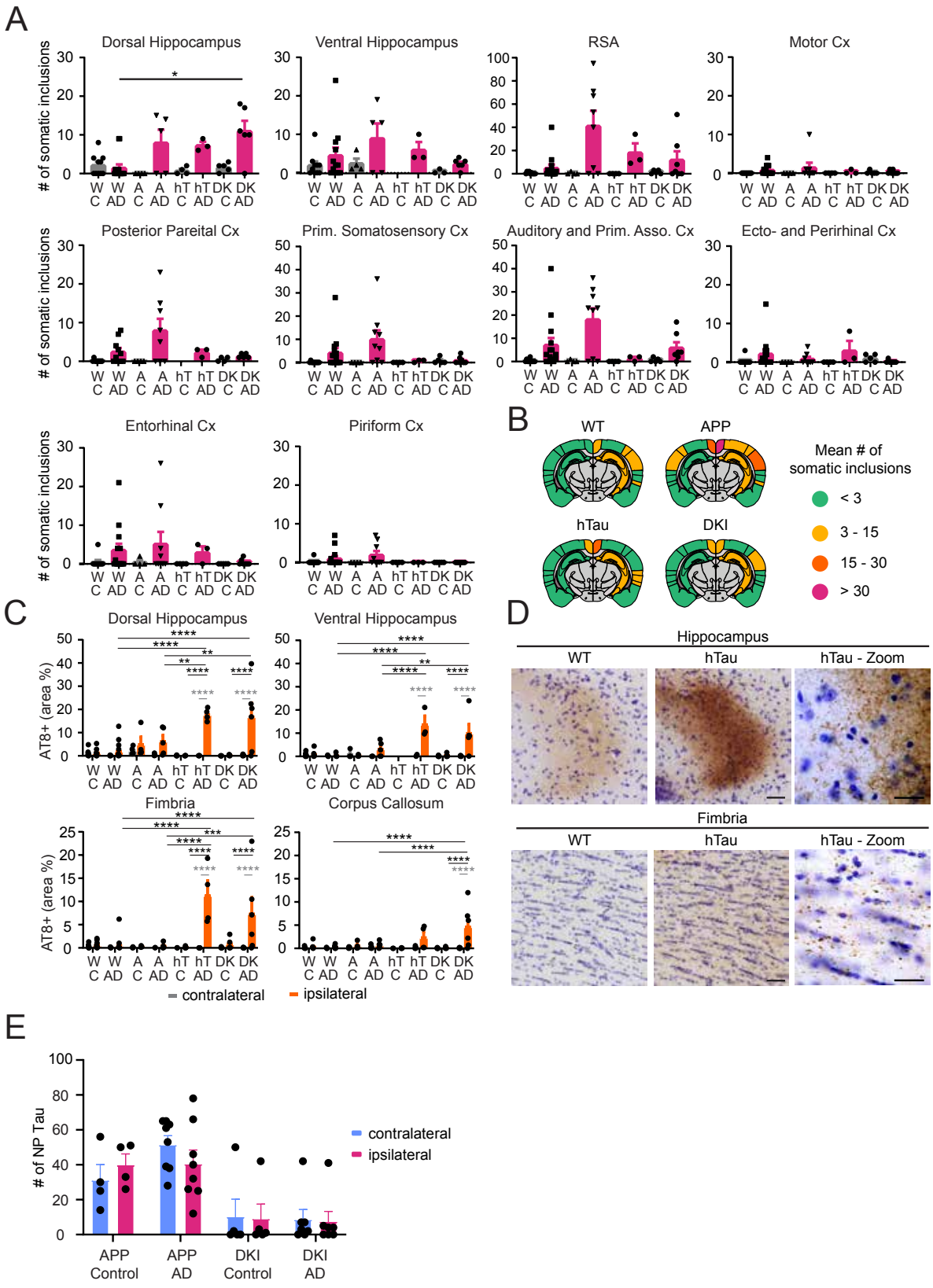

Figure 17: : Aß co-pathology has no impact on tau inclusion burden or spreading, but the presence of humanized tau enhances tau deposition.

A) Mean number of somatic inclusions in different ipsilateral brain regions of animals injected with tau extracts extracted from Control or AD brains. C=Control, W=WT, A=APP, hT =hTau, DK=DKI. Statistics: Kruskal-Wallis test (for dorsal HC - Approximate p-value=0.0155, Kruskal-Wallis statistic=10.39; for ventral HC - Approximate p-value=0.4352, Kruskal-Wallis statistic=2.730; for RSA - Approximate p-value=0.0155, Kruskal-Wallis

statistic=10.39; for Motor Cx - Approximate p-value=0.8045, Kruskal-Wallis statistic=0.9867; for Posterior Parietal - Approximate p-value=0.6084, Kruskal-Wallis statistic=1.83; for Primary Somatosensory Cx - Approximate p-value=0.1169, Kruskal-Wallis statistic=5.894; for Auditory Cx - Approximate p-value=0.2602, Kruskal-Wallis statistic=4.012; for Ecto- and Perirhinal CX - Approximate p-value=0.1885, Kruskal-Wallis statistic=4.781; for Entorhinal Cx - Approximate p-value=0.4783, Kruskal-Wallis statistic=2.484; for Piriform Cx - Approximate p-value=0.1606, Kruskal-Wallis statistic=5.158) with Dunn's multiple comparisons test. N represent individual animals. N(WT-C)=9-10, N(WT-AD)=14-15, N(APP-C)=4, N(APP-AD)=8-9, N(hT-C)=4, N(hT-AD)=3, N(DK-C)=5, N(DK-AD)=7. *p<0.05. **B)** Schematics of mean somatic inclusion burden of AD tau extract injected animals dependent on mouse genotype. Brain regions not analyzed are depicted in grey. Ipsilateral hemisphere is on the right. **C)** Area occupied by neuritic inclusions in four brain regions of animals injected with Control or AD tau extracts. Statistics: Ordinary Two-way ANOVA (for dorsal hippocampus - Interaction: F(7,88) = 8.073, p<0.0001; Row Factor: F(7,88) = 7.714, p<0.0001; Column Factor: F(1, 88) = 38.19, p<0.0001; for ventral hippocampus - Interaction: F(6,62) = 8.017, p<0.0001; Row Factor: F(6,62) = 7.733, p<0.0001; Column Factor: F(1,62) = 30.04, p<0.0001; for fimbria - Interaction: F(7,90) = 7.293, p<0.0001; Row Factor: F(7,90) = 7.084, p<0.0001; Column Factor: F(1,90) = 24.14, p<0.0001; for Corpus Callosum - Interaction: F(7,83) = 4.807, p=0.0001; Row Factor: F(7,83) = 4.837, p=0.0001; Column Factor: F(1,83) = 13.40, p=0.0004) with Sidak's multiple comparisons test. In grey: comparing ipsi- and contralateral hemisphere for the same injected extract. In black: comparing ipsilateral values of different tau extract injected groups. N represent individual animals. N(WT-C)=9-10, N(WT-AD)=14-15, N(APP-C)= 4, N(APP-AD)=5-9, N(hT-C)=0-4, N(hT-AD)=3-4, N(DK-C)=5, N(DK-AD)=5-6. *p<0.05, **p<0.01, ***p<0.005, ****p<0.0001. **D)** Representative images of neuritic inclusions in fimbria and hippocampus (scale bars: 50 µm (hTau) and 25 µm (hTau-Zoom)). **E)** Number of neuritic plaques (NP) with AT8-positive tau surrounding it. Statistics: Ordinary Two-way ANOVA with Sidak's multiple comparisons test. N(APP-Ctrl)=4, N(APP-AD)=8, N(DKI-Ctrl)=5, N(DKI-AD)=7. N represents individual animals with two sections analyzed per animal. Figure re-printed from JBC, Volume 297, Issue 4, Article 101159, Nies et al. 2021, *Spreading of Alzheimer tau seeds is enhanced by aging and template matching with limited impact of amyloid-ß,* doi: *https://doi.org/10.1016/j.jbc.2021.101159* , Figure 3, © 2021 Elsevier, with permission from Elsevier under the CC-BY license.

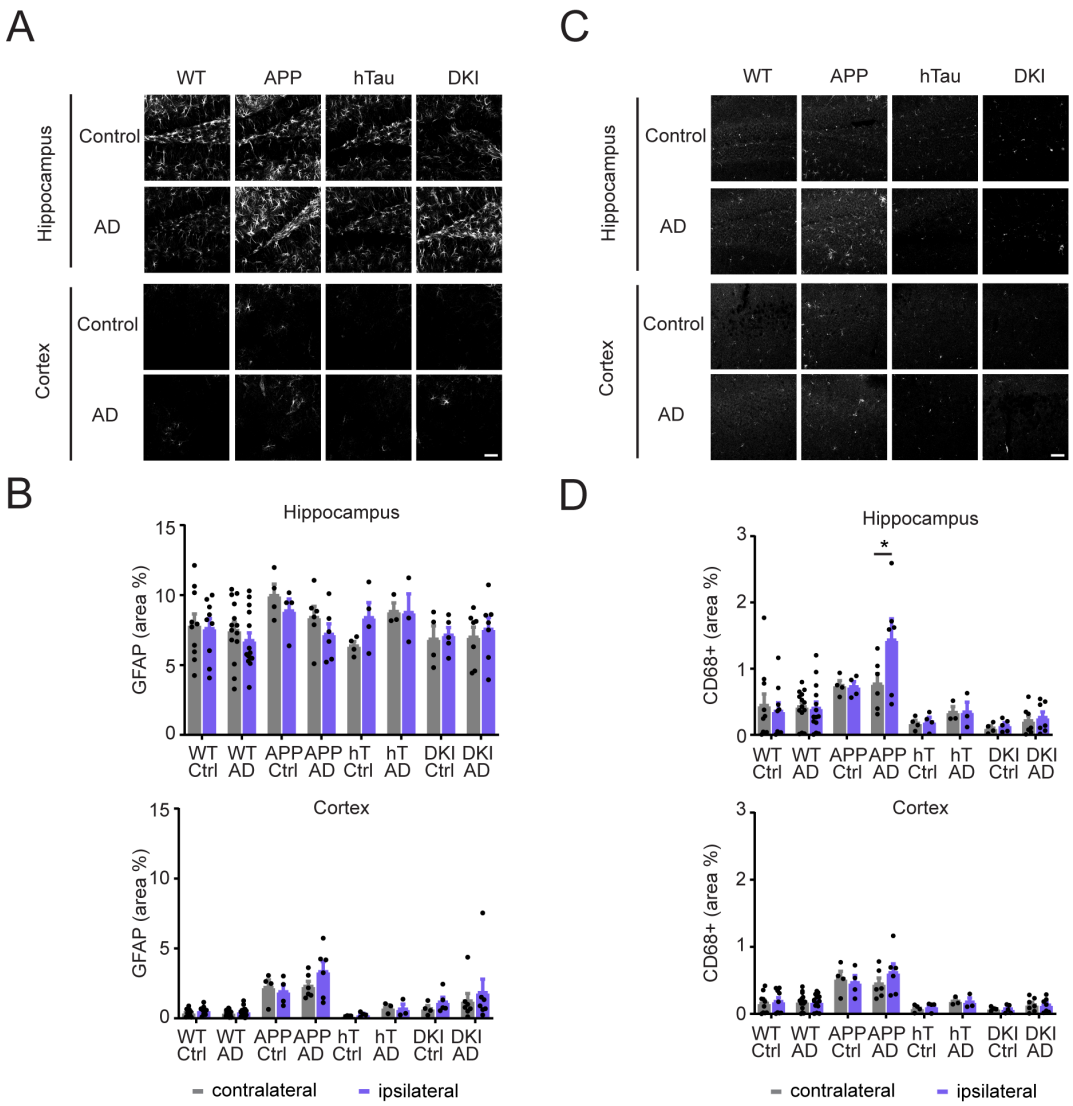

Figure 18: GFAP and CD68 area are not altered by tau injection.

A) Representative images of GFAP staining in the ipsilateral hemisphere hippocampus (DG) and cortex (layer I-III). Images were taken with a 20x objective (scale bar: 50 µm). **B)** Quantification of area occupied by GFAP staining in the dentate gyrus (left) and cortex layer I-III (right) in animals injected with Control or AD tau extracts. Statistics: Ordinary Two-way ANOVA test (for hippocampus - Interaction: F (7, 88) = 0.6645, p=0.7014; Row Factor: F (7, 88) = 1.654, p=0.1310; Column Factor: F (1, 88) = 0.01862, p=0.8918; for cortex - Interaction: F(7, 88) = 0.5127, p=0.8228; Row Factor: F(7, 88) = 10.59, p<0.0001; Column Factor: F(1, 88) = 1.424, p=0.2360) with Tukey's multiple comparisons test to compare same hemispheres across genotypes or with Sidak's multiple comparisons test to compare ipsi- and contralateral signals of the same genotype. N represent individual animals. N(WT-C)=9-10, N(WT-AD)=14-15, N(APP-C)=4, N(APP-AD)=6-8, N(hT-C)=4, N(hT-AD)=3, N(DK-C)=4-5, N(DK-AD)=7. **C)** Representative images of CD68 staining in the ipsilateral hemisphere hippocampus (DG) and cortex (layer I-III). Images were taken with a 20x objective (scale bar: 50 µm). **D)** Quantification of area occupied by CD68+ staining in the hippocampus (left) and cortex (right) in animals injected with Control or AD tau extracts. Statistics: Ordinary Two-way ANOVA test (for hippocampus -Interaction: F(7, 88) = 1.393, p=0.2185; Row Factor: F(7, 88) = 8.846, p<0.0001; Column Factor: F(1, 88) = 1.085, p=0.3005; for cortex - Interaction: F(7, 88) = 0.5283, p=0.8110; Row Factor: F(7, 88) = 13.76, p<0.0001; Column Factor: F(1, 88) = 0.2536, p=0.6158) with Sidak's multiple comparisons test to compare ipsi- and contralateral signals of the same genotype. N represent individual animals. N(WT-C)=9-10, N(WT-AD)=14-15, N(APP- C)=4, N(APP-AD)=6-8, N(hT-C)=4, N(hT-AD)=3, N(DK-C)=4-5, N(DK-AD)=7. Figure re-printed from JBC, Volume 297, Issue 4, Article 101159, Nies et al. 2021, *Spreading of Alzheimer tau seeds is enhanced by aging and template matching with limited impact of amyloid-ß,* doi: https://doi.org/10.1016/j.jbc.2021.101159 , Figure 3 E-F and Supplementary Figure 2 D-E, © 2021 Elsevier, with permission from Elsevier under the CC-BY license.

Aβ Present in AD Tau Extracts Induces Aβ Redistribution in AD Model Mice

Immunoblot analysis of tau extracts generated from human AD patients revealed small amounts of residual monomeric Aβ as well as aggregated Aβo in the AD-brain derived tau extracts (now called AD tau extracts), but not in the control brain-derived extract (Figure 19, A). We explored whether the Aβ in the tau extracts contributed to tau spreading and whether it might alter Aβ deposition in APP and DKI mice. We stained brain sections of the tau-injected animals (Figure 17) with an antibody recognizing the amino terminus of Aβ isoforms (D54D2) and thioflavin S (ThioS) to examine dense-core amyloid plaques (Figure 19). We then analyzed the percent area occupied by either stain in the whole hippocampus and cortex. When AD tau extracts containing Aβ are injected into mice, the ipsilateral hippocampus and parts of the overlying cortex exhibited a redistribution of Aβ along the hilus of the dentate gyrus, the outer edges of the dentate gyrus molecular layer, the hippocampal fissure, and the white matter surrounding the hippocampus and lower cortical regions (Figure 19, B and C). Conversely, this redistribution did not take place for Aβ that was part of dense-core plaques, since the ThioS signal was unaffected by AD extract injections (Figure 19, B and C). Redistribution was absent in Control extract-injected animals (Figure 19, B and C). In animals without existing Aβ plaques (WT and hTau), injecting tau extracts containing Aβ was not sufficient to induce Aβ accumulation (data not shown). Tile scanning of brain sections more posterior and anterior to the APP section analyzed in Figure 19, C showed that the redistribution was present at a distance in and around the hippocampus far away from the injection site (Figure 19, D).

To further clarify the extent of Aβ redistribution, we imaged at higher magnification and measured the percent area occupied by total Aβ and ThioS-positive dense-core plaques in different regions of the hippocampus and cortex in APP mice. Most notably, redistribution of total Aβ took place in the CA1 and corpus callosum, dentate gyrus and CA2, as well as medial and lateral cortex layer I to III, whereas dense-core plaque signal remained unaltered in all regions except an overall signal increase in the corpus callosum (Figure 21). Interestingly, comparing Aβ redistribution (Figure 19 and Figure 20) and the somatic and neuritic tau inclusions (Figure 17) seen in these animals revealed very different patterns. Aβ redistribution was localized to the hippocampus and inner cortex layers and spread along the anterior–posterior axis but did not reach ventral or lateral brain regions (e.g., EC). In comparison, somatic tau inclusions were present close to the injection site (hippocampus and RSA) and spread ventrally to the EC, potentially along synaptic connections.

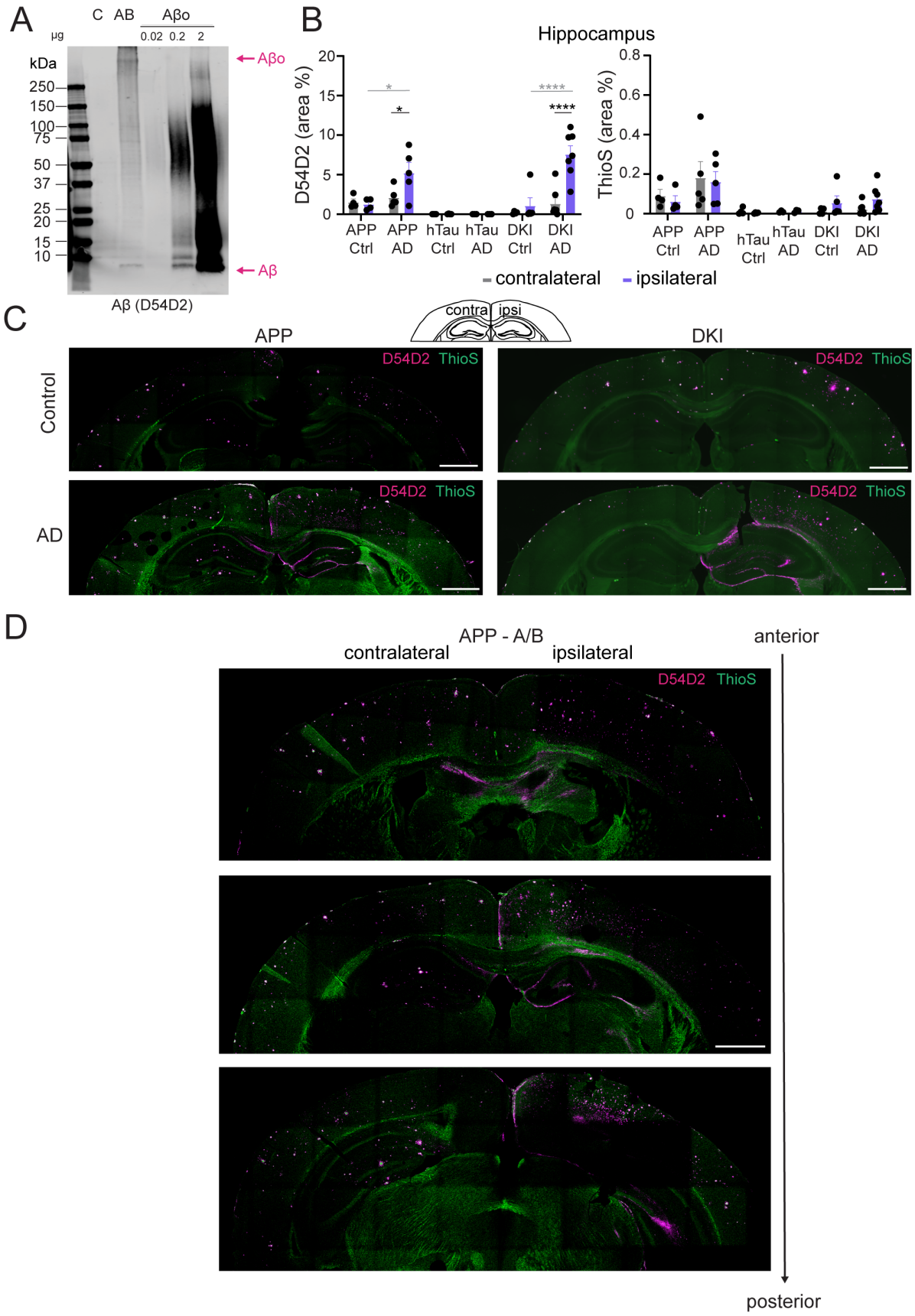

Figure 19: Aß in tau extracts leads to a redistribution of non-dense core plaque Aß in ipsilateral hemisphere, while dense-core plaque Aß remains unaffected.

A) Immunoblot of Control (C) and Brain A/B extract probed for Aβ with D54D2 antibody and compared to different amounts of synthetic biotinylated-Aβo. Samples were boiled for 5 minutes at 95°C with 10% BME. **B)** Quantification of the mean percent area occupied by D54D2-positive and ThioS-positive dense core plaques in the

hippocampus of Control and AD brain injected mice was measured by drawing ROIs around the brain region and thresholding images. Representative images can be found in Figure 4C and Figure S-3A. Statistics: Ordinary Two-way ANOVA (For D54D2 - Interaction: $F(5,43) = 5.939$, $p=0.0003$; Row Factor: $F(5,43) = 12.25$, $p<0.0001$; Column Factor: $F(1,43) = 11.62$, $p=0.0014$; For ThioS - Interaction: $F(5,43) = 0.4724$, $p=0.7947$; Row Factor: $F(5,43) = 5.546$, $p=0.0005$; Column Factor: $F(1,43) = 0.09148$, $p=0.7638$) with Sidak's multiple comparisons test comparing ipsi- and contralateral hemisphere within each group shown in black and Sidak's multiple comparisons test comparing ipsilateral hemispheres between Control and AD injected mice shown in grey. N represents individual animals. N(APP-C)=4, N(APP-AD)=5, N(hT-C)=4, N(hT-AD)=3, N(DKI-C)=4, N(DKI-AD)=7. *p<0.05, ****p<0.0001. **C)** Immunofluorescent staining with D54D2 (magenta) antibody for Amyloid-β and Thioflavine S (green) for dense-core amyloid-β plaques of APP and DKI mice injected with Control or AD brain tau extracts (scale bar: 1mm). **D)** Three coronal sections (anterior to posterior) of the same APP animal injected with AD tau extract and stained for with D54D2 (magenta) antibody for Aβ and ThioS (green) for dense-core amyloid plaques (scale bar: 1mm). Figure reprinted from JBC, Volume 297, Issue 4, Article 101159, Nies et al. 2021, *Spreading of Alzheimer tau seeds is enhanced by aging and template matching with limited impact of amyloid-ß,* doi: *https://doi.org/10.1016/j.jbc.2021.101159* , Figure 4 A-C and Figure S3 A and C, © 2021 Elsevier, with permission from Elsevier under the CC-BY license.

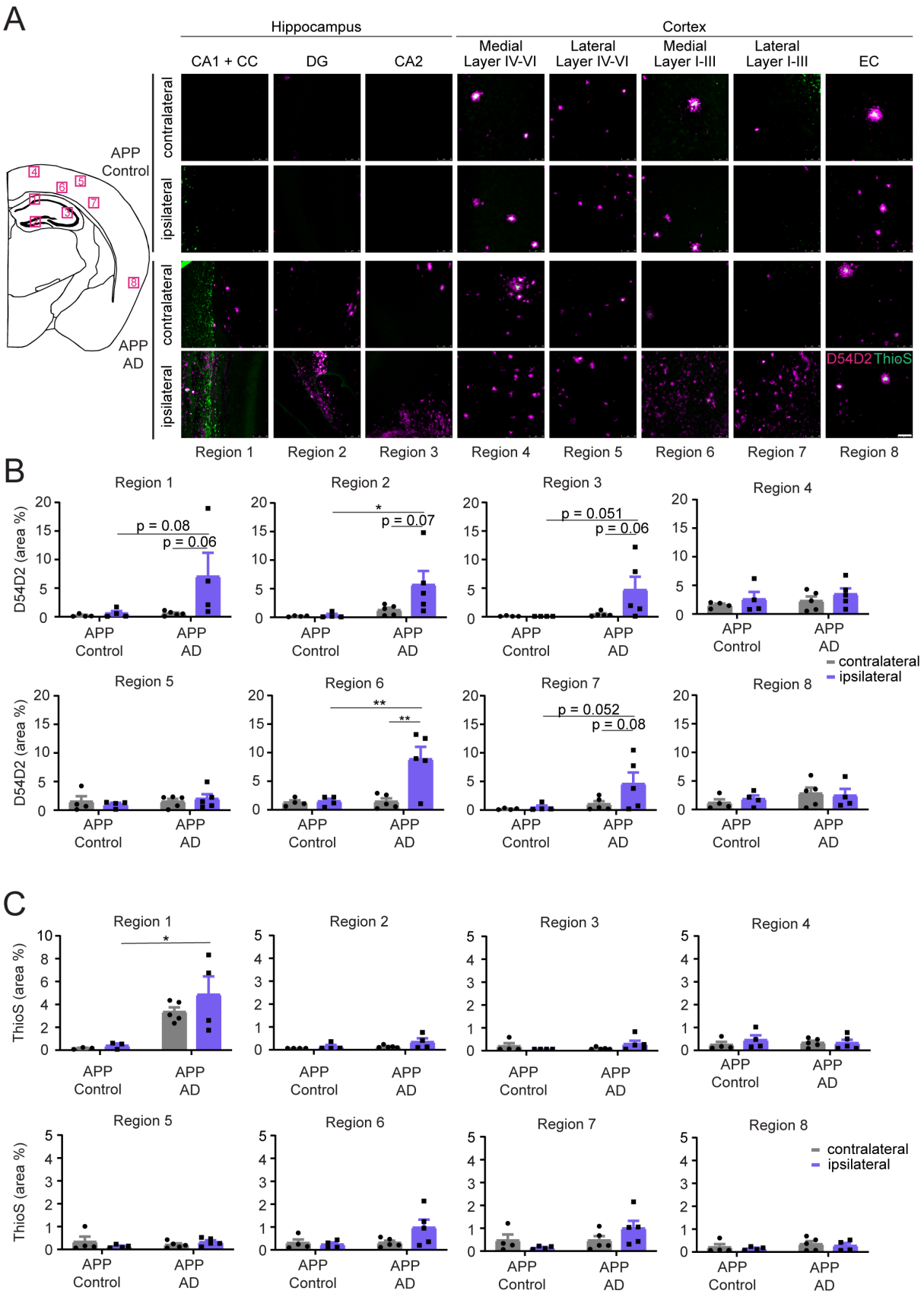

Figure 20: Redistribution of total Aβ takes place in the CA1, CA2, corpus callosum, dentate gyrus, as well as medial and lateral cortex layer I to III.

A) Representative images of D54D2 (magenta) and ThioS (green) staining taken with an 20x objective (scale bar: 50µm). Schematic on the left indicates the location of images in the brain. **B)** Quantification of D54D2 staining seen in A). Statistics: Ordinary Two-way ANOVA (For Region 1 - Interaction: F(1,13) = 2.449, p=0.1416; Row Factor: F(1,13) = 3.066, p=0.1035; Column Factor: F(1,13) = 3.131, p=0.1002; For Region 2 - Interaction: F(1,14) =

2.309, p=0.1509; Row Factor: F(1,14) = 5.332, p=0.0367; Column Factor: F(1,14) = 2.655, p=0.1255; Region 3 - Interaction: F(1,14) = 2.701, p=0.1225; Row Factor: F(1,14) = 3.560, p=0.0801; Column Factor: F(1,14) = 2.609, p=0.1285; Region 4 - Interaction: F(1,14) = 0.005899, p=0.9399; Row Factor: F(1,14) = 0.8148, p=0.3820; Column Factor: F(1,14) = 1.500, p=0.2410; Region 5 - Interaction: F(1,14) = 0.5541, p=0.4690; Row Factor: F(1,14) = 0.5692, p=0.4631; Column Factor: F(1,14) = 0.0001762, p=0.9896; Region 6 - Interaction: F(1,14) = 7.892, p=0.0139; Row Factor: F(1,14) = 8.591, p=0.0109; Column Factor: F(1,14) = 8.843, p=0.0100; Region 7 - Interaction: F(1,14) = 1.918, p=0.1877; Row Factor: F(1,14) = 4.515, p=0.0519; Column Factor: F(1,14) = 2.662, p=0.1251; Region 8 - Interaction: F(1,14) = 0.3087, p=0.5879; Row Factor: F(1,14) = 1.470, p=0.2470; Column Factor: F(1,14) = 0.02451, p=0.8780;) with Sidak's multiple comparisons test comparing ipsi- and contralateral hemisphere within each injection and ipsilateral results across injections. N represents individual animals. N(APP-C)=4, N(APP-AD)=4-5. *p<0.05, **p<0.01. **C)** Quantification of ThioS staining seen in A). Statistics: Ordinary Two-way ANOVA (For Region 1 - Interaction: F(1,11) = 0.4629, p=0.5103; Row Factor: F(1,11) = 17.11, p=0.0017; Column Factor: F(1,11) = 0.8951, p=0.3644; For Region 2 - Interaction: F(1,13) = 0.6931, p=0.4201; Row Factor: F(1,13) = 2.931, p=0.1106; Column Factor: F(1,13) = 3.046, p=0.1045; Region 3 - Interaction: F(1,14) = 2.825, p=0.1150; Row Factor: F(1,14) = 0.4270, p=0.5240; Column Factor: F(1,14) = 0.1024, p=0.7537; Region 4 - Interaction: F(1,14) = 0.6228, p=0.4432; Row Factor: F(1,14) = 0.02337, p=0.8807; Column Factor: F(1,14) = 0.5257, p=0.4804; Region 5 - Interaction: F(1,14) = 2.041, p=0.1750; Row Factor: F(1,14) = 0.07300, p=0.7910; Column Factor: F(1,14) = 0.1388, p=0.7151; Region 6 - Interaction: F(1,14) = 2.842, p=0.1140; Row Factor: F(1,14) = 2.980, p=0.1063; Column Factor: F(1,14) = 1.876, p=0.1924; Region 7 - Interaction: F(1,14) = 3.102, p=0.1000; Row Factor: F(1,14) = 3.089, p=0.1007; Column Factor: F(1,14) = 0.1771, p=0.6803; Region 8 - Interaction: F(1,13) = 0.00229, p=0.9625; Row Factor: F(1,13) = 1.370, p=0.2629; Column Factor: F(1,13) = 0.3419, p=0.5687) with Sidak's multiple comparisons test comparing ipsi- and contralateral hemisphere within each injection and ipsilateral results across injections. N represents individual animals. N(APP-C)=3-4, N(APP-AD)=4-5. *p<0.05, **p<0.01. Figure re-printed from JBC, Volume 297, Issue 4, Article 101159, Nies et al. 2021, *Spreading of Alzheimer tau seeds is enhanced by aging and template matching with limited impact of amyloid-ß,* doi: *https://doi.org/10.1016/j.jbc.2021.101159* , Figure 4 D-E and Figure S3B, © 2021 Elsevier, with permission from Elsevier under the CC-BY license.

To discern whether the Aβ redistribution is dependent on the Aβ present in the AD tau extracts, we next performed immunodepletion of Aβ from AD tau extracts. To remove Aß, we incubated brain D tau extracts with magnetic beads conjugated to D54D2 (D) antibody. Afterwards, any excess D54D2 antibody was cleared from the supernatant through an additional incubation with unconjugated beads. We immunoblotted untreated samples as well as Aβ-cleared extracts for total Aβ (Figure 21, A). After immunodepletion, monomeric Aβ was absent from tau extracts. Oligomeric Aβ was reduced by 74% in Aβ-cleared tau extracts, but small amounts remained. There was nonspecific reduction of tau during Aβ immunodepletion and thus, we adjusted the tau concentration of non-immunodepleted brain D extracts to match that of the Aβ D54D2-immunodepleted extracts for *in vivo* injections. With these tau-diluted samples, there was a lower somatic and neuritic inclusion burden on the ipsilateral and contralateral hemisphere of injected animals (Figure 21, B–D). We then examined whether the Aβ immunodepletion affected Aβ redistribution after injection of AD tau extracts into APP mice. Co-staining with D54D2 antibody and ThioS showed that the redistribution of hippocampal Aβ deposits was significantly reduced by the immunodepletion (Figure 21, E and F). As was the case prior to immunodepletion, ThioS- stained area in APP mice was unaltered by human brain extract injection.

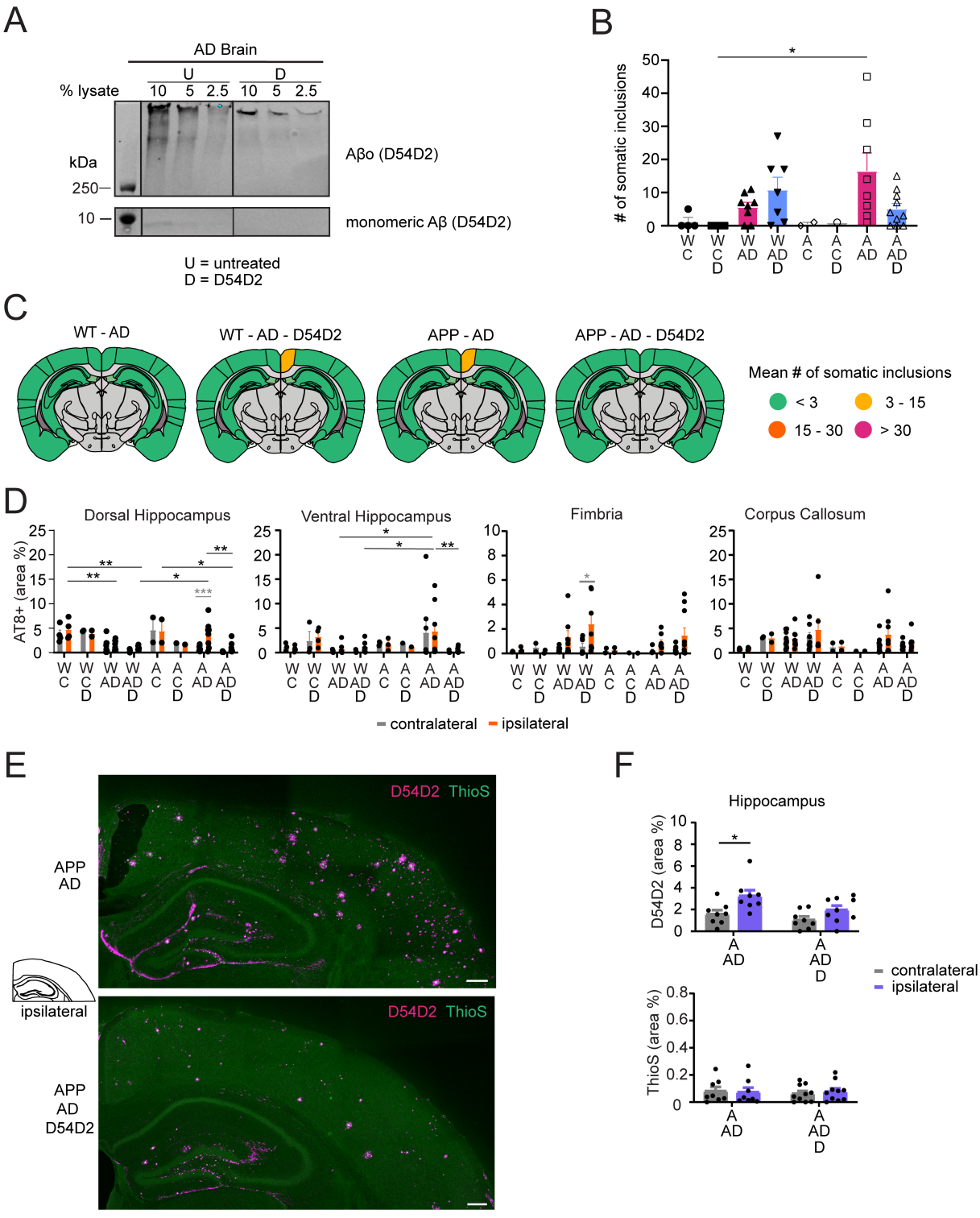

Figure 21: Immunodepleting Aβ from tau extracts ameliorates Aβ redistribution.

A) Immunoblots of tau extracts that had been incubated with D54D2 antibody conjugated to Protein G magnetic beads to remove Aβ from tau extracts. Blots shown were probed for Aβ (D54D2) to assess the removal of Aβ from the extracts. Bands shown were run on the same blot, but not next to each other and vertical black lines indicate splicing of the blot. U=untreated samples, D=D54D2-incubated samples. **B)** Mean number of somatic inclusions on the ipsilateral hemisphere of animals injected with Control (C) or AD brain tau extracts, or with Control or AD brain tau extracts that had been cleared of Aβ by incubating samples with D54D2 antibody conjugated to Protein G beads (C-D and AD-D samples). Statistics: Kruskal-Wallis test (Approximate p-value=0.0176, Kruskal-Wallis statistic=16.97) with Dunn's multiple comparisons test. N represent individual animals. N(WT-C)=4, N(WT-C-D)=4, N(WT-AD)=8, N(WT-AD-D)=7, N(APP-C)=2, N(APP-C-D)=1, N(APP-AD)=8, N(APP-AD-D)=10. *p<0.05**. C)** Schematics of mean somatic inclusion burden of tau extracts (extracted from AD brains, with or without Aβ removal) injected animals dependent on mouse genotype. Brain regions not analyzed are depicted in

grey. Ipsilateral hemisphere is on the right. **D)** Area occupied by neuritic inclusions in four brain regions of animals injected with Control or AD brain derived tau extracts with and without Aβ removal. Statistics: Ordinary Two-way ANOVA (for dorsal hippocampus - Interaction: F(7,68) = 1.680, p=0.1287; Row Factor: F(7,68) = 11.67, p<0.0001; Column Factor: F(1, 68) = 1.790, p=0.1864; for ventral hippocampus - Interaction: F(7,70) = 0.06833, p=0.9995; Row Factor: F(7,70) = 3.114, p=0.0064; Column Factor: F(1,70) = 0.07003, p=0.7921; for fimbria - Interaction: F(7,61) = 0.7205, p=0.6550; Row Factor: F(7,61) = 1.275, p=0.2777; Column Factor: F(1,61) = 2.317, p=0.1331; for Corpus Callosum - Interaction: F(7,67) = 0.2680, p=0.9573; Row Factor: F(7,67) = 1.825, p=0.0967; Column Factor: F(1,67) = 0.5514, p=0.4603) with Sidak's multiple comparisons test. In grey: comparing ipsi- and contralateral hemisphere for the same genotype and injected extract. In black: comparing ipsilateral values of different tau extract injected groups. N(WT-C) = 4, N(WT-C-D) = 2, N(WT-AD) = 8, N(WT-AD-D) = 6-7, N(APP-C) = 2, N(APP-C-D) = 1, N(APP-AD) = 8, N(APP-AD-D) = 10. *p<0.05, **p<0.01, ***p<0.005, ****p<0.0001. **E)** Representative images of the ipsilateral hippocampus with immunofluorescent staining of D54D2 (magenta) antibody for Aβ and ThioS (green) for dense-core amyloid plaques in APP mice injected with AD brain extracts with and without Aβ removal (scale bars: 250 µm). **F)** Quantification of the percent area occupied by D54D2 (top) and ThioS (bottom) in the hippocampus of APP mice injected with AD brain extracts with and without Aβ removal. Statistics: Ordinary Two-way ANOVA (For D54D2 - Interaction: F(1,29) = 0.9156, p=0.3465; Row Factor: F(1,29) = 5.346, p=0.0281; Column Factor: F(1,29) = 10.96, p=0.0025; For ThioS - Interaction: F(1,32) = 0.2028, p=0.6555; Row Factor: F(1,32) = 0.08193, p=0.7765; Column Factor: F(1,32) = 0.02327, p=0.8797) with Sidak's multiple comparisons test comparing ipsi- and contralateral hemisphere within each injection. N represents individual animals. N(APP-AD)=8, N(APP-AD-D)=8-10. *p<0.05. Figure re-printed from JBC, Volume 297, Issue 4, Article 101159, Nies et al. 2021, *Spreading of Alzheimer tau seeds is enhanced by aging and template matching with limited impact of amyloid-ß,* doi: *https://doi.org/10.1016/j.jbc.2021.101159* , Figure 5, © 2021 Elsevier, with permission from Elsevier under the CC-BY license.

Neither Ptk2b Deletion nor Treatment with the Fyn Inhibitor AZD0530 Altered Tau Spreading

Pyk2 was demonstrated to be a tau kinase[264], and Fyn kinase inhibition or deletion reduced tau deposition and rescued memory deficits in several tauopathy models[536,545,546]. Therefore, we sought to determine whether inhibiting Fyn kinase or knocking out Pyk2 would modify tau spreading. Mice were injected with control or AD tau extracts at 3 months of age, and Fyn kinase inhibitor treatment with AZD0530 (AZD) was started 2 weeks after the injection. WT and Ptk2b$^{-/-}$ brain tissue was collected 6 months after the injection, whereas vehicle versus AZD-treated WT animals were maintained until 9 months after injection (Figure 22, A). Overall, there were no significant changes in the number of somatic inclusions on the ipsilateral and contralateral hemispheres of injected animals when comparing WT to Ptk2b$^{-/-}$ animals and vehicle-dosed animals to AZD-treated animals (Figure 22, B and C). Interestingly, the three additional months of incubation time granted to the vehicle- and AZD-treated animals resulted in an increase of neuritic inclusions in the fimbria and corpus callosum independent of drug or vehicle treatment (Figure 22, D and E).

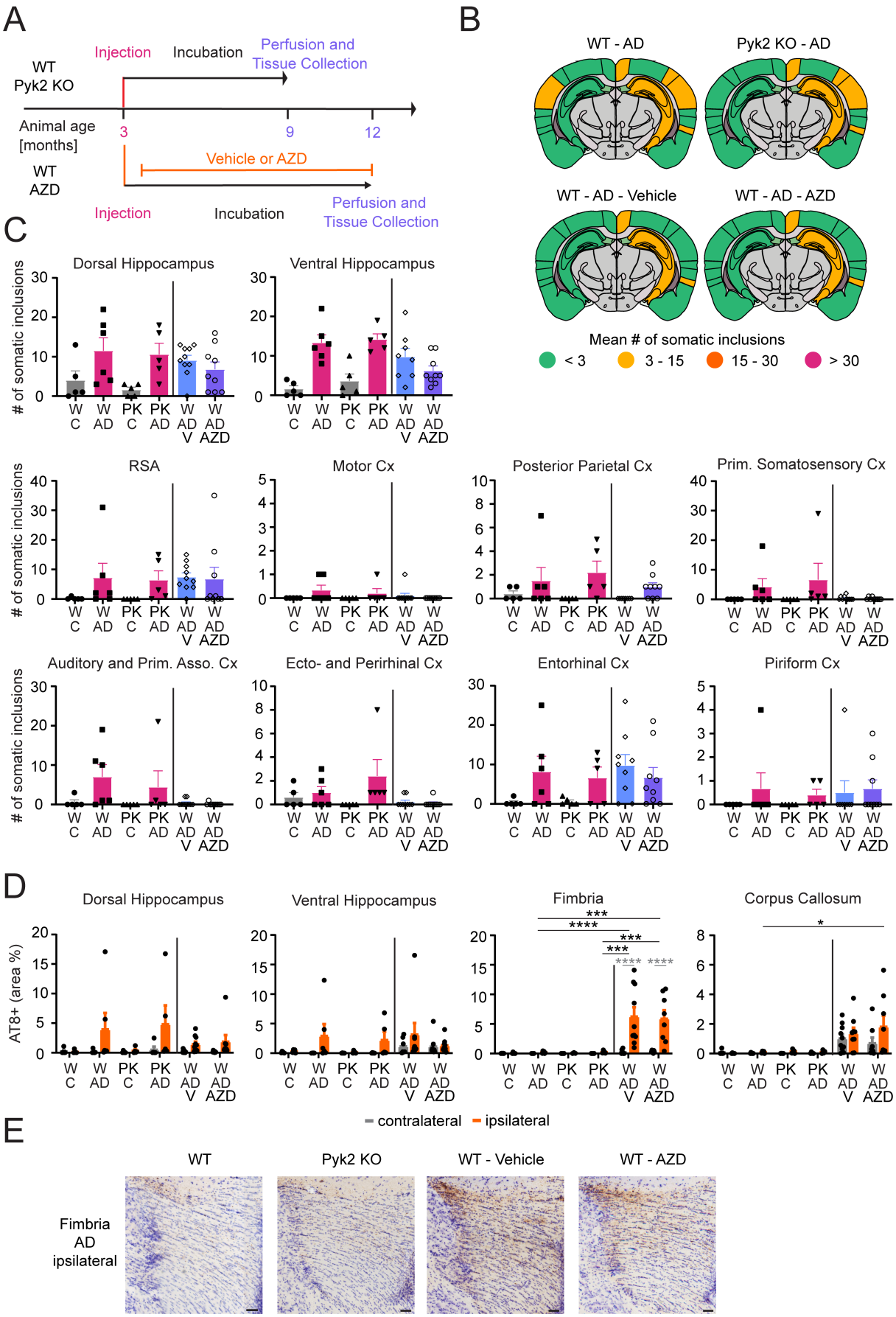

Figure 22: Ptk2b-/- or pharmacological inhibition of Fyn have no impact on tau spreading.

A) Mice in the WT vs Ptk2b$^{-/-}$ genotype comparison followed the established timeline of injection at 3 months of age, waiting period of 6 months, then tissue collection and analysis. WT animals treated with Vehicle or AZD0530

were also injected at 3 months of age, and then started on their AZD or vehicle treatment two weeks after tau injection. They were kept for 9 months before tissue was collected and analyzed. **B)** Schematics of mean somatic inclusion burden of AD tau extract injected animals dependent on mouse genotype. Brain regions not analyzed are depicted in grey. Ipsilateral hemisphere is on the right. **C)** Mean number of somatic inclusions in ipsilateral brain regions of animals injected with tau extracts extracted from Control or AD brains. C=Control, W=WT, PK=Ptk2b$^{-/-}$, V=Vehicle treated, AZD=AZD0530 treated. Statistics: Kruskal-Wallis test (for dorsal HC - Approximate p-value=0.563, Kruskal-Wallis statistic=2.046; for ventral HC - Approximate p-value=0.0153, Kruskal-Wallis statistic=10.43; for RSA - Approximate p-value=0.5301, Kruskal-Wallis statistic=2.209; for Motor Cx - Approximate p-value=0.3049, Kruskal-Wallis statistic=3.625; for Posterior Parietal - Approximate p-value=0.0217, Kruskal-Wallis statistic=9.663; for Primary Somatosensory Cx - Approximate p-value=0.0908, Kruskal-Wallis statistic=6.472; for Auditory Cx - Approximate p-value=0.0209, Kruskal-Wallis statistic=9.743; for Ecto- and Perirhinal CX - Approximate p-value=0.0077, Kruskal-Wallis statistic=11.9; for Entorhinal Cx - Approximate p-value=0.8443, Kruskal-Wallis statistic=0.8217; for Piriform Cx - Approximate p-value=0.8054, Kruskal-Wallis statistic=0.9828) with Dunn's multiple comparisons test. N represent individual animals. N(WT-C)=5, N(WT-AD)=6, N(PK-C)=5, N(PK-AD)=5, N(WT-AD-V)=8-10, N(WT-AD-AZD)=9. *p<0.05, **p<0.01. **D)** Area occupied by neuritic inclusions in four regions of animals injected with tau extracts. Statistics: Ordinary Two-way ANOVA (for dorsal hippocampus - Interaction: F(5,66) = 1.122, p=0.3574; Row Factor: F(5,66) = 1.341, p=0.2580; Column Factor: F(1, 66) = 8.063, p=0.0060; for ventral hippocampus - Interaction: F(5,63) = 0.7387, p=0.5973; Row Factor: F(5,63) = 1.155, p=0.3411; Column Factor: F(1,63) = 4.363, p=0.0408; for fimbria - Interaction: F(5,62) = 5.641, p=0.0002; Row Factor: F(5,62) = 6.684, p<0.0001; Column Factor: F(1,62) = 12.88, p=0.0007; for Corpus Callosum - Interaction: F(5,63) = 0.7336, p=0.6010; Row Factor: F(5,63) = 5.642, p=0.0002; Column Factor: F(1,63) = 1.505, p=0.2244) with Sidak's multiple comparisons test. In grey: comparing ipsi- and contralateral hemisphere of the same genotype and injected extract. In black: comparing ipsilateral values of different AD tau extract injected groups. N represent individual animals. N(WT-C)=5, N(WT-AD)=6, N(PK-C)=5, N(PK-AD)=5, N(WT-AD-V)=8-10, N(WT-AD-AZD)=8-9. *p<0.05, **p<0.01. **E)** Representative images of neuritic inclusions in the fimbria (scale bar: 50 µm). Figure re-printed from JBC, Volume 297, Issue 4, Article 101159, Nies et al. 2021, *Spreading of Alzheimer tau seeds is enhanced by aging and template matching with limited impact of amyloid-ß*, doi: https://doi.org/10.1016/j.jbc.2021.101159 , Figure 6, © 2021 Elsevier, with permission from Elsevier under the CC-BY license.

Deficiency of PGRN or TMEM106B Does Not Alter Tau Accumulation, but Aging Enhances Tau Spreading and Inclusion Burden

As PGRN and TMEM106B have both been reported to regulate lysosomal biology[499,525], we sought to evaluate whether PGRN or TMEM106B deficiency would modulate tau spreading. Here, we also considered whether advanced age would interact with the Tmem106b genotype since aging is a key risk factor for AD. Mice homozygous for the hypomorphic *Tmem106b* allele show some lysosomal abnormalities but have no observable alteration in life span facilitating these studies[520]. We injected WT (W) and Grn$^{-/-}$ (G) mice with control or AD patient–derived tau at 3 months of age, whereas aged WT (AW) and Tmem106b$^{-/-}$ (T) mice were 19 months old at the time of injection and 25 months at the end of the experiment (Figure 23, A). AD extract–injected animals showed comparable amounts of somatic inclusions on both hemispheres, regardless of animal age and genotype (Figure 23, B and C). Interestingly, the control extract injection induced somatic tau inclusions in aged mice but not in young mice. This phenomenon depended on mouse age, not genotype, and was spatially restricted close to the injection site (Figure 23, D). Furthermore, advanced mouse age also had an impact on the density of neuritic tau inclusions, causing significant increases in the ventral hippocampus, fimbria, and corpus callosum in AD extract–injected animals (Figure 23, E and F). As for somatic tau inclusions, mouse genotype did not alter the neuritic tau inclusion burden. These findings expand evidence that aging renders cells more susceptible to tau seeding and spreading. In contrast, disrupting lysosomal degradation by knocking out either PGRN or TMEM106B had no impact on tau spreading.

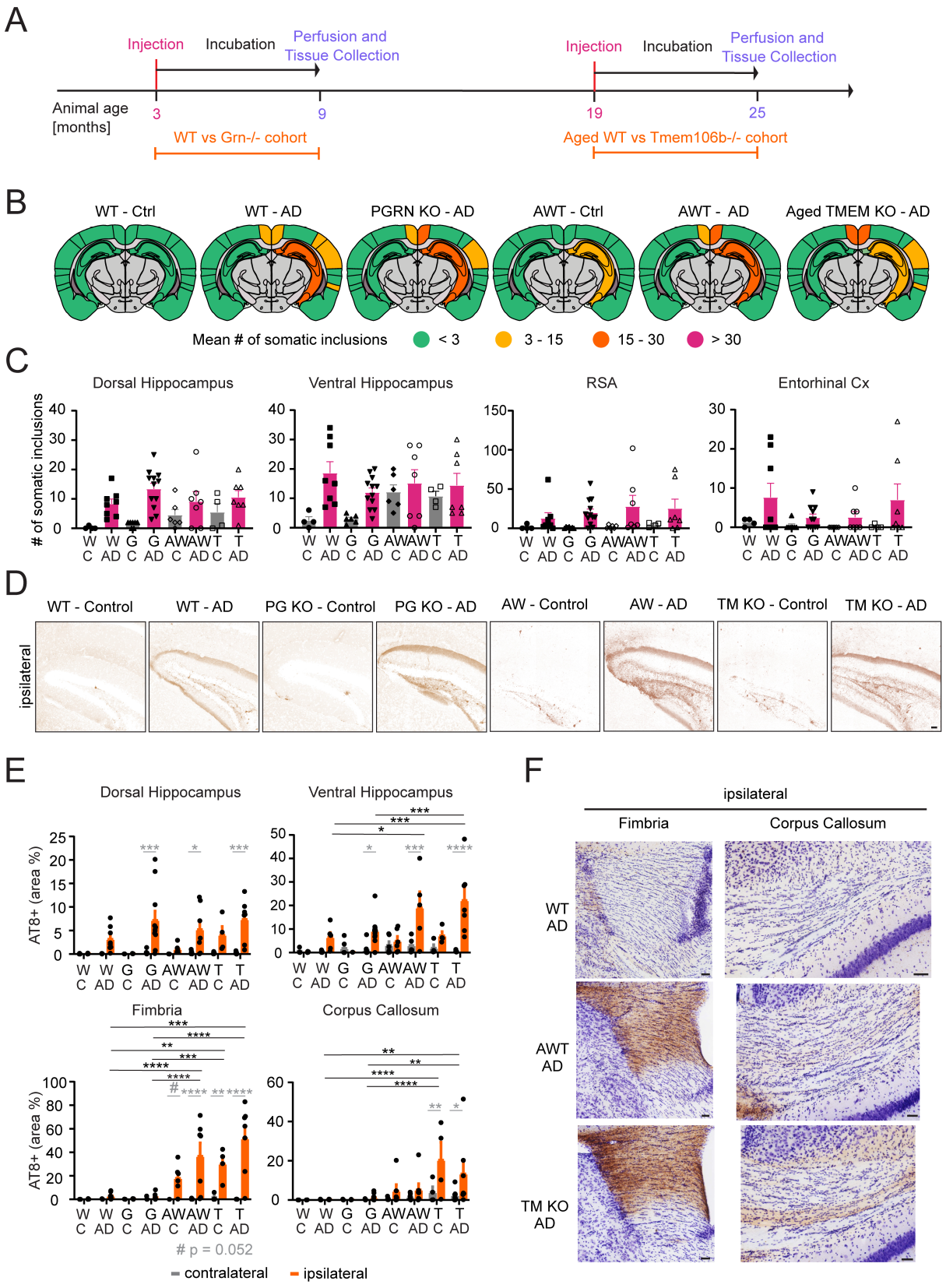

Figure 23: Grn-/- and Tmem106b-/- do not impact tau spreading, but advanced mice age exacerbates contralateral hippocampal inclusions and neuritic tau deposition.

A) WT and Grn$^{-/-}$ mice were injected according to the timeline previously described. Aged WT and Tmem106b$^{-/-}$ mice were injected at 19 months of age instead of 3 months of age and then followed the same timeline of 6 months waiting period, followed by mice perfusion, tissue collection and analysis. **B)** Schematics of mean somatic

inclusion burden of Control and AD tau extract injected animals dependent on mouse genotype and age at injection. Brain regions not analyzed are depicted in grey. Ipsilateral hemisphere is on the right. **C)** Mean number of somatic inclusions in ipsilateral brain regions of animals injected with tau extracts from Control or AD brains. C=Control, W=WT, G=Grn$^{-/-}$, AW=Aged WT, T=Tmem106b$^{-/-}$. Statistics: Kruskal-Wallis test (for dorsal HC - Approximate p-value=0.3227, Kruskal-Wallis statistic=3.485; for ventral HC - Approximate p-value=0.5686, Kruskal-Wallis statistic=2.018; for RSA - Approximate p-value=0.6358, Kruskal-Wallis statistic=1.705; for Entorhinal Cx - Approximate p-value=0.9075, Kruskal-Wallis statistic=0.5511) with Dunn's multiple comparisons test comparing AD injected groups. N represent individual animals. N(WT-C)=4, N(WT-AD)=8, N(G-C)=7, N(G-AD)=12, N(AWT-C)=6, N(AWT-AD)=7, N(T-C)=4, N(T-AD)=7. **D)** Representative images of ventral hippocampi of animals injected with Control or AD tau extracts (scale bar: 50 µm). **E)** Area occupied by neuritic inclusions in four brain regions of animals injected with Control or AD brain derived tau extracts. Statistics: Ordinary Two-way ANOVA (for dorsal hippocampus - Interaction: F(7,91) = 3.335, p=0.0033; Row Factor: F(7,91) = 3.823, p=0.0011; Column Factor: F(1, 91) = 32.08, p<0.0001; for ventral hippocampus - Interaction: F(7,83) = 5.547, p<0.0001; Row Factor: F(7,83) = 5.329, p<0.0001; Column Factor: F(1,83) = 32.05, p<0.0001; for fimbria - Interaction: F(7,94) = 10.82, p<0.0001; Row Factor: F(7,94) = 11.02, p<0.0001; Column Factor: F(1,94) = 59.22, p<0.0001; for Corpus Callosum - Interaction: F(7,94) = 2.355, p=0.0292; Row Factor: F(7,94) = 5.079, p<0.0001; Column Factor: F(1,94) = 12.36, p=0.0007) with Sidak's multiple comparisons test. In grey: comparing ipsi- and contralateral hemisphere for the same injected extract and genotype. In black: comparing ipsilateral values of AD tau extract injected groups. N represent individual animals. N(WT-C)=4, N(WT-AD)=8, N(G-C)=7, N(G-AD)=12, N(AWT-C)=6, N(AWT-AD)=7, N(T-C)=4, N(T-AD)=7. *p<0.05, **p<0.01, ***p<0.005, ****p<0.0001. **F)** Representative images of fimbria and corpus callosum neuritic tau inclusions (scale bars: 50 µm). Figure re-printed from JBC, Volume 297, Issue 4, Article 101159, Nies et al. 2021, *Spreading of Alzheimer tau seeds is enhanced by aging and template matching with limited impact of amyloid-ß,* doi: https://doi.org/10.1016/j.jbc.2021.101159 , Figure 7, © 2021 Elsevier, with permission from Elsevier under the CC-BY license.

Summary of Results

To better understand the interplay of Pyk2, Fyn and GSK3ß on phosphorylating tau, kinase phosphorylation was first studied in HEK-293T cells overexpressing the proteins of interest or in *in vitro* kinase assays. In these systems, Pyk2 and Fyn worked in synergy to increase GSK3ß and subsequent tau phosphorylation. Furthermore, GSK3ß co-immunoprecipitated with Pyk2 and Fyn kinase inhibition diminished its proximity to tau as well as reduced tau spreading in mouse cortical neuron cultures seeded with human tau. Thus, this initial data supported a role for the three kinases in contributing to tau hyperphosphorylation and spreading. To confirm these initial results, two more physiologically relevant model system of iPSC-derived neurons for further *in vitro* studies and of mice injected with human tau for *in vivo* tau spreading studies were established and validated.

In iPSC-derived neurons, the effects of pharmacologically inhibiting Fyn and Pyk2 were studied after successful validation of the model system. Contrary to previous results, no changes in GSK3ß phosphorylation were observed. In addition, tau phosphorylation on certain epitopes was surprisingly increased upon Pyk2 inhibition. To assess the potential impact of Aß-dependent PrP^{C}-mGluR5-Fyn signaling on tau phosphorylation, iPSC-derived neurons were incubated either short- or long-term with synthetic Aßo. Upon long-term treatment, neurons showed decreases in synaptic density as expected. In contrast though, short-term treatment with sAßo did not activate Pyk2 and Fyn kinases and showed no effect on GSK3ß, tau or other downstream targets. These results suggest that the observations from the over-expression model studies do not translate faithfully into other model systems and that likely more interaction partners and mechanisms are important for these kinases to act on tau in human cells.

To study the impact that different factors thought to modulate tau aggregation might have on tau spreading, mice were injected with tau extracted from human brains. Surprisingly, no changes in tau spreading were observed when Aß was present (APP/PS1 and hTau-App$^{NL\text{-}F/NL\text{-}F}$ mice), when kinases Fyn or Pyk2 were inhibited or when lysosomal homeostasis was

disrupted through knockout of *PGRN* or *TMEM106B*. In contrast, advanced mouse age and template matching (humanized Tau presence) increased the amount of neuritic tau deposition seen in AD tau injected mice. Overall, this suggests that mechanisms that are reported to be involved in the intracellular tau aggregation process only have limited impact on tau spreading.

Discussion

Intracellular Interactions of Fyn, Pyk2, GSK3ß and Tau Diverge in Different Cellular Model Systems

In the present study, the one aim was to characterize the interactions of Pyk2, Fyn and GSK3ß with one another and their effect on intracellular tau phosphorylation in the context of AD by using different *in vitro* model systems. Previously, the synergistic co-activation of Pyk2 and Fyn had already been described by several groups in different model systems[237,238,240,547–551]. Early publications[238,240] showed that Pyk2's kinase domain is necessary for the interaction of Pyk2 and Fyn to occur in in vitro kinase assays and in human embryonic kidney 293T (HEK-293T) cells [240]. Furthermore, they demonstrated that reciprocal activation of Pyk2 and Fyn takes place and is specific to Fyn over other Src family kinases[238]. This co-activation has since been confirmed in mouse fibroblasts[549] as well as model systems that do not rely on over-expression like human T cells[550,551] and mouse neurons[547]. Moreover, their interaction has been implicated in AD to lie downstream of amyloid-ß oligomer (Aßo) induced signaling via PrP^C and mGluR5[249,547,552].

In contrast, the connection between Pyk2 and GSK3ß as well as Fyn and GSK3ß in the context of AD is less well established and was a focus of this thesis. Many existing pieces of evidence rely on over-expression model systems and/or show correlations of kinase activation rather than direct interactions (e.g. co-localization in immunohistochemical staining). For Fyn – GSK3ß interaction, Lesort et al. published a study in 1999 suggesting that GSK3ß and subsequent tau phosphorylation were Fyn dependent[318]. They showed in SH-SY5Y neuroblastoma cells that phosphorylation of Tau upon insulin treatment correlated with increases in GSK3ß tyrosine phosphorylation levels, and that GSK3ß co-immunoprecipitated with Fyn after insulin stimulation. Furthermore, GSK3ß could be phosphorylated by purified active Fyn *in vitro*. In addition, a very recent study found that synaptosomal lipid rafts extracted from Aß overexpressing mice were enriched for Fyn, NR2B, GSK3ß, total tau, hyperphosphorylated tau and tau oligomers compared to lipid rafts extracted from WT mice[553]. For Pyk2 – GSK3ß interaction, over-expressed Pyk2 was shown to phosphorylate GSK3ß in transfected Chinese Hamster Ovary (CHO) cells[206], B103-LPA_1, SH-SY5Y neuroblastoma and PC12 cells[327]. These publications also demonstrated that an intact Pyk2 kinase domain is necessary for the interaction of Pyk2 with GSK3ß, and also showed co-immunoprecipitation of the two proteins from CHO and B103-LPA_1 cells[206,327].

In this thesis, we used an in vitro kinase assay to determine the K_M of Pyk2 – GSK3ß and Fyn – GSK3ß interaction. In accordance with previously published data, we found that both Pyk2 and Fyn can phosphorylate GSK3ß at Y216. When fitting Michaelis-Menten kinetics, the K_M of the Pyk2 – GSK3ß interaction is close to the mouse brain concentration of GSK3ß, making it plausible that this interaction could take place in mouse neurons under physiological conditions. To our knowledge, this is the first time K_M for these interactions were measured and compared to endogenous mouse brain protein levels. In addition, we used a HEK-293T over-expression system to study changes in phosphorylation of GSK3ß and tau upon co-transfection with either Pyk2, Fyn or both. In agreement with the data reported from previous phosphorylation studies in over-expression systems[206,318], we found that both Pyk2 and Fyn can activate GSK3ß through phosphorylation at Y216 and that they could act in synergy to further increase GSK3ß and subsequent tau phosphorylation at AT8. As expected, GSK3ß had to be present in the system for tau phosphorylation at AT8 to occur, since Pyk2 and Fyn are unable to phosphorylate tau at this epitope on their own. Of note, Pyk2 alone was able to cause a higher increase in GSK3ß and tau phosphorylation than Fyn alone. Furthermore, when GSK3ß and

Pyk2 were transfected into HEK-293T cells they co-immunoprecipitated, further confirming results from previous studies[206].

In addition to the GSK3ß-mediated tau phosphorylation, several papers have reported a direct and reciprocal interaction between Fyn and tau, in which Fyn can phosphorylate tau at epitope Y18 and tau is responsible for recruiting Fyn to dendritic spines[161,207,291,292,548,554,555]. A paper investigating tau's role in tethering Fyn to post synaptic densities found that truncation or deletion of tau in transgenic mice lead to the absence of tau in the dendritic compartment and resulted in mislocalization of Fyn away from postsynaptic densities. In addition, they suggested that the disruption of Fyn's interaction with NMDA receptor subunit NR2B in APP mice crossed with tau KO mice led to amelioration of the mice learning and memory deficits[161].

With regards to Fyn directly phosphorylating tau, it was first noted in the late 1990s that neurons showed co-labeling for hyperphosphorylated tau and elevated levels of Fyn in immunohistochemical staining of human AD brains[290]. Later on, Gloria Lee and colleagues investigated this connection further and identified that the SH3 domain of Fyn could bind to PXXP motifs on tau[292]. Furthermore, tau could be co-immunoprecipitated with Fyn *in vitro* as well as endogenously from SH-SY5Y neuroblastoma cells and upon co-transfection into different cell lines tau was tyrosine phosphorylated by Fyn[292]. This data was further expanded on in a follow up study determining that Fyn's phosphorylation site on tau was Y18[207]. In addition, they also identified in this study that phospho-Y18 could be detected in neurofibrillary tangles (NFT), but not neuropil threads or dystrophic neurites in AD patient brains. A third study from this group also examined if Fyn phosphorylation differed between tau isoforms and found that the tau 3R isoforms were better substrates for Fyn, that disease causing FTDP-17 mutations increased 4R tau probability to be phosphorylated by Fyn and that phosphorylation of tau Y18 takes place in a mouse model of FTD over-expressing P301L tau[291]. Another group recently crossed transgenic mice expressing P301L mutant tau with $Fyn^{-/-}$ mice[545]. They observed reduced NFT numbers, tau hyperphosphorylation and synaptic tau accumulation, and hypothesize that Fyn might occupy a central regulatory role in tau aggregation and pathology. Lastly, Fyn – Tau interaction was more closely tied to Aß-induced signaling by a study from Larson et al, where they showed that Aß oligomers could bind to a complex of PrP^C and Fyn in a PrP^C-dependent manner, increasing Fyn activation and subsequent tau pY18 phosphorylation in mouse primary neurons[554]. In addition, another way Fyn might facilitate tau accumulation was recently proposed, in which Aß oligomers trigger the activation of ERK/S6 signaling through Fyn, leading to increased local protein synthesis of tau and thus it's hyperphosphorylation and deposition in neurons somatodendritic domain[548]. In this thesis, we observed that direct interaction of Fyn and tau is dependent on Fyn's kinase activity in HEK-293T cells, and that Fyn inhibition can decrease tau seeding and spreading in cortical mouse neuron cultures. This is in accordance with the previously published data indicating that Fyn-tau interaction is important for modulating the proteins localization as well as tau pathology severity.

It should be noted, that Pyk2 might also be able to phosphorylate tau at residue Y18. First evidence supporting a role of Pyk2 in tau phosphorylation came from a study investigating tau phosphorylation in pR5 mice (expressing tau carrying the FTLD mutation P301L leading to tau deposits)[265]. In this study, immunohistochemical staining of mouse brain tissue showed that pY402 Pyk2 co-localized with activated GSK3ß as well as AT8/AT100 pS422 Tau in neuron cell bodies, suggesting that Pyk2 might act via GSK3ß or directly on tau to cause tau hyperphosphorylation[265]. In a follow up study, the pR5 mice were crossed with mice overexpressing Pyk2 in neurons[264]. In this model, phosphorylation of tau at Y18 was increased upon Pyk2 overexpression, but tau phosphorylation at other epitopes remained the same. The same study also

showed that Pyk2 can phosphorylate tau at Y18 in a HEK-293T cell overexpression model, as well as in an in vitro kinase assay.

One caveat many of the studies investigating Fyn and Pyk2 interactions with GSK3ß and tau share is that they employ mouse or cellular models reliant on (FTLD mutant) tau overexpression, which might distort the relevance of these interactions in human AD patients. When we moved into a model system of iPSC-derived neurons that did not rely on overexpression of our proteins of interest, the interactions previously seen in our HEK-293T over-expression model were not confirmed. Upon pharmacological inhibition of Pyk2, Fyn or both kinases, no changes in GSK3ß phosphorylation levels could be observed. In addition, the phosphorylation of tau epitope Y18, Fyn and Pyk2's reported direct phosphorylation site, also did not decrease upon kinase inhibition. Surprisingly, some tau epitopes like PHF-1 and AT8 even showed an increase in phosphorylation upon Pyk2 inhibition.

There could be several explanations for our conflicting results obtained from HEK-293T cells and iPSC-derived neurons. From a model system perspective, on the one hand it is possible that the overexpression of kinases in HEK-293T cells leads to an artificial hyperphosphorylation of tau that might not be physiologically relevant. On the other hand, iPSC-derived neurons have the caveat of being "young" cells that might not exhibit the amount of tau phosphorylation aged neurons in the brain of an AD patient might display. Thus, the baseline levels of phospho-tau epitopes like pY18 might be low and pharmacological inhibition of Fyn and Pyk2 might not cause further decreases due to the low baseline levels. To test this hypothesis, we would have to first increase tau pY18 levels and then observe the effects of inhibiting Pyk2 and/or Fyn. It is also possible though, that the lack of change in tau Y18 phosphorylation upon kinase inhibition in iPSC-derived neurons was physiologically relevant.

Support for this line of reasoning comes from the unexpected increases in tau phosphorylation that other tau epitopes (AT8 and PHF-1) showed upon Pyk2 inhibition, that cannot be explained by the argument of low baseline phospho-Tau. Instead, this would support the hypothesis of a more complex tau phosphorylation regulation system, in which we currently have not identified all players. We speculate that Pyk2 and Fyn are more important in indirectly regulating tau phosphorylation through their interactions with other kinases and/or by Fyn activity impacting tau binding and thus its localization. In support of this hypothesis, recently published data from our lab found that crossing PS19 mice with $Pyk2^{-/-}$ mice lead to an exacerbation of tau phosphorylation, earlier death and worsened spatial memory and increased hippocampal C1q deposition[544]. Furthermore, in the same study proteomic profiling comparing PS19-$Pyk2^{-/-}$ mice to PS19 mice was conducted and several potential protein kinases were identified. This included LKB1 and p38 MAPK, that are regulated by Pyk2 and could be involved in regulating tau pathology. A second study from our lab in support of this hypothesis found that pharmacologically inhibiting Fyn in PS19 mice did not alter tau Y18 phosphorylation, while serine/threonine epitopes like AT8 and PHF-1 showed decreased phosphorylation levels[536]. It is of note though that another group reported contradictory results, observing decreased tau Y18 phosphorylation in a newly generated mouse strain (obtained by crossing $Fyn^{-/-}$ mice with mice carrying the tau P301L mutation) compared to the tau transgenic mouse model with intact Fyn[545]. We speculate that the reasons for the discrepancies between the two studies might lie in the timing and duration of Fyn inhibition, since in the pharmacological Fyn inhibition model Fyn was only inhibited once mice had reached 2 months of age, while Fyn was never present in the Fyn deletion model.

Furthermore, to elucidate a potential role of Pyk2, Fyn and GSK3ß in connecting Aß and tau pathologies via PrP^{C}-mGluR5-Fyn-Pyk2 signaling, we incubated the iPSC-derived neurons with synthetic Aß oligomers (sAßo) for either 30 minutes or 7 days. As expected, we saw

decreases in synaptic density when we incubated iPSC-derived neurons with sAßo for one week, which was in accordance with previously published data from mouse primary neurons[243], brain slices[249,552] as well as other groups studying the impact of sAßo on iPSC-derived neurons[556–558].

In contrast, when we tried to stimulate Fyn and Pyk2 activity by incubating iPSC-derived neurons with sAßo for a shorter time, we were unable to detect consistent increases in Fyn or Pyk2 phosphorylation, suggesting that the signaling cascade was either not activated or we were unable to detect its activation. To our knowledge, no group has reported activation of Fyn upon short-term synthetic Aßo treatment in iPSC-derived neurons, but other changes in the phospho-proteome in response to sAßo treatment have been observed via mass spectrometry[559]. It would be of interest to incubate neurons short-term with sAßo and then investigate more broadly which proteins/kinases display changes in activity. The Aßo-PrP^C-mGluR5-Fyn signaling cascade has been described repeatedly in primary mouse neuronal culture[184,201], as well as studied extensively in mice where its disruption rescued mouse behavior and Aß pathology[211,212,214], suggesting that it might exist and be of importance in human neuronal culture and ultimately human AD. This leads us to believe, that technical reasons are most likely to blame for our inability to see activation of Fyn and Pyk2 upon sAßo incubation. This hypothesis is further supported by reports from another group that saw PrP^C-dependent decreases in synaptic damage upon Aßo treatment in iPSC-derived neurons, suggesting that PrP^C binding to Aßo is relevant to AD pathophysiology in this model system[558,560].

Potential reasons for our inability to detect increases in phosphorylation for Fyn and Pyk2 in response to short-term sAßo treatment include that we might work with too immature cell cultures, that we might try to observe phosphorylation events at the wrong time-point after treatment, that the type of synthetic Aßo we prepared might not interact with PrP^C or that we used too low concentrations of sAßo to achieve detectable signaling. Assumptions about at what time phosphorylation increases, which preparation of sAßo to use and at what monomer equivalent sAßo concentration to treat with have been based off primary mouse neuronal cultures. These assumptions might have to be revisited, since most signaling experiments in primary cultures have been conducted at DIV 21, where primary neurons are likely more mature and have more spines than iPSC-derived neuron cultures. We have validated, that the iPSC-derived neurons express all relevant signaling cascade proteins, but a lack of maturity of the cultures could also mean that they are not localized together at synapses yet. In the future, performing immunohistochemical staining of our signaling cascade components could confirm their synaptic localization.

Previous work in iPSC-derived neurons generated from familiar and sporadic AD patient cell lines has often focused on studying alterations in APP processing or clearance, and observed tau and GSK3ß phosphorylation as downstream effects of increased $Aß_{42}$ production[561,562]. The mechanisms leading to these increases in phosphorylation of tau and GSK3ß remain elusive though. We believe that it would be of great interest to the field to validate signaling cascades that had previously been studied in mice or other tissue culture systems to determine their translation into human neurons. In this thesis, we attempted to study Aßo-PrP^C-mGluR5-Fyn signaling in iPSC-derived neurons, but further optimization will be needed to determine, if this signaling cascade is faithfully replicated in this model system. If the existence of the signaling cascade can be confirmed, revisiting kinase inhibition experiments for Fyn and Pyk2 might be of interest to try to disrupt Aßo -induced signaling. At this point, the importance, and potential mechanisms of Pyk2 and Fyn interaction with GSK3ß and tau in human AD are under debate since conflicting data from different model systems exist. Data generated for this thesis was unable to clarify this question. Further studies in model

organisms that do not employ over-expression of kinases or mutant tau would likely be helpful to elucidate this question.

Tau Spreading is impacted by template matching and ageing, but not Aß presence, Pyk2 and Fyn kinase inhibition or lysosomal protein PGRN and TMEM106b ablation

We examined cellular and molecular processes that might modify tau spreading in the context of AD. We extracted tau seeds from human AD subject brains and injected them into WT and transgenic mice as described previously[431,444,485] and observed that Aβ pathology, Fyn or Pyk2 inhibition, and lysosomal dysregulation by PGRN or TMEM106B deficiency have no significant effects on tau spreading. In contrast, animal age and the presence of hTau promoted the deposition of neuritic, but not somatic, tau. We characterized the quality and seeding capabilities of our tau extracts. It appears that the extracts used in this study contain tau isoforms similar to those in the literature[444] and also contain low levels of Aβ. The *in vitro* seeding capabilities of our extracts also match previous findings[444]. As the tau / total protein ratio in our extracts ranged between 1.6 and 9.5% tau content by immunoblot, we injected 0.5 µg/site with brain AB extracts, whereas other groups used 1 to 4 µg/site[430,444,484,485]. While dose – response relationships were ill defined in our study, the lower concentrations may explain the limited somatic tau inclusions in WT animals, and why only regions with the highest amounts of tau deposition were significantly different from control-injected animals. However, the pattern of hippocampal and cortical regions with highest accumulation was consistent with previous studies[444].

There has been a longstanding debate regarding how Aβ-induced signaling and/or Aβ plaques themselves facilitate or even initiate the formation of tau deposits. On one hand, in mouse models overexpressing both mutant APP and mutant tau, NFT formation is accelerated by the presence of Aβ[531,532]. On the other hand, for models dealing with injected tau or Aβ, the evidence is less clear. Injecting artificial Aβ42 fibrils into a mouse model overexpressing P301L mutant tau led to a five-fold increase in NFTs[529]. In contrast, studies using a human tau injection model reported a decrease in the number of NFT in the hippocampus and EC in 5xFAD mice, accompanied by an increase in NP tau instead[485,563]. In this model, microglial ablation and TREM2 knockout further enhanced NP tau deposition[563]. In a third study, injecting the less severe $App^{NL\text{-}F/NL\text{-}F}$ mouse model did not alter NFT or NP tau burden[485]. In a fourth study, hTau mice were crossed with $App^{NL\text{-}G\text{-}F/NL\text{-}G\text{-}F}$ mice (carrying the Arctic mutation in addition to the Swedish and Iberian mutations) and injected with tau seeds[491]. That study observed an increase in tau deposition for mice carrying hTau in comparison to WT animals, and this increase was further exacerbated in mice carrying both hTau and $App^{NL\text{-}G\text{-}F/NL\text{-}G\text{-}F}$ mutations.

Here, we observed equally increased somatic inclusions in AD tau extract–injected hTau or hTau-$App^{NL\text{-}F/NL\text{-}F}$ (DKI) mice as compared with WT animals. Both groups had greater tau inclusions than mice with murine tau, and this aligns with evidence that the presence of hTau in mice increases tau deposition after tau seed injection[491], but that the $App^{NL\text{-}F/NL\text{-}F}$ genotype had no impact on tau spreading[485]. When analyzing another Aβ-overexpression mouse model (APPswe/PSEN1ΔE9, termed APP here), we expected to see a decrease in NFT and increase in NP tau similar to what was previously seen in 5xFAD mice, but we did not observe any changes in somatic inclusion burden. In addition, we detected no increase in NP tau in AD extract–injected DKI or APP animals. We hypothesize that this might be due to the greatly accelerated Aβ pathology in 5xFAD compared with APP or DKI mice, with 5xFAD mice showing higher plaque burden at a younger age[564]. Potentially, this provides an earlier and more aggressive

microenvironment around plaques that is conducive to the aggregation of NP tau. Thus, we speculate that injecting APP/PS1 mice at 9 months instead of 3 months of age might lead to a phenotype similar to the one observed in 5xFAD mice. Another observation supporting the hypothesis that only high levels of Aβ burden are able to impact tau accumulation is that hTau-App$^{NL\text{-}G\text{-}F/NL\text{-}G\text{-}F}$ mice injected with tau show increased tau deposition compared with hTau mice[491], while we observed no exacerbation in mice with the less severe Aβ phenotype, hTau-App$^{NL\text{-}F/NL\text{-}F}$ mice. The hypothesis of Aβ-independent tau spreading with moderate levels of Aβ accumulation is further supported by the fact that Aβ and tau show distinct spreading patterns in both human and animal models[42,442,443,565]. We observed a redistribution of Aβ accumulation on the ipsilateral hemisphere, whereas dense-core plaques and tau depositions remained unaffected by the injection. The redistribution was not induced by injecting control extract and was ameliorated by partial immunodepletion of Aβ. Thus, we conclude that the redistribution was dependent on the small amounts of residual Aβ in our tau extracts. In support of this notion, the pattern of redistribution we observed is similar to the deposition reported by other groups[147–149] when injecting Aβ extracted from human brains into mice. While Aβ pathology at the levels of APPswe/PSEN1ΔE9 or App$^{NL\text{-}F/NL\text{-}F}$ mice did not alter tau spreading from injected mature AD tau seeds, this does not address the question whether Aβ-dependent mechanisms initiate tau misfolding separately from the spread of preformed seeds.

As discussed earlier, Fyn and Pyk2 are tyrosine kinases that have been reported to directly interact with and phosphorylate tau[161,207,264,545] and to also increase the activity of glycogen synthase kinase 3β[206,327,356]. A recent study has shown increases in tau phosphorylation at Y18 in human Pyk2/P301L tau double transgenic mice[264]. Other studies found that Fyn also phosphorylated tau at Y18[207] and that tau recruits Fyn to synapses[161]. Furthermore, knocking out or pharmacologically inhibiting Fyn in human tauopathy models led to a decrease in NFT, tau phosphorylation, and synaptic tau accumulation[536,545,546]. We thus expected that inhibiting either one of these kinases in WT mice, by knocking out Pyk2 or pharmacologically inhibiting Fyn, might decrease tau phosphorylation, resulting in reduced tau deposition after tau seed injection. However, we observed no effect of kinase inhibition or deletion on tau spreading. There are several possible explanations for the negative results. The first one is that other kinases can compensate for the loss of one kinase. This would imply that we would have to disrupt several kinases at the same time to achieve an observable effect on tau spreading by AD tau seeds. Another one is that the phospho-tau epitopes targeted by Fyn and Pyk2 are important for the initial *de novo* tau misfolding and aggregation and but are not critical after the initial seeding event has taken place, when templating of conformation is key. By injecting exogenous "mature" tau seeds, the current study focuses exclusively on templating and spreading of tau but does not assess the initial *de novo* seed formation steps in tau pathology. There is also evidence in the literature supporting this hypothesis since inhibiting Fyn in WT animals immediately after tau pathology was induced by traumatic brain injury–reduced phospho-tau accumulation and synapse loss, while initiating Fyn inhibition 100 days after the injury showed no effect[536].

Another cellular process dysregulated in AD is autophagy[493,494]. We focused on two proteins (TMEM106B and PGRN) that regulate lysosomal function. Reduction of TMEM106B by hypomorphic Tmem106b alleles was reported to decrease levels of lysosomal enzymes and to disrupt lysosomal acidification, one of the final steps in autophagy, leading to impaired degradation[507]. PGRN deficiency was reported to cause increases in lipofuscin and in the levels of many lysosomal enzymes[507]. Furthermore, decreasing PGRN levels were reported to enhance tau phosphorylation in P301L mutant tau mice[504,505]. However, the mechanistic details of this enhanced tau phosphorylation remain elusive. Given the previously reported effects of

TMEM106B and PGRN deficiency, we hypothesized an increase in tau spreading in the two knockout mice. Surprisingly, we observed no significant effects on tau spreading when disrupting expression of either TMEM106B or PGRN. We speculate that the lack of effect on tau spreading might be due to compensation by other cellular mechanisms (e.g., upregulated ubiquitin–proteasome response). Alternatively, as for the synaptic tyrosine kinases, lysosomal degradation may be more relevant for clearing *de novo* seed formation than for modulating tau templating and propagation.

Tau spreading was strongly increased by the presence of human tau and by advanced mouse age. We were able to confirm that the presence of hTau increases neuritic tau deposition in mice. Previous studies reported that tau from a particular species might template best onto tau of that same species[430,491]. This matches with the idea that a substrate with an amino acid match to the seed is more energetically favored to match the misfolded state of the seed. The effect of age on tau spreading is most interesting, and an increase in somatic and neuritic tau seeding has been detected in older mice previously[444]. In humans, aging is one of the most important risk factors for developing sporadic AD, and it is suspected that a variety of factors, including impaired protein clearance mechanisms, contribute to susceptibility and development of neurodegenerative diseases[566]. Our data indicate that tau deposition is increased when injecting tau seeds into older animals but disrupting lysosome-mediated clearance in aged mice by knocking out TMEM106B did not further increase tau deposition.

Since most mechanisms explored in this thesis did not have an impact on tau spreading, the question remains what factors mitigate tau spreading? In the last two years, several studies implicating different cellular mechanisms have been published. One study investigated the effect of TREM2 knockout and microglial depletion on neuritic plaque tau after tau injection into a transgenic APP mouse model[563]. They found that both TREM2 KO and microglial ablation increased neuritic plaque tau seeding and spreading and hypothesize that the protective effects conveyed by TREM2/microglia were most likely due to the activated state of the microglia surrounding plaques. Other studies used tau overexpression models combined with tau injections of various origin (human or mutant recombinant tau) to investigate tau spreading. One group studied the selective vulnerability of one of the earliest sites of AD tau accumulation, noradrenergic neurons in the locus coeruleus (LC). They found that a monoamine oxidase A metabolite of norepinephrine can interact with tau at residue K353, promoting its aggregation and subsequent propagation, rendering these neurons more susceptible to tau pathology[567]. Another study found that tau acetylation can shift its degradation from both macroautophagy and chaperone-mediated autophagy (CMA) towards mostly macroautophagy. In return, when CMA is inhibited in mice, acetylated tau accumulates in neurons and spreads to more recipient neurons than in WT mice[478]. A third study investigated the effects of different APOE isoforms on tau spreading in PS19 mice crossed with mice homozygous for different APOE alleles. Surprisingly, they found APOE3 to cause the highest increase in tau spreading compared to PS19 mice or PS19 mice carrying with the other APOE alleles[84]. This might be explained by the absence of other pathologies (e.g. Aß) that interact with APOE and might change its impact on tau spreading.

Future Directions

As the contradicting results from previous studies and this thesis show, the specific role of Pyk2 and Fyn in tau aggregation remains unclear, with different model systems displaying differential regulation of tau phosphorylation. Further research is needed to clarify which model system(s) best recapitulate AD pathology in humans and if the role of Pyk2 and Fyn on GSK3ß and tau in neurons is direct or indirect, and relevant to human AD tau pathology. In the future,

moving away from model systems that rely on overexpression of FTLD tau mutants might be of interest for tau phosphorylation research in the context of AD. Another useful approach might be to identify interaction partners of Pyk2 and Fyn in non-AD patient-derived iPSC-derived neurons that could phosphorylate tau. After their identification, their (dys)regulation could be studied in AD patient-derived cells and/or in mouse models.

Moreover, Fyn and Pyk2 are both expressed in microglia, albeit at lower levels than in neurons[241,249,568]. So far, their roles in microglia in the context of AD have not been extensively studied, but Fyn has been suggested to regulate α-synuclein uptake into microglia in Parkinson's Disease[568]. A recent publication has underscored the importance of microglia for tau spreading[563], and thus, characterizing interaction partners of Pyk2 and Fyn in microglia might be of interest in the context of tau aggregation and spreading.

To optimize the experiments in which iPSC-derived neurons were treated with sAßo to induce PrP^C-mGluR5-Fyn-Pyk2 signaling, several approaches could be taken. First, the binding of the sAßo species should be assessed via immunohistochemistry, to confirm successful binding of sAßo to PrP^C. If binding is successful, assessing downstream signaling events and identifying potential new proteins that respond to Aß binding would be important. Furthermore, perturbing the system through CRISPR/Cas9-mediated PrP^C knockdown or competitive inhibition would be of interest to confirm the importance of PrP^C in inducing downstream signaling events. In addition, the co-localization of the signaling cascade components in post-synaptic densities and/or dendritic spines could be confirmed through confocal imaging. If binding of the currently used sAßo species is not successful, other sAßo preparations should be tested for their binding abilities. Ultimately, studying the effects of highly purified Aß from human AD patient brains would be useful to observe differences from synthetics Aßo preparations.

To further study the factors impacting tau spreading, the scope of studied factors in mice should be broadened. Of note, a recent study found significant differences in tau spreading dependent on the genetic background of different WT mice strains[492]. In the study, the background strain used in this thesis (C57BL6) was found to be among the more resilient ones regarding tau spreading. It raises the question, if factors with a small impact on tau spreading would potentially not show any effect in our background strain but would have shown an effect in a different, more susceptible one. In addition, it also demonstrates that our understanding of the factors underlying tau spreading remains incomplete and a more thorough understanding of different mouse model genetic profiles might be necessary to compare studies within the field.

Another interesting research target would be to dissect which age-dependent mechanisms impact initial tau seed formation versus tau spreading versus both. From a technical perspective, heparin-independent aggregation of synthetic tau was shown to generate fibrils that are similar to brain-extracted tau fibrils[569]. Evaluating their seeding potential in mice models would be important, since we did observe differences in seeding density between extracts of different human brains, and these fibrils could be a useful tool to standardize future tau injection studies. Lastly, expanding on existing tau spreading and accumulation studies in *in vitro* systems would be of interest to further differentiate between factors impacting intracellular tau aggregation and trans-synaptic tau spreading.

Identifying those mechanisms that are necessary and sufficient to generate de novo tau seeds may be most relevant for the development of early intervention treatments for AD. Conversely, understanding of how tau spreading is regulated could pave the way for treatments of later stages of this devastating disease, when first tau deposition has taken place, but pathology has not spread throughout the brain yet.

References

1. Hippius, H. & Neundörfer, G. The discovery of Alzheimer's disease. *Dialogues Clin. Neurosci.* **5**, 101 (2003).
2. Jucker, M., Beyreuther, K., Haass, C., Nitsch, R. & Christen, Y. *Alzheimer: 100 Years and Beyond*. (Springer, 2006).
3. Alzheimer, A. Über eine eigenartige Erkrankung der Hirnrinde. *Allg. Zeitschrift für Psychiatr. und Psych. Medizin.* 146–148 (1907).
4. Perusini, G. Über klinisch und histologisch eigenartige psychische Erkrankungen des späteren Lebensalters. *Histol. und Histopathol. Arb.* **Band III**, 2 (1909).
5. Goedert, M. Oskar Fischer and the study of dementia. *Brain* **132**, 1102 (2009).
6. Cipriani, G., Dolciotti, C., Picchi, L. & Bonuccelli, U. Alzheimer and his disease: a brief history. *Neurol. Sci.* **32**, 275–279 (2010).
7. Fischer, O. Miliare Nekrosen mit drusigen Wucherungen der Neurofibrillen, eine regelmässige Veränderung der Hirnrinde bei seniler Demenz. *Monatsschr. Psychiatr. Neurol.* **22**, 361–72 (1907).
8. Alzheimer, A. Über eigenartige Krankheitsfälle des späteren Alters. *Zeitschrift für die gesamte Neurol. und Psychiatr.* **4**, 356–85 (1911).
9. Fischer, O. Die presbyophrene Demenz, deren anatomische Grundlage und klinische Abgrenzung. *Zeitschrift für die gesamte Neurol. und Psychiatr.* **3**, 371–471 (1910).
10. Fischer, O. Der spongiöse Rindenschwund, ein besonderer Destruktionsprozess der Hirnrinde. *Zeitschrift für die gesamte Neurol. und Psychiatr.* **7**, 1–33 (1911).
11. Fischer, O. Ein weiterer Beitrag zur Klinik und Pathologie der presbyophrenen Demenz. *Zeitschrift für die gesamte Neurol. und Psychiatr.* **12**, 99–135 (1912).
12. Kraepelin, E. *Psychiatrie. Ein Lehrbuch für Studierende und Ärzte, Band II: Klinische Psychiatrie.* (Barth, 1910).
13. Golde, T. E. Alzheimer's disease – the journey of a healthy brain into organ failure. *Mol. Neurodegener.* **17**, 1–19 (2022).
14. Congdon, E. E. & Sigurdsson, E. M. Tau-targeting therapies for Alzheimer disease. *Nat. Rev. Neurol.* **14**, 399 (2018).
15. Walker, L. C., Schelle, J. & Jucker, M. The prion-like properties of Amyloid-β assemblies: Implications for Alzheimer's Disease. *Cold Spring Harb. Perspect. Med.* **6**, a024398 (2016).
16. Hodges, J. R. Alzheimer's centennial legacy: origins, landmarks and the current status of knowledge concerning cognitive aspects. *Brain* **129**, 2811–2822 (2006).
17. Hane, F. T., Lee, B. Y. & Leonenko, Z. Recent Progress in Alzheimer's Disease Research, Part 1: Pathology. *J. Alzheimer's Dis.* **57**, 1–28 (2017).
18. Robinson, M., Lee, B. Y. & Hane, F. T. Recent Progress in Alzheimer's Disease Research, Part 2: Genetics and Epidemiology. *J. Alzheimer's Dis.* **57**, 317–330 (2017).
19. Hane, F. T. *et al.* Recent Progress in Alzheimer's Disease Research, Part 3: Diagnosis and Treatment. *J. Alzheimer's Dis.* **57**, 645–665 (2017).
20. Roth, M., Tomlinson, B. E. & Blessed, G. Correlation between scores for dementia and counts of 'senile plaques' in cerebral grey matter of elderly subjects. *Nature* **209**, 109–

110 (1966).

21. Blessed, G., Tomlinson, B. E. & Roth, M. The association between quantitative measures of dementia and of senile change in the cerebral grey matter of elderly subjects. *Br. J. Psychiatry* **114**, 797–811 (1968).

22. Heindel, W. C., Salmon, D. P., Shults, C. W., Walicke, P. A. & Butters, N. Neuropsychological evidence for multiple implicit memory systems: a comparison of Alzheimer's, Huntington's, and Parkinson's disease patients. *J. Neurosci.* **9**, 582–587 (1989).

23. Moss, M. B., Albert, M. S., Butters, N. & Payne, M. Differential patterns of memory loss among patients with Alzheimer's disease, Huntington's disease, and alcoholic Korsakoff's syndrome. *Arch. Neurol.* **43**, 239–246 (1986).

24. Kopelman, M. D. Rates of forgetting in Alzheimer-type dementia and Korsakoff's syndrome. *Neuropsychologia* **23**, 623–638 (1985).

25. Butters, N., Granholm, E., Salmon, D. P., Grant, I. & Wolfe, J. Episodic and semantic memory: a comparison of amnesic and demented patients. *J. Clin. Exp. Neuropsychol.* **9**, 479–497 (1987).

26. Petersen, R. C., Smith, G. E., Ivnik, R. J., Kokmen, E. & Tangalos, E. G. Memory function in very early Alzheimer's disease. *Neurology* **44**, 867–872 (1994).

27. Petersen, R. C. *et al.* Mild cognitive impairment: clinical characterization and outcome. *Arch. Neurol.* **56**, 303–308 (1999).

28. Fabrigoule, C. *et al.* Cognitive process in preclinical phase of dementia. *Brain* **121**–**1**, 135–141 (1998).

29. Hodges, J. The amnestic prodrome of Alzheimer's disease. *Brain* **121**–**9**, 1601–1602 (1998).

30. Bäckman, L., Small, B. J. & Fratiglioni, L. Stability of the preclinical episodic memory deficit in Alzheimer's disease. *Brain* **124**, 96–102 (2001).

31. Flicker, C., Ferris, S. H. & Reisberg, B. Mild cognitive impairment in the elderly: predictors of dementia. *Neurology* **41**, 1006–1009 (1991).

32. Linn, R. T. *et al.* The 'preclinical phase' of probable Alzheimer's disease. A 13-year prospective study of the Framingham cohort. *Arch. Neurol.* **52**, 485–490 (1995).

33. De Jager, C. A., Hogervorst, E., Combrinck, M. & Budge, M. M. Sensitivity and specificity of neuropsychological tests for mild cognitive impairment, vascular cognitive impairment and Alzheimer's disease. *Psychol. Med.* **33**, 1039–1050 (2003).

34. Ball, H. A. *et al.* Functional cognitive disorder: dementia's blind spot. *Brain* **143**, 2895–2903 (2020).

35. Liss, J. L. *et al.* Practical recommendations for timely, accurate diagnosis of symptomatic Alzheimer's disease (MCI and dementia) in primary care: a review and synthesis. *J. Intern. Med.* **290**, 310–334 (2021).

36. Jack, C. R. *et al.* Hypothetical model of dynamic biomarkers of the Alzheimer's pathological cascade. *Lancet Neurol.* **9**, 119–128 (2010).

37. Drachman, D. A. & Leavitt, J. Human Memory and the Cholinergic System: A Relationship to Aging? *Arch. Neurol.* **30**, 113–121 (1974).

38. Bowen, D. M., Smith, C. B., White, P. & Davison, A. N. Neurotransmitter-related

Enzymes and Indices of Hypoxia in Senile Dementia and Other Abiotrophies. *Brain* **99**, 459–496 (1976).

39. Terry, A. V. & Buccafusco, J. J. The Cholinergic Hypothesis of Age and Alzheimer's Disease-Related Cognitive Deficits: Recent Challenges and Their Implications for Novel Drug Development. *J. Pharmacol. Exp. Ther.* **306**, 821–827 (2003).
40. Hardy, J. A. & Higgins, G. A. Alzheimer's disease: The amyloid cascade hypothesis. *Science (80-.).* **256**, 184–185 (1992).
41. Hyman, B. T., Van Hoesen, G. W., Damasio, A. R. & Barnes, C. L. Alzheimer's Disease: Cell-Specific Pathology Isolates the Hippocampal Formation. *Science (80-.).* **225**, 1168–1170 (1984).
42. Braak, H. & Braak, E. Neuropathological stageing of Alzheimer-related changes. *Acta Neuropathol.* **82**, 239–259 (1991).
43. Braak, H. & Braak, E. Staging of Alzheimer's disease-related neurofibrillary changes. *Neurobiol. Aging* **16**, 271–278 (1995).
44. Simard, D., Olesen, J., Paulson, O. B., Lassen, N. A. & Skinhøj, E. Regional cerebral blood flow and its regulation in dementia. *Brain* **94**, 273–288 (1971).
45. Frackowiak, R. S. J. *et al.* Regional cerebral oxygen supply and utilization in dementia. A clinical and physiological study with oxygen-15 and positron tomography. *Brain* **104**, 753–778 (1981).
46. Klunk, W. E. *et al.* Imaging brain amyloid in Alzheimer's disease with Pittsburgh Compound-B. *Ann. Neurol.* **55**, 306–319 (2004).
47. Cook, R. H., Ward, B. E. & Austin, J. H. Studies in aging of the brain: IV. Familial Alzheimer disease: Relation to transmissible dementia, aneuploidy, and microtubular defects. *Neurology* **29**, 1402–1412 (1979).
48. Masters, C. L., Gajdusek, D. C. & Gibbs, C. J. The familial occurrence of Creutzfeldt-Jakob disease and Alzheimer's disease. *Brain* **104**, 535–558 (1981).
49. Bird, T. D. *et al.* Phenotypic heterogeneity in familial Alzheimer's disease: a study of 24 kindreds. *Ann. Neurol.* **25**, 12–25 (1989).
50. St. George-Hyslop, P. H. *et al.* The genetic defect causing familial Alzheimer's disease maps on chromosome 21. *Science* **235**, 885–890 (1987).
51. Goate, A. *et al.* Segregation of a missense mutation in the amyloid precursor protein gene with familial Alzheimer's disease. *Nature* **349**, 704–706 (1991).
52. Sherrington, R. *et al.* Cloning of a gene bearing missense mutations in early-onset familial Alzheimer's disease. *Nature* **375**, 754–760 (1995).
53. Corder, E. H. *et al.* Gene dose of apolipoprotein E type 4 allele and the risk of Alzheimer's disease in late onset families. *Science* **261**, 921–923 (1993).
54. Strittmatter, W. J. *et al.* Apolipoprotein E: high-avidity binding to beta-amyloid and increased frequency of type 4 allele in late-onset familial Alzheimer disease. *Proc. Natl. Acad. Sci. U. S. A.* **90**, 1977–1981 (1993).
55. Reitz, C., Brayne, C. & Mayeux, R. Epidemiology of Alzheimer disease. *Nat. Rev. Neurol.* **7**, 137 (2011).
56. Haass, C., Kaether, C., Thinakaran, G. & Sisodia, S. Trafficking and proteolytic processing of APP. *Cold Spring Harb. Perspect. Med.* **2**, (2012).

57. Kunkle, B. W. *et al.* Genetic meta-analysis of diagnosed Alzheimer's disease identifies new risk loci and implicates Aβ, tau, immunity and lipid processing. *Nat. Genet.* **51**, 414–430 (2019).

58. Smith, L. M. & Strittmatter, S. M. Binding Sites for Amyloid-β Oligomers and Synaptic Toxicity. *Cold Spring Harb. Perspect. Med.* a024075 (2016) doi:10.1101/cshperspect.a024075.

59. Scheltens, P. *et al.* Alzheimer's disease. *Lancet* **397**, 1577–1590 (2021).

60. Busche, M. A. & Hyman, B. T. Synergy between amyloid-β and tau in Alzheimer's disease. *Nat. Neurosci.* **23**, 1183–1193 (2020).

61. Hyman, B. T. *et al.* National Institute on Aging–Alzheimer's Association guidelines for the neuropathologic assessment of Alzheimer's disease. *Alzheimer's Dement.* **8**, 1 (2012).

62. Grangeon, L. *et al.* Cerebrospinal Fluid Profile of Tau, Phosphorylated Tau, Aβ42, and Aβ40 in Probable Cerebral Amyloid Angiopathy. *J. Alzheimer's Dis.* 1–12 (2022) doi:10.3233/JAD-215208.

63. Lang, L. *et al.* Prevalence and determinants of undetected dementia in the community: a systematic literature review and a meta-analysis. *BMJ Open* **7**, e011146 (2017).

64. McKhann, G. M. *et al.* The diagnosis of dementia due to Alzheimer's disease: recommendations from the National Institute on Aging-Alzheimer's Association workgroups on diagnostic guidelines for Alzheimer's disease. *Alzheimer's Dement.* **7**, 263–269 (2011).

65. Alzheimer's Association. 2021 Alzheimer's disease facts and figures special report Race, Ethnicity and Alzheimer's in America. *Alzheimer's Dement.* **17**, 327–406 (2021).

66. Gatz, M. *et al.* Role of genes and environments for explaining Alzheimer disease. *Arch. Gen. Psychiatry* **63**, 168–174 (2006).

67. Sherrington, R. *et al.* Alzheimer's Disease Associated with Mutations in Presenilin 2 is Rare and Variably Penetrant. *Hum. Mol. Genet.* **5**, 985–988 (1996).

68. Rogaev, E. I. *et al.* Familial Alzheimer's disease in kindreds with missense mutations in a gene on chromosome 1 related to the Alzheimer's disease type 3 gene. *Nature* **376**, 775–778 (1995).

69. Levy-Lahad, E. *et al.* A Familial Alzheimer's Disease Locus on Chromosome 1. *Science (80-.).* **269**, 970–973 (1995).

70. Cruts, M. *et al.* Molecular genetic analysis of familial early-onset Alzheimer's disease linked to chromosome 14q24.3. *Hum. Mol. Genet.* **4**, 2363–2371 (1995).

71. Campion, D. *et al.* Mutations of the presenilin I gene in families with early-onset Alzheimer's disease. *Hum. Mol. Genet.* **4**, 2373–2377 (1995).

72. Rovelet-Lecrux, A. *et al.* APP locus duplication causes autosomal dominant early-onset Alzheimer disease with cerebral amyloid angiopathy. *Nat. Genet.* **38**, 24–26 (2006).

73. Guerreiro, R. J. *et al.* Genetic screening of Alzheimer's disease genes in Iberian and African samples yields novel mutations in presenilins and APP. *Neurobiol. Aging* **31**, 725–731 (2010).

74. Wallon, D. *et al.* The French series of autosomal dominant early onset Alzheimer's disease cases: mutation spectrum and cerebrospinal fluid biomarkers. *J. Alzheimer's Dis.* **30**, 847–856 (2012).

75. ALZFORUM. APP. https://www.alzforum.org/mutations/app.

76. ALZFORUM. PSEN-1. https://www.alzforum.org/mutations/psen-1.

77. ALZFORUM. PSEN-2. https://www.alzforum.org/mutations/psen-2.

78. O'Brien, R. J. & Wong, P. C. Amyloid precursor protein processing and Alzheimer's disease. *Annu. Rev. Neurosci.* **34**, 185–204 (2011).

79. Mullan, M. *et al.* A pathogenic mutation for probable Alzheimer's disease in the APP gene at the N-terminus of beta-amyloid. *Nat. Genet.* **1**, 345–347 (1992).

80. Eckman, C. B. *et al.* A new pathogenic mutation in the APP gene (I716V) increases the relative proportion of A beta 42(43). *Hum. Mol. Genet.* **6**, 2087–2089 (1997).

81. Kamino, K. *et al.* Linkage and mutational analysis of familial Alzheimer disease kindreds for the APP gene region. *Am. J. Hum. Genet.* **51**, 998 (1992).

82. Nilsberth, C. *et al.* The 'Arctic' APP mutation (E693G) causes Alzheimer's disease by enhanced Aβ protofibril formation. *Nat. Neurosci.* **4**, 887–893 (2001).

83. Tokuda, T. *et al.* Lipidation of apolipoprotein E influences its isoform-specific interaction with Alzheimer's amyloid beta peptides. *Biochem. J.* **348 Pt 2**, 359–65 (2000).

84. Williams, T. *et al.* Impact of APOE genotype on prion-type propagation of tauopathy. *Acta Neuropathol. Commun.* **10**, 57 (2022).

85. Kim, J., Basak, J. M. & Holtzman, D. M. The role of apolipoprotein E in Alzheimer's Disease. *Neuron* **63**, 287–303 (2009).

86. Singh, P. P., Singh, M. & Mastana, S. S. APOE distribution in world populations with new data from India and the UK. *Ann. Hum. Biol.* **33**, 279–308 (2006).

87. Kleinberger, G. *et al.* TREM2 mutations implicated in neurodegeneration impair cell surface transport and phagocytosis. *Sci. Transl. Med.* **6**, 243ra86 (2014).

88. Morenas-Rodríguez, E. *et al.* Soluble TREM2 in CSF and its association with other biomarkers and cognition in autosomal-dominant Alzheimer's disease: a longitudinal observational study. *Lancet Neurol.* **21**, 329–341 (2022).

89. Rochoy, M. *et al.* Factors Associated with Alzheimer's Disease: An Overview of Reviews. *J. Prev. Alzheimer's Dis.* **6**, 121–134 (2019).

90. Chêne, G. *et al.* Gender and incidence of dementia in the Framingham Heart Study from mid-adult life. *Alzheimer's Dement.* **11**, 310 (2015).

91. Tecalco-Cruz, A. C., Zepeda–Cervantes, J. & Ortega-Domínguez, B. Estrogenic hormones receptors in Alzheimer's disease. *Mol. Biol. Rep.* **48**, 7517–7526 (2021).

92. Buckley, R. F. *et al.* Sex Differences in the Association of Global Amyloid and Regional Tau Deposition Measured by Positron Emission Tomography in Clinically Normal Older Adults. *JAMA Neurol.* **76**, 542–551 (2019).

93. Fisher, R. A., Miners, J. S. & Love, S. Pathological changes within the cerebral vasculature in Alzheimer's disease: New perspectives. *Brain Pathol.* **00**, e13061 (2022).

94. Pendlebury, S. T. & Rothwell, P. M. Prevalence, incidence, and factors associated with pre-stroke and post-stroke dementia: a systematic review and meta-analysis. *Lancet Neurol.* **8**, 1006–1018 (2009).

95. Michailidis, M. *et al.* Alzheimer's Disease as Type 3 Diabetes: Common Pathophysiological Mechanisms between Alzheimer's Disease and Type 2 Diabetes. *Int. J. Mol. Sci.* **23**, 2687 (2022).

96. Zhu, X. & Zhao, Y. Sleep-disordered breathing and the risk of cognitive decline: a meta-analysis of 19,940 participants. *Sleep Breath.* **22**, 165–173 (2018).

97. Fleminger, S., Oliver, D. L., Lovestone, S., Rabe-Hesketh, S. & Giora, A. Head injury as a risk factor for Alzheimer's disease: the evidence 10 years on; a partial replication. *J. Neurol. Neurosurg. Psychiatry* **74**, 857 (2003).

98. Zhang, J., Zhang, Y., Zou, J. & Cao, F. A meta-analysis of cohort studies: Traumatic brain injury and risk of Alzheimer's Disease. *PLoS One* **16**, e0253206 (2021).

99. Caamaño-Isorna, F., Corral, M., Montes-Martínez, A. & Takkouche, B. Education and dementia: a meta-analytic study. *Neuroepidemiology* **26**, 226–232 (2006).

100. Zhang, J. *et al.* An updated meta-analysis of cohort studies: Diabetes and risk of Alzheimer's disease. *Diabetes Res. Clin. Pract.* **124**, 41–47 (2017).

101. Futch, H. S., Croft, C. L., Truong, V. Q., Krause, E. G. & Golde, T. E. Targeting psychologic stress signaling pathways in Alzheimer's disease. *Mol. Neurodegener.* **12**, (2017).

102. Yusufov, M., Weyandt, L. L. & Piryatinsky, I. Alzheimer's disease and diet: a systematic review. *Int. J. Neurosci.* **127**, 161–175 (2017).

103. Stern, Y., Barnes, C. A., Grady, C., Jones, R. N. & Raz, N. Brain reserve, cognitive reserve, compensation, and maintenance: operationalization, validity, and mechanisms of cognitive resilience. *Neurobiol. Aging* **83**, 124–129 (2019).

104. Kochhar, R. & Oates, R. *Attitudes about Aging: A Global Perspective*. (2014).

105. World Health Organization. The top 10 causes of death. https://www.who.int/news-room/fact-sheets/detail/the-top-10-causes-of-death (2020).

106. World Health Organization. *Towards a dementia- inclusive society: WHO toolkit for dementia-friendly initiatives (DFIs)*. (2021).

107. Andersen, K. *et al.* Gender differences in the incidence of AD and vascular dementia: The EURODEM Studies. EURODEM Incidence Research Group. *Neurology* **53**, 1992–1997 (1999).

108. Alzheimer's Impact Movement. *Realizing the National Plan to Address Alzheimer's Disease*. https://alzimpact.org/media/serve/id/5eab1509d8322 (2022).

109. Kaiser, J. The Alzheimer's gamble: NIH tries to turn billions in new funding into treatment for deadly brain disease. *Science (80-.).* (2018) doi:10.1126/SCIENCE.AAV2455.

110. Breijyeh, Z., Karaman, R., Muñoz-Torrero, D. & Dembinski, R. Comprehensive Review on Alzheimer's Disease: Causes and Treatment. *Molecules* **25**, 5789 (2020).

111. Vaz, M. & Silvestre, S. Alzheimer's disease: Recent treatment strategies. *Eur. J. Pharmacol.* **887**, 173554 (2020).

112. The Medical Letter. 1628: Aducanumab (Aduhelm) for Alzheimer's Disease. **63**, (2021).

113. US National Library of Medicine. 221AD302 Phase 3 Study of Aducanumab (BIIB037) in Early Alzheimer's Disease. https://clinicaltrials.gov/ct2/show/NCT02484547.

114. US National Library of Medicine. 221AD301 Phase 3 Study of Aducanumab (BIIB037) in Early Alzheimer's Disease (ENGAGE). https://clinicaltrials.gov/ct2/show/NCT02477800.

115. Kuller, L. H. & Lopez, O. L. ENGAGE and EMERGE: Truth and consequences? *Alzheimer's Dement.* **17**, 692–695 (2021).

116. Fillit, H. & Green, A. Aducanumab and the FDA — where are we now? *Nat. Rev. Neurol.*

17, 129–130 (2021).

117. Lee, J. *et al.* Adaptor Protein Sorting Nexin 17 Regulates Amyloid Precursor Protein Trafficking and Processing in the Early Endosomes. *J. Biol. Chem.* **283**, 11501 (2008).
118. Young-Pearse, T. L. *et al.* A critical function for beta-amyloid precursor protein in neuronal migration revealed by in utero RNA interference. *J. Neurosci.* **27**, 14459–14469 (2007).
119. Ashley, J., Packard, M., Ataman, B. & Budnik, V. Fasciclin II signals new synapse formation through amyloid precursor protein and the scaffolding protein dX11/Mint. *J. Neurosci.* **25**, 5943–55 (2005).
120. Zheng, H. *et al.* beta-Amyloid precursor protein-deficient mice show reactive gliosis and decreased locomotor activity. *Cell* **81**, 525–531 (1995).
121. Oh, E. S. *et al.* Amyloid precursor protein increases cortical neuron size in transgenic mice. *Neurobiol. Aging* **30**, 1238–1244 (2009).
122. Herms, J. *et al.* Cortical dysplasia resembling human type 2 lissencephaly in mice lacking all three APP family members. *EMBO J.* **23**, 4106–4115 (2004).
123. Koo, E. H. *et al.* Precursor of amyloid protein in Alzheimer disease undergoes fast anterograde axonal transport. *Proc. Natl. Acad. Sci. U. S. A.* **87**, 1561–5 (1990).
124. Kinoshita, A. *et al.* Demonstration by FRET of BACE interaction with the amyloid precursor protein at the cell surface and in early endosomes. *J. Cell Sci.* **116**, 3339–3346 (2003).
125. Bachurin, S. O., Bovina, E. V. & Ustyugov, A. A. Drugs in Clinical Trials for Alzheimer's Disease: The Major Trends. *Med. Res. Rev.* **37**, 1186–1225 (2017).
126. Walker, L. C., Schelle, J. & Jucker, M. The Prion-Like Properties of Amyloid-β Assemblies: Implications for Alzheimer's Disease. *Cold Spring Harb. Perspect. Med.* **6**, a024398 (2016).
127. Jankowsky, J. L. *et al.* Mutant presenilins specifically elevate the levels of the 42 residue beta-amyloid peptide in vivo: evidence for augmentation of a 42-specific gamma secretase. *Hum. Mol. Genet.* **13**, 159–70 (2004).
128. Shen, J. & Kelleher, R. J. The presenilin hypothesis of Alzheimer's disease: evidence for a loss-of-function pathogenic mechanism. *Proc. Natl. Acad. Sci. U. S. A.* **104**, 403–9 (2007).
129. Bergmans, B. A. & De Strooper, B. γ-secretases: from cell biology to therapeutic strategies. *Lancet Neurol.* **9**, 215–226 (2010).
130. Chow, V. W., Mattson, M. P., Wong, P. C. & Gleichmann, M. An overview of APP processing enzymes and products. *Neuromolecular Med.* **12**, 1–12 (2010).
131. Nelson, R. *et al.* Structure of the cross-β spine of amyloid-like fibrils. *Nature* **435**, 773 (2005).
132. Laganowsky, A. *et al.* Atomic View of a Toxic Amyloid Small Oligomer. *Science* **335**, 1228 (2012).
133. Buchete, N. V., Tycko, R. & Hummer, G. Molecular Dynamics Simulations of Alzheimer's β-Amyloid Protofilaments. *J. Mol. Biol.* **353**, 804–821 (2005).
134. Qiang, W., Yau, W. M., Luo, Y., Mattson, M. P. & Tycko, R. Antiparallel β-sheet architecture in Iowa-mutant β-amyloid fibrils. *Proc. Natl. Acad. Sci. U. S. A.* **109**, 4443–

4448 (2012).

135. Wälti, M. A., Orts, J., Vögeli, B., Campioni, S. & Riek, R. Solution NMR Studies of Recombinant Aβ(1–42): From the Presence of a Micellar Entity to Residual β-Sheet Structure in the Soluble Species. *ChemBioChem* **16**, 659–669 (2015).

136. Yang, Y. *et al.* Cryo-EM structures of amyloid-b 42 filaments from human brains. *Science (80-.).* **375**, 167–172 (2022).

137. Yu, X. & Zheng, J. Polymorphic Structures of Alzheimer's β-Amyloid Globulomers. *PLoS One* **6**, e20575 (2011).

138. Lu, J. X. *et al.* Molecular structure of β-amyloid fibrils in Alzheimer's disease brain tissue. *Cell* **154**, 1257 (2013).

139. Sandberg, A. *et al.* Stabilization of neurotoxic Alzheimer amyloid-β oligomers by protein engineering. *Proc. Natl. Acad. Sci. U. S. A.* **107**, 15595–15600 (2010).

140. Braak, H. & Braak, E. Frequency of Stages of Alzheimer-Related Lesions in Different Age Categories. *Neurobiol. Aging* **18**, 351–357 (1997).

141. Sengoku, R. Aging and Alzheimer's disease pathology. *Neuropathology* **40**, 22–29 (2020).

142. Iwatsubo, T. *et al.* Visualization of Aβ42(43) and Aβ40 in senile plaques with end-specific Aβ monoclonals: Evidence that an initially deposited species is Aβ42(43). *Neuron* **13**, 45–53 (1994).

143. Langer, F. *et al.* Soluble aβ seeds are potent inducers of cerebral β-amyloid deposition. *J. Neurosci.* **31**, 14488–14495 (2011).

144. Novotny, R. *et al.* Conversion of Synthetic Aβ to In Vivo Active Seeds and Amyloid Plaque Formation in a Hippocampal Slice Culture Model. *J. Neurosci.* **36**, (2016).

145. Ye, Lan; Hamaguchi, Tsuyoshi; Fritschi, Sarah K.; Eisele, Yvonne S.; Obermüller, Ulrike; Jucker, Mathias; Walker, L. C. Progression of seed-induced Abeta deposition within the limbic connectome. *Physiol. Behav.* **176**, 139–148 (2019).

146. Heilbronner, G. *et al.* Seeded strain-like transmission of β-amyloid morphotypes in APP transgenic mice. *EMBO Rep.* **14**, 1017–1022 (2013).

147. Eisele, Y. S. *et al.* Induction of cerebral β-amyloidosis: Intracerebral versus systemic Aβ inoculation. *Proc. Natl. Acad. Sci. U. S. A.* **106**, 12926–12931 (2009).

148. Kane, M. D. *et al.* Evidence for Seeding of β-Amyloid by Intracerebral Infusion of Alzheimer Brain Extracts in β-Amyloid Precursor Protein-Transgenic Mice. *J. Neurosci.* **20**, 3606–3611 (2000).

149. Meyer-Luehmann, M. *et al.* Exogenous induction of cerebral β-amyloidogenesis is governed bf agent and host. *Science (80-.).* **313**, 1781–1784 (2006).

150. Weller, R. O., Preston, S. D., Subash, M. & Carare, R. O. Cerebral amyloid angiopathy in the aetiology and immunotherapy of Alzheimer disease. *Alzheimers. Res. Ther.* **1**, 6 (2009).

151. DaRocha-Souto, B. *et al.* Brain oligomeric β-amyloid but not total amyloid plaque burden correlates with neuronal loss and astrocyte inflammatory response in amyloid precursor protein/tau transgenic mice. *J. Neuropathol. Exp. Neurol.* **70**, 360–76 (2011).

152. Lue, L. F. *et al.* Soluble amyloid beta peptide concentration as a predictor of synaptic change in Alzheimer's disease. *Am. J. Pathol.* **155**, 853–862 (1999).

153. Giannakopoulos, P., Hof, P. R., Michel, J. P., Guimon, J. & Bouras, C. Cerebral cortex pathology in aging and Alzheimer's disease: a quantitative survey of large hospital-based geriatric and psychiatric cohorts. *Brain Res. Rev.* **25**, 217–245 (1997).

154. Kostylev, M. A. *et al.* Prion-Protein-interacting Amyloid-β oligomers of high molecular weight are tightly correlated with memory impairment in multiple Alzheimer mouse models. *J. Biol. Chem.* **290**, 17415–38 (2015).

155. Shankar, G. M. *et al.* Amyloid-β protein dimers isolated directly from Alzheimer's brains impair synaptic plasticity and memory. *Nat. Med.* **14**, 837–842 (2008).

156. Walker, L. C. Aβ Plaques. *Free Neuropathol.* **1**, 1–42 (2020).

157. Lee, H. G. *et al.* Challenging the Amyloid Cascade Hypothesis: Senile Plaques and Amyloid-β as Protective Adaptations to Alzheimer Disease. *Ann. N. Y. Acad. Sci.* **1019**, 1–4 (2004).

158. Greer, M. M. J. Inflammation and the pathophysiology of Alzheimer's disease. *Dialogues Clin. Neurosci.* **2**, 233–239 (2022).

159. Abramov, E. *et al.* Amyloid-beta as a positive endogenous regulator of release probability at hippocampal synapses. *Nat. Neurosci.* **12**, 1567–76 (2009).

160. Kamenetz, F. *et al.* APP processing and synaptic function. *Neuron* **37**, 925–37 (2003).

161. Ittner, L. M. *et al.* Dendritic function of tau mediates Amyloid-β toxicity in Alzheimer's Disease mouse models. *Cell* **142**, 387–397 (2010).

162. Heneka, M. T. *et al.* Neuroinflammation in Alzheimer's disease. *Lancet Neurol.* **14**, 388–405 (2015).

163. Schaefer, P. M., von Einem, B., Walther, P., Calzia, E. & von Arnim, C. A. F. Metabolic characterization of intact cells reveals intracellular Amyloid Beta but not its precursor protein to reduce mitochondrial respiration. *PLoS One* **11**, e0168157 (2016).

164. Aleardi, A. M. *et al.* Gradual alteration of mitochondrial structure and function by β-Amyloids: Importance of membrane viscosity changes, energy deprivation, reactive oxygen species production, and cytochrome c release. *J. Bioenerg. Biomembr.* **37**, 207–225 (2005).

165. Xu, L.-L. *et al.* Mitochondrial dynamics changes with age in an APPswe/PS1dE9 mouse model of Alzheimer's disease. *Neuroreport* **28**, 1 (2017).

166. Smith, L. M., Kostylev, M. A., Lee, S. & Strittmatter, S. M. Systematic and standardized comparison of reported amyloid-β receptors for sufficiency, affinity, and Alzheimer's disease relevance. *J. Biol. Chem.* **294**, 6042 (2019).

167. Kuner, P., Schubenel, R. & Hertel, C. Amyloid Binds to p75 NTR and Activates NFB in Human Neuroblastoma Cells. *J. Neurosci. Res.* **54**, 798–804 (1998).

168. Woolf, N. J., Gould, E. & Butcher, L. L. Nerve growth factor receptor is associated with cholinergic neurons of the basal forebrain but not the pontomesencephalon. *Neuroscience* **30**, 143–152 (1989).

169. Mufson, E. J. & Kordower, J. H. Cortical neurons express nerve growth factor receptors in advanced age and Alzheimer disease. *Proc. Natl. Acad. Sci. U. S. A.* **89**, 569–573 (1992).

170. Yaar, M. *et al.* Binding of beta-amyloid to the p75 neurotrophin receptor induces apoptosis. A possible mechanism for Alzheimer's disease. *J. Clin. Invest.* **100**, 2333 (1997).

171. Yan, S. Du *et al.* RAGE and amyloid-β peptide neurotoxicity in Alzheimer's disease. *Nature* **382**, 685–691 (1996).

172. Neeper, M. *et al.* Cloning and expression of a cell surface receptor for advanced glycosylation end products of proteins. *J. Biol. Chem.* **267**, 14998–15004 (1992).

173. Schmidt, A. M. *et al.* Isolation and characterization of two binding proteins for advanced glycosylation end products from bovine lung which are present on the endothelial cell surface. *J. Biol. Chem.* **267**, 14987–14997 (1992).

174. Hori, O. *et al.* The receptor for advanced glycation end products (RAGE) is a cellular binding site for amphoterin. Mediation of neurite outgrowth and co-expression of rage and amphoterin in the developing nervous system. *J. Biol. Chem.* **270**, 25752–25761 (1995).

175. Deane, R. *et al.* RAGE mediates amyloid-beta peptide transport across the blood-brain barrier and accumulation in brain. *Nat. Med.* **9**, 907–913 (2003).

176. Vodopivec, I. *et al.* RAGE does not affect amyloid pathology in transgenic ArcAbeta mice. *Neurodegener. Dis.* **6**, 270–280 (2009).

177. Hogg, R. C., Raggenbass, M. & Bertrand, D. Nicotinic acetylcholine receptors: from structure to brain function. *Rev. Physiol. Biochem. Pharmacol.* **147**, 1–46 (2003).

178. Wang, H. Y., Lee, D. H. S., Davis, C. B. & Shank, R. P. Amyloid peptide Abeta(1-42) binds selectively and with picomolar affinity to alpha7 nicotinic acetylcholine receptors. *J. Neurochem.* **75**, 1155–1161 (2000).

179. Dineley, K. T. *et al.* Beta-amyloid activates the mitogen-activated protein kinase cascade via hippocampal alpha7 nicotinic acetylcholine receptors: In vitro and in vivo mechanisms related to Alzheimer's disease. *J. Neurosci.* **21**, 4125–4133 (2001).

180. Park, J. H. *et al.* Alzheimer precursor protein interaction with the Nogo-66 receptor reduces amyloid-beta plaque deposition. *J. Neurosci.* **26**, 1386–1395 (2006).

181. Park, J. H. *et al.* Subcutaneous Nogo Receptor Removes Brain Amyloid-β and Improves Spatial Memory in Alzheimer's Transgenic Mice. *J. Neurosci.* **26**, 13279–13286 (2006).

182. Xie, L. *et al.* Alzheimer's beta-amyloid peptides compete for insulin binding to the insulin receptor. *J. Neurosci.* **22**, RC221 (2002).

183. Zhao, W. *et al.* Amyloid beta oligomers induce impairment of neuronal insulin receptors. *FASEB J.* **22**, 246–260 (2008).

184. Laurén, J., Gimbel, D. A., Nygaard, H. B., Gilbert, J. W. & Strittmatter, S. M. Cellular prion protein mediates impairment of synaptic plasticity by amyloid-β oligomers. *Nature* **457**, 1128–1132 (2009).

185. Wang, L. *et al.* Epidermal growth factor receptor is a preferred target for treating amyloid-β-induced memory loss. *Proc. Natl. Acad. Sci. U. S. A.* **109**, 16743–16748 (2012).

186. Cissé, M. *et al.* Reversing EphB2 depletion rescues cognitive functions in Alzheimer model. *Nature* **469**, 47–52 (2011).

187. Fu, A. K. Y. *et al.* Blockade of EphA4 signaling ameliorates hippocampal synaptic dysfunctions in mouse models of Alzheimer's disease. *Proc. Natl. Acad. Sci. U. S. A.* **111**, 9959–9964 (2014).

188. Kam, T. I. *et al.* FcγRIIb mediates amyloid-β neurotoxicity and memory impairment in Alzheimer's disease. *J. Clin. Invest.* **123**, 2791–2802 (2013).

189. Amin, L. & Harris, D. A. Aβ receptors specifically recognize molecular features displayed by fibril ends and neurotoxic oligomers. *Nat. Commun.* **12**, 3451 (2021).

190. Kim, T. *et al.* Human LilrB2 is a β-amyloid receptor and its murine homolog PirB regulates synaptic plasticity in an Alzheimer's model. *Science* **341**, 1399–1404 (2013).

191. Hu, T., Wang, S., Chen, C., Sun, J. & Yang, X. Real-Time Analysis of Binding Events between Different Aβ 1-42 Species and Human Lilrb2 by Dual Polarization Interferometry. *Anal. Chem.* **89**, 2606–2612 (2017).

192. Cao, Q. *et al.* Inhibiting amyloid-β cytotoxicity through its interaction with the cell surface receptor LilrB2 by structure-based design. *Nat. Chem.* **10**, 1213–1221 (2018).

193. Carlo, A. S. *et al.* The Pro-Neurotrophin Receptor Sortilin Is a Major Neuronal Apolipoprotein E Receptor for Catabolism of Amyloid-β Peptide in the Brain. *J. Neurosci.* **33**, 358–370 (2013).

194. Nygaard, H. B., van Dyck, C. H. & Strittmatter, S. M. Fyn kinase inhibition as a novel therapy for Alzheimer's disease. *Alzheimers. Res. Ther.* **6**, 8 (2014).

195. Brody, A. H. & Strittmatter, S. M. *Synaptotoxic Signaling by Amyloid Beta Oligomers in Alzheimer's Disease Through Prion Protein and mGluR5*. *Advances in Pharmacology* vol. 82 (Elsevier Inc., 2017).

196. Salazar, S. V. & Strittmatter, S. M. Cellular prion protein as a receptor for amyloid-β oligomers in Alzheimer's disease. *Biochem. Biophys. Res. Commun.* **483**, 1143–47 (2016).

197. Chen, S., Yadav, S. P. & Surewicz, W. K. Interaction between human prion protein and amyloid-beta (Abeta) oligomers: role OF N-terminal residues. *J. Biol. Chem.* **285**, 26377–83 (2010).

198. Balducci, C. *et al.* Synthetic amyloid-beta oligomers impair long-term memory independently of cellular prion protein. *Proc. Natl. Acad. Sci. U. S. A.* **107**, 2295–300 (2010).

199. Um, J. W. *et al.* Alzheimer amyloid-β oligomer bound to postsynaptic prion protein activates Fyn to impair neurons. *Nat. Neurosci.* **15**, 1227–1235 (2012).

200. Haas, L. T. *et al.* Metabotropic glutamate receptor 5 couples cellular prion protein to intracellular signalling in Alzheimer's disease. *Brain* **139**, 526–46 (2016).

201. Um, J. W. *et al.* Metabotropic glutamate receptor 5 is a coreceptor for Alzheimer Aβ oligomer bound to cellular prion protein. *Neuron* **79**, 887–902 (2013).

202. Hu, N.-W. *et al.* mGlu5 receptors and cellular prion protein mediate amyloid-β-facilitated synaptic long-term depression in vivo. *Nat. Commun.* **5**, 3374 (2014).

203. Rushworth, J. V., Griffiths, H. H., Watt, N. T. & Hooper, N. M. Prion protein-mediated toxicity of amyloid-β oligomers requires lipid rafts and the transmembrane LRP1. *J. Biol. Chem.* **288**, 8935–8951 (2013).

204. Larson, M. *et al.* The complex PrP(c)-Fyn couples human oligomeric Aβ with pathological tau changes in Alzheimer's disease. *J. Neurosci.* **32**, 16857–71a (2012).

205. Lambert, J.-C. *et al.* Meta-analysis of 74,046 individuals identifies 11 new susceptibility loci for Alzheimer's disease. *Nat. Genet.* **45**, 1452–1458 (2013).

206. Hartigan, J. A., Xiong, W.-C. & Johnson, G. V. W. Glycogen Synthase Kinase 3β Is Tyrosine Phosphorylated by PYK2. *Biochem. Biophys. Res. Commun.* **284**, 485–489 (2001).

207. Lee, G. *et al.* Phosphorylation of Tau by Fyn: Implications for Alzheimer's Disease. *J. Neurosci.* **24**, 2304–2312 (2004).

208. Conn, P. J. & Pin, J. P. Pharmacology and functions of metabotropic glutamate receptors. *Annu. Rev. Pharmacol. Toxicol.* **37**, 205–237 (1997).

209. Lev, S. *et al.* Protein tyrosine kinase PYK2 involved in Ca2+-induced regulation of ion channel and MAP kinase functions. *Nature* **376**, 737–745 (1995).

210. Gimbel, D. A. *et al.* Memory impairment in transgenic Alzheimer mice requires cellular prion protein. *J. Neurosci.* **30**, 6367–74 (2010).

211. Kaufman, A. C. *et al.* Fyn inhibition rescues established memory and synapse loss in Alzheimer mice. *Ann. Neurol.* **77**, 953–71 (2015).

212. Spurrier, J. *et al.* Reversal of synapse loss in Alzheimer mouse models by targeting mGluR5 to prevent synaptic tagging by C1Q. *Sci. Transl. Med.* **14**, (2022).

213. Ma, T. *et al.* Inhibition of AMP-activated protein kinase signaling alleviates impairments in hippocampal synaptic plasticity induced by amyloid β. *J. Neurosci.* **34**, 12230–8 (2014).

214. Salazar, S. V *et al.* Conditional Deletion of Prnp Rescues Behavioral and Synaptic Deficits after Disease Onset in Transgenic Alzheimer's Disease. *J. Neurosci.* **37**, 9207–9221 (2017).

215. Barry, A. E. *et al.* Alzheimer's disease brain-derived amyloid-β-mediated inhibition of LTP in vivo is prevented by immunotargeting cellular prion protein. *J. Neurosci.* **31**, 7259–7263 (2011).

216. Freir, D. B. *et al.* Interaction between prion protein and toxic amyloid β assemblies can be therapeutically targeted at multiple sites. *Nat. Commun.* **2**, 336 (2011).

217. Klyubin, I. *et al.* Peripheral Administration of a Humanized Anti-PrP Antibody Blocks Alzheimer's Disease Aβ Synaptotoxicity. *J. Neurosci.* **34**, 6140–6145 (2014).

218. Chung, E. *et al.* Anti-PrPC monoclonal antibody infusion as a novel treatment for cognitive deficits in an Alzheimer's disease model mouse. *BMC Neurosci.* **11**, (2010).

219. Fluharty, B. R. *et al.* An N-terminal Fragment of the Prion Protein Binds to Amyloid-β Oligomers and Inhibits Their Neurotoxicity in Vivo. *J. Biol. Chem.* **288**, 7857 (2013).

220. Cox, T. O. *et al.* Anti-PrPC antibody rescues cognition and synapses in transgenic alzheimer mice. *Ann. Clin. Transl. Neurol.* **6**, 554 (2019).

221. Bate, C. & Williams, A. Amyloid-β-induced Synapse Damage Is Mediated via Cross-linkage of Cellular Prion Proteins. *J. Biol. Chem.* **286**, 37955 (2011).

222. Calella, A. M. *et al.* Prion protein and Aβ-related synaptic toxicity impairment. *EMBO Mol. Med.* **2**, 306–314 (2010).

223. Kessels, H. W., Nguyen, L. N., Nabavi, S. & Malinow, R. The prion protein as a receptor for amyloid-β. *Nature* **466**, E3–E4 (2010).

224. Cissé, M. *et al.* Ablation of Cellular Prion Protein Does Not Ameliorate Abnormal Neural Network Activity or Cognitive Dysfunction in the J20 Line of Human Amyloid Precursor Protein Transgenic Mice. *J. Neurosci.* **31**, 10427 (2011).

225. Nicoll, A. J. *et al.* Amyloid-β nanotubes are associated with prion protein-dependent synaptotoxicity. *Nat. Commun.* **4**, 1–9 (2013).

226. Dohler, F. *et al.* High molecular mass assemblies of amyloid-β oligomers bind prion

protein in patients with Alzheimer's disease. *Brain* **137**, 873–886 (2014).

227. Selkoe, D. J. & Hardy, J. The amyloid hypothesis of Alzheimer's disease at 25 years. *EMBO Mol. Med.* **8**, 595 (2016).

228. Games, D. *et al.* Alzheimer-type neuropathology in transgenic mice overexpressing V717F beta-amyloid precursor protein. *Nature* **373**, 523–527 (1995).

229. Citron, M. *et al.* Mutant presenilins of Alzheimer's disease increase production of 42-residue amyloid beta-protein in both transfected cells and transgenic mice. *Nat. Med.* **3**, 67–72 (1997).

230. Puoliväli, J. *et al.* Hippocampal A beta 42 levels correlate with spatial memory deficit in APP and PS1 double transgenic mice. *Neurobiol. Dis.* **9**, 339–347 (2002).

231. Oddo, S., Caccamo, A., Kitazawa, M., Tseng, B. P. & LaFerla, F. M. Amyloid deposition precedes tangle formation in a triple transgenic model of Alzheimer's disease. *Neurobiol. Aging* **24**, 1063–1070 (2003).

232. Perez-Nievas, B. G. *et al.* Dissecting phenotypic traits linked to human resilience to Alzheimer's pathology. *Brain* **136**, 2510–2526 (2013).

233. Ingelsson, M. *et al.* Early Abeta accumulation and progressive synaptic loss, gliosis, and tangle formation in AD brain. *Neurology* **62**, 925–931 (2004).

234. Sasaki, H. *et al.* Cloning and characterization of cell adhesion kinase, a novel protein-tyrosine kinase of the focal adhesion kinase subfamily. *J. Biol. Chem.* **270**, 21206–21219 (1995).

235. Avraham, S. *et al.* Identification and characterization of a novel related adhesion focal tyrosine kinase (RAFTK) from megakaryocytes and brain. *J. Biol. Chem.* **270**, 27742–51 (1995).

236. Xiong, W. C., Macklem, M. & Parsons, J. T. Expression and characterization of splice variants of PYK2, a focal adhesion kinase-related protein. *J. Cell Sci.* **111**, 1981–91 (1998).

237. Park, S.-Y., Avraham, H. K. & Avraham, S. RAFTK/Pyk2 activation is mediated by trans-acting autophosphorylation in a Src-independent manner. *J. Biol. Chem.* **279**, 33315–22 (2004).

238. Qian, D. *et al.* Tyrosine phosphorylation of Pyk2 is selectively regulated by Fyn during TCR signaling. *J. Exp. Med.* **185**, 1253–9 (1997).

239. Zhao, M., Finlay, D., Zharkikh, I. & Vuori, K. Novel role of Src in priming Pyk2 phosphorylation. *PLoS One* **11**, e0149231 (2016).

240. Dikic, Ivan, Tokiwa, George, Lev, Sima, Courtneidge, Sara A., Schlessinger, J. A role for Pyk2 and Src in linking G-protein-coupled receptors with MAP kinase activation. *Nature* **383**, 547–550 (1996).

241. Pins, B. de, Mendes, T., Giralt, A. & Girault, J.-A. The Non-receptor Tyrosine Kinase Pyk2 in Brain Function and Neurological and Psychiatric Diseases. *Front. Synaptic Neurosci.* **13**, 749001 (2021).

242. Kumar, R., Tiwari, V. & Dey, S. Role of proline-rich tyrosine kinase 2 (Pyk2) in the pathogenesis of Alzheimer's disease. *Eur. J. Neurosci.* 1–11 (2021) doi:10.1111/EJN.15569.

243. Lee, S., Salazar, S. V., Cox, T. O. & Strittmatter, S. M. Pyk2 signaling through graf1 and rhoA GTPase is required for amyloid-β oligomer-triggered synapse loss. *J. Neurosci.* **39**,

1910–1929 (2019).

244. López-Molina, L. *et al.* Pyk2 Regulates MAMs and Mitochondrial Dynamics in Hippocampal Neurons. *Cells* **11**, 842 (2022).

245. Astier, A. *et al.* The related adhesion focal tyrosine kinase is tyrosine-phosphorylated after beta1-integrin stimulation in B cells and binds to p130cas. *J. Biol. Chem.* **272**, 228–32 (1997).

246. Berg, N. N. & Ostergaard, H. L. T cell receptor engagement induces tyrosine phosphorylation of FAK and Pyk2 and their association with Lck. *J. Immunol.* **159**, 1753–7 (1997).

247. Xiong, W. & Parsons, J. T. Induction of apoptosis after expression of PYK2, a tyrosine kinase structurally related to focal adhesion kinase. *J. Cell Biol.* **139**, 529–39 (1997).

248. Xu, L. H. *et al.* Attenuation of the expression of the focal adhesion kinase induces apoptosis in tumor cells. *Cell Growth Differ.* **7**, 413–8 (1996).

249. Salazar, S. V *et al.* Alzheimer's Disease Risk Factor Pyk2 Mediates Amyloid-β Induced Synaptic Dysfunction and Loss. *J. Neurosci.* **39**, 758–772 (2018).

250. Tse, K. W. K. *et al.* Small molecule inhibitors of the Pyk2 and FAK kinases modulate chemoattractant-induced migration, adhesion and Akt activation in follicular and marginal zone B cells. *Cell. Immunol.* **275**, 47–54 (2012).

251. Oakley, H. *et al.* Intraneuronal β-Amyloid Aggregates, Neurodegeneration, and Neuron Loss in Transgenic Mice with Five Familial Alzheimer's Disease Mutations: Potential Factors in Amyloid Plaque Formation. *J. Neurosci.* **26**, 10129–10140 (2006).

252. Giralt, A. *et al.* PTK2B/Pyk2 overexpression improves a mouse model of Alzheimer's disease. *Exp. Neurol.* **307**, 62–73 (2018).

253. Kilinc, D. *et al.* Pyk2 overexpression in postsynaptic neurons blocks amyloid β 1-42-induced synaptotoxicity in microfluidic co-cultures. *Brain Commun.* **2**, (2020).

254. Snyder, E. M. *et al.* Regulation of NMDA receptor trafficking by amyloid-β. *Nat. Neurosci.* **8**, 1051–1058 (2005).

255. Xu, J. *et al.* Striatal-enriched Protein-tyrosine Phosphatase (STEP) Regulates Pyk2 Kinase Activity. *J. Biol. Chem.* **287**, 20942 (2012).

256. Xu, J. *et al.* Inhibitor of the tyrosine phosphatase STEP reverses cognitive deficits in a mouse model of Alzheimer's disease. *PLoS Biol.* **12**, e1001923 (2014).

257. Kurup, P. *et al.* Aβ-Mediated NMDA Receptor Endocytosis in Alzheimer's Disease Involves Ubiquitination of the Tyrosine Phosphatase STEP61. *J. Neurosci.* **30**, 5948–5957 (2010).

258. Chan, G. *et al.* CD33 modulates TREM2: convergence of Alzheimer loci. *Nat. Neurosci.* **18**, 1556–1558 (2015).

259. Harwood, J. C. *et al.* Defining functional variants associated with Alzheimer's disease in the induced immune response. *Brain Commun.* **3**, (2021).

260. Combs, C. K., Johnson, D. E., Cannady, S. B., Lehman, T. M. & Landreth, G. E. Identification of microglial signal transduction pathways mediating a neurotoxic response to amyloidogenic fragments of beta-amyloid and prion proteins. *J. Neurosci.* **19**, 928–939 (1999).

261. Alawieyah Syed Mortadza, S., Sim, J. A., Neubrand, V. E. & Jiang, L.-H. A critical role of

TRPM2 channel in Aβ 42 -induced microglial activation and generation of tumor necrosis factor-α. *Glia* **66**, 562–575 (2018).

262. Yamamoto, S. *et al.* TRPM2-mediated Ca2+influx induces chemokine production in monocytes that aggravates inflammatory neutrophil infiltration. *Nat. Med.* **14**, 738–747 (2008).
263. Dourlen, P. *et al.* Functional screening of Alzheimer risk loci identifies PTK2B as an in vivo modulator and early marker of Tau pathology. *Mol. Psychiatry* **22**, 874–883 (2017).
264. Li, C. & Götz, J. Pyk2 is a Novel Tau Tyrosine Kinase that is Regulated by the Tyrosine Kinase Fyn. *J. Alzheimer's Dis.* **64**, 205–221 (2018).
265. Köhler, C., Dinekov, M. & Götz, J. Active glycogen synthase kinase-3 and tau pathology-related tyrosine phosphorylation in pR5 human tau transgenic mice. *Neurobiol. Aging* **34**, 1369–1379 (2013).
266. Goldsmith, J. F., Hall, C. G. & Atkinson, T. P. Identification of an alternatively spliced isoform of the fyn tyrosine kinase. *Biochem. Biophys. Res. Commun.* **298**, 501–504 (2002).
267. Boggon, T. J. & Eck, M. J. Structure and regulation of Src family kinases. *Oncogene* **23**, 7918–7927 (2004).
268. Thomas, S. M. & Brugge, J. S. Cellular functions regulated by Src family kinases. *Annu. Rev. Cell Dev. Biol.* **13**, 513–609 (1997).
269. Cooke, M. & Perlmutter, R. Expression of a novel form of the fyn proto-oncogene in hematopoietic cells. *New Biol.* **1**, 66–74 (1989).
270. Ohnishi, H., Murata, Y., Okazawa, H. & Matozaki, T. Src family kinases: modulators of neurotransmitter receptor function and behavior. *Trends Neurosci.* **34**, 629–637 (2011).
271. Guglietti, B., Sivasankar, S., Mustafa, S., Corrigan, F. & Collins-Praino, L. E. Fyn Kinase Activity and Its Role in Neurodegenerative Disease Pathology: a Potential Universal Target? *Mol. Neurobiol.* **58**, 5986–6005 (2021).
272. Appleby, M. W. *et al.* Defective T cell receptor signaling in mice lacking the thymic isoform of p59fyn. *Cell* **70**, 751–763 (1992).
273. Sugie, K., Jeon, M. S. & Grey, H. M. Activation of naïve CD4 T cells by anti-CD3 reveals an important role for Fyn in Lck-mediated signaling. *Proc. Natl. Acad. Sci. U. S. A.* **101**, 14859–14864 (2004).
274. Sugie, K. *et al.* Fyn tyrosine kinase associated with Fc epsilon RII/CD23: possible multiple roles in lymphocyte activation. *Proc. Natl. Acad. Sci. U. S. A.* **88**, 9132 (1991).
275. Tamura, T. *et al.* Impairment in the expression and activity of Fyn during differentiation of naive CD4+ T cells into the Th2 subset. *J. Immunol.* **167**, 1962–1969 (2001).
276. Li, X. *et al.* Alphavbeta6-Fyn signaling promotes oral cancer progression. *J. Biol. Chem.* **278**, 41646–41653 (2003).
277. Fresno Vara, J. A., Domínguez Cáceres, M. A., Silva, A. & Martín-Pérez, J. Src family kinases are required for prolactin induction of cell proliferation. *Mol. Biol. Cell* **12**, 2171–2183 (2001).
278. Horak, I. D., Corcoran, M. L., Thompson, P. A., Wahl, L. M. & Bolen, J. B. Expression of p60fyn in human platelets. *Oncogene* **5**, 597–602 (1990).
279. Reddy, K. B., Smith, D. M. & Plow, E. F. Analysis of Fyn function in hemostasis and

αIIbβ3-integrin signaling. *J. Cell Sci.* **121**, 1641 (2008).

280. Hannon, R. A. *et al.* Effects of the Src kinase inhibitor saracatinib (AZD0530) on bone turnover in healthy men: a randomized, double-blind, placebo-controlled, multiple-ascending-dose phase I trial. *J. Bone Miner. Res.* **25**, 463–471 (2010).
281. Umemori, H., Satot, S., Yagi, T., Aizawal, S. & Yamamoto, T. Initial events of myelination involve Fyn tyrosine kinase signalling. *Nature* **367**, 572–576 (1994).
282. Nygaard, H. B. Targeting Fyn Kinase in Alzheimer's Disease. *Biol. Psychiatry* **83**, 369 (2018).
283. Tezuka, T., Umemori, H., Akiyama, T., Nakanishi, S. & Yamamoto, T. PSD-95 promotes Fyn-mediated tyrosine phosphorylation of the N-methyl-D-aspartate receptor subunit NR2A. *Proc. Natl. Acad. Sci. U. S. A.* **96**, 435–440 (1999).
284. Suzuki, T. & Okumura-Noji, K. NMDA receptor subunits epsilon 1 (NR2A) and epsilon 2 (NR2B) are substrates for Fyn in the postsynaptic density fraction isolated from the rat brain. *Biochem. Biophys. Res. Commun.* **216**, 582–8 (1995).
285. Nakazawa, T. *et al.* Characterization of Fyn-mediated tyrosine phosphorylation sites on GluR epsilon 2 (NR2B) subunit of the N-methyl-D-aspartate receptor. *J. Biol. Chem.* **276**, 693–699 (2001).
286. Bliss, T. V. P. & Lømo, T. Long-lasting potentiation of synaptic transmission in the dentate area of the anaesthetized rabbit following stimulation of the perforant path. *J. Physiol.* **232**, 331–356 (1973).
287. Lambert, M. P. *et al.* Diffusible, nonfibrillar ligands derived from Abeta1-42 are potent central nervous system neurotoxins. *Proc. Natl. Acad. Sci. U. S. A.* **95**, 6448–6453 (1998).
288. Chin, J. *et al.* Fyn kinase modulates synaptotoxicity, but not aberrant sprouting, in human amyloid precursor protein transgenic mice. *J. Neurosci.* **24**, 4692–4697 (2004).
289. Chin, J. *et al.* Fyn kinase induces synaptic and cognitive impairments in a transgenic mouse model of Alzheimer's disease. *J. Neurosci.* **25**, 9694–9703 (2005).
290. Shirazi, S. K. & Wood, J. G. The protein tyrosine kinase, fyn, in Alzheimer's disease pathology. *Neuroreport* **4**, 435–437 (1993).
291. Bhaskar, K., Yen, S.-H. & Lee, G. Disease-related modifications in tau affect the interaction between Fyn and Tau. *J. Biol. Chem.* **280**, 35119–25 (2005).
292. Lee, G., Newman, S. T., Gard, D. L., Band, H. & Panchamoorthy, G. Tau interacts with src-family non-receptor tyrosine kinases. *J. Cell Sci.* **111 Pt.2**, 3167–77 (1998).
293. Li, C. & Götz, J. Somatodendritic accumulation of Tau in Alzheimer's disease is promoted by Fyn-mediated local protein translation. *EMBO J.* **36**, e201797724 (2017).
294. Nguyen, T. H., Liu, J. & Lombroso, P. J. Striatal enriched phosphatase 61 dephosphorylates Fyn at phosphotyrosine 420. *J. Biol. Chem.* **277**, 24274–24279 (2002).
295. Schenone, S. *et al.* Fyn kinase in brain diseases and cancer: the search for inhibitors. *Curr. Med. Chem.* **18**, 2921–2942 (2011).
296. Hennequin, L. F. *et al.* N-(5-chloro-1,3-benzodioxol-4-yl)-7-[2-(4-methylpiperazin-1-yl)ethoxy]-5- (tetrahydro-2H-pyran-4-yloxy)quinazolin-4-amine, a novel, highly selective, orally available, dual-specific c-Src/Abl kinase inhibitor. *J. Med. Chem.* **49**, 6465–6488 (2006).
297. Zhao, M., Finlay, D., Zharkikh, I. & Vuori, K. Novel Role of Src in Priming Pyk2

Phosphorylation. *PLoS One* **11**, e0149231 (2016).

298. Dubreuil, P. *et al.* Masitinib (AB1010), a potent and selective tyrosine kinase inhibitor targeting KIT. *PLoS One* **4**, e7258 (2009).

299. Li, T. *et al.* Effects of Chronic Masitinib Treatment in APPswe/PSEN1dE9 Transgenic Mice Modeling Alzheimer's Disease. *J. Alzheimer's Dis.* **76**, 1339–1345 (2020).

300. ALZFORUM. Positive Phase 2 Results Claimed for Masitinib in Alzheimer's. https://www.alzforum.org/news/research-news/positive-phase-2-results-claimed-masitinib-alzheimers (2020).

301. Boschelli, F., Arndt, K. & Gambacorti-Passerini, C. Bosutinib: a review of preclinical studies in chronic myelogenous leukaemia. *Eur. J. Cancer* **46**, 1781–1789 (2010).

302. Boschelli, D. H. *et al.* Optimization of 4-phenylamino-3-quinolinecarbonitriles as potent inhibitors of Src kinase activity. *J. Med. Chem.* **44**, 3965–3977 (2001).

303. O'Hare, T. *et al.* AP24534, a Pan-BCR-ABL Inhibitor for Chronic Myeloid Leukemia, Potently Inhibits the T315I Mutant and Overcomes Mutation-Based Resistance. *Cancer Cell* **16**, 401 (2009).

304. Das, J. *et al.* 2-aminothiazole as a novel kinase inhibitor template. Structure-activity relationship studies toward the discovery of N-(2-chloro-6-methylphenyl)-2-[[6-[4-(2-hydroxyethyl)-1- piperazinyl)]-2-methyl-4-pyrimidinyl]amino)]-1,3-thiazole-5-carboxamide (dasatin. *J. Med. Chem.* **49**, 6819–6832 (2006).

305. Dhawan, G. & Combs, C. K. Inhibition of Src kinase activity attenuates amyloid associated microgliosis in a murine model of Alzheimer's disease. *J. Neuroinflammation* **9**, 117 (2012).

306. Kreutzman, A. *et al.* Expansion of highly differentiated CD8+ T-cells or NK-cells in patients treated with dasatinib is associated with cytomegalovirus reactivation. *Leukemia* **25**, 1587–1597 (2011).

307. Smith, L. M., Zhu, R. & Strittmatter, S. M. Disease-modifying benefit of Fyn blockade persists after washout in mouse Alzheimer's model. *Neuropharmacology* **130**, 54–61 (2018).

308. Toyonaga, T. *et al.* In Vivo Synaptic Density Imaging with 11 C-UCB-J Detects Treatment Effects of Saracatinib in a Mouse Model of Alzheimer Disease. *J. Nucl. Med.* **60**, 1780–1786 (2019).

309. Nygaard, H. B. *et al.* A phase Ib multiple ascending dose study of the safety, tolerability, and central nervous system availability of AZD0530 (saracatinib) in Alzheimer's disease. *Alzheimers. Res. Ther.* **7**, 35 (2015).

310. Van Dyck, C. H. *et al.* Effect of AZD0530 on Cerebral Metabolic Decline in Alzheimer Disease: A Randomized Clinical Trial. *JAMA Neurol.* **76**, 1219–1229 (2019).

311. EMBI, N., RYLATT, D. B. & COHEN, P. Glycogen Synthase Kinase-3 from Rabbit Skeletal Muscle. *Eur. J. Biochem.* **107**, 519–527 (1980).

312. Rylatt, D. B., Embi, N. & Cohen, P. Glycogen synthase kinase-2 from rabbit skeletal muscle is activated by the calcium-dependent regulator protein. *FEBS Lett.* **98**, 76–80 (1979).

313. Itartet, E. & Huangg, K.-P. Purification and Properties of Cyclic AMP-independent Glycogen Synthase Kinase 1 from Rabbit Skeletal Muscle*. *J. Biol. Chem.* **254**, 4052–4057 (1979).

314. Woodgett, J. R. Molecular cloning and expression of glycogen synthase kinase-3/factor A. *EMBO J.* **9**, 2431 (1990).

315. Force, T. & Woodgett, J. R. Unique and overlapping functions of GSK-3 isoforms in cell differentiation and proliferation and cardiovascular development. *J. Biol. Chem.* **284**, 9643–9647 (2009).

316. Kaidanovich-Beilin, O. *et al.* Abnormalities in brain structure and behavior in GSK-3alpha mutant mice. *Mol. Brain* **2**, 1–23 (2009).

317. Hoeflich, K. P. *et al.* Requirement for glycogen synthase kinase-3β in cell survival and NF-κB activation. *Nature* **406**, 86–90 (2000).

318. Lesort, M., Jope, R. S. & Johnson, G. V. Insulin transiently increases tau phosphorylation: involvement of glycogen synthase kinase-3beta and Fyn tyrosine kinase. *J. Neurochem.* **72**, 576–84 (1999).

319. Cole, A., Frame, S. & Cohen, P. Further evidence that the tyrosine phosphorylation of glycogen synthase kinase-3 (GSK3) in mammalian cells is an autophosphorylation event. *Biochem. J.* **377**, 249–55 (2004).

320. Beurel, E., Grieco, S. F. & Jope, R. S. Glycogen synthase kinase-3 (GSK3): Regulation, actions, and diseases. *Pharmacol. Ther.* **148**, 114–131 (2015).

321. Frame, S., Cohen, P. & Biondi, R. M. A Common Phosphate Binding Site Explains the Unique Substrate Specificity of GSK3 and Its Inactivation by Phosphorylation. *Mol. Cell* **7**, 1321–1327 (2001).

322. ter Haar, E. *et al.* Structure of GSK3β reveals a primed phosphorylation mechanism. *Nat. Struct. Biol.* **8**, 593–596 (2001).

323. Dajani, R. *et al.* Structural basis for recruitment of glycogen synthase kinase 3β to the axin—APC scaffold complex. *EMBO J.* **22**, 494–501 (2003).

324. Cole, A. R. *et al.* GSK-3 Phosphorylation of the Alzheimer Epitope within Collapsin Response Mediator Proteins Regulates Axon Elongation in Primary Neurons *. *J. Biol. Chem.* **279**, 50176–50180 (2004).

325. Singh, S. A. *et al.* FLEXIQinase, a mass spectrometry–based assay, to unveil multikinase mechanisms. *Nat. Methods* **9**, 504–508 (2012).

326. Hanger, D. P., Hughes, K., Woodgett, J. R., Brion, J.-P. & Anderton, B. H. Glycogen synthase kinase-3 induces Alzheimer's disease-like phosphorylation of tau: Generation of paired helical filament epitopes and neuronal localisation of the kinase. *Neurosci. Lett.* **147**, 58–62 (1992).

327. Sayas, C. L., Ariaens, A., Ponsioen, B. & Moolenaar, W. H. GSK-3 is activated by the tyrosine kinase Pyk2 during LPA1-mediated neurite retraction. *Mol. Biol. Cell* **17**, 1834–44 (2006).

328. Moreno-Jiménez, E. P. *et al.* Adult hippocampal neurogenesis is abundant in neurologically healthy subjects and drops sharply in patients with Alzheimer's disease. *Nat. Med.* **25**, 554–560 (2019).

329. Morales-Garcia, J. A. *et al.* Glycogen synthase kinase 3 inhibition promotes adult hippocampal neurogenesis in vitro and in vivo. *ACS Chem. Neurosci.* **3**, 963–971 (2012).

330. Gao, C. *et al.* FAK/PYK2 promotes the Wnt/β-catenin pathway and intestinal tumorigenesis by phosphorylating GSK3β. *Elife* **4**, e10072 (2015).

331. Peineau, S. *et al.* LTP Inhibits LTD in the Hippocampus via Regulation of GSK3β. *Neuron*

53, 703–717 (2007).

332. Hooper, C. *et al.* Glycogen synthase kinase-3 inhibition is integral to long-term potentiation. *Eur. J. Neurosci.* **25**, 81–86 (2007).

333. Yuskaitis, C. J. & Jope, R. S. Glycogen synthase kinase-3 regulates microglial migration, inflammation, and inflammation-induced neurotoxicity. *Cell. Signal.* **21**, 264–273 (2009).

334. Linding, R. *et al.* Systematic Discovery of In Vivo Phosphorylation Networks. *Cell* **129**, 1415–1426 (2007).

335. Sutherland, C. What Are the bona fide GSK3 Substrates? *Int. J. Alzheimers. Dis.* **2011**, 1–23 (2011).

336. Takashima, A. *et al.* Exposure of rat hippocampal neurons to amyloid β peptide (25–35) induces the inactivation of phosphatidyl inositol-3 kinase and the activation of tau protein kinase I/glycogen synthase kinase-3β. *Neurosci. Lett.* **203**, 33–36 (1996).

337. Ferrari, A., Hoerndli, F., Baechi, T., Nitsch, R. M. & Götz, J. β-Amyloid Induces Paired Helical Filament-like Tau Filaments in Tissue Culture. *J. Biol. Chem.* **278**, 40162–40168 (2003).

338. Phiel, C. J., Wilson, C. A., Lee, V. M. Y. & Klein, P. S. GSK-3α regulates production of Alzheimer's disease amyloid-β peptides. *Nature* **423**, 435–439 (2003).

339. Ryder, J. *et al.* Divergent roles of GSK3 and CDK5 in APP processing. *Biochem. Biophys. Res. Commun.* **312**, 922–929 (2003).

340. Su, Y. *et al.* Lithium, a Common Drug for Bipolar Disorder Treatment, Regulates Amyloid-β Precursor Protein Processing. *Biochemistry* **43**, 6899–6908 (2004).

341. Tesco, G. & Tanzi, R. E. GSK3β Forms a Tetrameric Complex with Endogenous PS1-CTF/NTF and β-Catenin: Effects of the D257/D385A and FAD-linked Mutations. *Ann. N. Y. Acad. Sci.* **920**, 227–232 (2000).

342. Kirschenbaum, F., Hsu, S.-C., Cordell, B. & Mccarthy, J. V. Glycogen Synthase Kinase-3Î² Regulates Presenilin 1 C-terminal Fragment Levels*. *J. Biol. Chem.* **276**, 30701–30707 (2001).

343. Maesako, M. *et al.* Effect of glycogen synthase kinase 3 β-mediated presenilin 1 phosphorylation on amyloid β production is negatively regulated by insulin receptor cleavage. *Neuroscience* **177**, 298–307 (2011).

344. Ly, P. T. T. *et al.* Inhibition of GSK3β-mediated BACE1 expression reduces Alzheimer-associated phenotypes. *J. Clin. Invest.* **123**, 224–235 (2013).

345. Chen, C. H. *et al.* Increased NF-κB signalling up-regulates BACE1 expression and its therapeutic potential in Alzheimer's disease. *Int. J. Neuropsychopharmacol.* **15**, 77–90 (2012).

346. Li, Q., Liu, Y. & Sun, M. Autophagy and Alzheimer's Disease. *Cell. Mol. Neurobiol.* **37**, 377–388 (2017).

347. Kurochkin, I. V. & Goto, S. Alzheimer's β-amyloid peptide specifically interacts with and is degraded by insulin degrading enzyme. *FEBS Lett.* **345**, 33–37 (1994).

348. Caccamo, A. *et al.* mTOR regulates tau phosphorylation and degradation: implications for Alzheimer's disease and other tauopathies. *Aging Cell* **12**, 370–380 (2013).

349. Jolivalt, C. G. *et al.* Defective insulin signaling pathway and increased glycogen synthase

kinase-3 activity in the brain of diabetic mice: Parallels with Alzheimer's disease and correction by insulin. *J. Neurosci. Res.* **86**, 3265–3274 (2008).

350. Lauretti, E., Dincer, O. & Praticò, D. Glycogen synthase kinase-3 signaling in Alzheimer's disease. *Biochim. Biophys. Acta - Mol. Cell Res.* **1867**, 118664 (2020).
351. Jackson, G. R. *et al.* Human Wild-Type Tau Interacts with wingless Pathway Components and Produces Neurofibrillary Pathology in Drosophila. *Neuron* **34**, 509–519 (2002).
352. Pérez, M. *et al.* Formation of aberrant phosphotau fibrillar polymers in neural cultured cells. *Eur. J. Biochem.* **269**, 1484–1489 (2002).
353. Wang, J. Z., Grundke-Iqbal, I. & Iqbal, K. Kinases and phosphatases and tau sites involved in Alzheimer neurofibrillary degeneration. *Eur. J. Neurosci.* **25**, 59–68 (2007).
354. Leroy, K., Yilmaz, Z. & Brion, J.-P. Increased level of active GSK-3? in Alzheimer's disease and accumulation in argyrophilic grains and in neurones at different stages of neurofibrillary degeneration. *Neuropathol. Appl. Neurobiol.* **33**, 43–55 (2007).
355. Lee, S. J. *et al.* Age-related changes in glycogen synthase kinase 3β (GSK3β) immunoreactivity in the central nervous system of rats. *Neurosci. Lett.* **409**, 134–139 (2006).
356. Terwel, D. *et al.* Amyloid Activates GSK-3β to Aggravate Neuronal Tauopathy in Bigenic Mice. *Am. J. Pathol.* **172**, 786–798 (2008).
357. Ma, Q.-L. *et al.* Antibodies against β-amyloid reduce aβ oligomers, glycogen synthase kinase-3β activation and τ phosphorylation in vivo and in vitro. *J. Neurosci. Res.* **83**, 374–384 (2006).
358. Bian, H. *et al.* RNA Interference Silencing of Glycogen Synthase Kinase 3β Inhibites Tau Phosphorylation in Mice with Alzheimer Disease. *Neurochem. Res.* **41**, 2470–2480 (2016).
359. Magdesian, M. H. *et al.* Amyloid-β Binds to the Extracellular Cysteine-rich Domain of Frizzled and Inhibits Wnt/β-Catenin Signaling. *J. Biol. Chem.* **283**, 9359–9368 (2008).
360. D'mello, S. R. When Good Kinases Go Rogue: GSK3, p38 MAPK and CDKs as Therapeutic Targets for Alzheimer's and Huntington's Disease. *Int. J. Mol. Sci.* **22**, 5911 (2021).
361. Sun, M., Herrmann, N. & Shulman, K. I. Lithium Toxicity in Older Adults: a Systematic Review of Case Reports. *Clin. Drug Investig.* **38**, 201–209 (2018).
362. Roux, M. & Dosseto, A. From direct to indirect lithium targets: a comprehensive review of omics data. *Metallomics* **9**, 1326–1351 (2017).
363. Gómez-Isla, T. *et al.* Neuronal loss correlates with but exceeds neurofibrillary tangles in Alzheimer's disease. *Ann. Neurol.* **41**, 17–24 (1997).
364. Giannakopoulos, P. *et al.* Tangle and neuron numbers, but not amyloid load, predict cognitive status in Alzheimer's disease. *Neurology* **60**, 1495–1500 (2003).
365. Goedert, M., Spillantini, M. G., Potier, M. C., Ulrich, J. & Crowther, R. A. Cloning and sequencing of the cDNA encoding an isoform of microtubule-associated protein tau containing four tandem repeats: differential expression of tau protein mRNAs in human brain. *EMBO J.* **8**, 393 (1989).
366. Himmler, A., Drechsel, D., Kirschner, M. W., Martin, D. W. & Jr. Tau consists of a set of proteins with repeated C-terminal microtubule-binding domains and variable N-terminal domains. *Mol. Cell. Biol.* **9**, 1381 (1989).

367. Iqbal, K., Liu, F. & Gong, C. X. Tau and neurodegenerative disease: the story so far. *Nat. Rev. Neurol.* **12**, 15–27 (2016).

368. Lu, M. & Kosik, K. S. Competition for Microtubule-binding with Dual Expression of Tau Missense and Splice Isoforms. *Mol. Biol. Cell* **12**, 171 (2001).

369. Mandelkow, E., Von Bergen, M., Biernat, J. & Mandelkow, E. M. Structural Principles of Tau and the Paired Helical Filaments of Alzheimer's Disease. *Brain Pathol.* **17**, 83 (2007).

370. Noble, W., Hanger, D. P., Miller, C. C. J. & Lovestone, S. The importance of tau phosphorylation for neurodegenerative diseases. *Front. Neurol.* **4**, 83 (2013).

371. Drubin, D. G. & Kirschner, M. W. Tau protein function in living cells. *J. Cell Biol.* **103**, 2739 (1986).

372. Cleveland, D. W., Hwo, S. Y. & Kirschner, M. W. Purification of tau, a microtubule-associated protein that induces assembly of microtubules from purified tubulin. *J. Mol. Biol.* **116**, 207–225 (1977).

373. Lidón, L. *et al.* Tau Protein as a New Regulator of Cellular Prion Protein Transcription. *Mol. Neurobiol.* (2020) doi:10.1007/s12035-020-02025-x.

374. Asada-Utsugi, M. *et al.* Failure of DNA double-strand break repair by tau mediates Alzheimer's disease pathology in vitro. *Commun. Biol.* **5**, 358 (2022).

375. Van Hummel, A. *et al.* No Overt Deficits in Aged Tau-Deficient C57Bl/6.Mapt tm1(EGFP)Kit GFP Knockin Mice. *PLoS One* **11**, e0163236 (2016).

376. Dawson, H. N. *et al.* Inhibition of neuronal maturation in primary hippocampal neurons from tau deficient mice. *J. Cell Sci.* **114**, 1179–1187 (2001).

377. Kovacs, G. G. Invited review: Neuropathology of tauopathies: principles and practice. *Neuropathol. Appl. Neurobiol.* **41**, 3–23 (2015).

378. Leveille, E., Ross, O. A. & Gan-Or, Z. Tau and MAPT genetics in tauopathies and synucleinopathies. *Parkinsonism Relat. Disord.* **90**, 142–154 (2021).

379. Lee, V. M., Goedert, M. & Trojanowski, J. Q. Neurodegenerative tauopathies. *Annu. Rev. Neurosci.* **24**, 1121–59 (2001).

380. Kurt, M. A., Davies, D. C. & Kidd, M. Paired helical filament morphology varies with intracellular location in Alzheimer's disease brain. *Neurosci. Lett.* **239**, 41–44 (1997).

381. Goedert, M. *et al.* Molecular dissection of the paired helical filament. *Neurobiol. Aging* **16**, 325–334 (1995).

382. Jakes, R., Novak, M., Davison, M. & Wischik, C. M. Identification of 3- and 4-repeat tau isoforms within the PHF in Alzheimer's disease. *EMBO J.* **10**, 2725–2729 (1991).

383. Zilka, N. *et al.* Truncated tau from sporadic Alzheimer's disease suffices to drive neurofibrillary degeneration in vivo. *FEBS Lett.* **580**, 3582–3588 (2006).

384. Ye, H., Han, Y., Li, P., Su, Z. & Huang, Y. The Role of Post-Translational Modifications on the Structure and Function of Tau Protein. *J. Mol. Neurosci.* 1–15 (2022) doi:10.1007/s12031-022-02002-0.

385. Shane Arnold, C. *et al.* The microtubule-associated protein tau is extensively modified with O-linked N-acetylglucosamine. *J. Biol. Chem.* **271**, 28741–28744 (1996).

386. Liu, F., Iqbal, K., Grundke-Iqbal, I., Hart, G. W. & Gong, C. X. O-GlcNAcylation regulates phosphorylation of tau: a mechanism involved in Alzheimer's disease. *Proc. Natl. Acad. Sci. U. S. A.* **101**, 10804–10809 (2004).

387. Pérez, M., Valpuesta, J. M., Medina, M., Montejo De Garcini, E. & Avila, J. Polymerization of tau into filaments in the presence of heparin: the minimal sequence required for tau-tau interaction. *J. Neurochem.* **67**, 1183–1190 (1996).

388. Yuzwa, S. A. *et al.* Mapping O-GlcNAc modification sites on tau and generation of a site-specific O-GlcNAc tau antibody. *Amino Acids* **40**, 857–868 (2011).

389. Liu, Y., Liu, F., Grundke-Iqbal, I., Iqbal, K. & Gong, C. X. Brain glucose transporters, O-GlcNAcylation and phosphorylation of tau in diabetes and Alzheimer's disease. *J. Neurochem.* **111**, 242–249 (2009).

390. Lindwall, G. & Cole, R. D. Phosphorylation affects the ability of tau protein to promote microtubule assembly. *J. Biol. Chem.* **259**, 5301–5305 (1984).

391. Alonso, A. D. C., Zaidi, T., Grundke-Iqbal, I. & Iqbal, K. Role of abnormally phosphorylated tau in the breakdown of microtubules in Alzheimer disease. *Proc. Natl. Acad. Sci. U. S. A.* **91**, 5562 (1994).

392. Sengupta, A., Novak, M., Grundke-Iqbal, I. & Iqbal, K. Regulation of Phosphorylation of Tau by Cyclin-dependent Kinase 5 and Glycogen Synthase Kinase-3 at Substrate Level. *FEBS Lett.* **580**, 5925 (2006).

393. Reynolds, C. H. *et al.* Phosphorylation regulates tau interactions with Src homology 3 domains of phosphatidylinositol 3-kinase, phospholipase Cγ1, Grb2, and Src family kinases. *J. Biol. Chem.* **283**, 18177–18186 (2008).

394. Usardi, A. *et al.* Tyrosine phosphorylation of tau regulates its interactions with Fyn SH2 domains, but not SH3 domains, altering the cellular localization of tau. *FEBS J.* **278**, 2927–2937 (2011).

395. Pooler, A. M. *et al.* Dynamic association of tau with neuronal membranes is regulated by phosphorylation. *Neurobiol. Aging* **33**, 431.e27-431.e38 (2012).

396. Le Corre, S. *et al.* An inhibitor of tau hyperphosphorylation prevents severe motor impairments in tau transgenic mice. *Proc. Natl. Acad. Sci. U. S. A.* **103**, 9673–9678 (2006).

397. Noble, W. *et al.* Inhibition of glycogen synthase kinase-3 by lithium correlates with reduced tauopathy and degeneration in vivo. *Proc. Natl. Acad. Sci. U. S. A.* **102**, 6990–5 (2005).

398. Cruz, J. C., Tseng, H. C., Goldman, J. A., Shih, H. & Tsai, L. H. Aberrant Cdk5 Activation by p25 Triggers Pathological Events Leading to Neurodegeneration and Neurofibrillary Tangles. *Neuron* **40**, 471–483 (2003).

399. Noble, W. *et al.* Cdk5 Is a Key Factor in Tau Aggregation and Tangle Formation In Vivo. *Neuron* **38**, 555–565 (2003).

400. Lucas, J. J. *et al.* Decreased nuclear β-catenin, tau hyperphosphorylation and neurodegeneration in GSK-3β conditional transgenic mice. *EMBO J.* **20**, 27–39 (2001).

401. Louis, J. V. *et al.* Mice lacking phosphatase PP2A subunit PR61/B'δ (Ppp2r5d) develop spatially restricted tauopathy by deregulation of CDK5 and GSK3β. *Proc. Natl. Acad. Sci. U. S. A.* **108**, 6957–6962 (2011).

402. Lovestone, S. *et al.* Alzheimer's disease-like phosphorylation of the microtubule-associated protein tau by glycogen synthase kinase-3 in transfected mammalian cells. *Curr. Biol.* **4**, 1077–86 (1994).

403. Baumann, K., Mandelkow, E. M., Biernat, J., Piwnica-Worms, H. & Mandelkow, E.

Abnormal Alzheimer-like phosphorylation of tau-protein by cyclin-dependent kinases cdk2 and cdk5. *FEBS Lett.* **336**, 417–424 (1993).

404. Mairet-Coello, G. *et al.* The CAMKK2-AMPK Kinase Pathway Mediates the Synaptotoxic Effects of Aβ Oligomers through Tau Phosphorylation. *Neuron* **78**, 94–108 (2013).

405. Thornton, C., Bright, N. J., Sastre, M., Muckett, P. J. & Carling, D. AMP-activated protein kinase (AMPK) is a tau kinase, activated in response to amyloid β-peptide exposure. *Biochem. J.* **434**, 503–512 (2011).

406. Hanger, D. P. *et al.* Novel phosphorylation sites in tau from Alzheimer brain support a role for casein kinase 1 in disease pathogenesis. *J. Biol. Chem.* **282**, 23645–54 (2007).

407. Andorfer, C. A. & Davies, P. PKA Phosphorylations on Tau: Developmental Studies in the Mouse. *Dev. Neurosci.* **22**, 303–309 (2000).

408. Wang, D. *et al.* β2 Adrenergic Receptor, Protein Kinase A (PKA) and c-Jun N-terminal Kinase (JNK) Signaling Pathways Mediate Tau Pathology in Alzheimer Disease Models. *J. Biol. Chem.* **288**, 10298–10307 (2013).

409. Sheppard, O. *et al.* Altered regulation of tau phosphorylation in a mouse model of down syndrome aging. *Neurobiol. Aging* **33**, 828.e31-828.e44 (2012).

410. Woods, Y. L. *et al.* The kinase DYRK phosphorylates protein-synthesis initiation factor eIF2Bε at Ser539 and the microtubule-associated protein tau at Thr212: potential role for DYRK as a glycogen synthase kinase 3-priming kinase. *Biochem. J.* **355**, 609–615 (2001).

411. Drewes, G. *et al.* Microtubule-associated protein/microtubule affinity-regulating kinase (p110mark). A novel protein kinase that regulates tau-microtubule interactions and dynamic instability by phosphorylation at the Alzheimer-specific site serine 262. *J. Biol. Chem.* **270**, 7679–7688 (1995).

412. Lee, S., Wang, J. W., Yu, W. & Lu, B. Phospho-dependent ubiquitination and degradation of PAR-1 regulates synaptic morphology and tau-mediated Aβ toxicity in Drosophila. *Nat. Commun.* **3**, 1–12 (2012).

413. Cancino, G. I. *et al.* c-Abl tyrosine kinase modulates tau pathology and Cdk5 phosphorylation in AD transgenic mice. *Neurobiol. Aging* **32**, 1249–1261 (2011).

414. Lebouvier, T. *et al.* The microtubule-associated protein tau is phosphorylated by Syk. *Biochim. Biophys. Acta* **1783**, 188 (2008).

415. Gong, C. -X, Singh, T. J., Grundke-Iqbal, I. & Iqbal, K. Phosphoprotein phosphatase activities in Alzheimer disease brain. *J. Neurochem.* **61**, 921–927 (1993).

416. Gong, C. X., Grundke-Iqbal, I. & Iqbal, K. Dephosphorylation of Alzheimer's disease abnormally phosphorylated tau by protein phosphatase-2A. *Neuroscience* **61**, 765–772 (1994).

417. Bennecib, M., Gong, C. X., Grundke-Iqbal, I. & Iqbal, K. Role of protein phosphatase-2A and -1 in the regulation of GSK-3, cdk5 and cdc2 and the phosphorylation of tau in rat forebrain. *FEBS Lett.* **485**, 87–93 (2000).

418. Tanimukai, H., Grundke-Iqbal, I. & Iqbal, K. Up-Regulation of Inhibitors of Protein Phosphatase-2A in Alzheimer's Disease. *Am. J. Pathol.* **166**, 1761 (2005).

419. Basurto-Islas, G., Grundke-Iqbal, I., Tung, Y. C., Liu, F. & Iqbal, K. Activation of Asparaginyl Endopeptidase Leads to Tau Hyperphosphorylation in Alzheimer Disease. *J. Biol. Chem.* **288**, 17495 (2013).

420. Arif, M., Kazim, S. F., Grundke-Iqbal, I., Garruto, R. M. & Iqbal, K. Tau pathology involves protein phosphatase 2A in parkinsonism-dementia of Guam. *Proc. Natl. Acad. Sci. U. S. A.* **111**, 1144–1149 (2014).

421. Berger, Z. *et al.* Accumulation of Pathological Tau Species and Memory Loss in a Conditional Model of Tauopathy. *J. Neurosci.* **27**, 3650–3662 (2007).

422. Tai, H. C. *et al.* The synaptic accumulation of hyperphosphorylated tau oligomers in Alzheimer disease is associated with dysfunction of the ubiquitin-proteasome system. *Am. J. Pathol.* **181**, 1426–1435 (2012).

423. Caamaño-Moreno, M. & Gargini, R. Tauopathies: The Role of Tau in Cellular Crosstalk and Synaptic Dysfunctions. *Neuroscience* (2022) doi:10.1016/j.neuroscience.2022.02.034.

424. Hoover, B. R. *et al.* Tau mislocalization to dendritic spines mediates synaptic dysfunction independently of neurodegeneration. *Neuron* **68**, 1067–1081 (2010).

425. Zempel, H., Thies, E., Mandelkow, E. & Mandelkow, E. M. Abeta oligomers cause localized Ca(2+) elevation, missorting of endogenous Tau into dendrites, Tau phosphorylation, and destruction of microtubules and spines. *J. Neurosci.* **30**, 11938–11950 (2010).

426. Zempel, H. & Mandelkow, E. M. Linking amyloid-β and tau: amyloid-β induced synaptic dysfunction via local wreckage of the neuronal cytoskeleton. *Neurodegener. Dis.* **10**, 64–72 (2012).

427. Wang, D. *et al.* The Structure Biology of Tau and Clue for Aggregation Inhibitor Design. *Protein J.* **40**, 656–668 (2021).

428. Zeng, Y. *et al.* The structure and phase of tau: from monomer to amyloid filament. *Cell. Mol. Life Sci.* **78**, 1873–1886 (2020).

429. Sanders, D. W. *et al.* Distinct Tau Prion Strains Propagate in Cells and Mice and Define Different Tauopathies. *Neuron* **82**, 1271–1288 (2014).

430. He, Z. *et al.* Transmission of tauopathy strains is independent of their isoform composition. *Nat. Commun.* **11**, 7 (2020).

431. Narasimhan, S. *et al.* Pathological tau strains from human brains recapitulate the diversity of tauopathies in non-transgenic mouse brain. *J. Neurosci.* **37**, 1230–17 (2017).

432. Xu, H. *et al.* In vitro amplification of pathogenic tau conserves disease-specific bioactive characteristics. *Acta Neuropathol.* **141**, 193–215 (2021).

433. Dujardin, S. & Hyman, B. T. Tau Prion-Like Propagation: State of the Art and Current Challenges. *Adv. Exp. Med. Biol.* **1184**, 305–325 (2019).

434. Vaquer-Alicea, J., Diamond, M. I. & Joachimiak, L. A. Tau strains shape disease. *Acta Neuropathol.* **142**, 57 (2021).

435. Chastagner, P. *et al.* Fate and propagation of endogenously formed Tau aggregates in neuronal cells. *EMBO Mol. Med.* **12**, e12025 (2020).

436. Vingtdeux, V., Sergeant, N. & Buée, L. Potential contribution of exosomes to the prion-like propagation of lesions in Alzheimer's disease. *Front. Physiol.* **3 JUL**, 229 (2012).

437. Scheres, S. H., Zhang, W., Falcon, B. & Goedert, M. Cryo-EM structures of tau filaments. *Curr. Opin. Struct. Biol.* **64**, 17–25 (2020).

438. Dregni, A. J. *et al.* Fluent molecular mixing of Tau isoforms in Alzheimer's disease

neurofibrillary tangles. *Nat. Commun.* **13**, 2967 (2022).

439. Daebel, V. *et al.* β-sheet core of tau paired helical filaments revealed by solid-state NMR. *J. Am. Chem. Soc.* **134**, 13982–13989 (2012).

440. Andronesi, O. C. *et al.* Characterization of Alzheimer's-like paired helical filaments from the core domain of tau protein using solid-state NMR spectroscopy. *J. Am. Chem. Soc.* **130**, 5922–5928 (2008).

441. Bibow, S. *et al.* The Dynamic Structure of Filamentous Tau. *Angew. Chemie Int. Ed.* **50**, 11520–11524 (2011).

442. Braak, H., Alafuzoff, I., Arzberger, T., Kretzschmar, H. & Tredici, K. Staging of Alzheimer disease-associated neurofibrillary pathology using paraffin sections and immunocytochemistry. *Acta Neuropathol.* **112**, 389–404 (2006).

443. Kaufman, S. K., Del Tredici, K., Thomas, T. L., Braak, H. & Diamond, M. I. Tau seeding activity begins in the transentorhinal/entorhinal regions and anticipates phospho-tau pathology in Alzheimer's disease and PART. *Acta Neuropathol.* **136**, 57–67 (2018).

444. Guo, J. L. *et al.* Unique pathological tau conformers from Alzheimer's brains transmit tau pathology in nontransgenic mice. *J. Exp. Med.* **213**, 2635–2654 (2016).

445. Dujardin, S. *et al.* Neuron-to-neuron wild-type Tau protein transfer through a trans-synaptic mechanism: Relevance to sporadic tauopathies. *Acta Neuropathol. Commun.* **2**, 1–14 (2014).

446. Kfoury, N., Holmes, B. B., Jiang, H., Holtzman, D. M. & Diamond, M. I. Trans-cellular Propagation of Tau Aggregation by Fibrillar Species. *J. Biol. Chem.* **287**, 19440–19451 (2012).

447. Polanco, J. C. & Götz, J. Exosomal and vesicle-free tau seeds—propagation and convergence in endolysosomal permeabilization. *FEBS J.* febs.16055 (2021) doi:10.1111/febs.16055.

448. Yamada, K. *et al.* Neuronal activity regulates extracellular tau in vivo. *J. Exp. Med.* **211**, 387–393 (2014).

449. Dujardin, S. *et al.* Ectosomes: A New Mechanism for Non-Exosomal Secretion of Tau Protein. *PLoS One* **9**, e100760 (2014).

450. Asai, H. *et al.* Depletion of microglia and inhibition of exosome synthesis halt tau propagation. *Nat. Neurosci.* **18**, 1584–1593 (2015).

451. Saman, S. *et al.* Exosome-associated Tau Is Secreted in Tauopathy Models and Is Selectively Phosphorylated in Cerebrospinal Fluid in Early Alzheimer Disease. *J. Biol. Chem.* **287**, 3842–3849 (2012).

452. Wang, Y. *et al.* The release and trans-synaptic transmission of Tau via exosomes. *Mol. Neurodegener.* **12**, 5 (2017).

453. Katsinelos, T. *et al.* Unconventional Secretion Mediates the Trans-cellular Spreading of Tau. *Cell Rep.* **23**, 2039–2055 (2018).

454. Fontaine, S. N. *et al.* DnaJ/Hsc70 chaperone complexes control the extracellular release of neurodegenerative-associated proteins. *EMBO J.* **35**, 1537–1549 (2016).

455. Kanmert, D. *et al.* C-Terminally Truncated Forms of Tau, But Not Full-Length Tau or Its C-Terminal Fragments, Are Released from Neurons Independently of Cell Death. *J. Neurosci.* **35**, 10851–10865 (2015).

456. Kim, W. *et al.* Interneuronal Transfer of Human Tau Between Lamprey Central Neurons in situ. *J. Alzheimer's Dis.* **19**, 647–664 (2010).

457. Pooler, A. M., Phillips, E. C., Lau, D. H. W., Noble, W. & Hanger, D. P. Physiological release of endogenous tau is stimulated by neuronal activity. *EMBO Rep.* **14**, 389–394 (2013).

458. Mohamed, N. V., Plouffe, V., Rémillard-Labrosse, G., Planel, E. & Leclerc, N. Starvation and inhibition of lysosomal function increased tau secretion by primary cortical neurons. *Sci. Rep.* **4**, 1–11 (2014).

459. Wu, J. W. *et al.* Neuronal activity enhances tau propagation and tau pathology in vivo. *Nat. Neurosci.* **19**, 1085–1092 (2016).

460. Frost, B., Jacks, R. L. & Diamond, M. I. Propagation of Tau Misfolding from the Outside to the Inside of a Cell. *J. Biol. Chem.* **284**, 12845–12852 (2009).

461. Nobuhara, C. K. *et al.* Tau Antibody Targeting Pathological Species Blocks Neuronal Uptake and Interneuron Propagation of Tau in Vitro. *Am. J. Pathol.* **187**, 1399–1412 (2017).

462. Takeda, S. *et al.* Neuronal uptake and propagation of a rare phosphorylated high-molecular-weight tau derived from Alzheimer's disease brain. *Nat. Commun.* **6**, (2015).

463. Martini-Stoica, H. *et al.* TFEB enhances astroglial uptake of extracellular tau species and reduces tau spreading. *J. Exp. Med.* **215**, 2355–2377 (2018).

464. Piacentini, R. *et al.* Reduced gliotransmitter release from astrocytes mediates tau-induced synaptic dysfunction in cultured hippocampal neurons. *Glia* **65**, 1302–1316 (2017).

465. Castillo-Carranza, D. L. *et al.* Specific Targeting of Tau Oligomers in Htau Mice Prevents Cognitive Impairment and Tau Toxicity Following Injection with Brain-Derived Tau Oligomeric Seeds. *J. Alzheimer's Dis.* **40**, S97–S111 (2014).

466. Holmes, B. B. *et al.* Heparan sulfate proteoglycans mediate internalization and propagation of specific proteopathic seeds. *Proc. Natl. Acad. Sci. U. S. A.* **110**, E3138 (2013).

467. Rauch, J. N. *et al.* Tau Internalization is Regulated by 6-O Sulfation on Heparan Sulfate Proteoglycans (HSPGs). *Sci. Rep.* **8**, 1–10 (2018).

468. Stopschinski, B. E. *et al.* Specific glycosaminoglycan chain length and sulfation patterns are required for cell uptake of tau versus α-synuclein and β-amyloid aggregates. *J. Biol. Chem.* **293**, 10826–10840 (2018).

469. Rauch, J. N. *et al.* LRP1 is a master regulator of tau uptake and spread. *Nature* **580**, 381–385 (2020).

470. Calafate, S., Flavin, W., Verstreken, P. & Moechars, D. Loss of Bin1 Promotes the Propagation of Tau Pathology. *Cell Rep.* **17**, 931–940 (2016).

471. Falcon, B., Noad, J., McMahon, H., Randow, F. & Goedert, M. Galectin-8–mediated selective autophagy protects against seeded tau aggregation. *J. Biol. Chem.* **293**, 2438–2451 (2018).

472. Flavin, W. P. *et al.* Endocytic vesicle rupture is a conserved mechanism of cellular invasion by amyloid proteins. *Acta Neuropathol.* **134**, 629–653 (2017).

473. Robert, A., Schöll, M. & Vogels, T. Tau Seeding Mouse Models with Patient Brain-Derived Aggregates. *Int. J. Mol. Sci.* **22**, 6132 (2021).

474. Liu, L. *et al.* Trans-Synaptic Spread of Tau Pathology In Vivo. *PLoS One* **7**, e31302 (2012).

475. De Calignon, A. *et al.* Propagation of Tau Pathology in a Model of Early Alzheimer's Disease. *Neuron* **73**, 685–697 (2012).

476. Harris, J. A. *et al.* Human P301L-Mutant Tau Expression in Mouse Entorhinal-Hippocampal Network Causes Tau Aggregation and Presynaptic Pathology but No Cognitive Deficits. *PLoS One* **7**, e45881 (2012).

477. Wegmann, S. *et al.* Removing endogenous tau does not prevent tau propagation yet reduces its neurotoxicity. *EMBO J.* **34**, 3028–3041 (2015).

478. Caballero, B. *et al.* Acetylated tau inhibits chaperone-mediated autophagy and promotes tau pathology propagation in mice. *Nat. Commun.* **12**, 1–18 (2021).

479. Wegmann, S. *et al.* Experimental evidence for the age dependence of tau protein spread in the brain. *Sci. Adv.* **5**, 6404–6430 (2019).

480. Smolek, T. *et al.* First-in-Rat Study of Human Alzheimer's Disease Tau Propagation. *Mol. Neurobiol.* **56**, 621–631 (2019).

481. Ferrer, I., Andrés-Benito, P., Sala-Jarque, J., Gil, V. & del Rio, J. A. Capacity for Seeding and Spreading of Argyrophilic Grain Disease in a Wild-Type Murine Model; Comparisons With Primary Age-Related Tauopathy. *Front. Mol. Neurosci.* **13**, 101 (2020).

482. Audouard, E. *et al.* High–Molecular-Weight Paired Helical Filaments from Alzheimer Brain Induces Seeding of Wild-Type Mouse Tau into an Argyrophilic 4R Tau Pathology in Vivo. *Am. J. Pathol.* **186**, 2709–2722 (2016).

483. Lasagna-Reeves, C. A. *et al.* Identification of oligomers at early stages of tau aggregation in Alzheimer's disease. *FASEB J.* **26**, 1946–59 (2012).

484. Narasimhan, S. *et al.* Human tau pathology transmits glial tau aggregates in the absence of neuronal tau. *J. Exp. Med.* **217**, e20190783 (2020).

485. He, Z. *et al.* Amyloid-β plaques enhance Alzheimer's brain tau-seeded pathologies by facilitating neuritic plaque tau aggregation. *Nat. Med.* **24**, 29–38 (2017).

486. Hu, W. *et al.* Hyperphosphorylation determines both the spread and the morphology of tau pathology. *Alzheimer's Dement.* **12**, 1066–1077 (2016).

487. Nies, S. H. *et al.* Spreading of Alzheimer tau seeds is enhanced by aging and template matching with limited impact of amyloid-β. *J. Biol. Chem.* **297**, 101159 (2021).

488. Zareba-Paslawska, J., Patra, K., Kluzer, L., Revesz, T. & Svenningsson, P. Tau Isoform-Driven CBD Pathology Transmission in Oligodendrocytes in Humanized Tau Mice. *Front. Neurol.* **11**, 1825 (2021).

489. Oddo, S. *et al.* Triple-transgenic model of Alzheimer's disease with plaques and tangles: intracellular Abeta and synaptic dysfunction. *Neuron* **39**, 409–421 (2003).

490. Belfiore, R. *et al.* Temporal and regional progression of Alzheimer's disease-like pathology in 3xTg-AD mice. *Aging Cell* **18**, e12873 (2019).

491. Saito, T. *et al.* Humanization of the entire murine Mapt gene provides a murine model of pathological human tau propagation. *J. Biol. Chem.* **294**, 12754–12765 (2019).

492. Dujardin, S. *et al.* Tau propagation is dependent on the genetic background of mouse strains. *Brain Commun.* **4**, 1–8 (2022).

493. Nixon, R. A. & Yang, D. S. Autophagy and Neuronal Cell Death in Neurological Disorders. *Cold Spring Harb. Perspect. Biol.* **4**, a008839 (2012).

494. Menzies, F. M., Fleming, A. & Rubinsztein, D. C. Compromised autophagy and neurodegenerative diseases. *Nat. Rev. Neurosci.* **16**, 345–357 (2015).

495. Mariño, G., Madeo, F. & Kroemer, G. Autophagy for tissue homeostasis and neuroprotection. *Curr. Opin. Cell Biol.* **23**, 198–206 (2011).

496. Lee, S., Sato, Y. & Nixon, R. A. Lysosomal proteolysis inhibition selectively disrupts axonal transport of degradative organelles and causes an Alzheimer's-like axonal dystrophy. *J. Neurosci.* **31**, 7817–7830 (2011).

497. Avrahami, L. *et al.* Inhibition of glycogen synthase kinase-3 ameliorates β-amyloid pathology and restores lysosomal acidification and mammalian target of rapamycin activity in the Alzheimer disease mouse model: in vivo and in vitro studies. *J. Biol. Chem.* **288**, 1295–1306 (2013).

498. Nicholson, A. M. & Rademakers, R. What we know about TMEM106B in neurodegeneration. *Acta Neuropathol.* **132**, 639–651 (2016).

499. Paushter, D. H., Du, H., Feng, T. & Hu, F. The lysosomal function of progranulin, a guardian against neurodegeneration. *Acta Neuropathol.* **136**, 1–17 (2018).

500. Chitramuthu, B. P., Bennett, H. P. J. & Bateman, A. Progranulin: a new avenue towards the understanding and treatment of neurodegenerative disease. *Brain* **140**, 3081–3104 (2017).

501. Feng, T., Lacrampe, A. & Hu, F. Physiological and pathological functions of TMEM106B: a gene associated with brain aging and multiple brain disorders. *Acta Neuropathol.* **141**, 327–339 (2021).

502. Smith, K. R. *et al.* Strikingly Different Clinicopathological Phenotypes Determined by Progranulin-Mutation Dosage. *Am. J. Hum. Genet.* **90**, 1102–1107 (2012).

503. Baker, M. *et al.* Mutations in progranulin cause tau-negative frontotemporal dementia linked to chromosome 17. *Nature* **442**, 916–919 (2006).

504. Takahashi, H. *et al.* Opposing effects of progranulin deficiency on amyloid and tau pathologies via microglial TYROBP network. *Acta Neuropathol.* **133**, 785–807 (2017).

505. Hosokawa, M. *et al.* Progranulin Reduction Is Associated With Increased Tau Phosphorylation in P301L Tau Transgenic Mice. *J. Neuropathol. Exp. Neurol.* **74**, 158–165 (2015).

506. Xu, W. *et al.* The FAM171A2 gene is a key regulator of progranulin expression and modifies the risk of multiple neurodegenerative diseases. *Sci. Adv.* **6**, eabb3063 (2020).

507. Klein, Z. A. *et al.* Loss of TMEM106B Ameliorates Lysosomal and Frontotemporal Dementia-Related Phenotypes in Progranulin-Deficient Mice. *Neuron* **95**, 281-296.e6 (2017).

508. Tanaka, Y., Chambers, J. K., Matsuwaki, T., Yamanouchi, K. & Nishihara, M. Possible involvement of lysosomal dysfunction in pathological changes of the brain in aged progranulin-deficient mice. *Acta Neuropathol. Commun.* **2**, 1–15 (2014).

509. Ahmed, Z. *et al.* Accelerated Lipofuscinosis and Ubiquitination in Granulin Knockout Mice Suggest a Role for Progranulin in Successful Aging. *Am. J. Pathol.* **177**, 311–324 (2010).

510. Kämäläinen, A. *et al.* GRN Variant rs5848 Reduces Plasma and Brain Levels of Granulin in Alzheimer's Disease Patients. *J. Alzheimer's Dis.* **33**, 23–27 (2013).

511. Lee, M. J., Chen, T. F., Cheng, T. W. & Chiu, M. J. rs5848 Variant of Progranulin Gene Is

a Risk of Alzheimer's Disease in the Taiwanese Population. *Neurodegener. Dis.* **8**, 216–220 (2011).

512. Sheng, J., Su, L., Xu, Z. & Chen, G. Progranulin polymorphism rs5848 is associated with increased risk of Alzheimer's disease. *Gene* **542**, 141–145 (2014).
513. Hsiung, G. Y. R., Fok, A., Feldman, H. H., Rademakers, R. & MacKenzie, I. R. A. rs5848 polymorphism and serum progranulin level. *J. Neurol. Sci.* **300**, 28–32 (2011).
514. Minami, S. S. *et al.* Progranulin protects against amyloid β deposition and toxicity in Alzheimer's disease mouse models. *Nat. Med.* **20**, 1157–1164 (2014).
515. Van Kampen, J. M. & Kay, D. G. Progranulin gene delivery reduces plaque burden and synaptic atrophy in a mouse model of Alzheimer's disease. *PLoS One* **12**, e0182896 (2017).
516. Hosokawa, M. *et al.* Progranulin haploinsufficiency reduces amyloid beta deposition in Alzheimer's disease model mice. *Exp. Anim.* **67**, 63–70 (2018).
517. Lüningschrör, P. *et al.* The FTLD Risk Factor TMEM106B Regulates the Transport of Lysosomes at the Axon Initial Segment of Motoneurons. *Cell Rep.* **30**, 3506-3519.e6 (2020).
518. Schwenk, B. M. *et al.* The FTLD risk factor TMEM 106 B and MAP 6 control dendritic trafficking of lysosomes. *EMBO J.* **49**, 1–18 (2013).
519. Stagi, M., Klein, Z. A., Gould, T. J., Bewersdorf, J. & Strittmatter, S. M. Lysosome size, motility and stress response regulated by fronto-temporal dementia modifier TMEM106B. *Mol. Cell. Neurosci.* **61**, 226–240 (2014).
520. Perez-Canamas, A., Takahashi, H., Lindborg, J. A. & Strittmatter, S. M. Fronto-temporal dementia risk gene TMEM106B has opposing effects in different lysosomal storage disorders. *Brain Commun.* **3**, (2020).
521. Schweighauser, M. *et al.* Age-dependent formation of TMEM106B amyloid filaments in human brains. *Nature* (2022) doi:10.1038/S41586-022-04650-Z.
522. Jiang, Y. X. *et al.* Amyloid fibrils in disease FTLD-TDP are composed of TMEM106B not TDP-43. *Nature* 1–10 (2022) doi:10.1038/s41586-022-04670-9.
523. Chang, A. *et al.* Homotypic fibrillization of TMEM106B across diverse neurodegenerative diseases. *Cell* **185**, 1346-1355.e15 (2022).
524. Simons, C. *et al.* A recurrent de novo mutation in TMEM106B causes hypomyelinating leukodystrophy. *Brain* **140**, 3105–3111 (2017).
525. Feng, T. *et al.* A role of the frontotemporal lobar degeneration risk factor TMEM106B in myelination. *Brain* **143**, 2255–2271 (2020).
526. Zhou, X. *et al.* Loss of Tmem106b exacerbates <scp>FTLD</scp> pathologies and causes motor deficits in progranulin-deficient mice. *EMBO Rep.* **21**, e50197 (2020).
527. Van Deerlin, V. M. *et al.* Common variants at 7p21 are associated with frontotemporal lobar degeneration with TDP-43 inclusions. *Nat. Genet.* **42**, 234–239 (2010).
528. Rutherford, N. J. *et al.* TMEM106B risk variant is implicated in the pathologic presentation of Alzheimer disease. *Neurology* **79**, 717 (2012).
529. Götz, J., Chen, F., Van Dorpe, J. & Nitsch, R. M. Formation of neurofibrillary tangles in P301L tau transgenic mice induced by Aβ42 fibrils. *Science (80-.).* **293**, 1491–1495 (2001).

530. Lewis, J. *et al.* Enhanced neurofibrillary degeneration in transgenic mice expressing mutant tau and APP. *Science (80-.).* **293**, 1487–1491 (2001).

531. Hurtado, D. E. *et al.* Aβ Accelerates the Spatiotemporal Progression of Tau Pathology and Augments Tau Amyloidosis in an Alzheimer Mouse Model. *Am. J. Pathol.* **177**, 1977–1988 (2010).

532. Bennett, R. E. *et al.* Enhanced Tau Aggregation in the Presence of Amyloid β. *Am. J. Pathol.* **187**, 1601–1612 (2017).

533. Makin, S. The amyloid hypothesis on trial. *Nature* **559**, S4–S7 (2018).

534. Sousa, A. M. M. *et al.* Molecular and cellular reorganization of neural circuits in the human lineage. *Science* **358**, 1027–1032 (2017).

535. Tian, R. *et al.* CRISPR Interference-Based Platform for Multimodal Genetic Screens in Human iPSC-Derived Neurons. *Neuron* **104**, 239-255.e12 (2019).

536. Tang, S. J. *et al.* Fyn kinase inhibition reduces protein aggregation, increases synapse density and improves memory in transgenic and traumatic Tauopathy. *Acta Neuropathol. Commun.* **8**, 96 (2020).

537. Rush, T. *et al.* A peptide inhibitor of Tau-SH3 interactions ameliorates amyloid-β toxicity. *Neurobiol. Dis.* **134**, 104668 (2020).

538. Zhong, L. *et al.* A rapid and cost-effective method for genotyping apolipoprotein e gene polymorphism. *Mol. Neurodegener.* **11**, 1–8 (2016).

539. Okigaki, M. *et al.* Pyk2 regulates multiple signaling events crucial for macrophage morphology and migration. *Proc. Natl. Acad. Sci. U. S. A.* **100**, 10740–10745 (2003).

540. Kayasuga, Y. *et al.* Alteration of behavioural phenotype in mice by targeted disruption of the progranulin gene. *Behav. Brain Res.* **185**, 110–118 (2007).

541. Saito, T. *et al.* Single App knock-in mouse models of Alzheimer's disease. *Nat. Neurosci.* **17**, 661–3 (2014).

542. Bachmanov, A. A., Reed, D. R., Beauchamp, G. K. & Tordoff, M. G. Food intake, water intake, and drinking spout side preference of 28 mouse strains. *Behav. Genet.* **32**, 435–443 (2002).

543. Schindelin, J. *et al.* Fiji: an open-source platform for biological-image analysis. *Nat. Methods* **9**, 676–682 (2012).

544. Brody, A. H. *et al.* Alzheimer Risk Gene Product Pyk2 Suppresses Tau Phosphorylation and Phenotypic Effects of Tauopathy. *Mol. Neurodegener.* **17**, 1–33 (2022).

545. Briner, A., Götz, J. & Polanco, J. C. Fyn Kinase Controls Tau Aggregation In Vivo. *Cell Rep.* **32**, 108045 (2020).

546. Liu, G. *et al.* Fyn depletion ameliorates tauP301L-induced neuropathology. *Acta Neuropathol. Commun.* **8**, 1–15 (2020).

547. Kaufman, A. C. *et al.* Fyn inhibition rescues established memory and synapse loss in Alzheimer mice. *Ann. Neurol.* **77**, 953–971 (2015).

548. Li, C. & Götz, J. Somatodendritic accumulation of Tau in Alzheimer's disease is promoted by Fyn-mediated local protein translation. *EMBO J.* **36**, e201797724 (2017).

549. Andreev, J. *et al.* Src and Pyk2 Mediate G-protein-coupled Receptor Activation of Epidermal Growth Factor Receptor (EGFR) but Are Not Required for Coupling to the Mitogen-activated Protein (MAP) Kinase Signaling Cascade. *J. Biol. Chem.* **276**, 20130–

20135 (2001).

550. Collins, M. *et al.* The T cell receptor-mediated phosphorylation of Pyk2 tyrosines 402 and 580 occurs via a distinct mechanism than other receptor systems. *J. Leukoc. Biol.* **87**, 691–701 (2010).

551. Collins, M., Bartelt, R. R. & Houtman, J. C. D. T cell receptor activation leads to two distinct phases of Pyk2 activation and actin cytoskeletal rearrangement in human T cells. *Mol. Immunol.* **47**, 1665–1674 (2010).

552. Lee, S., Salazar, S. V., Cox, T. O. & Strittmatter, S. M. Pyk2 Signaling through Graf1 and RhoA GTPase Is Required for Amyloid-β Oligomer-Triggered Synapse Loss. *J. Neurosci.* **39**, 1910–1929 (2019).

553. Kawarabayashi, T. *et al.* Lipid Rafts Act as a Common Platform for Amyloid-β Oligomer-Induced Alzheimer's Disease Pathology. *J. Alzheimer's Dis.* **87**, 1189–1203 (2022).

554. Larson, M. *et al.* The Complex PrPc-Fyn Couples Human Oligomeric Aβ with Pathological Tau Changes in Alzheimer's Disease. *J. Neurosci.* **32**, 16857 (2012).

555. Padmanabhan, P., Martínez-Mármol, R., Xia, D., Götz, J. & Meunier, F. A. Frontotemporal dementia mutant Tau promotes aberrant Fyn nanoclustering in hippocampal dendritic spines. *Elife* **8**, (2019).

556. Nieweg, K., Andreyeva, A., van Stegen, B., Tanriöver, G. & Gottmann, K. Alzheimer's disease-related amyloid-β induces synaptotoxicity in human iPS cell-derived neurons. *Cell Death Dis.* **6**, e1709 (2015).

557. Bassil, R. *et al.* Improved modeling of human AD with an automated culturing platform for iPSC neurons, astrocytes and microglia. *Nat. Commun.* **12**, 1–21 (2021).

558. Corbett, G. T. *et al.* PrP is a central player in toxicity mediated by soluble aggregates of neurodegeneration-causing proteins. *Acta Neuropathol.* **139**, 503–526 (2020).

559. Sackmann, C. & Hallbeck, M. Oligomeric amyloid-β induces early and widespread changes to the proteome in human iPSC-derived neurons. *Sci. Rep.* **10**, 1–12 (2020).

560. Mengel, D. *et al.* PrP-grafted antibodies bind certain amyloid β-protein aggregates, but do not prevent toxicity. *Brain Res.* **1710**, 125 (2019).

561. Rowland, H. A., Hooper, N. M. & Kellett, K. A. B. Modelling Sporadic Alzheimer's Disease Using Induced Pluripotent Stem Cells. *Neurochem. Res.* **43**, 2179–2198 (2018).

562. Wu, Y. Y., Chiu, F. L., Yeh, C. S. & Kuo, H. C. Opportunities and challenges for the use of induced pluripotent stem cells in modelling neurodegenerative disease. *Open Biol.* **9**, 180177 (2019).

563. Gratuze, M. *et al.* Activated microglia mitigate Aβ-associated tau seeding and spreading. *J. Exp. Med.* **218**, 1–11 (2021).

564. Kostylev, M. A. *et al.* Prion-Protein-interacting Amyloid-β Oligomers of High Molecular Weight Are Tightly Correlated with Memory Impairment in Multiple Alzheimer Mouse Models. *J. Biol. Chem.* **290**, 17415–17438 (2015).

565. Katsuno, T. *et al.* Independent accumulations of tau and amyloid β-protein in the human entorhinal cortex. *Neurology* **64**, 687–692 (2005).

566. Hou, Y. *et al.* Ageing as a risk factor for neurodegenerative disease. *Nat. Rev. Neurol. 2019 1510* **15**, 565–581 (2019).

567. Kang, S. S. *et al.* Tau modification by the norepinephrine metabolite DOPEGAL

stimulates its pathology and propagation. *Nat. Struct. Mol. Biol.* **29**, 292–305 (2022).

568. Panicker, N. *et al.* Fyn kinase regulates misfolded α-synuclein uptake and NLRP3 inflammasome activation in microglia. *J. Exp. Med.* **216**, 1411 (2019).

569. Chakraborty, P. *et al.* Co-factor-free aggregation of tau into seeding-competent RNA-sequestering amyloid fibrils. *Nat. Commun.* **12**, 4231 (2021).

Statement of Contributions

Contribution overview of Nies et al. 2021

Nies SH, Takahashi H, Herber CS, Huttner A, Chase A, Strittmatter SM. Spreading of Alzheimer tau seeds is enhanced by aging and template matching with limited impact of amyloid-β. *J Biol Chem*. 2021;297(4):101159. doi:10.1016/j.jbc.2021.101159

Sarah Helena Nies (SHN) designed the research and wrote the original draft of the paper together with SMS. Furthermore, she acquired a Ph.D. fellowship (BIF) for funding, as well as acquired and analyzed all data contained in this paper except for the data in Figure 1E.

Hideyuki Takahashi (HT) cultured mouse neurons, applied tau fibrils to them, as well as imaged and analyzed that dataset (Figure 1E). He also bred the $Grn^{-/-}$ mice used in this study.

Charlotte S. Herber established the human tau extraction procedure in the lab and tau extracts from Brain A and B were extracted by SHN and Charlotte S. Herber together.

Anita Huttner is a pathologist at Yale, who provided the human brain autopsy tissue to the lab.

Alison Chase was a summer student, working with SHN. She counted inclusions and imaged brain sections for Fig. 4 B-C in collaboration with SHN.

Stephen M. Strittmatter (SMS) supervised and provided funding for the research. He collaborated with SHN to design the research and to write the original draft of the paper.

All authors reviewed and edited the final draft. The authors read and approved the final manuscript.

Contribution overview of Tang et al. 2020

Tang SJ*, Fesharaki-Zadeh A*, Takahashi H*, **Nies SH,** Smith LM, Luo A, Chyung A, Chiasseu M, Strittmatter SM. Fyn kinase inhibition reduces protein aggregation, increases synapse density and improves memory in transgenic and traumatic Tauopathy. *Acta Neuropathol Commun*. 2020 Jul 1;8(1):96. doi: 10.1186/s40478-020-00976-9. PMID: 32611392; PMCID: PMC7329553.

Si Jie Tang (SJT) designed research and wrote the original draft of the paper in collaboration with SMS, HT and AFZ. She treated mice with AZD and performed all associated staining and behavior in collaboration with LMS and HT (Figures 1-3, 4A-D, S1-S3).

Arman Fesharaki-Zadeh (AFZ) wrote the original draft of the paper in collaboration with SMS, HT and SJT. He conducted experiments involving traumatic brain injury (Figures 5, S4-S6) in collaboration with MC.

Hideyuki Takahashi (HT) designed research and wrote the original draft of the paper in collaboration with SMS, SJT and AFZ. He supervised work done by SJT for Figures 1-3, 4A-D, S1-S3. He performed the analysis of the fyn-tau PLA assay (Fig. 4F-I), mouse neuron culture, treatment and data analysis in collaboration with SHN (Figure 6B-D)

Sarah Helena Nies (SHN) extracted human Tau and performed quality control (Figure 6A). She treated primary neurons with human Tau, stained them and analyzed the data in collaboration with HT (Figure 6B-D). She also stained and imaged the fyn-tau PLA assay (Figure 4E) and performed the data analysis in collaboration with HT (Figure 4F-I).

Levi M. Smith (LMS) treated mice with AZD in collaboration with SJT and HT.

Anin Luo and Anabelle Chyung (AL and AC) stained and analyzed mouse brain tissue in collaboration with LMS and SJT.

Marius Chiasseu (MC) worked with AFZ to establish the brain injury mouse model, operated mice and performed experiments with AFZ..

Stephen M. Strittmatter (SMS) supervised and provided funding for the research. He designed the research and wrote the original draft of the paper in collaboration with SJT, HT and AFZ.

All authors reviewed and edited the final draft. The authors read and approved the final manuscript.

Contribution overview of Brody et al. 2022

Brody AH, **Nies SH,** Guan F, Smith L, Mukherjee B, Salazar S, Lee S, Lam T, Strittmatter SM. Alzheimer Risk Gene Product Pyk2 Suppresses Tau Phosphorylation and Phenotypic Effects of Tauopathy. *In revision at Molecular Neurodegeneration*

Alex Harrison Brody (AHB) designed the research and wrote the original draft of the paper in collaboration with SMS. He conducted all experiments and data analysis not attributed to other people below.

Sarah Helena Nies (SHN) cultured iPSC-derived neurons used in this study together with AHB (Figures 2E-I, 7A-C and S8).

Fulin Guan (FG) conducted the phosphorylation assays in HEK293T cells (Figure 1).

Levi M. Smith (LMS) acquired mass spectrometry dataset in collaboration with AHB and SAS (Figures 6, 8, 9).

Bandhan Mukherjee (BM) conducted the slice experiments in collaboration with AHB (Figure 2A-D).

Santiago A. Salazar (SAS) acquired mass spectrometry dataset in collaboration with AHB and SAS (Figures 6, 8, 9).

Suho Lee (SL) cloned the constructs used in phosphorylation experiments in HEK239T cells (Figure 1).

Tuk Lam (TL) ran the mass spectrometry samples on MS machines (Figures 6, 8, 9).

All authors reviewed and edited the final draft. The authors read and approved the final manuscript.

Contributions to human iPSC-derived neuron culture

Framework of joint project: SHN and AHB established a culture of iPSC-derived neurons in the Strittmatter lab based off an already published protocol using dual-SMAD inhibition. The goal of the project is to investigate signaling downstream of amyloid-ß (Aß) in these neurons, with a focus on kinase signaling and tau hyperphosphorylation downstream of Aß binding to PrP^{C}-mGluR5.

Sarah Helena Nies (SHN) cultured the "Gibco" cell line in collaboration with AHB through differentiation with the dual-SMAD inhibition protocol. She performed experiments using Fyn and Pyk2 inhibitors in these cells in collaboration with AHB. In addition, she treated cells with synthetic Aß-oligomers (sAßo) for seven days to assess post-synaptic density decreases through immunohistochemistry. Furthermore, she also cultured and performed all

experiments shown with the “i3N” cell line (obtained from the Kampmann lab at UCSF, see Tian et al. 2019).

Alex Harrison Brody (AHB) cultured the “Gibco” cell line in collaboration with SHN through differentiation with the dual-SMAD inhibition protocol. He performed experiments using Fyn and Pyk2 inhibitors in these cells in collaboration with SHN.

Acknowledgements

First and foremost, I would like to thank Stephen Strittmatter for providing me with the opportunity to be a part of his lab and for his guidance throughout my doctoral project. It was a pleasure to conduct my thesis work in a place, where scientific collaboration and exchange of knowledge are the highest priority. I got to learn many new techniques, and was allowed great independence in conducting my research, which I value very highly.

Next, I would like to extend my gratitude to Peter Heutink and Philipp Kahle for being part of my advisory board and for agreeing to have Zoom advisory board meetings long before a global pandemic made them a common occurrence. Their feedback and support shaped this thesis and helped me succeed. I would also like to thank the staff of the Graduate Training Center for Neuroscience in Tübingen, especially Susanne Kamphausen, Petya Georgieva and Monika Lam for answering all my questions regarding coursework, accreditations, and other organizational matters around my dissertation. Without their support, writing a thesis while conducting most of the research abroad would not have been possible.

Furthermore, I would like to thank all the lab members that I had the pleasure of working with throughout the years. Many have become dear friends and without them, work would have been significantly less fun. Harry, you were my reliable partner-in-crime for all things iPSC and a fellow Ph.D. student to discuss the ups and downs of being a doctoral student with. Leire and Azu, you were the best coffee-buddies anyone could have wished for, and I valued your expertise, compassion and friendship greatly. Misha, you are a scientist whose intuition I admire. You have also organized many memorable backyard barbecues, with always excellent food and interesting people from all around New Haven. Bandhan, Graham, Erik, Carmen, LaShae and Yangyi, I want to thank you for your camaraderie in the lab and all the philosophical discussions we had about art, life, books, food and all other topics under the sun. In addition, I am grateful for Laura Haas for introducing me to the Steve and the Strittmatter lab during my master's degree, which lead to me doing my thesis work there.

I would also like to thank my dear friends Samantha Schmaul, Malte Kölling, Raymond Townsend, Yuxuan Wu and Carmen Dege for all the interesting and intelligent discussions we had in the last years. I'm very also grateful to my family for always believing that I could achieve the goals I set for myself. More specifically, I want to thank my parents for helping me organize things back home and my brother Jasper for always lending an open ear, being in my corner and overall, being the greatest brother, one could wish for. I also want to thank my grandmother, Ama, for being so invested in what her granddaughter is up to, sending me regular updates about the hassles of retirement I get to look forward to in 50 years' time and her unconditional love and support. I would also like to take a moment to remember the three family members that have unfortunately passed away during this thesis: my grandfather Hans-Karl Batsch, my grandmother Ingeborg Nies and my uncle Nicolas Batsch. They have been an influential part of my life and I remember them fondly.

Last but certainly not least, I would like to thank my partner Hope and our mischievous, but incredibly cute cat, Aisha. Hope has been my anchor throughout long workdays, complicated experiments and arduous paper and thesis writing processes and always managed to make me smile at the end of the day. I love you, our shared sense of adventure for new places, food and experiences and that we never run out of things to talk about.

To conclude, thank you all for making my Ph.D. work and my life in New Haven the wonderful experience it has been!